# P-T ESTIMATES OF PEAK BUSHVELD METAMORPHISM IN THE EASTERN BUSHVELD COMPLEX, LIMPOPO PROVINCE, SOUTH AFRICA: CONSTRAINTS FROM P-T PSEUDOSECTIONS

**Denni Raubenheimer**

**Submitted in partial fulfilment of the requirements for the degree Masters in Geology in the Faculty of Natural & Agricultural Sciences, University of Pretoria, Pretoria**

**July 2012.**

**Supervisors: M.J. Rigby and J. Roberts**

# STATEMENT

I, Denni Raubenheimer, declare that this thesis, which I hereby submit for the degree Masters in Geology at the University of Pretoria, is my own work and has not previously been submitted by me for a degree at this or any other tertiary institution.

Signed: _____

Date: 27 July 2012

# ABSTRACT

The Bushveld Igneous Complex (BIC) is the largest layered mafic intrusion in the world and contains the largest known deposits of vanadium, chromium and Platinum group elements on the planet, as well as large deposits of iron, nickel, copper, tin and fluorite. To aid and improve our understanding of the tectonics that prevailed during the emplacement of the Bushveld Complex relevant data can still be extracted from the metamorphic aureole of the Complex, not the least among which are accurate determinations of pressure conditions during peak metamorphism. A relatively large number of geothermobarometric investigations have been performed on the Bushveld Complex aureole. The summation of all the thermobarometric studies on the Bushveld Complex aureole produces a dataset with largely divergent pressure-estimates, ranging from 1.5 kbar to 5.5 kbar. This study's main aim was to produce new thermobarometric data for the Eastern Bushveld Complex aureole. To this ends metapelites from the aureole were sampled between Lydenburg and somewhat northwest of Penge. Polished thin-sections were produced for a number of samples and studied under microscope. After XRF analyses were performed on a refined number of samples, pseudosections for these samples were produced using Perplex. Electron microprobe analyses were used to analyze mineral chemistries of five samples and the resultant data used to construct isopleths for these samples in Perplex. The isopleth data was then used to scrutinize and, where possible, refine PT-estimates. The principal results obtained from mineral equilibrium modeling were the pseudosections and isopleths of samples DY09-54 and DY09-56. These samples' cumulate results suggest that the metapelites of their sampling locality, which lies roughly ~36 km northwest of Penge, reached 530-565 ºC and 2230-2960 bar during peak metamorphism. Modelled isopleths of MnO/(MnO+CaO+FeO+MgO) suggest that these estimates be refined to 550 ± 5 ºC and 2650 ± 20 bar. These pressure estimates agree well with the majority of barometric studies in the literature that post-date the nineteen-eighties. The pressure estimates of 2230-2960 bar suggest that DY09-54 and DY09-56 were at a crustal depth of 7.9-10.4 km during peak metamorphism, assuming that a roughly 1.5 km thick load of rock, mainly of the Rooiberg Group and/or the Lebowa Granite Suite, were situated above the Rustenburg Layered Suite and at the top of the pile that overlay the samples. In such a case the Rustenburg Layered Suite's contribution to the load would have represented a 4.2-6.7 km thick pile of these mafic rocks and, assuming that the load of Pretoria Group strata in the floor to the Complex had a thickness of 2350 m, the base of the Rustenburg Layered Suite would have been at a crustal depth of 5.6-8.0 km during peak metamorphism and directly above samples DY09-54 and DY09-56. Modelled palaeogeotherms together with the peak-metamorphic crustal depths estimated for samples DY09-54 and DY09-56

suggest that at peak metamorphism the samples' temperatures had been elevated by no less than 320-355 °C, assuming that no thermal metamorphic effect was active on the samples just prior to the intrusion of the Bushveld Complex.

# INDEX

# ACKNOWLEDGEMENTS

I would like to thank the following persons for the roles they played in the completion of my thesis:

Martin Rigby for his help and guidance throughout my project.

James Roberts for all his assistance and help in the final stages of my write-up.

My wife, Yolandé, for all her encouragement, patience and help with Photoshop problems.

Ingrid Booysen for producing such excellent figures.

Philane Mavimbela for helping me with numerous small issues.

Professor P.G. Eriksson for his advice and help with my literature review and other issues.

# CHAPTER 1

## INTRODUCTION

### 1.1. General Background

The Bushveld Igneous Complex (BIC) is the largest layered mafic intrusion in the world (Webb *et al.*, 2004; Clarke *et al.*, 2009). Its outcrops occur over a wide area, occurring in four Provinces of South Africa, namely Gauteng, North West, Limpopo and Mpumalanga (Fig. 1). The Bushveld Complex contains the largest known deposits of vanadium, chromium and Platinum group elements on the planet (Clarke *et al.*, 2009), as well as large deposits of iron, nickel, copper, tin and fluorite (Eriksson *et al.*, 1995). The latter two deposit-types are restricted to the felsic portions of the Complex (Eriksson *et al.*, 1995), which represents the Lebowa Granite Suite, while the mafic-ultramafic portions of the Complex represent the Rustenburg Layered Suite (RLS) (Johnson *et al.*, 2004; Clarke *et al.*, 2009). The tectonic settings which prevailed in the Transvaal Basin, wherein most of the BIC is found (Eriksson *et al.*, 1995), just prior to- and after the intrusion of the Bushveld Complex has been much debated, though resolution on this matter has somewhat improved (Eriksson *et al.*, 1991; Eriksson *et al.*, 1995; Clarke *et al.*, 2009). Bushveld tectonics must have been related to convergence of the Kaapvaal and Zimbabwe cratons (Clarke *et al.*, 2009), while the emplacement of the Complex must have been influenced by the Transvaal-Murchison Lineament (TML) (Eriksson *et al.*, 1991; Clarke *et al.*, 2009). Regarding the former, Clarke *et al.*, 2009 surmised that contemporaneous to intrusion of the BIC, the Kaapvaal and Zimbabwe cratons must have been subject to a NW-SE compressional regime. With regards to the latter, Eriksson *et al.* (1991) suggested that the TML was subjected to extensional reactivation during deposition of the Pretoria Group and that the latter was deposited in a series of half-grabens. To aid and improve our understanding of the tectonics that prevailed during the emplacement of the Bushveld Complex relevant data can still be extracted from the metamorphic aureole of the Complex. Accurate determinations of pressure conditions during peak metamorphism in the aureole can be used to determine the depth of intrusion of the Bushveld Complex and thus be used to better scrutinize the tectonic models for the evolution of the Complex.


**Fig. 1.** Map of South Africa showing the distribution of the Bushveld Complex in green, modified after Impala Platinum Holdings Limited (2004).

The metamorphic aureole of the Bushveld Complex occurs in the rocks of the Transvaal Supergroup (Eriksson *et al.*, 1995; Waters and Lovegrove, 2002), though its manifestation is mostly restricted to the successions of the Pretoria Group (Hall. 1932). Stratigraphically, the aureole has a maximum thickness of over 5 km (Uken, 1998). This translates to the aureole being up to 25 km wide in outcrop, perpendicular to the igneous contact (Waters and Lovegrove, 2002).

In southeastern Limpopo, in the area surrounding Burgersfort, the eastern limb of the Bushveld Complex lies directly on top of the Silverton, Magaliesberg, Vermont and Lakenvlei formations of the Pretoria Group (Waters and Lovegrove, 2002). Here, the aureole's thickness and width increases from south to north (Hall, 1932). At Lydenburg the aureole extends midway into the Silverton Formation, around Ohrigstad into the Timeball Hill Formation and, northwest of Penge, it extends into the calc-silicates of the Chuniespoort Group (Hall, 1932). In the study area, which stretches from just north-

northwest of Lydenburg, past Burgersfort, to roughly 40 km northwest of Penge, the aureole is thus largely manifested in Pretoria Group successions, which are rich in pelitic rocks, thus making ideal subjects for thermobarometric studies.

A relatively large number of geothermobarometric investigations have been performed on the Bushveld Complex aureole. Some of the earliest works being those of Human (1975) and Engelbrecht (1976) and some of the most recent being that of Kaneko *et al.* (2005). The summation of all the thermobarometric studies on the Bushveld Complex aureole produces a dataset with largely divergent pressure-estimates, ranging from 1.5 kbar (Kaneko *et al*., 2005) to 5.5 kbar (Sharpe, 1982). Such discrepancies are far too large to be accounted for by variations in stratigraphic depth between studies. One very plausible reason for this large divergence is the fact that many different geobarometers and geobarometric methods, as well as different thermodynamic datasets, have been applied. Furthermore, a large proportion of studies from the late nineteen-nineties and onwards have obtained their PT-estimates via PT-grids and the construction of pseudosections. These modern thermobarometric techniques have tended to produce more modest and rather consistent pressure estimates of peak metamorphism in the aureole (Uken, 1998; Pitra and De Waal, 2001; Waters and Lovegrove, 2002; Johnson *et al*., 2003; Johnson *et al*. 2004). It can be argued that a pseudosection approach to producing thermobarometric data of peak metamorphism in the aureole is far superior to more traditional thermobarometric techniques, as it produces results specific to a sample's bulk-composition and with errors and uncertainties that are comparable between studies when the thermodynamic dataset of Holland and Powell (1998) is applied.

This study provides new geothermobarometric data of peak metamorphism in the eastern Bushveld Complex aureole using modern geothermobarometric techniques, i.e. the modelling program Perplex, and the internally consistent thermodynamic dataset of Holland and Powell (1998).

## 1.2. Aims

This study was conducted to refine pressure estimates of peak metamorphism in the thermal aureole of the eastern limb of the BIC. Furthermore, the obtained metamorphic

pressures would be used to infer the depth of samples during peak metamorphism and if possible to estimate the depth of intrusion of the Rustenburg Layered Suite.

## 1.3. Study Area

The sampling area stretches from just north of the Rooipoort River, north-northwest of Mecklenburg, Limpopo Province, to less than 20 km west-northwest of Lydenburg, Mpumalanga Province (Fig. 2A).

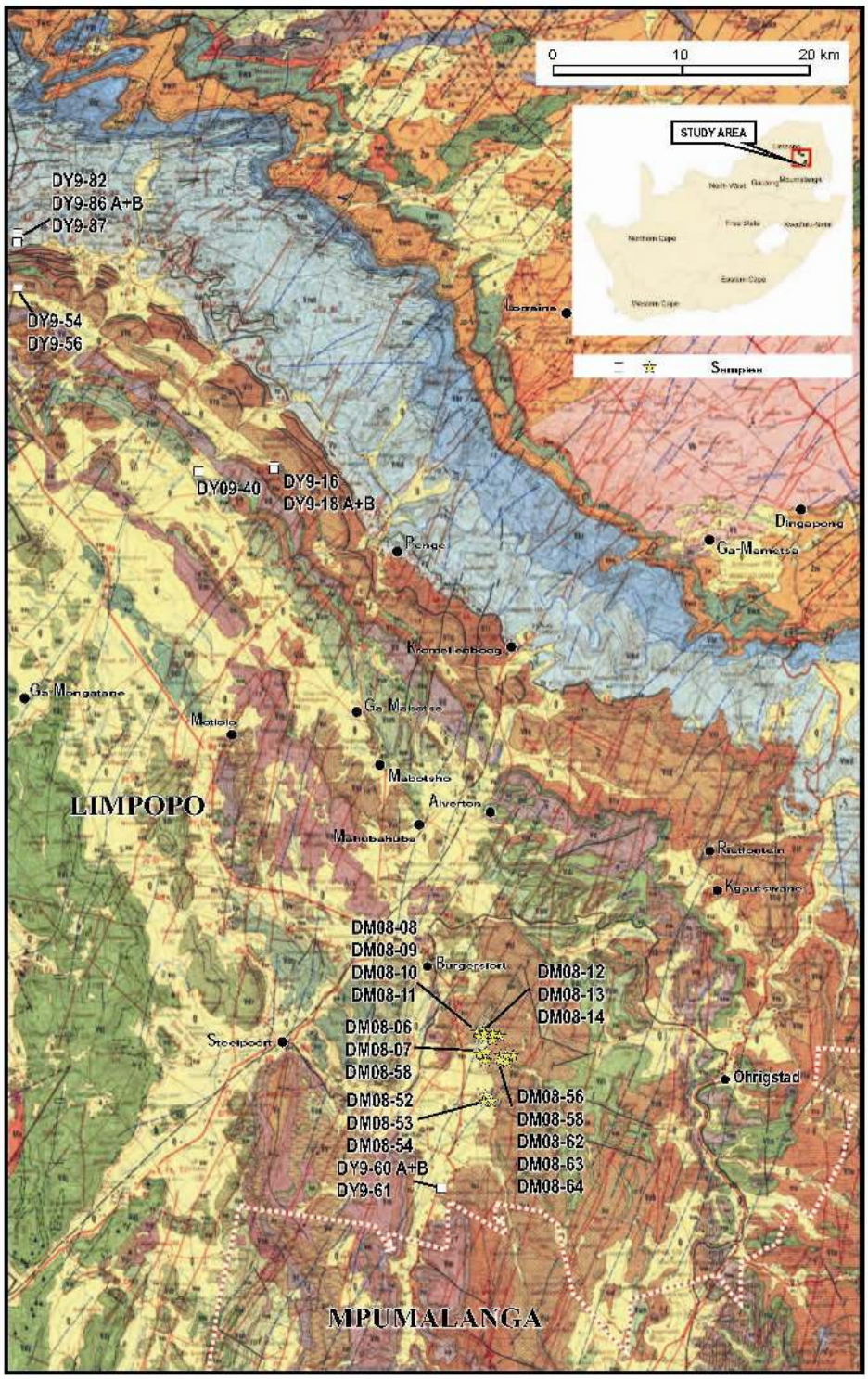


**Fig. 2A.** Geological map of study area showing sampling locations of all analysed samples; modified after Department of Mineral and Energy Affairs and the Geological Survey (1986).

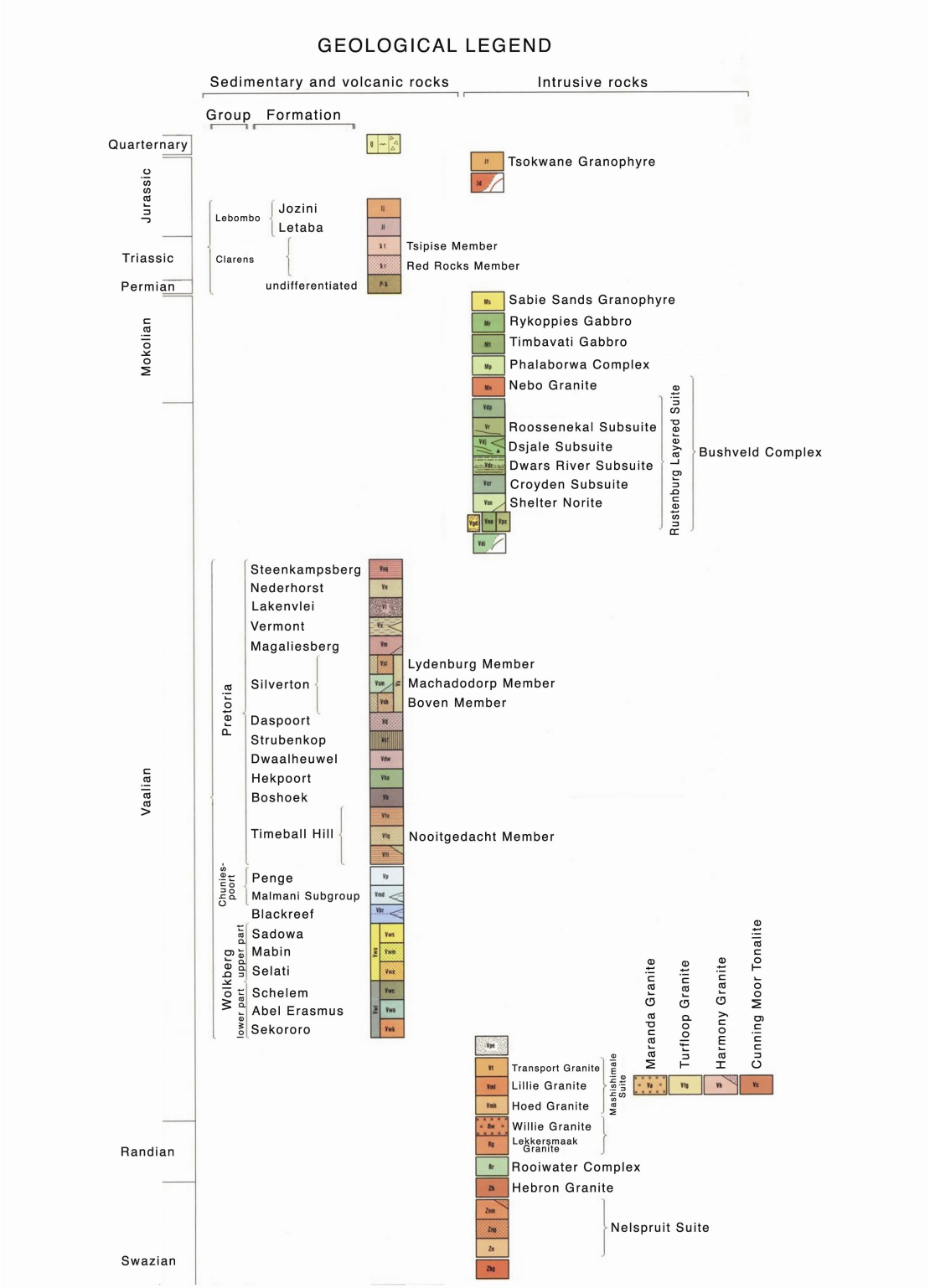


**Fig. 2B.** Geological legend of study area map modified after Department of Mineral and Energy Affairs and the Geological Survey (1986).

# CHAPTER 2

## GEOLOGICAL SETTING AND PREVIOUS METAMORPHIC STUDIES

### 2.1. Regional Geology

The ~2.05-2.06 Ga old (Walraven *et al.*, 1990; Buick *et al.*, 2001; Cawthorn and McKenna, 2006; Scoates and Friedman, 2007) Bushveld Igneous Complex is made up of two suites of plutonic rock, namely the Lebowa Granite Suite and the Rustenburg Layered Suite (Johnson *et al.*, 2004; Clarke *et al.*, 2009). The Lebowa granites post-date the RLS and largely intruded the mafic- to ultramafic rocks of the RLS (Clarke *et al.*, 2009). Prior to this intrusion the RLS intruded the rocks of the Transvaal Supergroup around ~2.05 Ga (Scoates and Friedman, 2007).

The RLS occurs mainly within the Transvaal Basin (Eriksson *et al.*, 1995) and intruded the Transvaal Sequence largely subconcordantly (Clarke *et al.*, 2009). In many areas the Rooiberg Group, of the upper Transvaal Sequence, forms the roof of the RLS. The floor rocks of the Rustenburg Layered Suite are, in most areas, the upper units of the Pretoria Group (Eales and Cawthorn, 1996). However, the RLS transgresses onto the Archaean basement of the Kaapvaal Craton in the northern limb of the Bushveld Complex (Eales and Cawthorn, 1996).

Today the RLS is exposed at surface in five different areas, collectively covering a total area of outcrop of >65000 $km^2$ (Cawthorn and McKenna, 2006). These five areas are known as the northern, far western, western, south-eastern and eastern limbs and evidence suggests that these might be connected at depth forming a giant sill (Cawthorn *et al.*, 1998; Cawthorn and McKenna, 2006). In the eastern BIC the RLS has a maximum thickness around 8 km (Cawthorn and Walraven, 1998).

Shortly after intrusion, the rocks of the RLS subsided owing to their greater density relative to the rocks they intruded. It is not known exactly how this subsidence affected the structure of the surrounding rocks of the Transvaal Supergroup. However, it is known that the underlying rock units often dip towards the centre of the BIC and that the dips tend to increase as the contact with the BIC is approached (Button, 1975). In northern Mpumalanga, dips increase from below 5º to more than 15º as the igneous contact is

approached, while in south-eastern Limpopo, dips greater than 40º have been measured near the contact (Button, 1975).

In general, the Pretoria Group rocks in the northern portion of the eastern BIC have steeper dips than those in the middle and southern sections. The northern portion is also anomalous in dip direction. As this portion is approached from the south, dip directions change from roughly south-westwards to roughly southwards.

The Transvaal Supergroup was deposited on the Archaean aged basement of the Kaapvaal Craton between 2550-2100 Ma (Waters and Lovegrove, 2002). This Supergroup is divided, from bottom to top, into the Wolkberg Group, the Black Reef Formation, the Chuniespoort Group and the Pretoria Group, and is dominated by sedimentary rocks that were deposited in relatively shallow-water conditions (Catuneanu and Eriksson, 1999). The maximum thicknesses of these subdivisions from bottom to top, are 2000 m, 500 m, 3000 m and 8000 m, respectively (Button, 1975).

The Pretoria Group mainly consists of alternating units of shale and quartzite (Eriksson *et al.*, 1991), although it contains various volcanic horizons (Eriksson *et al.*, 1995). From bottom to top, the Pretoria Group is divided into the Rooihoogte (shale, quartzite/sandstone and conglomerate), Timeball Hill (mainly shale), Boshoek (diamictite, conglomerate and quartzite/sandstone), Hekpoort (basaltic andesite), Dwaalheuwel (diamictite, conglomerate and quartzite/sandstone), Strubenkop (mainly shales), Daspoort (mainly quartzite/sandstone), Silverton (mainly shale), Magaliesberg (mainly quartzite/sandstone), Vermont (mainly shale), Lakenvlei (mainly quartzites/sandstone), Nederhorst (shale and quartzite/sandstone), Steenkampsberg (mainly quartzite/sandstone) and Houtenberg (shales, quartzite/sandstone and limestone) formations (Hartzer, 1995; Catuneanu and Eriksson, 1999). Reczco (1994) performed a thorough study of the geochemistry of the Pretoria Group. He found that two distinct groups of shales can be distinguished in the Pretoria Group, based on chemistry and mineralogy, namely Al-rich shales with predominantly kaolinite-mica clay mineral assemblages, and Mg-Ca-Na-rich shales with mica-plagioclase mineral assemblages. The Al-rich shales are typical of the shales found between the bottom of the Pretoria Group and the Daspoort Formation, while the Mg-Ca-Na-rich shales are typical of the Silverton Formation and the shale units

occurring above the Magaliesberg Formation (Reczco, 1994). Of particular interest to this study are the shales of the Timeball Hill and Silverton formations.

Waters and Lovegrove (2000) reported that in the area around Burgersfort the Timeball Hill Formation consists of Fe- and Al-rich shales, siltstones and quartzites. They also reported that these rocks are often graphite rich. According to Reczco (1994), in the eastern Transvaal (as well as in the western Transvaal, Botswana and in the Dennilton Fragment inlier) the Timeball Hill Formation consists of a lower unit of shale, a middle unit of sandstone and/or quartzite and an upper unit of shale. His work shows that the lower unit of shale is typically enriched in $Al_2O_3$ and depleted in MgO, CaO and $Na_2O$ relative to average shale estimates. He reported that this same enrichment and depletion is typically observed in the upper unit of shales, although the upper unit also shows enrichment for $P_2O_5^-$ relative to average shale estimates. The total thickness of the Timeball Hill Formation in the eastern Transvaal was reported by Button (1973) as 700-1300 m.

Reczco (1994) reported that in northern Mpumalanga and south-eastern Limpopo the Silverton Formation is divided, from bottom to top, into the Boven Shale Member, the Machadodorp Volcanic Member and the Lydenburg Shale Member. He observed that the Boven Shale Member shows enrichment in $SiO_2$ and depletion in $Fe_2O_3$(t), MnO, MgO, CaO and $K_2O$ when compared to average shale estimates. For the Lydenburg Shale Member he reported enrichment in $SiO_2$ and depletion in $Al_2O_3$, $K_2O$ and $TiO_2$ relative to average shale estimates and that in the case of titanium oxide the depletion is minor. According to Reczco (1994) in northern Mpumalanga the approximate thicknesses of the the Boven Shale Member and the Lydenburg Shale Member is 300 m and 700 m, respectively. Button (1976) reported that in northern Mpumalanga the Boven Shale Member has a thickness varying between 170-300 m, while the Machadodorp Volcanic Member has a maximum thickness of 400 m in the south, which decreases irregularly to the north. The Lydenburg Shale has a thickness varying between 1200 and 1700 m (Button, 1976).

According to Johnson *et al.* (2003), the metamorphic aureole of the Bushveld Complex has a maximum width adjacent to the northern portion of the Eastern Bushveld Complex, where it stretches at least 25 km away from the contact with the RLS. This area

corresponds to the northern portion of the study area. At and near the contact with the RLS the Bushveld aureole exhibits high to ultra-high grades of metamorphism (Nell, 1985; Engelbrecht, 1990; Johnson *et al.*, 2003; Kaneko *et al.*, 2005), as well as migmatitic textures (Johnson *et al.*, 2003). Though the aureole is well developed its outcrops are not ubiquitous around the BIC (Johnson *et al.*, 2003).

## 2.2. Previous Metamorphic Studies

Gau (1907) gave a brief description of the geology of the area around the intersection of the Olifants and Elands rivers, in northern Mpumalanga. He reported that the Pretoria Group dips to the east at about 25º in that area and also noted a number of metamorphosed pelites within the Group. These include a relatively thin band of pelite occurring just above the Chuniespoort Group. The pelite reportedly displays black pigment, locally separated into black spots, which Gau (1907) interpreted as being caused by contact metamorphism. He also described a metapelite occurring just below quartzites (probably Daspoort or Magaliesberg). He described it as a micaceous schist and reported it to contain chiastolite. He ascribed the metamorphism to a diabase occurring above the overlying quartzites. Another metapelite was reported to occur between quartzites and an amygdaloidal diabase, on the farm Elandsdrift close to the Elands River. This pelite also contains andalusite. Finally, Gau (1907) also described a dark, compact rock with a concoidal fracture and an appearance similar to chert. These rocks form hills along the Moos River and Gau (1907) reported that it can contains fine-grained quartz and feldspar, as well as large crystals of plagioclase. He concluded that it might be a type of hornfels and that its metamorphism might have been caused by the thermal action of large basic intrusives to the north and south, combined with the influence of stress.

Hall (1932) performed a broad study of the Bushveld Complex, which includes a section focusing on the metamorphism associated with the igneous complex. He reported on the geographic variation in the thickness of the aureole noting that the aureole had a minimum thickness of approximately 366 metres north of Pretoria Central and a maximum thickness of roughly 4020 m at Malips Drift (south-eastern Limpopo). Hall (1932) reported that the most common rock-type in the aureole are the pelites of the Pretoria Group. These were grouped into three categories of metamorphic character, namely the “Groothoek

Type", the "Longsight Type" and the "Malips River Type". The Groothoek Type reportedly consists mainly of holocrystalline cordierite-hornfels from which the sedimentary structures have been obliterated. Hall (1932) reported that the Groothoek Type seldom reaches beyond the inner aureole and typically contains the following minerals: biotite, cordierite, quartz, andalusite, garnet, feldspar, sillimanite and tourmaline, though pyroxene and amphibole might also be present. The Longsight Type is described as a slate with visible contact metamorphic minerals that still displays its sedimentary origin. These rocks occur in the outer aureole and often contain abundant chiastolite. When chiastolite is less abundant, or absent, these rocks may be characterised by andalusite, or, in south-eastern Limpopo, by staurolite. The Malips River Type is essentially those rocks within the inner aureole that display a gneissic or schistose texture. They are reportedly restricted to south-eastern Limpopo and commonly contain sillimanite, garnet and muscovite, as well as often-abundant cordierite and sometimes andalusite, but no chiastolite.

According to Hall (1932), the inner aureole is characterised by cordierite-bearing hornfels, while the outer aureole is characterised by chiastolite- and/or andalusite-bearing metapelites. Furthermore, staurolite, though only occurring in south-eastern Limpopo, is reportedly restricted to the outer aureole.

Concerning metamorphism of roof-rocks Hall (1932) reported acute felspathisation of roof-quartzites together with increased grain-size, which varies between beds (although both the former characteristics are also observed in floor-quartzites). Furthermore, Hall (1932) reported that the xenoliths occurring in the Rustenburg Layered Suite show intense metamorphism, similar to that of the inner aureole, but with widespread partial melting and contamination from the Rustenburg Layered Suite. In the xenoliths, sedimentary structures were reported as totally, or almost totally, erased.

Hall (1932) concluded that the aureole was predominantly formed by thermal influences, except in south-eastern Limpopo where pressure played a significant role. He further interpreted the Rustenburg Layered Suite as the predominant source of the thermal energy.

Willemse (1959) reported that the presence of akermanite, monticellite and wollastonite in calc-silicate xenoliths in the Hendriksplaas norite, Steelpoort area (eastern

BIC), could indicate temperatures of 700-750 ºC. His reason was that the reaction akermanite ($Ca_2MgSi_2O_7$) = monticellite ($CaMgSiO_4$) + wollastonite ($CaSiO_3$) will occur at these temperatures at pressures of 2.1-4.2 kbar.

Schwellnus *et al.* (1962) conducted a thorough study of the geology of the Olifants River area, in south-eastern Limpopo. The following minerals were identified in the hornfelses in their study area: quartz, andalusite, staurolite, biotite, chlorite, spinel, diopside, sillimanite, chloritoid, garnet, amphibole, cordierite, tourmaline, muscovite, sericite, feldspar and plagioclase. The occurrence of these minerals in the study area of Schwellnus *et al.* (1962) was described as follows. Quartz is present in all the metapelites, while andalusite commonly occurs from below the Magaliesberg Formation, into the Timeball Hill pelites. The abundance of andalusite decreases upwards in the Pretoria Group stratigraphy – being completely absent above the Magaliesberg Formation. Staurolite is as abundant in the Timeball Hill Formation and said to contain inclusions of quartz and opaque minerals. Biotite is present in the studied pelites in varying amounts, occurring mainly as porphyroblasts. Chlorite is also present in these pelites and inferred to be a secondary product of biotite. Spinel and diopside occur in calcareous strata above the Magaliesberg Formation. Gneissic rocks occurring just below the Magaliesberg quartzites sometimes contain fine-grained fibrous sillimanite formed from biotite. Chloritoid occurs in metapelites of the Timeball Hill Formation near Penge. Garnet is apparently only found in the Timeball Hill and Daspoort formations. It occurs in schists, hornfelses and granulites. Amphibole occurs in granulites throughout most of the Pretoria Group. Cordierite characterises the metapelites just below the Magaliesberg quartzites and is widespread throughout the studied area. Tourmaline is common at stratigraphic levels near the Daspoort-Timeball Hill contact, but sparsely distributed throughout other stratigraphic horizons. Muscovite is a relatively minor component in the studied metapelites, but sericite common. Feldspar is restricted to Timeball Hill and Daspoort metapelites, but plagioclase and K-felspar are common in the cordierite hornfels of the Magaliesberg Formation and ubiquitous below this Formation. Finally, feldspars are also abundant in the feldspathised quartzites of Daspoort and post-Magaliesberg ages.

Schwellnus *et al.* (1962) reported evidence for regional metamorphism in their study area. These are:

1) Schistose rocks developed by shearing within the Daspoort Formation. This shearing was parallel to the strike of the strata.

2) Preservation of all phases of progressive metamorphism from andalusite hornfels to sericite schists.

3) The occurence of staurolite- and quartz schists.

4) The Daspoort conglomerate shows a schistose fabric and elongated pebbles.

5) Certain Magaliesberg-aged pelitic sediments are altered to schists.

6) Certain cordierite hornfels below the Magaliesberg quartzites were converted to cordierite gneiss containing sillimanite.

Schwellnus *et al.* (1962) inferred that medium- and high grades of metamorphism are recorded in their study area, the medium grade represented by the presence of andalusite, cordierite and/or staurolite, and the high-grade indicated by mobilised hornfels, cordierite-sillimanite gneiss and hypersthene granulite.

Schwellnus *et al.* (1962) interpreted the Hendriksplaas norite (i.e. Rustenburg Layered Suite) as the most likely cause of the thermal-component of the regional metamorphism recoded in the Olifants River area. They also interpreted the stress-component of the metamorphism to have been coeval with folding and to have post-dated the thermal metamorphism, thus overprinting it. According to Schwellnus *et al.* (1962), the thermal metamorphism could also have been caused by mafic magmatism prior to the emplacement of the Hendriksplaas norite. In such a case a) the intrusion of the Hendriksplaas norite could have caused the stresses that lead to the regional metamorphic character of the area, and b) later emplacement of mafic magma could have caused the high-grade metamorphism. Finally, Schwellnus *et al.* (1962) inferred that gneissic fabrics in their area of study could indicate that such rocks had schistose fabric prior to metamorphism, or might just be the result of high-grade metamorphism.

Human (1975) investigated the Havercroft-Streatham andalusite deposit in south-eastern Limpopo. He reported that the deposit is hosted in the upper pelitic unit of the Timeball Hill Formation and that the formation dips to the southwest at 14-17 ° in that area. A 12-15 m thick diabase sill reportedly divides the upper Timeball Hill pelitic unit from the Timeball Hill quartzite. A quartz-epidote-hornblende hornfels occurs as <1 m thick lenses

directly above this sill. Above these hornfels Human (1975) reported staurolite-biotite-muscovite hornfelses, 8-10 m in thickness when covered by garnet hornfels, but 20-22 m thick when the garnet hornfels are absent. The garnet hornfels, which is 10-12 m thick in places, is reportedly often buried under tallus or alluvium. Human (1975) reported that biotite-staurolite hornfels, 18-22 m thick, occur directly above the garnet-hornfels. Within the biotite-staurolite hornfels many <2.5 m thick lenses of andalusite-staurolite-biotite hornfels were reported. Finally, a roughly 50 m thick andalusite-hornfels apparently occurs directly above the biotite-staurolite hornfels and is mined for andalusite.

Human (1975) reported that the roughly 50 m thick andalusite hornfels zone consists of a basal zone of hard andalusite-garnet-staurolite hornfels, <1.5 m thick, which is overlain by a "giant crystal zone", which in turn is covered by a banded andalusite hornfels. The "giant crystal zone" contains andalusite porphyroblasts up to 12 cm in length, while the banded andalusite hornfels contains interbedded layers of biotite hornfels, staurolite hornfels and ziosite-garnet hornfels.

Human (1975) also investigated the petrography of the deposit. He reported that the andalusites in the "giant crystal zone" sometimes have idioblastic to subidioblastic crystals measuring up to 15×16×120 mm in dimension. Inclusions of carbonaceous matter and minor staurolite and chloritoid were reported to occur in the deposit's andalusite. Human (1975) reported that staurolite idioblasts up to 4 mm in length, as well as biotite xenoblasts up to 0.7 mm in length occur in the studied hornfelses. The hornfelses, reportedly, typically have matrices of fine-grained quartz, biotite and sericite, and also minor iron oxides.

Except for accessory minerals, the minerals present in the studied hornfelses are biotite, muscovite, quartz, chlorite, chloritoid, cordierite, staurolite, andalusite, garnet, sillimanite, fibrolite, ziosite, hornblende, minor calcite and iron-oxides (Human, 1975). These minerals reportedly show abnormal sequences of crystallisation, which Human (1975) interpreted as suggesting chemical disequilibrium and non-simultaneous crystallisation. Furthermore, Human (1975) interpreted the metamorphic minerals to have formed directly from the pre-existing quartz and muscovite, as well as minor chloritoid, biotite and chlorite.

Based on constructed PT-grids and the presence of staurolite and cordierite, Human (1975) concluded that the peak metamorphism caused by the Bushveld Complex recorded in the Havercroft pelites occurred at temperatures of 500-530 ºC, ± 10 ºC and pressures between 1-2 kbar.

Engelbrecht (1976) studied the metamorphic aureole of the Bushveld Complex in the area north-east of Zeerust, along the western limb of the Complex. He identified and described a number of metamorphic mineral assemblages that are here summarised.

1) Andalusite-muscovite-biotite assemblage: This assemblage commonly occurs in chiastolite-bearing slates of Timeball Hill and Daspoort ages. The horizons bearing this assemblage are typically characterised by chiastolite porphyroblasts occurring in a groundmass of quartz, muscovite and biotite, as well as variable amounts of ilmenite and hematite.

2) Anthophyllite-cordierite-biotite assemblage: This assemblage seems sparse and occurs within the Daspoort and Magaliesberg Formations. Anthophyllite crystals up to 5 mm in length are reported.

3) Andalusite-muscovite assemblage: Within the Daspoort Formation a bed occurs consisting mainly of andalusite and muscovite, with lesser amounts of quartz. Andalusite porphyroblasts up to 250 mm long and 12 mm thick are reported to occur in this horizon.

4) Garnet-andalusite-muscovite (-biotite) assemblage: This assemblage occurs within the Daspoort Formation. It is found in alternating layers of almandine-rich and andalusite-rich metapelite and consists of garnet, andalusite, quartz, muscovite, opaque minerals and secondary chlorite.

5) Almandine-grunerite assemblage: This assemblage was only found in the lowest metapelites of the Magaliesberg Formation. The garnets of this assemblage are intergrown with amphibole and the grunerite is light brown to colourless and has a decussate texture.

6) Cordierite-biotite (-K-feldspar, -muscovite, -andalusite, -plagioclase) assemblage: This assemblage is commonly found in the lower portion of the Silverton Formation, but also occurs within the Magaliesberg Formation. In rocks containing this assemblage cordierite increases at the expense of andalusite. The cordierite is sometimes very xenoblastic and has varying amounts of inclusions, ranging from virtually zero to large amounts thereof. The inclusions are typically quartz, muscovite and biotite.

7) Garnet-muscovite-K-feldspar-biotite assemblage: This assemblage occurs in metapelites near the base of the Magaliesberg Formation. It consists of porphyroblasts of orthoclase, almandine, muscovite, chlorite and biotite in a groundmass of quartz, biotite and lesser muscovite.

8) Hornblende (-cordierite, -biotite, -plagioclase, -K-felspar, -clinoziosite) assemblage: The hornblende of this assemblage is "apple green" to "olive green" in colour and highly pleochroic. The cummingtonite sometimes occurs as exsolution textures in the hornblende, or as rims of the hornblende. Cordierite and clinoziosite are usually only present in small amounts.

9) Hornblende-cummingtonite (-biotite) assemblage: This assemblage is found in a very fine-grained rock within the Magaliesberg Formation that reportedly resembles a tuff. A zoned amphibole was discovered consisting of hornblende in its core and with cummingtonite forming its rim. Hornblende with exsolution lamellae of amphibole was also reported.

10) Diopside (-plagioclase, -hornblende, -calcite) assemblage: This assemblage is found in a band of chert that occurs within the Ongeluk lava. The chert contains diopside with lesser calcite, hornblende and clinoziosite.

11) Diopside-scapolite-hornblende-clinoziosite assemblage: This last assemblage occurs in an impure chert layer, within the Magaliesberg Formation, sandwiched between a sill and quartzite. The scapolite occurs as large poikiloblasts and the clinoziosite is inferred to have formed from the hornblende and diopside in the rock.

Engelbrecht (1976) found that the identified mineral assemblages are characteristic of the hornblende-hornfels facies of metamorphism. He estimated that the conditions of metamorphism were between 530-630 ºC and of a pressure <2.5 kbar. The temperature estimates were based on constructed PT-grids using curves of Evans (1965), Richardson *et al.* (1969) and Winkler (1970). The pressure constraint was based on Evans (1965) and Fyfe *et al.* (1958), who defined the upper limit of the hornblende-hornfels facies as 2.5 kbar of pressure. Finally, Engelbrecht (1976) concluded that the Rustenburg Layered Suite is the only reasonable source of the thermal energy responsible for the formation of the aureole in the study area.

Hulbert and Sharpe (1981) produced pressure-temperature estimates of metamorphism for a number of sites around Burgersfort, as well as for a site near Lydenburg and for another near Belfast. They estimated 500 ° C at 5.3 kbar and 710 ºC at 5.3 kbar, respectively, for two sites east of Burgersfort, 530 ºC at 5.2 kbar for rocks located roughly 40 km north-northwest of Burgersfort and 700 ºC at 5.2 kbar for roof rocks located west of Burgersfort. For a xenolith located west-northwest of Lydenburg they estimated 1200 ºC at 4.5 kbar and for rocks located roughly 48 km north of Belfast - 600 ºC at 4.0 kbar. The pressure estimates were based on the following inferred equilibria:

1) plagioclase = garnet + sillimanite + quartz (Ghent, 1976; Schmid and Wood, 1976)

and 2) cordierite = garnet + sillimanite + quartz (Wood and Fraser, 1976).

The temperature estimates were obtained from biotite-garnet pairs, according to the method of Ferry and Spear (1978), and from cordierite-biotite pairs by utilizing their $Mg/Mg+Fe^{2+}$ values.

Hulbert and Sharpe (1981) also produced preliminary isotherms for 600- and 700 ºC. The 600 ºC isotherm is restricted to the Silverton Formation to the south of Burgersfort, and cuts across the Daspoort Formation into the Timeball Hill Formation, roughly east-northeast of Burgersfort. The 700 ºC isotherm is restricted to the Silverton pelites close to Burgersfort.

Sharpe and Fortsch (1981) calculated metamorphic temperatures of 535 ºC and 589 ºC by the methods of Raheim and Green (1974) and Wells (1979), respectively, for metamorphosed limestones at Houtenberg. These calculations were performed for an assumed pressure of 3.5 kbar as based on stratigraphic summation. The estimates were based on garnet-clinopyroxene assemblages that were interpreted to reflect the equilibrium: clinopyroxene + almandine = clinopyroxene + pyrope.

Sharpe (1982) produced a map showing the following calculated conditions for the Burgersfort area: 500 ºC and 5.2 kbar for a location west of Burgersfort and near Ohrigstad, 700 ºC and 5.3 kbar at Burgersfort, 705 ºC and 5.5 kbar for a location southwest of Burgersfort, 533 ºC and 5.2 kbar for a location north-northwest of Burgersfort, 1150 ºC and

4.5 kbar for a location west-northwest of Burgersfort, 1150 ºC and 4.5 kbar for a location southwest of Burgersfort and 575 ºC and 3.5 kbar for a location south-southwest of Burgersfort (and southwest of Lydenburg) and near Dullstroom. These temperature and pressure pairs were obtained by the same methods used by Hulbert and Sharpe (1981).

Nell (1984) gave evidence for two stages of metamorphism preserved near Potgietersrus. He determined that initial maximum temperatures of 750 ºC were reached at 1.5 kbar based on cordierite + olivine + orthopyroxene ± spinel ± quartz assemblages. The inferred second stage of metamorphism occurred at approximately 850-900 ºC and 4 to 5 kbar as was obtained via the following assemblages:

1) Garnet + cordierite + orthopyroxene + biotite.
2) Clinopyroxene + plagioclase + quartz**.**
3) Cordierite + spinel ± sillimanite ± corundum ± orthopyroxene ± olivine.

The inferred metamorphic conditions mentioned above were interpreted from various estimates of metamorphic conditions that were performed on numerous samples and calculated according to a number of methods. The methods and/or geothermobarometers used are:

a) Garnet-biotite thermometry according to the methods of Thompson (1976 b), Holdaway and Lee (1977) and Ferry and Spear (1978).

b) Garnet-cordierite thermometry, applying the methods Thompson (1976 b), Wells (1976 a) and Holdaway and Lee (1977).

c) Garnet-orthopyroxene thermometry according to the method of Powell (1978 a).

d) Two-pyroxene thermometry, applying the methods of Wood and Banno (1973), Wells (1977) and Powell (1978 a).

e) Cordierite-spinel thermometry according to the method of Vielzeuf (1983) and a method prepared by Nell himself.

f) Garnet-cordierite ion-exchange barometry according to the work of Hensen and Green (1973).

g) A geobarometer centred on the reaction: ferrosilite = fayalite + quartz, according to the work of Bohlen and Boettcher (1981) and Berg (1977 b).

h) The assemblage olivine + cordierite + orthopyroxene + spinel, utilizing the work of Hsu and Burnham (1969), Schreyer (1976), Lal and Seifert (1979), Frost (1979) and Abraham & Schreyer (1973).

i) Garnet-orthopyroxene barometry according to the method of Wood (1974).

j) The Ca-Tschermaks molecule – plagioclase – quartz barometer (applying the method of S. Reed as described by M.R. Sharpe during personal communication with Nell).

k) The assemblage cordierite + spinel + corundum + sillimanite according to the method of Wells and Richardson (1979).

l) The assemblage cordierite + spinel + quartz according to the method of Harris (1981).

Nell (1984) interpreted the first stage of metamorphism to be related to the intrusion of the lower zone of the Bushveld Complex, while attributing the second to the intrusion of the upper critical-, main- and upper zones of the Complex. He perceived that, according to the preserved regional geology, the large increase in pressure estimated for the second stage exceeds the expected increase in pressure resulting from the added overburden of the critical-, main- and upper zones. However, Nell (1984) proposed a solution to this conundrum. The excess pressure could be due to anisotropic stress active during metamorphism together with an overburden roughly 1 kbar greater than suggested by the region's geology.

Engelbrecht (1986) calculated maximum metamorphic temperatures ranging between 615 - 789 ºC and pressures of 4.2 and 4.3 kbar for granofels near Nietverdiend (western BIC). His geothermometry was based on the inferred equilibrium:

phlogopite + almandine = annite + pyrope

according to the methods of Thompson (1976), Holdaway and Lee (1977) and Ferry and Spear (1978). For the calculations based on the work of Holdaway and Lee (1977) and Ferry and Spear (1978), two sets of calculations were performed, namely one set assuming a pressure of 2 kbar and the other assuming 4 kbar. The barometry was based on the inferred reaction:

cordierite + hypersthene = garnet + quartz

and the method of Hensen and Green (1973).

Hammerbeck (1986) studied the andalusite deposits of the Bushveld Complex aureole. He found that along the south-western limb of the Bushveld Complex chiastolite is the predominant species of andalusite within the Timeball Hill Formation. This area was divided into four metamorphic zones by Blain (1974), which Hammerbeck (1986) named Zones A-D. Hammerbeck (1986) reported that no stress-component was active in the metamorphism of these rocks. He described Zone A as consisting of shale and slate which contain ubiquitous chiastolite and biotite and moderate amounts of andalusite, epidote and cordierite. Zone B was described as consisting of blue, grey and green biotite- and chiastolite-bearing slates, which are similar to those of Zone A, except that they don't contain cordierite. Hammerbeck (1986) also reported that Zone B had the largest area of outcrop of all four zones. Zone C is reportedly characterised by incipient andalusite growths, and its few chiastolite porphyroblasts are almost all pseudomorphed by quartz and sericite. Finally, Zone D is characterised by spotted shales and slates with characteristic anhedral biotite. In some cases this zone contains totally altered chiastolite porphyroblasts.

Hammerbeck (1986) described the metamorphic zones of Blain (1975), which occur along the eastern limb the Bushveld Complex, and named them Zones A-E. He described these as follows. Zone A, which occurs in the region of Malipsdrif, records regional metamorphism. This zone is bounded in the south and north-west by shear zones and consists of cordierite- and sillimanite-bearing schists, as well as schists containing relict andalusite grains that are sericitized. Zone B is restricted to north of Burgersfort and was produced by thermal metamorphism. It consists of very fine-grained dark cordierite-bearing metapelites. Zone C stretches over most of the eastern Bushveld Complex aureole and is manifested in the Silverton to Timeball Hill formations. It contains andalusite- and staurolite-bearing metapelites and assemblages containing chiastolite-muscovite-biotite, garnet-staurolite-biotite, and chiastolite-staurolite-biotite (along northernmost portions of eastern limb). Low-grade metamorphism caused by the Bushveld Complex is evident in Zone D, which is characterised by chloritoid-bearing metapelites. Zone E also represents low-grade metamorphism and consists of spotted slates between Lydenburg and Penge. These slates contain chiastolite that has been totally pseudomorphed by sericite and quartz. This zone is manifested in rocks of the Silverton, Daspoort and Timeball Hill formations.

The metamorphic rocks of the aureole along the north-western margin of the Bushveld Complex, surrounding Thabazimbi, were also described by Hammerbeck (1986). These he described as follows. The metapelites of the Silverton Formation are reported as being characterised by dark-grey and fine-grained cordierite-bearing hornfelses. Andalusite, *sensu stricto,* and chiastolite are apparently only seldom present in the rocks. The upper Timeball Hill Formation has poor exposure along this margin of the Complex, nevertheless chiastolite-bearing rock, rich in quartz, was reported to occur in these parts of the Formation. The lower unit of the Timeball Hill Formation has a larger area of outcrop in his study area and contains abundant chiastolite. These pelites are described as iron-rich with iron-stained chiastolite. Pseudomorphs of chlorite after chiastolite were also reported. East of Middelwit, Hammerbeck (1986) tells of evidence for polymetamorphism. Here muscovite-biotite-quartz schists are developed which are totally absent in the same stratigraphic units to the west. Hammerbeck (1986) reported chiastolite-rich shists north of Rooiberg. In these rocks the chiastolite crystals are orientated parallel to bedding.

Human and Collins (1986) also studied the Havercroft-Streatham andalusite deposit in south-eastern Limpopo. They largely recited the mineralogical variation with stratigraphic position, as well as the petrological observations of Human (1975), but also contributed further data on the deposit. Human and Collins (1986) reported that a zone of staurolite-andalusite-garnet hornfels with a thickness of 25-30 m occurs above the 50 m thick zone of andalusite hornfels of Human (1975). Furthermore, directly above these staurolite-andalusite-garnet hornfels occur a “Mixed Zone” of garnet-staurolite hornfels, andalusite-staurolite hornfels and biotite hornfels. The two researchers also reported that andalusite in the eastern Bushveld Complex aureole occurs from south of Lydenburg up to Malipsdrif.

Hartzer (1987) inferred estimates of the peak metamorphic conditions recorded in the argillaceous and calc-silicate rocks of the Crocodile River Fragment (western BIC). He identified two mineral assemblages, useful for thermobarometric inferences, in the argillites, namely:

muscovite, quartz, chlorite and K-feldspar

andalusite, biotite, muscovite and quartz.

He inferred that the reaction of Turner (1968) was responsible for the formation of these assemblages. This reaction is:

muscovite + quartz = K-feldspar + andalusite + $H_2O$.

The work of Evans (1965) gives evidence that this reaction occurs at pressures of 0-2.5 kbar and temperatures of 470-620 ºC. Further constraints were identified as given by the presence of biotite and chlorite. According to Winkler (1976) biotite will only start forming between 410-470 ºC, at all pressures.

Hartzer (1987) interpreted the presence of chlorite, as well as the absence of cordierite, staurolite and sillimanite, in the argillites as additional indicators of the relatively low-grade of metamorphism. According to Winkler (1976), at all pressures, cordierite and staurolite will only start forming at temperatures between 510-570 ºC. Furthermore, considering that the Fragment was probably metamorphosed below 2.5 kbar of pressure, the work of Evans (1965) suggests that sillimanite would only have formed at temperatures exceeding 650 ºC.

Hartzer (1987) inferred the following two reactions for the calc-silicates of the Crocodile River Fragment:

3 dolomite + 4 quartz + $H_2O$ = 1 talc + 3 calcite + 3 $CO_2$

5 talc + 6 calcite + 4 quartz = 3 tremolite + 6 $CO_2$+ 2 $H_2O$.

The first mentioned reaction will occur between 400-490 ºC, at a pressure of 1 kbar (Winkler, 1976), and at a maximum temperature of 520 ºC, at 2.5 kbar (Winkler, 1976). The latter reaction will occur at temperatures between 450-530 ºC at pressures of 0-2.5 kbar (Winkler, 1976), but based on the absence of diopside, Hartzer (1987) inferred a temperature range between 470-530 ºC.

Hartzer (1987) also reported on the metamorphism of the Penge Formation iron stones, and of the Hekpoort Formation volcanics, of the Crocodile River Fragment. The iron stones reportedly consist of chert, magnetite and grunerite and it was reported that according to Burt (1971) grunerite forms from carbonate minerals between 300-700 ºC. Lastly, Hartzer (1987) reported that the mineral assemblage present in the Hekpoort

volcanics is hornblende, quartz, plagioclase, biotite and muscovite, which corresponds to the hornblende-hornfels facies of metamorphism according to Turner (1968).

Miyano *et al.* (1987) gave evidence that amphibolitic sills in the Penge Iron Formation, at Penge, post-date the peak metamorphism caused by the intrusion of the Bushveld Complex. Their evidence was based on the discovery of a contact-metamorphic assemblage related to the sills and containing hornblende, clinopyroxene and fayalite, which overprints a grunerite-bearing assemblage ascribed to contact-metamorphism caused by the Bushveld Complex. They also reported that the metamorphic assemblage ascribed to Bushveld Complex contact-metamorphism in these ironstones, at Penge and Mafefe, consists of grunerite, quartz, biotite, calcite, magnetite, ankerite, K-feldspar, pyrrhotite, pyrite, chalcopyrite and sphalerite, in estimated order of abundance.

Working on calc-silicate xenoliths of the Marginal and Critical Zones of the Bushveld Complex near Steelpoort, Wallmach *et al*. (1989) gave evidence that metamorphic temperatures had exceeded 1200 ºC, and that overburden pressures of 0.6-1.6 kbar and 1.1-2.4 kbar are recorded in these xenoliths. The former pressure range they ascribed to the emplacement of the magmas of the critical zone and the latter to those of the main zone. They also emphasised the overlap of 1.1-1.6 kbar between the two pressure ranges. Their evidence was based on the following:

1) The mineral assemblages: calcite + akermanite + monticellite (with polygonal texture), calcite + forsterite + monticellite, akermanite + diopside + monticellite and diopside + forsterite + monticellite, for xenoliths of the Marginal Zone, and calcite + periclase + monticellite, merwinite + akermanite + monticellite and forsterite + periclase + monticellite (with polygonal texture), for xenoliths of the Critical Zone.
2) Forsterite exsolution in monticellite with anomalously positive optical signature.
3) Dehydroxylated Ba-rich phlogopite.

The pressure determinations were performed by the construction of a P-T diagram assuming maximum temperatures between 1200-1300 ºC.

Working adjacent to the western-most lobe, Engelbrecht (1990) gave thermobarometric evidence for peak metamorphic conditions between 646-760 ºC and 2.1-3.2 kbar. The barometric results were obtained from orthopyroxene-garnet-cordierite-

biotite-plagioclase-quartz assemblages by applying the research of Bowlen *et al.* (1983), Newton and Perkins (1982), Perkins and Chipera (1985) and Powell and Holland (1988). For the same samples they obtained pressures of 4.2-5.6 kbar by applying the barometric methods of Hensen and Green (1973) and Bhattacharya (1986) for the assemblage cordierite + hypersthene + garnet + quartz. These higher pressure results were however rejected as erroneous by Engelbrecht. Despite his thermobarometric results, Engelbrecht (1990) argued that field and petrographic evidence suggest pressures less than 2.2 kbar. His thermometric results were calculated by garnet-biotite pairs of the inferred equilibrium: almandine + phlogopite = pyrope + annite, according to the method of Ferry and Spear (1978), as well as by garnet-cordierite pairs according to the equilibrium: pyrope + Fe-cordierite = almandine + Mg-cordierite, as described by Ferry and Spear (1978), Holdaway and Lee (1977), Perchuk *et al.* (1981) and Thompson (1976).

Kaneko *et al*. (1990a) calculated pressure and temperature estimates for two stratigraphic levels of metapelites of the Pretoria Group samples near Penge. Stratigraphically these two levels occur 1.7 and 2.9 km below the Bushveld-Pretoria Group contact, respectively. Their pressure estimates were based on the equilibrium:

anorthite = grossular + andalusite + quartz

and performed according to the method of Newton and Haselton (1981), while applying the experimental dataset of Koziol and Newton (1988). The results were 2.0 and 2.3 kbar for the shallower stratigraphic level and 2.6 kbar for the deeper level. Their temperature estimates were based on the equilibria:

almandine + phlogopite = pyrope + Fe-cordierite

and almandine + Mg-cordierite = pyrope + Fe-cordierite.

The method of Hodges and Spear (1982) was utilized for the former equilibrium and produced temperatures of 560 ° and 570 ° C for the shallower stratigraphic level and 540º C for the deeper level. For the latter equilibrium, the method of Thompson (1976) was implemented, producing 570 ° and 560 ºC for the shallower stratigraphic position. This second equilibrium was not applicable to the deeper level.

Kaneko *et al*. (1990b) investigated the occurrence of fibrolite in the eastern Bushveld Complex aureole. They reported that fibrolite has an X-ray powder diffraction pattern very similar to that of sillimanite in a bulk-form. It was found that fibrolite was often formed by the replacement of biotite. They reported that andalusite most often occurs as poikiloblasts or idioblastic chiastolite and discovered that fibrolite very seldom coexists with poikiloblasts of andalusite in the chiastolite zone of Hammerbeck (1986). Based on fibrolite's restricted occurrence in the eastern Bushveld aureole, Kaneko *et al*. (1990b) concluded that fibrolite could be regarded as an index mineral, occurring at lower temperatures than sillimanite. Furthermore, they estimated that fibrolite formed between 550-650 ºC in their study area, based on its regional distribution and the work of Kaneko and Miyano (1990).

In an excursion guide he compiled, Von Gruenewaldt (1991) reported the following:

1) That the mineral assemblages of garnet-biotite schists, orthopyroxene-biotite-garnet hornfelses and forsterite-diopside marbles of the Vermont Formation in the Steelpoort Pericline suggest conditions of ~ 750 ºC and ~ 4.5 kbar.

2) Sillimanite hornfelses of the Silverton formation at Witgatboom (Burgersfort area) were partially melted and metamorphosed by the Apiesdoorndraai peridotite sill at peak-temperatures of 750-800 ºC.

3) Metamorphic conditions reflected by the andalusite/sillimanite isograd at Dresden, near Burgersfort, were estimated with the application of metamorphic grids to be ~ 650 ºC and ~ 4.5 kbar.

4) Calc-silicate xenoliths found in the Marginal Zone of the BIC, near Burgersfort, were interpreted to have recorded the reaction: akermanite + forsterite + calcite = monticellite + $CO_2$. Assuming peak metamorphic temperatures of 1200-1300 ºC, this reaction would have occurred at 2.5-3.5 kbar.

5) Garnet-biotite thermometry indicates that metapelites of the Timeball Hill Formation north of Havercroft were metamorphosed at temperatures of 520-540 ºC. The reaction of Ghent (1976): $3CaAl_2Si_2O_8 = Ca_3Al_2Si_3O_{12} + 2Al_2SiO_5 + SiO_2$, indicate that these metapelites were metamorphosed at ~ 5 kbar.

In his model for metamorphism Hartzer (1994) concluded that metamorphic temperatures for the Transvaal inliers, namely the Crocodile River Dome and Rooiberg

Fragment (western BIC) as well as the Dennilton Dome, Marble Hall Dome and Stavoren Fragment (eastern BIC), reached temperatures up to 800 ºC, based on index minerals and mineral assemblages.

In his study Hartzer (1994) also reported on the metamorphic-facies, and their distribution, in the Transvaal Supergroup inliers of the Bushveld Complex. These facies are the albite-epidote-hornfels facies, the hornblende-hornfels facies and the pyroxene-hornfels facies. Hartzer (1994) reported that the albite-epidote-hornfels facies is developed in pelitic rocks of the southern and central parts of the Marble Hall Dome (according to De Waal (1963)) and also in certain central areas of the Crocodile River Fragment and the Dennilton Dome.

Hartzer (1994) stated that the hornblende-hornfels facies is manifested in the rocks in the eastern portion of the Marble Hall Dome, in most of the Crocodile River fragment rocks, as well as in rocks of the Dennilton Dome that occur close to the contact with the BIC. He also reported the minerals associated with this facies in the inliers. In the pelitic rocks they are quartz, muscovite, cordierite, plagioclase, biotite, andalusite and garnet, in the carbonate rocks - diopside, hornblende, grossularite, tremolite, plagioclase and prehnite and in the volcanic rocks - hornblende and plagioclase.

Hartzer (1994) reported that the rocks in which the pyroxene-hornfels facies is developed are those in the northern and western portions of the Marble Hall Dome, as well as those in very close proximity to the contact with the BIC in the Dennilton Dome. He reported that the minerals cordierite, chiastolite, sillimanite, orthoclase, quartz, biotite, hypersthene and andalusite are typical of this facies in the pelites of these inliers, but that sillimanite only occurs in metapelites just next to the Bushveld granite-Marble Hall dome contact. In the volcanic rocks of these domes the minerals associated with this facies were reported as plagioclase, biotite, hypersthene, augite and hornblende.

Wallmach et al. (1995) gave evidence that peak metamorphism of two calc-silicate xenoliths sampled from the Upper Zone of the BIC, had undergone peak metamorphism at temperatures of 1100-1200 ºC and pressures below 1.5 kbar. The xenoliths occur close to Roossenekal and roughly 30 km east-southeast of Steelpoort, respectively. Their evidence was based on the following:

1) The reactions:

calcite + diopside = akermanite + $CO_2$

and calcite + forsterite + akermanite = monticellite + $CO_2$.

2) Experimental research by Otto and Wyllie (1993), which suggests that monticellite and akermanite will be in equilibrium with the melt phase at temperatures exceeding 1100 ºC.

3) The lack of complete melting, which they suggested to probably reflect temperatures below 1200 ºC and a maximum pressure of 1.5 kbar.

4) The likelihood that the Upper Zone xenoliths had reached similar peak temperatures than those of the Critical and Marginal Zones.

In his study of the northern portion of the eastern Bushveld aureole, Uken (1998) performed garnet-biotite and garnet-cordierite thermometry, as well as garnet-staurolite barometry on Timeball Hill metapelites. The garnet-biotite geothermometry was based on the inferred reaction:

Fe-garnet + Mg-biotite = Mg-garnet + Fe-biotite,

and performed according to the methods of Thompson (1976), Holdaway and Lee (1977) and Ferry and Spear (1978). The results are shown in Table 1.

| **SAMPLE** | **AQ/X** | **HWU** | **M/1** | **OB5** | **16/7.** |
|---|---|---|---|---|---|
| | | | | | |
| **Thompson (1976)** | | | | | |
| **T (core) (ºC)** | 527 | 546 | 476 | 514 | 549 |
| **T (rim) (ºC)** | 523 | 538 | 501 | 544 | 556 |
| | | | | | |
| **Holdaway and Lee (1977)** | | | | | |
| **2 kbar** | | | | | |
| **T (core) (ºC)** | 539 | 557 | 493 | 528 | 528 |
| **T (rim) (ºC)** | 537 | 548 | 515 | 554 | 554 |
| **3 kbar** | | | | | |
| **T (core) (ºC)** | 548 | 560 | 496 | 531 | 531 |
| **T (rim) (ºC)** | 540 | 552 | 518 | 552 | 557 |
| **4 kbar** | | | | | |
| **T (core) (ºC)** | 546 | 563 | 499 | 534 | 534 |
| **T (rim) (ºC)** | 543 | 555 | 522 | 561 | 561 |
| | | | | | |
| **Ferry and Spear (1978)** | | | | | |
| **2 kbar** | | | | | |
| **T (core) (ºC)** | 524 | 549 | 460 | 507 | 552 |

| | | | | | |
|---|---|---|---|---|---|
| **T (rim) (ºC)** | 519 | 537 | 490 | 545 | 562 |
| **3 kbar** | | | | | |
| **T (core) (ºC)** | 528 | 553 | 462 | 511 | 556 |
| **T (rim) (ºC)** | 522 | 541 | 494 | 549 | 566 |
| **4 kbar** | | | | | |
| **T (core) ºC** | 531 | 556 | 466 | 515 | 560 |
| **T (rim) (ºC)** | 526 | 545 | 497 | 553 | 570 |

**Table 1.** Results of the biotite-garnet thermometry of Uken (1998).
Table modified after Table 6.4 (Uken, 1998).

The garnet-cordierite geothermometry of Uken (1998) was based on the inferred reaction:

Fe-cordierite + pyrope = Mg-cordierite + almandine.

It was conducted according to the methods of Thompson (1976), Wells (1976), Holdaway and Lee (1977) and Wells (1979). The results are shown in Table 2.

| **SAMPLE** | **HWU** | **16/7.** | **19/12.** |
|---|---|---|---|
| | | | |
| **Thompson (1976)** | | | |
| **T (core) (ºC)** | 548 | 545 | 488 |
| **T (rim) (ºC)** | 531 | 545 | 525 |
| | | | |
| **Wells (1976)** | | | |
| **2 kbar** | | | |
| **T (core) (ºC)** | 619 | 615 | 560 |
| **T (rim) (ºC)** | 602 | 615 | 596 |
| **3 kbar** | | | |
| **T (core) (ºC)** | 615 | 611 | 556 |
| **T (rim) (ºC)** | 598 | 611 | 595 |
| **4 kbar** | | | |
| **T (core) (ºC)** | 611 | 607 | 553 |
| **T (rim) (ºC)** | 594 | 607 | 589 |
| | | | |
| **Holdaway and Lee (1977)** | | | |
| **2 kbar** | | | |
| **T (core) (ºC)** | 555 | 552 | 501 |
| **T (rim) (ºC)** | 539 | 552 | 534 |
| **3 kbar** | | | |
| **T (core) (ºC)** | 559 | 556 | 504 |
| **T (rim) (ºC)** | 543 | 556 | 538 |
| **4 kbar** | | | |
| **T (core) (ºC)** | 563 | 560 | 508 |
| **T (rim) (ºC)** | 547 | 560 | 542 |
| | | | |
| **Wells (1979)** | | | |

| | | | |
|---|---|---|---|
| **2 kbar** | | | |
| **T (core) (ºC)** | 554 | 550 | 493 |
| **T (rim) (ºC)** | 536 | 540 | 530 |
| **3 kbar** | | | |
| **T (core) (ºC)** | 549 | 545 | 488 |
| **T (rim) (ºC)** | 531 | 545 | 526 |
| **4 kbar** | | | |
| **T (core) (ºC)** | 545 | 541 | 484 |
| **T (rim) (ºC)** | 527 | 541 | 521 |

**Table 2.** Temperature results of the garnet-cordierite thermometry of Uken (1998). Table modified after Table 6.5 (Uken, 1998).

The garnet-staurolite geobarometry conducted by Uken (1998) was based on the following equilibria:

Fe-garnet + Mg-staurolite = Mg-garnet + Fe-staurolite

and staurolite + quartz + muscovite = biotite + garnet + $Al_2SiO_5$ + $H_2O$.

The method of Perchuk (1977) was applied and the results are shown in Table 3.

| **SAMPLE** | **AQ/X** | **HWU** | **M/1** | **OB5** |
|---|---|---|---|---|
| | | | | |
| **Perchuk (1977)** | | | | |
| **T (core) (kbar)** | 3.2 | 4.1 | 4.3 | 3.3 |
| **T (rim) (kbar)** | 3.2 | 3.8 | 4.8 | 4.2 |

**Table 3.** Pressure results of the staurolite-garnet baromometry of Uken (1998). Table modified after Table 6.6 (Uken, 1998).

Uken (1998) also inferred peak-metamorphic conditions, for the andalusite zone of the Timeball Hill Formation in his study area, with the use of petrogenetic grids in the KFMASH system. A petrogenetic grid constructed by Dymoke and Sandiford (1992) with the dataset of Holland and Powell (1990) produced useful results. This grid was constructed for $\alpha(H_2O) \approx 1$ and biotite, quartz and muscovite in excess. Uken (1998) identified the assemblage cordierite + staurolite + biotite + muscovite + quartz in the andalusite zone, which represented a field lying between 535-563 ºC and 2.8-3.2 kbar in Dymoke and Sandiford (1992)'s grid.

Having applied two-pyroxene geothermometry on metapelites of the Vermont Formation, Mizuno and Miyano (1999) concluded that peak-metamorphic temperatures between 700-780 ºC had been attained. Their samples were collected just southeast of Steelpoort (sample 1402C) and just northwest of Burgersfort (sample 1413B), respectively.

The methods they applied were those of Kretz (1982), Lindsley (1983), Wells (1977) and Wood and Banno (1973). For their calculations a pressure of 1.8 kbar was assumed, however a pressure of 5 kbar was assumed for those performed by the method of Lindsley (1983). The method of Kretz (1982) comprises two equations- one for the gradient of the clinopyroxene limb of the Ca-Fe-Mg pyroxene slope and the other based on the dependence of the Fe- Mg distribution coefficient on temperature. The results obtained from these two equations are shown below in Table 4.

| **Results from the equation based on the gradient of the clinopyroxene limb of the Ca-Fe-Mg pyroxene slope of Kretz (1982):** | |
|---|---|
| **Sample 1413B** | **Sample 1402C** |
| 753 | 783 |
| 760 | 779 |
| 760 | 761 |
| 699 | |
| 722 | |
| 783 | |
| **Results from the equation based on the temperature dependence of the Fe- Mg distribution coefficient of Kretz (1982):** | |
| **Sample 1413B** | **Sample 1402C** |
| 757 | 739 |
| 782 | 776 |
| 774 | 733 |
| 719 | |
| 783 | |
| 806 | |

**Table 4.** Temperature results from the two equations of Kretz (1982).

The method of Lindsley (1983) yielded the results shown below in Table 5.

| **Results from the method of Lindsley (1983):** | |
|---|---|
| **Sample 1413B** | **Sample 1402C** |
| 750 | 680 |
| 740 | 700 |
| 740 | 600 |
| 720 | |
| 800 | |

**Table 5.** Temperature results from the method of Lindsley (1983).

Mizuno and Miyano (1999) interpreted the results obtained from the methods of Wells (1983) and Wood and Banno (1973) as inaccurate. The temperatures obtained from these two methods are shown below in Table 6.

| Results from the method of Wells (1983) | | | Results from the method of Wood and Banno (1973) | |
|---|---|---|---|---|
| **Sample 1413B** | **Sample 1402C** | | **Sample 1413B** | **Sample 1402C** |
| 878 | 900 | | 875 | 864 |
| 882 | 899 | | 876 | 861 |
| 879 | 879 | | 873 | 849 |
| 845 | | | 851 | |
| 859 | | | 864 | |
| 891 | | | 887 | |

**Table 6.** Temperature results from the methods of Wells (1983) and Wood and Banno (1973).

Mizuno *et al*. (1999) described the petrography of partially melted orthopyroxene-bearing metapelites sampled close to Steelpoort. The sampled orthopyroxene-hornfels occur in the Vermont Formation less than 1.5 km from the contact with the BIC. These rocks were found to occur close to the 700 ºC isotherm of Sharpe and Chadwich (1982) and to plot within the cordierite/sillimanite hornfels zone of Hammerbeck (1986). They reported that the hornfels sample, 1401B, contains poikiloblasts of orthopyroxene up to 5 mm in diameter that are often rimmed by K-feldspar. This was interpreted to signify biotite having reacted to orthopyroxene and K-feldspar. They also reported on the mineralogy of the leucocratic samples 1305B, 1306A and 1306B. Sample 1305B contains biotite, K-feldspar, quartz, plagioclase, Fe-Ti oxides and/or cordierite, as well as hornblende of lesser proportions. The core and outer shell of sample 1306A can be mineralogically differentiated- the core consisting mainly of K-feldspar, quartz, plagioclase and biotite, and the outer shell mainly of K-feldspar, biotite, orthopyroxene and cordierite. Sample 1306B was collected from the same location as 1306A and contains orthopyroxene, biotite, plagioclase and minor K-feldspar. Mizuno *et al*. (1999) also analysed their samples' chemistries. Based on the Mg-contents of the orthopyroxene-biotite assemblages, they concluded that melting had occurred under conditions of high water activity.

Further research on xenoliths of the BIC was performed by Buick *et al*. (2000). They gave evidence that xenoliths from the Rustenburg Layered Suite were metasomatised after peak-metamorphism, at 2059 ± 1.1 Ma, by 600-700 ºC retrograde fluids. They inferred that these fluids were in near-equilibrium with the mafic rocks of the Rustenburg Layered Suite, with regards to oxygen-isotopic compositions. It was also found that with increasing metamorphic grade: a) marbles within the aureole show roughly 5-10 ‰

lowering in oxygen-isotope concentrations, and b) mineral assemblages were chemically buffered to higher concentrations of carbon dioxide (with the exception of the highest metamorphic grades). They interpreted their findings to generally suggest variable fluid flow produced by devolitilisation of metapelites sufficiently close to the Rustenburg Layered Suite. Finally, they also inferred the pre-existence of a fluid with limited occurrence, low $^{18}O$ values and compositions in equilibrium with the Rustenburg Layered Suite, which occurred in fault-zones within the aureole.

Kaneko *et al*. (2000) investigated the microstructures and mineral-chemistry of silicates of Timeball Hill metapelites, with a focus on pseudomorphs and ghost structures. Their study area covered most of the portion of the eastern Bushveld aureole that occurs somewhat north of Burgersfort. They found that the metapelites that contain pseudomorphs and ghost structures typically contain the following mineral assemblages:

biotite + andalusite + staurolite + muscovite + quartz

± chlorite ± garnet ± plagioclase.

It was discovered that pseudomorphs and ghost structures in andalusite and staurolite are restricted to the Timeball Hill Formation in their study area. It was also reported that in the hornfelses containing poikiloblastic andalusite, or poikiloblastic staurolite, the ghost structures are restricted to the poikiloblasts.

In the samples that Kaneko *et al*. (2000) studied, various forms of andalusite are present, e.g. xenoblasts, idioblasts and subidioblasts. They reported that poikiloblastic andalusites were found to contain inclusions of quartz, muscovite, biotite, garnet, staurolite, chlorite and opaque minerals. Staurolite was found to occur in poikiloblastic to idioblastic forms and the minerals included in poikiloblastic staurolite was reported as mainly quartz and ilmenite, with minor plagioclase, biotite and garnet. Biotite was reported to occur in xenoblastic to subidioblastic forms and to contain inclusions of quartz, muscovite, plagioclase, ilmenite and zircon. In some of the samples garnet and chorite were identified. Garnet occurs in idioblastic to subidioblastic forms and was found to mainly overgrow biotite, staurolite and chlorite. For chlorite they reported idioblastic to subidioblastic forms, and that it overgrows biotite, though only seldom. Lastly, muscovite was found to occur as a) acicular or tabular grains in many hornfelses' matrixes, b) tabular poikiloblasts that cover biotite, and c) lath-shapes in some ghost structures and matrixes.

Studying the mineral chemistries of the silicates in their samples, Kaneko *et al*. (2000) found andalusite to have uniform compositions, with no compositional variation between portions of poikiloblasts that are inclusion-rich and portions that are inclusion-poor (which contain ghost structures). They reported that biotite shows no compositional zoning, nor any difference in composition between biotites in matrix, ghost structures or pseudomorphs. Similar to biotite, chlorite was found to display no compositional zoning. Garnet did display compositional zoning, with cores enriched in Fe and Mn, and rims enriched in Mg and Ca.

Kaneko *et al*. (2000) concluded that the pseudomorphs and ghost structures in their samples had formed simultaneously with andalusite and stuarolite poikiloblasts, and at the expense of Al-bearing minerals. They also concluded that biotite was the most likely precursor to the pseudomorphs and ghost structures in the metapelites that they studied.

Pitra and De Waal (2001) gave evidence of two-stage metamorphism being preserved in metapelites of the Marble Hall Fragment. The first stage reflects conditions of 550-600 ºC at 0.15-0.25 GPa. This was determined by the construction of average P-T diagrams and P-T pseudosections in THERMOCALC in the KFMASH + $H_2O$ system for the inferred assemblages andalusite + cordierite + biotite + quartz ± garnet. The second stage, which they interpreted as reflecting peak-conditions >720 ºC at similar pressure, was determined by P-T and T-X pseudosections constructed in THERMOCALC from inferred garnet + cordierite + biotite + K-feldspar + quartz and sillimanite + cordierite + K-feldspar + quartz assemblages as well as quartz under-saturated cordierite-spinel symplectites. The T-X pseudosections were constructed for 0.20 GPa.

Waters and Lovegrove (2002) reported that metapelites of the inner aureole located near Burgersfort were metamorphosed at ~3 kbar, as indicated by the following inferred reactions:

And = Sill

Ms + Qtz = Ksp + And/Sill + $H_2O$

Ms + Bt + Qtz = Crd + Ksp + $H_2O$

Bt + And/Sill + Qtz = Crd + Ksp + $H_2O$,

which give a pressure of 3.0 ± 0.5 kbar. They also reported that metamorphic temperatures >700 ºC are recorded near the contact close to Penge.

Harris *et al*. (2003) gave evidence that metapelites collected around the eastern limb of the BIC were partially melted >700 ºC. This was based on a PT-pseudosection which included the $H_2O$ saturated pelite solidus of Le Breton and Thompson (1988), the muscovite dehydration reaction of Patiňo Douce and Harris (1998), the biotite-sillimanite-plagioclase-quartz dehydration solidus of Le Breton and Thompson (1988) and isopleths of Holtz and Johannes (1991) for approximate melt fractions.

Johnson *et al*. (2003) calculated temperatures of 750 º ± 100 ºC, 600-650 ºC and 650-800 ºC for garnet-bearing granofels, lower-grade metatexites and granofels together with diatexites, respectively, for areas around Steelpoort and Burgersfort. The temperature results for the garnet granofels were obtained by the application of garnet-cordierite Fe-Mg thermometry for which the dataset of Holland and Powell (1998) was used. The results for the lower-grade metatexites and the granofels and diatexites were inferred from the concentrations of Na in cordierite crystals. Johnson *et al*. (2003) advocated peak metamorphic temperatures of ~680-690 ºC for lower grade migmatites and of ~720 ºC for higher grade migmatites from their study area. These judgments were based on their conductive heating model and T-X pseudosections at 3kbar in the NCKFMASH system using THERMOCALC. Furthermore, they also determined pressures of 3.5 ± 1.5 kbar for the rocks they studied. To this ends they used the dataset of Holland and Powell (1998) and the program AX (to determine activities of end-members).

Buick *et al*. (2004) performed an experimental study on a medium- and a high-grade hornfels sample of the Bushveld Complex aureole, respectively. The high-grade sample that was used was collected close to Burgersfort and the medium-grade sample - somewhat north-west of Lydenburg. It was found that the lower grade sample, containing roughly 4.4 weight% $H_2O$, achieved about 50-65 % partial melting at temperatures ≥750 ºC. The higher grade sample, containing roughly 1.2 weight% $H_2O$, only showed such high levels of partial melting at 1000 ºC. Both experiments were performed at 3 kbar of pressure. They interpreted the results to imply that highly restitic metapelites, as do occur in the aureole, can be explained by sufficiently rapid heating of relatively highly-hydrated pelites.

After having constructed pseudosections in the MnNCKFMASHT system Johnson *et al*. (2004) concluded that peak metamorphic conditions >720 ºC and around 3 kbar, as well as retrograde diapiric rise which had passed through conditions of 1.5-2 kbar at temperatures >700 ºC, is recorded in the Phepane dome rocks north of Burgersfort.

Kaneko *et al*. (2005) calculated metamorphic conditions for a number of rocks around the Burgersfort area. They calculated pressures by applying the garnet-aluminosilicate-plagioclase-quartz (GASP) barometer, modified to be applied on rocks metamorphosed in the stability field of andalusite according to the method of Kaneko and Miyano (1990). For samples for which the GASP barometer was not applicable they inferred pressures from calculated pressure values at other stratigraphic levels, by pressure conversions from stratigraphic corrections using the average Pretoria Group density data (2.75 g/cm$^3$) of Molyneux and Klinkert (1978). Their resulting pressure estimates at the contact between the Bushveld Complex and its floor rocks were 0.146 and 0.166 GPa in the Burgersfort and Penge areas, respectively. They also applied the petrogenetic grids of Pattison *et al*. (2002) which they reported as applicable to the metapelites of the Silverton Formation and obtained rough pressure estimates of 0.15-0.25 and 0.22-0.31 GPa for the Lydenburg Shale and Boven Shale Members, of the Silverton Formation, respectively. Applying orthopyroxene-cordierite (Sakai and Kawasaki, 1997) and orthopyroxene-biotite (Mizuno, 2000) thermometry they calculated temperature estimates of 750-805 ºC and 755-820 ºC, respectively, for a sample collected < 10 km roughly northeast of Burgersfort containing the paragenesis bt + crd + opx + kfs + plg + qtz, assuming a pressure of 0.15 GPa. By garnet-cordierite thermometry (Kaneko and Miyano, 2004) they obtained temperature estimates of 740-790 ºC for a sample collected <20 km southwest of Burgersfort. Samples from three different locations <10 km from Penge produced temperature estimates of 550-595 ºC by garnet-biotite thermometry (Kaneko and Miyano 2004). Applying this same thermometer and method they also calculated estimates of 635-665 ºC for a sample collected <20 km southwest of Penge and of 450-475 ºC for a sample collected <5 km north of Penge. Both temperature and pressure estimates could be calculated for samples collected from two locations- one roughly 5 km west of Penge and the other roughly 10 km southwest of Penge. Conditions of 570 ± 20 ºC and 0.24 ± 0.04

GPa, for the former location and of 600 ± 30 ºC and 0.21 ± 0.03 GPa for the latter were obtained.

In summary, when the literature is consulted concerning the pressures that prevailed during the formation of the Eastern Bushveld Complex aureole, widely divergent results are encountered. Ignoring xenoliths, these results range from 1.5 kbar (Kaneko *et al*., 2005) to 5.5 kbar (Sharpe, 1982). There is also a trend with regards to how long ago the studies were performed. The studies performed before 1992 tend to have produced pressure estimates in the region 5 kbar (Von Gruenewaldt, 1991, Sharpe, 1982 and Hulbert and Sharpe, 1981), while the majority of research conducted after these tended to produced more conservative pressure estimates, typically in the region of 3 kbar (Uken, 1998, Waters and Lovegrove, 2002, Johnson *et al*., 2003, Johnson *et al*., 2004, Kaneko *et al*., 2005). Finally, it is noteworthy that the work of Kaneko *et al*. (2005) provides evidence that the pressures of peak metamorphism increase with distance from the contact of the aureole with the Rustenburg Layered Suite (i.e. with stratigraphic depth). The studies that produced pressure- and/or temperature data are tabulated in Table 7 and their results largely illustrated in Fig. 3. Furthermore, the geographic distribution of pressure- and temperature estimates, together with simplified geology and metamorphic facies in the study area, are shown in Fig. 4.

| PRESSURE (kbar) | TEMPERATURE (ºC) | METHOD | AUTHOR | LOCATION |
|---|---|---|---|---|
| 2.1-4.2* | 700-750# | Inferred from presence of akermanite, monticellite and wollastonite | Willemse (1959) | Steelpoort area |
| 1.0-2.0 | 500-530, ± 10 | PT-grids | Human (1975) | Havercroft-Streatham andalusite deposit (near Penge) |
| <2.5 | 530-630 | PT-grids | Engelbrecht (1976) | North-east of Zeerust |
| A) 5.3, B) 5.3, C) 5.2, D) 5.2, E) 4.5 and F) 4.0 | A) 500, B) 710, C) 530, D) 700, E) 1200# and F) 600 | The pressure estimates were based on the equilibria: 1) plagioclase = garnet + sillimanite + quartz (Ghent, 1976 and Schmid and Wood, 1976) and 2) cordierite = garnet + sillimanite + quartz (Wood and Fraser, 1976). The temperature estimates were obtained from biotite-garnet pairs and cordierite-biotite pairs. | Hulbert and Sharpe (1981) | Study area covered most of the Eastern Bushveld Complex aureole. A) somewhat east of Burgersfort: S 24.69° E 30.49°, B) somewhat east of Burgersfort: S 24.65° E 30.41°, C) roughly 40 km north-northwest of Burgersfort: S 24.34° E 30.20°, D) roof rocks west of Burgersfort: S 24.77° E 30.10°, E) west-northwest of Lydenburg: S 24.98° E 30.13° and F) roughly 48 km north of Belfast: S 25.26° E 30.09° |
| 3.5* | 535 and 589 respectively | Garnet-clinopyroxene thermometry | Sharpe and Fortsch (1981) | On farms Klipbankspruit and Houtenbek near Belfast |
| A) 5.2, B) 5.3, C) 5.5, D) 5.2, E) 4.5#, F) 4.5# and G) 3.5 | A) 500, B) 700, C) 705, D) 533, E) 1150#, F) 1150# and G) 575 | Same methods as those employed by Hulbert and Sharpe (1981) | Sharpe (1982) | Large area surrounding Burgersfort. A) west of Burgersfort B) at Burgersfort C) south-west of Burgersfort D) north-northwest of Burgersfort E) west-northwest of Burgersfort F) south-west of Burgersfort and G) south-west of Lydenburg near Dullstroom |
| 1.5 (first stage) and 4-5 (second stage) | ~750 (first stage) and 850-900 (second stage) | Garnet-biotite thermometry, garnet-cordierite thermometry, garnet-orthopyroxene thermometry, two-pyroxene thermometry, cordierite-spinel thermometry, garnet-cordierite ion-exchange barometry, a geobarometer centred on the reaction: ferrosilite = | Nell (1984) | North of Potgietersrus |

| | | | | |
|---|---|---|---|---|
| | | fayalite + quartz, according to the work of Bohlen and Boettcher (1981) and Berg (1977 b), the assemblage olivine + cordierite + orthopyroxene + spinel, utilizing the work of Hsu and Burnham (1969), Schreyer (1976), Lal and Seifert (1979), Frost (1979) and Abraham & Schreyer (1973), garnet-orthopyroxene barometry, Ca-Tschermaks molecule – plagioclase – quartz barometry, the assemblage cordierite + spinel + corundum + sillimanite according to the method of Wells and Richardson (1979) and the assemblage cordierite + spinel + quartz according to the method of Harris (1981). | | |
| A) 4.2, B) 4.4 and C) 4.6 | A) 720, B) 740 and C) 680 | - | Nell (1985) | North of Potgietersrus: A) S 24.08° E 28.97°, B)S 24.10° E 28.98° and C) S 24.12° E 28.98° |
| 4.2-4.3 | 615-789 | The geothermometry was based on the equilibrium: phlogopite + almandine = annite + pyrope according to the methods of Thompson (1976), Holdaway and Lee (1977) and Ferry and Spear (1978). The barometry was based on the equilibrium cordierite + hypersthene = garnet + quartz according to the method of Hensen and Green (1973). | Engelbrecht (1986) | Near Nietverdiend (adjacent to western-most limb of BIC) |
| <2.5 assumed for metapelite temperature estimate | >650 and 470-530, respectively, for metapelites and calc-silicates of the Crocodile River Fragment | Temperature estimates of metapelites were based on the assemblages 1) muscovite, quartz, chlorite and K-feldspar and 2) andalusite, biotite, muscovite and quartz and based on the work of Evans (1965) and Winkler (1976), while temperature estimates for calc-silicates were based on the reactions 1) 3 dolomite + 4 quartz + $H_2O$ = 1 talc + 3 calcite + 3 | Hartzer (1987) | Crocodile River Fragment (western BIC) |

| | | | | |
|---|---|---|---|---|
| | | $CO_2$ and 2) 5 talc + 6 calcite + 4 quartz = 3 tremolite + 6 $CO_2$+ 2 $H_2O$ as based on the work of Winkler (1976). | | |
| 0.6-1.6 # and 1.1-2.4 # | >1200 # | Based on the assemblages: calcite + akermanite + monticellite, calcite + forsterite + monticellite, akermanite + diopside + monticellite and diopside + forsterite + monticellite and calcite + periclase + monticellite, merwinite + akermanite + monticellite and forsterite + periclase + monticellite, as well as forsterite exsolution in monticellite and dehydroxylated Ba-rich phlogopite. | Wallmach *et al.* (1989) | Near Steelpoort |
| 2.1-3.2 | 646-760 | The barometric results were obtained from orthopyroxene-garnet-cordierite-biotite-plagioclase-quartz assemblages by applying the research of Bowlen *et al.* (1983), Newton and Perkins (1982), Perkins and Chipera (1985) and Powell and Holland (1988). The temperatures were based on garnet-biotite and garnet-cordierite pairs. | Engelbrecht (1990) | Near Nietverdiend (adjacent to the western-most lobe) |
| 2.0 and 2.3 (for the shallower stratigraphic level) and 2.6 kbar (for the deeper level) | 560-570 (for the shallower stratigraphic level) and 540 (for the deeper level) | The pressure estimates were based on the equilibrium: anorthite = grossular + andalusite + quartz according to the method of Newton and Haselton (1981), while the temperature estimates were based on garnet-cordierite Fe-Mg exchange thermometry (not applicable to the deeper level) and the equilibria almandine + phlogopite = pyrope + Fe-cordierite according to the method of Hodges and Spear (1982). | Kaneko *et al.* (1990a) | Near Penge |
| - | 550-650 (for the formation of fibrolite | Based on fibrolite's regional distribution and the work of Kaneko and Miyano | Kaneko *et al.* (1990b) | Eastern Bushveld Complex aureole. |

| | | | | |
|---|---|---|---|---|
| | in the Bushveld Complex aureole) | (1990). | | |
| 1) ~4.5, 2) -, 3) ~4.5, 4) 2.5-3.5#, and 5) ~5 | 1) ~750, 2) 750-800, 3) ~650, 4) 1200-1300*#, and 5) 520-540 | 1) Based on mineral assemblages of garnet-biotite schists, orthopyroxene-biotite-garnet hornfelses and forsterite-diopside marbles, 2) -, 3) metamorphic grids, 4) based on the reaction: akermanite + forsterite + calcite = monticellite + $CO_2$, and 5) Garnet-biotite thermometry and the reaction of Ghent (1976): $3CaAl_2Si_2O_8 = Ca_3Al_2Si_3O_{12} + 2Al_2SiO_5 + SiO_2$. | Von Gruenewaldt (1991) | 1) Steelpoort Pericline, 2) Witgatboom, 3) at Dresden, near Burgersfort, 4) near Burgersfort and 5) north of Havercroft Mine |
| - | ≤800 | Based on index minerals and mineral assemblages. | Hartzer (1994) | Crocodile River Dome, Rooiberg Fragment, Dennilton Dome, Marble Hall Dome and Stavoren Fragment (eastern BIC) |
| <1.5 # | 1100-1200 # | Based on the reactions: 1) calcite + diopside = akermanite + $CO_2$ and 2) calcite + forsterite + akermanite = monticellite + $CO_2$, experimental research by Otto and Wyllie (1993), lack of complete melting and the likelihood that the Upper Zone xenoliths had reached similar peak temperatures than those of the Critical and Marginal Zones. | Wallmach et al. (1995) | Close to Roossenekal and north-west of Steelpoort, respectively |
| 2.8-3.2 (based on PT-grid) and 3.2-4.8 (based on staurolite-garnet barometry) | 535-563 (based on PT-grid) and 460-619 (based on biotite-garnet and garnet-cordierite thermometry) | Temperatures based on garnet-biotite and garnet-cordierite Fe-Mg exchange thermometry. Pressure estimates were produced by garnet-staurolite barometry based on the reactions: 1) Fe-garnet + Mg-staurolite = Mg-garnet + Fe-staurolite and 2) staurolite + quartz + muscovite = biotite + garnet + $Al2SiO_5$ + $H_2O$ and also with utilization of the petrogenetic grid of Dymoke and Sandiford (1992). | Uken (1998) | Northern portion of the eastern Bushveld aureole. The study area lies between 24°08' - 24°30' south and 29°30' - 29°08' east and |
| 1.8* (though a pressure of 5 | 700-780 | Two-pyroxene geothermometry according to the methods of Kretz (1982), | Mizuno and Miyano (1999) | Just south-east of Steelpoort and just northwest of Burgersfort |

| | | | | |
|---|---|---|---|---|
| kbar was assumed for the thermometry done according to Lindsley (1983)) | | Lindsley (1983), Wells (1977) and Wood and Banno (1973). | | |
| 1.5-2.5 (first and second stage) | 550-600 (first stage) and >720 (second stage) | P-T diagrams, P-T pseudosections in the KFMASH + $H_2O$ system using THERMOCALC and T-X pseudosections using THERMOCALC. | Pitra and De Waal (2001) | Marble Hall Fragment |
| 3.0 ± 0.5 | - | Pressure estimate based on the reactions: 1) And = Sill, 2) Mu + Q = Ksp + And/Sill + $H_2O$, 3) Mu + Bi + Q = Cd + Ksp + $H_2O$ and 4) Bi + And/Sill + Q = Cd + Ksp + $H_2O$ | Waters and Lovegrove (2002) | West of Penge: M32) S 24.31° E 30.20°, M33) S 24.36° E 30.25° and DLB-9) S 24.37° E 30.26° |
| - | >700 | Based on a PT-pseudosection which included the $H_2O$ saturated pelite solidus of Le Breton and Thompson (1988), the muscovite dehydration reaction of Patiňo Douce and Harris (1998), the biotite-sillimanite-plagioclase-quartz dehydration solidus of Le Breton and Thompson (1988) and isopleths of Holtz and Johannes (1991) for approximate melt fractions. | Harris *et al.* (2003) | Eastern Bushveld Complex aureole (samples scattered from close to Lydenburg up to northern limits of Eastern Bushveld Complex aureole). S24º21•044' E30º06•137'; S24º13•818' E30º49•507'; S24º00•043' E30º13•731'; S24º55•905' E30º19•762'; S24º58•627' E30º22•881'; S24º42•385' E30º20•893'; S24º38•762' E30º22•475'; S24º37•223' E30º20•990'; S24º38•518' E30º19•424'; S24º20•287' E30º03•036'; S24º18•298' E30º00•178'; S24º18•702' E30º39•312'; S24º13•818' E30º49•507'; S24º21•044' E30º06•137'; S24º21•647' E30º05•615' |
| 3.5 ± 1.5 | 750 ± 100, 600-650 and 650-800 (for | The temperature estimates for the garnet granofels were obtained by garnet- | Johnson *et al.* (2003) | Around Steelpoort and Burgersfort and further north near northern limit |

| | | | | |
|---|---|---|---|---|
| | garnet-bearing granofels, lower-grade metatexites and granofels together with diatexites, respectively) as well as ~680-690 and ~720 (for lower grade migmatites and higher grade migmatites, respectively) | cordierite Fe-Mg thermometry, the second and third set of temperature results were obtained from the concentrations of Na in cordierite crystals and the latter two sets (those for lower and higher grade metatexites) were obtained from conductive heat modelling and T-X pseudosections at 3 kbar using THERMOCALC. The pressure estimate was also obtained with the use of THERMOCALC. | | of eastern limb. Metatexites: S24º37•35' E30º21•07' and S24º37•31' E30º21•03', leucosomes: S24º19•41' E30º02•68' and S24º21•56' E30º42•57' and diatexite: S24º21•56' E30º42•57' |
| 3 (first stage) and 1.5-2 (second stage) | >720 (first stage) and >700 (second stage) | Pseudosections in the MnNCKFMASHT system constructed through the use of THERMOCALC | Johnson *et al.* (2004) | Phepane Dome north of Burgersfort |
| 1) 0.146 and 0.166 GPa (pressure estimates for contact); 2) 0.15-0.25 and 0.22-0.31 GPa (for the Lydenburg Shale and Boven Shale Members, respectively); 3) 0.24 ± 0.04 GPa 4) 0.21 ± 0.03 GPa | A) 750-805, B) 755-820, C) 740-790, D) 550-595, E) 635-665, F) 450-475, G) 570 ± 20 and H) 600 ± 30 | For pressure estimates at contact the garnet-aluminosilicate-plagioclase-quartz (GASP) barometer, or stratigraphic pressure correction coupled with GASP barometer data, was used. Pressure estimates for the Lydenburg Shale and Boven Shale Members were obtained from the petrogenetic grid of Pattison et al. (2002). For the other two pressure results the method used is unknown. For temperature estimates A-X: A) orthopyroxene-cordierite thermometry, B) orthopyroxene-biotite thermometry, C) garnet-cordierite thermometry, D,E&F) garnet-biotite thermometry and G&H) unknown. | Kaneko *et al.* (2005) | Burgersfort area and most of the Eastern Bushveld Complex aureole north of Burgersfort. Pressure estimates: 1) -, 2) -, 3) S 24.36° E 30.23° and 4) S 24.42° E 30.18°. Temperature estimates: A&B) S 24.74° E 30.38°, C) S 24.90° E 30.19°, D) T-range corresponds to that of three samples at locations: S 24.43° E 30.28°; S 24.36° E 30.21° and S 24.40° E 30.26°, respectively, E) S 24.48° E 30.16°, F) S 24.33° E 30.28°, G) S 24.36° E 30.23° and H) S 24.42° E 30.18° |

**Table 7.** Summary of all reviewed geothermobarometry on the Bushveld Complex aureole. In the pressure and temperature columns values with stars represent assumed values and values with hashes were obtained for xenoliths.

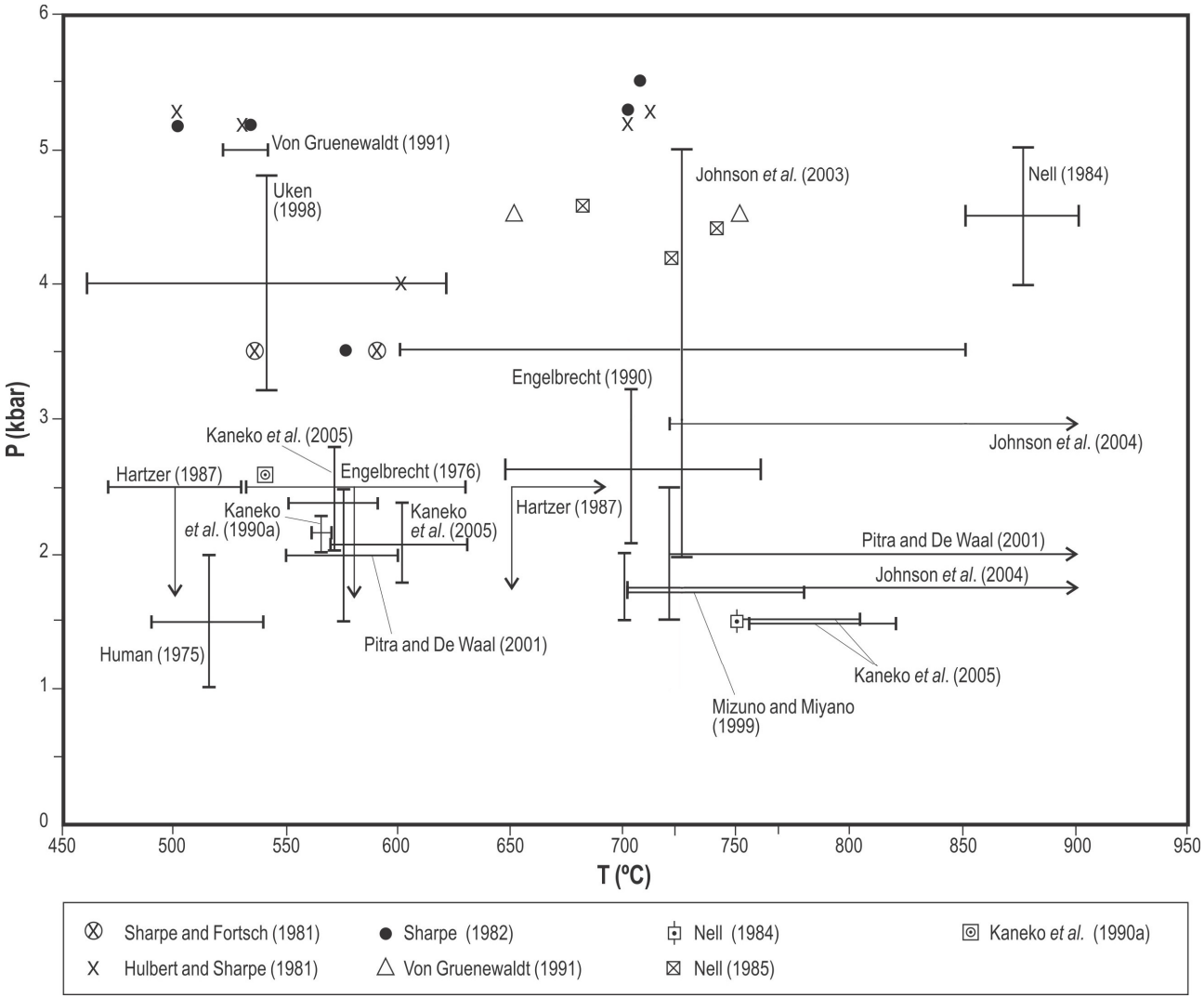


**Fig. 3.**

PT-diagram with geo-thermobarometric results from the reviewed studies. Diagram excludes all results obtained from xenoliths and all temperature estimates that could not be paired with pressure estimates, and vice versa. For the graphed results of Human (1975), Johnson *et al.* (2003) and Kaneko *et al.* (2005) errors were added to graphed results (e.g. 3.5 ± 1.5 kbar was graphed as 2-5 kbar).

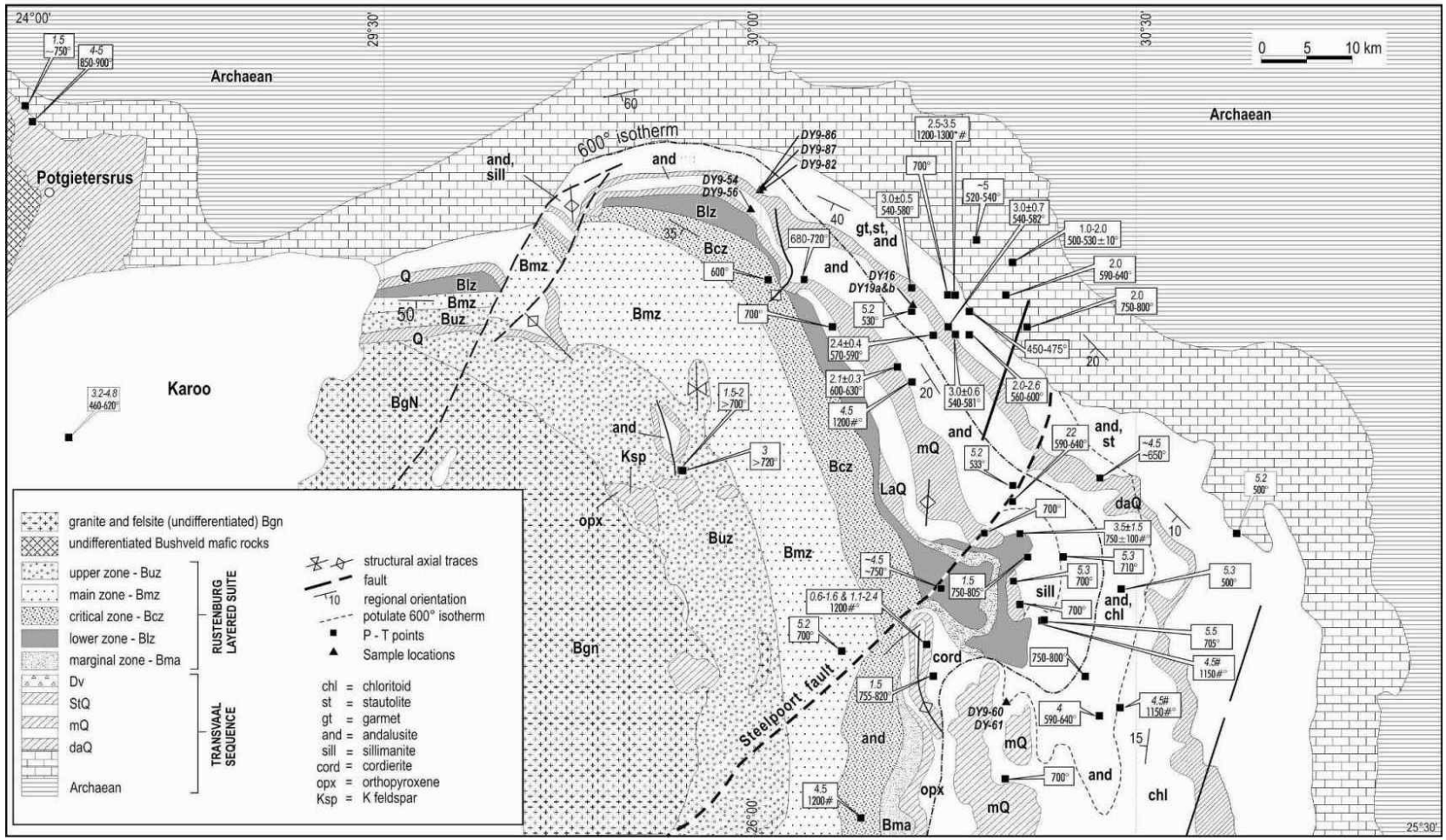


**Fig. 4.** Simplified geological map of Eastern Bushveld Complex, including Potgietersrus and its immediate surroundings, with metamorphic facies and pressure- and temperature estimates from the literature (Mavimbela, 2012).

# CHAPTER 3

## METHODOLOGY

For the purpose of this study samples of metapelites from varying stratigraphic positions were collected during 2008 and 2009 over a large portion of the eastern Bushveld Complex aureole. These samples were collected using five pound- and geological hammers. Coordinates of sampling were noted using hand-held GPS devises. During the sampling in 2009 strike and dip measurements were taken at numerous locations during fieldwork. In total roughly 150 samples were collected.

Polished thin-sections were prepared for a selection of 30 samples. These had been chosen according to their classification, their state of weathering and, when possible, their mineralogies. After studying the thin sections under polarised microscope, a further selection of samples, namely samples DM08-06, DM08-07, DM08-09, DM08-12, DM08-13, DM08-14, DM08-16, DM08-52, DM08-53, DM08-54, DM08-56, DM08-58, DM08-62, DM08-63, DY09-18A, DY09-18B, DY09-40, DY09-54, DY09-56, DY09-60A, DY09-60B, DY09-66, DY09-82, DY09-86B and DY09-87, was chosen for analyses of bulk-rock compositions by X-ray fluorescence spectroscopy (XRF). These samples were chosen according to the variance of their identified mineral assemblages (assemblages with low variance were primary targets), the state of weathering visible under polarised microscope and in some cases the textural relationships between phases. For the XRF analyses the samples were ground to <75µm in a Tungsten Carbide milling vessel, roasted at 1000ºC to determine Loss On Ignition values and after adding 1g sample to 6g $Li_2B_4O_7$ fused into glass beads. The major element analyses were executed on the fused beads using an ARL9400XP+ spectrometer.

Pseudosections for all samples analysed for bulk-rock composition were then constructed in the MnNCKFMASHT system using PERPLEX. The pressure-temperature window used in the modelling was 500 - 700 ºC and 1000 – 5000 bar. The solid solution phases that were modelled were St(HP), Chl(HP), Opx(HP), TiBio(HP), Gt(HP), Ep(HP) Ctd(HP), IlGHPy and hCrd of Holland and Powell (1998), melt(HP) (Holland and Powell, 2001), feldspar (Furman and Lindsley, 1988) and Mica(CH2) (Coggon and Holland,

2002). A few samples were also modelled in the NCKFMASHT system in an attempt to circumnavigate certain modelling difficulties. In all modelling water was assumed to be in excess as the assemblages were below the onset of partial melting.

For a selection of five samples, namely DM08-52B, DY09-54, DY09-56, DY09-82 and DY09-87, mineral chemistries had been measured by wavelength dispersive spectrometry. The selection criteria for these samples had been that they contain high variance mineral assemblages and that they had to have shown promising results from early modelling. Major element compositions of minerals in these samples had been analysed using a CAMECA SX-100 electron microprobe at the University of Pretoria, at an accelerated voltage of 15 kV and a beam current of 20 nA. Element concentrations were determined from relative peak intensities using the internal PAP-correction software of Pouchou and Pichoir (1991). $Fe^{3+}$ concentrations were calculated by stoichiometric criteria using the method of Droop (1987).

Isopleths were then constructed for all samples that had been analysed for mineral chemistries and that had pseudosections with fields matching those identified under optical microscope. Isopleth data was then compared to analysed mineral chemistries. Where isopleths showed overlap with analysed mineral chemistries and cut through relevant assemblage fields in constructed pseudosections isopleth data was used to further refine pressure and temperature estimates of peak metamorphism.

For the interpretation of P-T estimates and of isopleth modelling it was attempted to quantify the errors implicit to the modelling. This was done as follows. The standard deviation of XRF data was propagated through the modelling for both pseudosections and isopleths. This was done by adding the standard deviation values (of XRF data) to thermodynamic component compositions in the relevant files produced though “build.exe” and then re-modelling the relevant pseudosections and isopleths. Errors were then quantified by comparing these pseudosections and isopleths to the originals at a number of arbitrary pressures and temperatures. Furthermore, errors originating from errors on the enthalpies of formation of phases in the Holland and Powell (1998) dataset were also propagated through the modelling. This was done by subtracting the errors on

the enthalpies of formation from the relevant values in “hp02ver.dat” and then re-modelling the relevant pseudosections.

Pressure-estimates obtained from the constructed pseudosections were converted to depths during peak metamorphism. These depths were then related to the Rustenburg Layered Suite, in terms of structural and spatial relations.

# CHAPTER 4

## PETROGRAPHY

The following mineral abbreviations will be encountered in the remainder of the text: bi = biotite; mu= muscovite; q = quartz; pl = plagioclase; st = staurolite; g = garnet; and = andalusite; sill = sillimanite; ilm = ilmenite; tml = tourmaline; ctd = chloritoid; ru = rutile.

DM08-06

Minerals present: bi + mu + tml + q + pl + ilm. Biotite and quartz are the most abundant minerals in the sample. Biotite seems to display a preferred orientation, although some grains have a decussate texture. Biotite often appears acicular along the the thin section's surface. Ilmenite is sparse and most commonly relatively equant. The majority of ilmenite grains had c-axes smaller than 200 µm in length. Muscovite crystals tend to have larger grain sizes than biotite. The latter typically having maximum diameters of around 100 µm. A granoblastic texture dominates, although a few 120º grain boundaries are present.

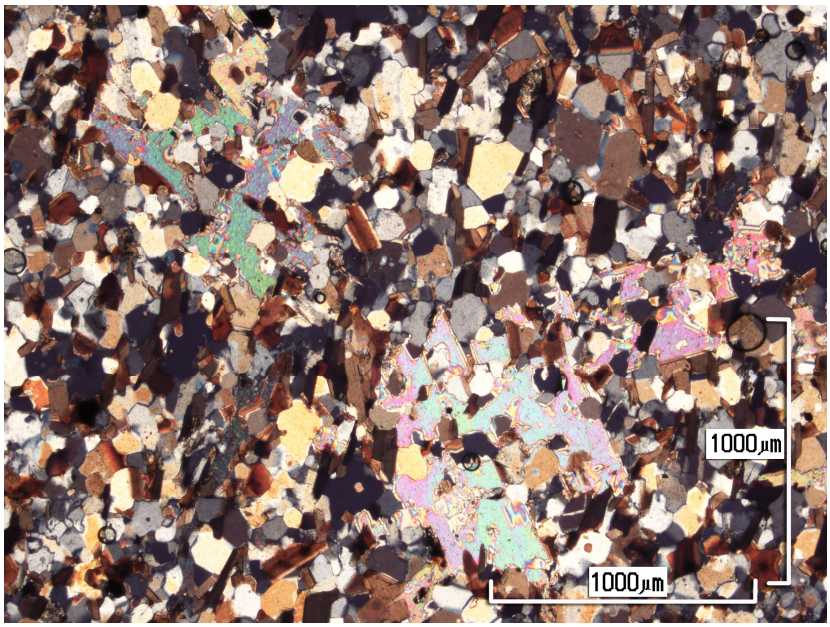


**Fig. 5.** Photomicrograph of sample DM08-06 under crossed polars with 1000 µm scalebars.

DM08-07

Minerals present: bi + ilm + tml + pl + q + mu. Biotite and quartz are the most abundant minerals in the sample. As in DM08-06 muscovite crystals tend to be of larger grains sizes than biotite. Ilmenite is very sparse and tends to be relatively fine grained with the majority of ilmenite grains having maximum diameters below 100 µm. A granoblastic texture dominates, although a very few 120º grain boundaries are present, as is the case with certain biotite grain boundaries.

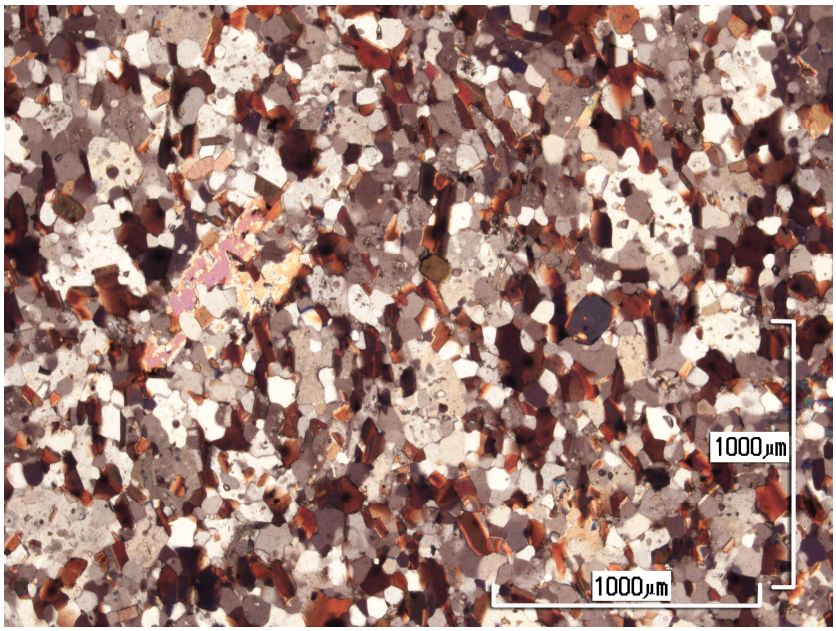


**Fig. 6.** Photomicrograph of sample DM08-07 under crossed polars.

DM08-08

Minerals present: bi + ilm + tml + pl + q + mu. Biotite and quartz are the most abundant minerals in the sample. As in DM08-07 certain biotite grains display decussate texture and muscovite crystals are on average of larger grains sizes than that of biotite. The majority of ilmenite grains have maximum diameters below 100 µm and are of equant shape. A granoblastic texture dominates the sample.

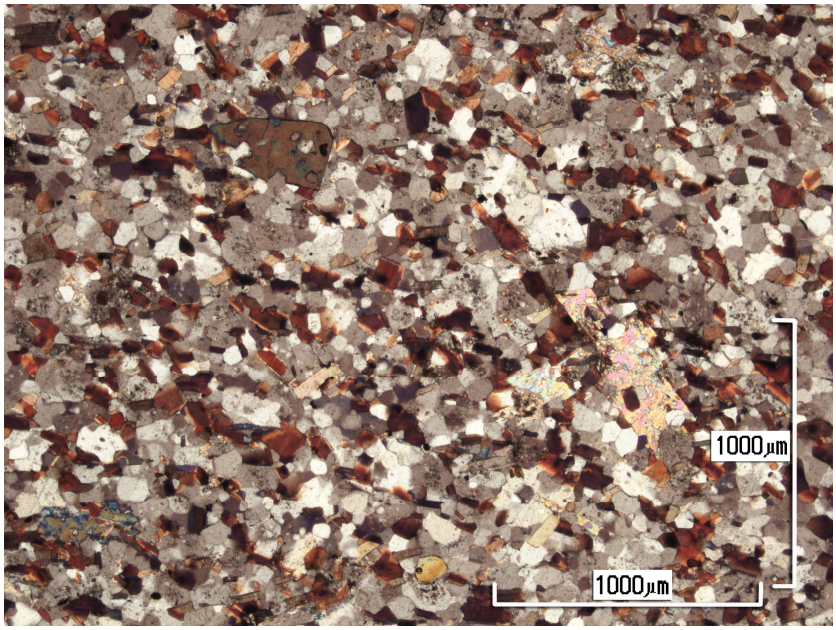


**Fig. 7.** Photomicrograph of sample DM08-08 under crossed polars.

DM08-09

Minerals present: bi + mu + pl + q + tml + ilm. Biotite and quartz are the most abundant minerals in the sample. Muscovite appears to be the third most abundant mineral in the sample. Biotites display a preference in orientation. Ilmenite is sparser than in most samples and has similar grain sizes than in DM08-07 and DM08-08. Equant ilmenite crystals are more abundant than acicular crystals. Apart from the preferred orientation of biotite, a granoblastic texture dominates the sample.

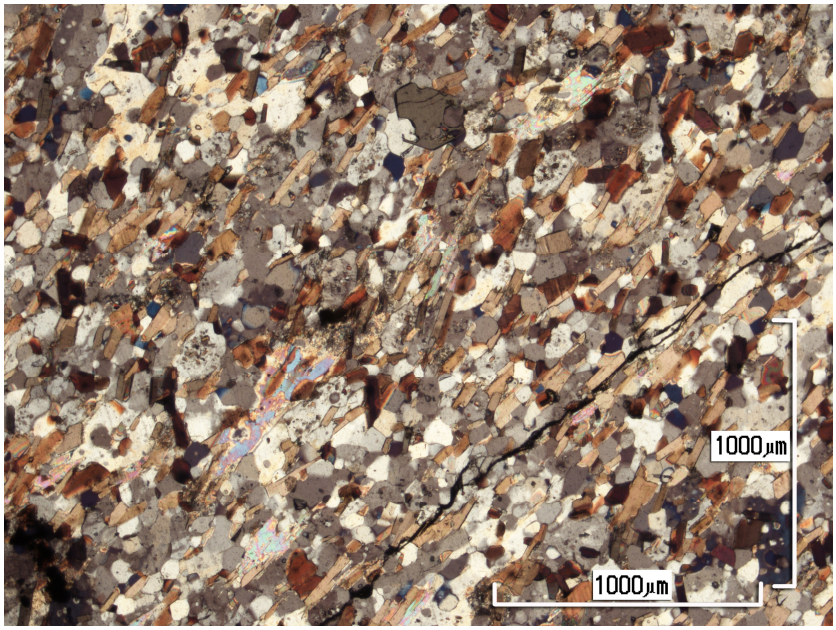


**Fig. 8.** Photomicrograph of sample DM08-09 under crossed polars.

DM08-10

Minerals present: bi + mu + q + ilm + pl + tml. All phases, except possibly ilmenite, are finer grained than in the previous samples. Quartz and biotite appear to be the foremost and second-most abundant minerals in the sample, respectively. Ilmenite is most commonly subhedral and acicular. In terms of grain shape, -size and -relationships, the sample is similar in texture to DM08-09, -12 and -13, but seems to contain more quartz. Polygonal grain boundaries are relatively common, but a granoblastic texture dominates.

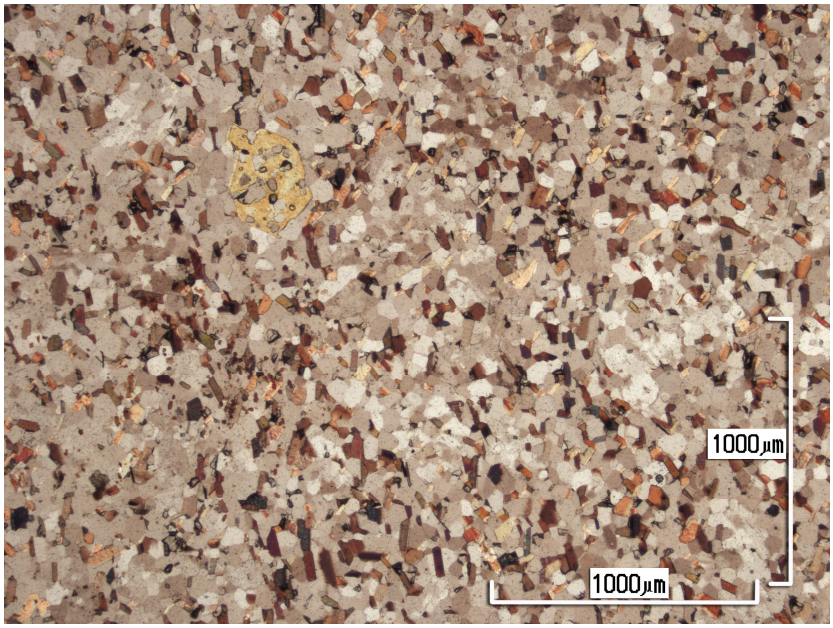


**Fig. 9.** Photomicrograph of sample DM08-10 through uncrossed polars.

DM08-11

Minerals present: bi + mu + q + ilm + pl + tml. Biotite and quartz are the most abundant minerals in the sample. Micas are randomly orientated. A granoblastic texture dominates the plagioclase grain boundaries, though polygonal grain boundaries are not uncommon. Furthermore, decussate texture is apparent in biotite grain relationships. Ilmenite most often occurs as subhedral acicular crystals, but equant grains also occur.

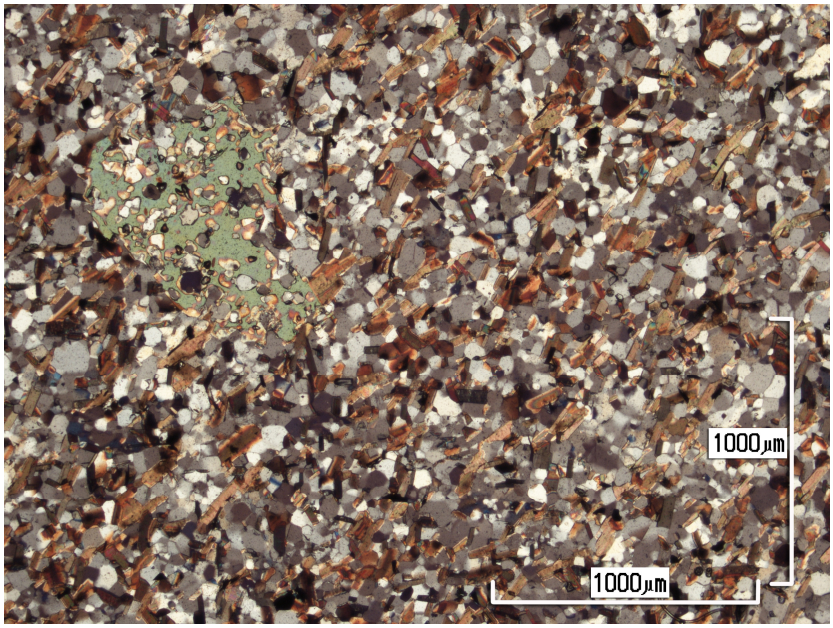


**Fig. 10.** Photomicrograph of sample DM08-11 under crossed polars.

DM08-12

Minerals present: bi + mu + q + ilm + pl + tml. Biotite and quartz appear to be the most abundant minerals in the sample. Ilmenite is most commonly subhedral and occurs as either acicular crystals, or as more equant grains. A small portion of acicular crystals of ilmenite are more than 200 µm in length. Granoblastic texture dominates the sample, although polygonal grain boundaries are relatively common. Furthermore, decussate texture is apparent in many biotite-biotite grain relationships.

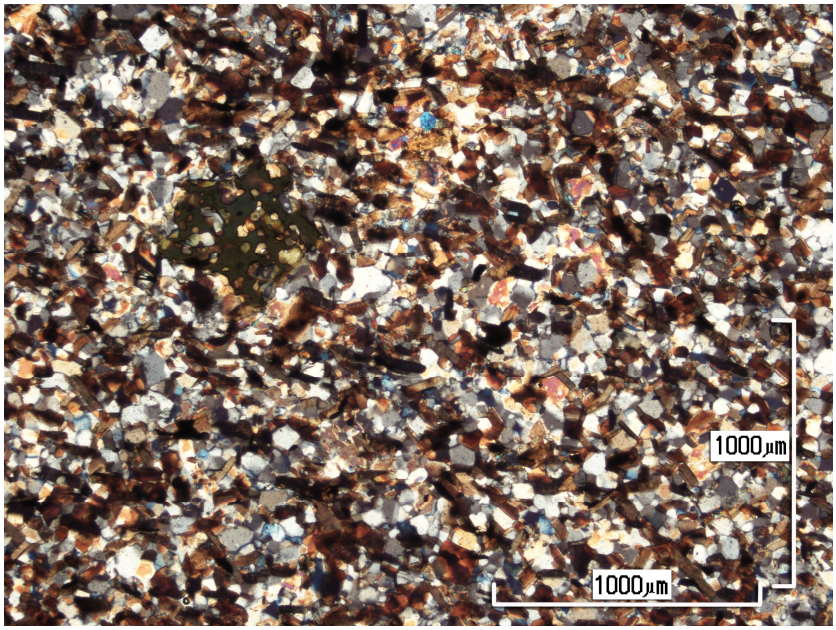


**Fig. 11.** Photomicrograph of sample DM08-12 under crossed polars.

DM08-13

Minerals present: bi + mu + q + ilm + pl. Biotite and quartz are the most abundant minerals in the sample. The sample is rather texturally homogeneous (in terms of grain size and granoblastic texture) and has similar grain sizes than DM08-12. The majority of ilmenite grains are relatively equant and have grain sizes below 90 µm in diameter. Micas are randomly orientated. The sample has a granoblastic texture, although polygonal grain relationships are relatively common.

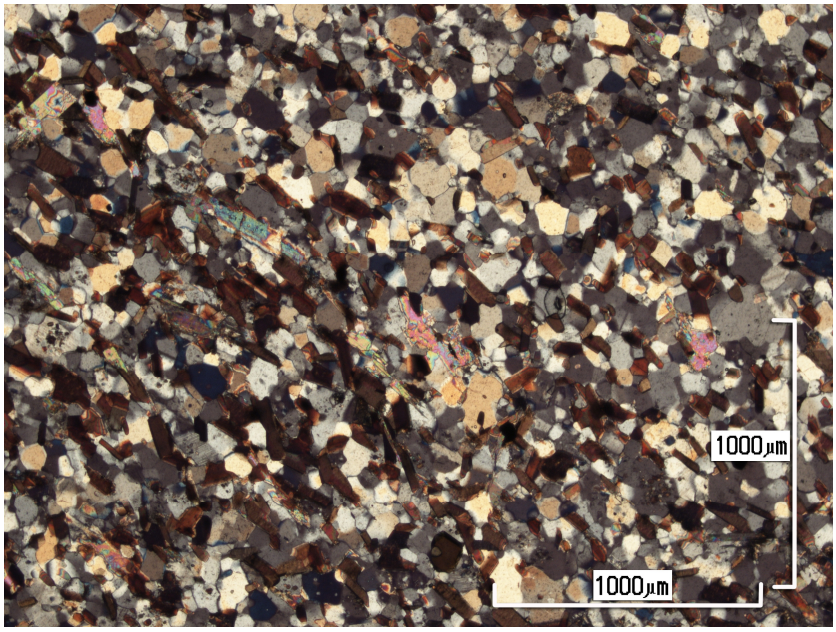


**Fig. 12.** Photomicrograph of sample DM08-13 under crossed polars.

DM08-14

Minerals present: mu + bi + tml + ilm + pl + q. Biotite and quartz are the most abundant minerals in the sample – quartz appearing to be more abundant. Ilmenite is mostly subhedral and much more commonly equant than acicular. Decussate biotite is present and the sample predominantly has a granoblastic texture, although polygonal grain boundaries do occur.

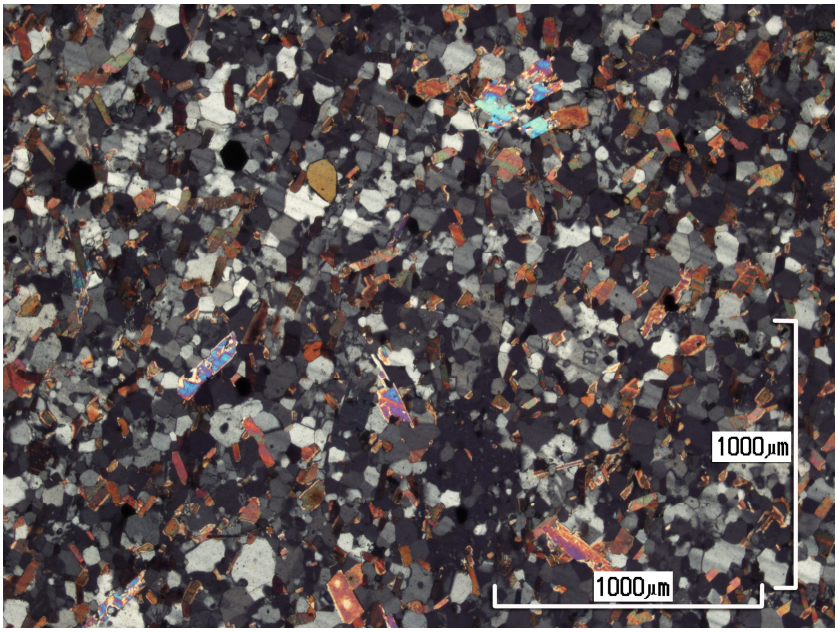


**Fig. 13.** Photomicrograph of sample DM08-14 under crossed polars.

DM08-52A

Minerals present: and + sill + bi + mu + q + ilm + pl. Biotite appears to be the most abundant phase in the sample. Compositional banding within the sample is visible with the naked eye. Sillimanite occurs in much smaller amounts than andalusite and displays acicular texture. Inclusions in sillimanite are hard to discern due to crystals typically being very thin, but microscope investigation shows that ilmenite and possibly quartz and plagioclase are inclusions within this phase. Andalusite is typically porphyroblastic. Andalusite contains inclusions of muscovite, biotite, ilmenite, plagioclase and quartz. Ilmenite is ubiquitous over all but a small band of the thin section. The mineral is mostly equant and typically subhedral, though many acicular crystals are present. Decussate mica dominates the sample, although the small band depleted in ilmenite displays a dominantly granoblastic texture with only a moderate amount of polygonal grain relationships.

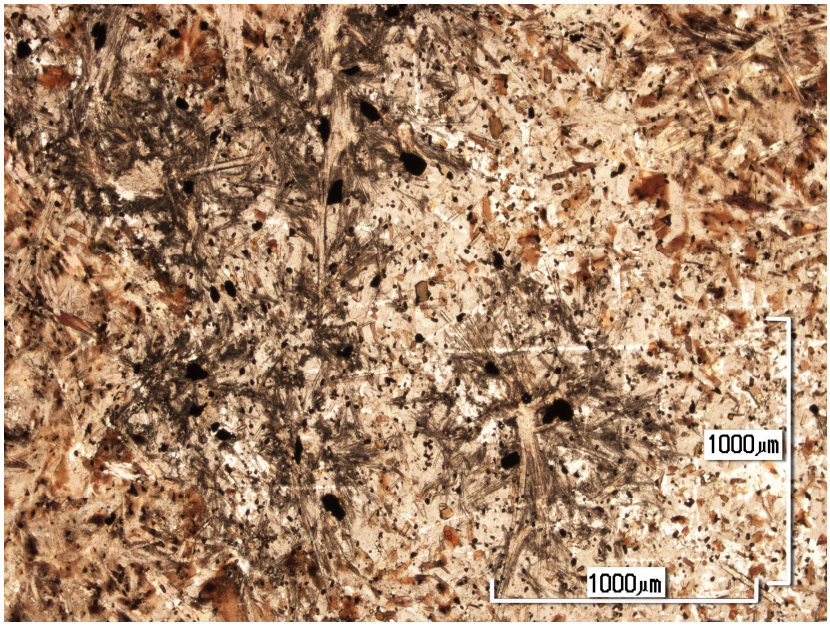


**Fig. 14.** Photomicrograph of sample DM08-52A through uncrossed polars. Acicular sillimanite can be seen in the central and top-left portions of the image.

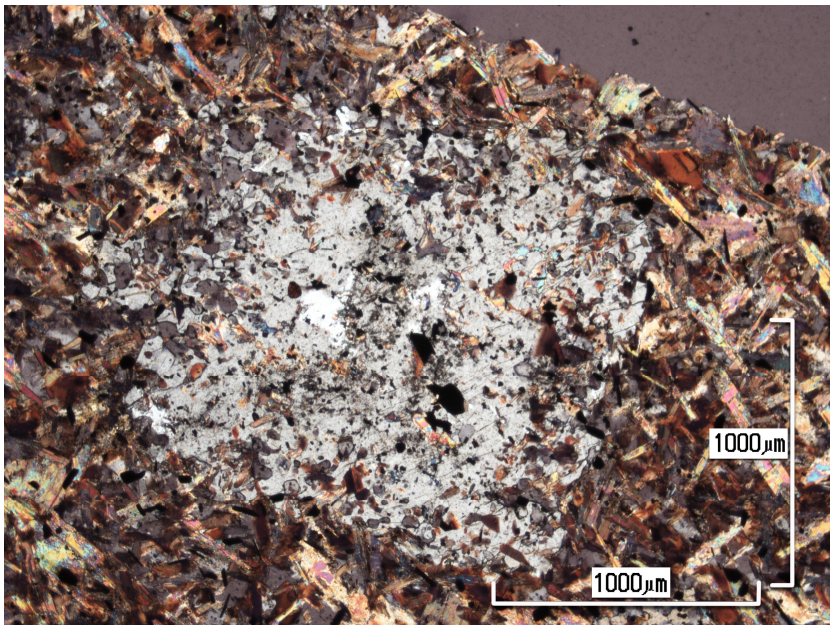


**Fig. 15.** Photomicrograph of sample DM08-52A under crossed polars. A large poikiloblast of andalusite features in the centre of the photomicrograph. The poikiloblast has a diameter of roughly 1600 µm and inclusions of biotite, muscovite, quartz and ilmenite.

DM08-52B

Minerals present: and + sill + bi + mu + q + ilm + pl. Biotite seems to be the most abundant mineral present. Micas display decussate texture. Andalusite is much more abundant than sillimanite. Sillimanite displays acicular texture similar than in DM08-52A. The most probable inclusions in sillimanite are ilmenite grains. Andalusite is typically porphyroblastic and contains inclusions of biotite, ilmenite, muscovite, plagioclase and quartz. Ilmenite is ubiquitous over the whole sample and although it is mostly equant, acicular crystals are common. If compositional banding is present its manifestation in the thin-section is very vague.

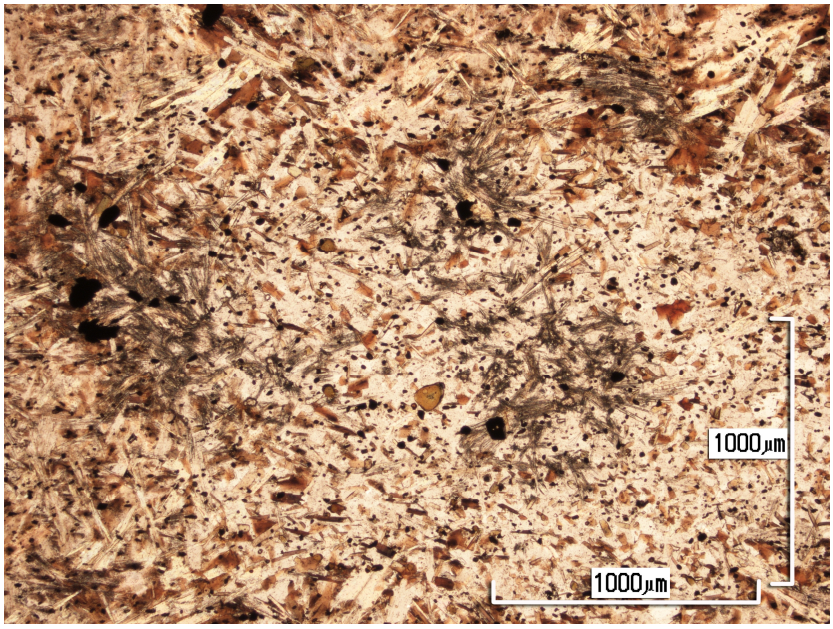


**Fig. 16.** Photomicrograph of sample DM08-52B through uncrossed polars. Greyish acicular sillimanite can be seen in the central, left and top-right portions of the photomicrograph.

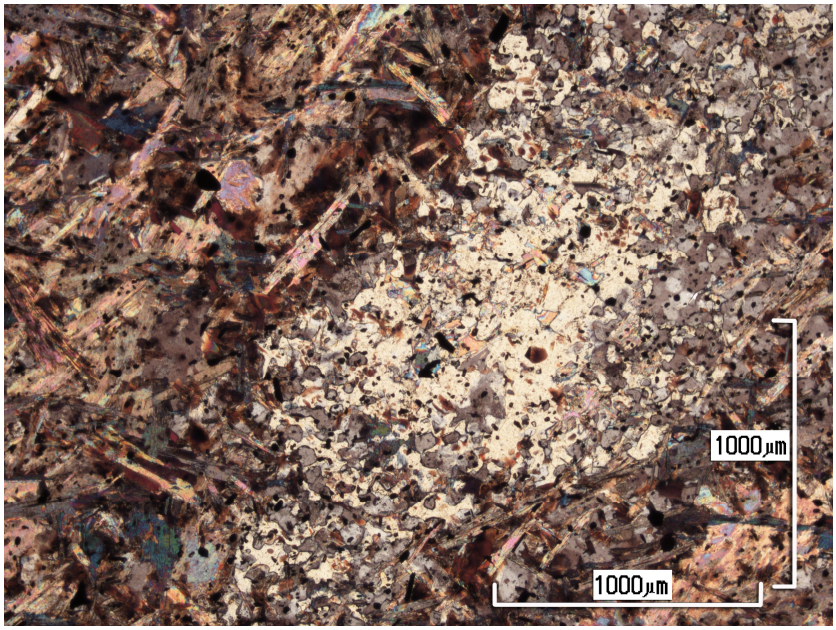


**Fig. 17.** Photomicrograph of sample DM08-52B under crossed polars. A large poikiloblast of andalusite transects the image from its top-right corner to somewhat right of its bottom-left corner. In this photomicrograph the poikiloblast covers an area of roughly 2.5 $mm^2$. It can also be seen to contain inclusions of biotite, muscovite, ilmenite and quartz and/or plagioclase.

DM08-53

Minerals present: bi + mu + pl + q + tml + ilm. Biotite and quartz are the most abundant minerals in the sample. Ilmenite is mostly relatively equant and finer grained than in most samples with the majority of grains having diameters below 80 µm. Biotite is mostly anhedral and it seems to displays a vague preference in orientation. Indistinct foliation that is visible to the naked eye supports this interpretation. Granoblastic texture dominates the sample, although 120º grain boundaries are present.

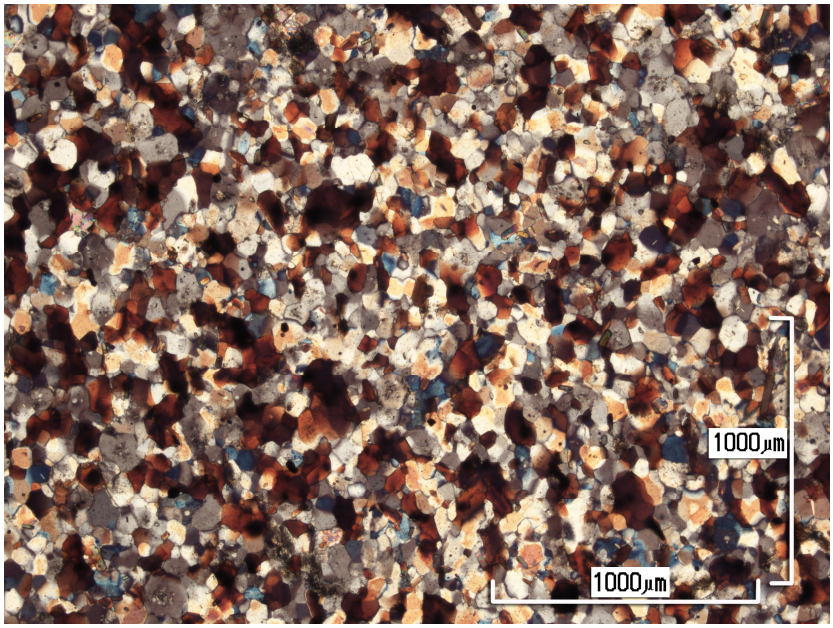


**Fig. 18.** Photomicrograph of sample DM08-53 under crossed polars.

DM08-54

Minerals present: bi + pl + q + ilm + and + sill + mu. The sample contains compositional banding. Ilmenite is ubiquitous, although some bands contain significantly less ilmenite than others. This mineral is mostly subhedral and occurs in a spectrum of acicular to equant grains. Biotite also occurs everywhere and may well be the most voluminous mineral in the sample. Biotite displays random orientation and deccusate texture. Andalusite occurs as either porphyroblasts or poikiloblasts. These contain inclusions of muscovite, biotite, ilmenite, quartz and plagioclase. Similar to DM08-52A biotite is less dominant in the bands characterised by small amounts of ilmenite. In these bands quartz is abundant and a granoblastic texture is dominant.

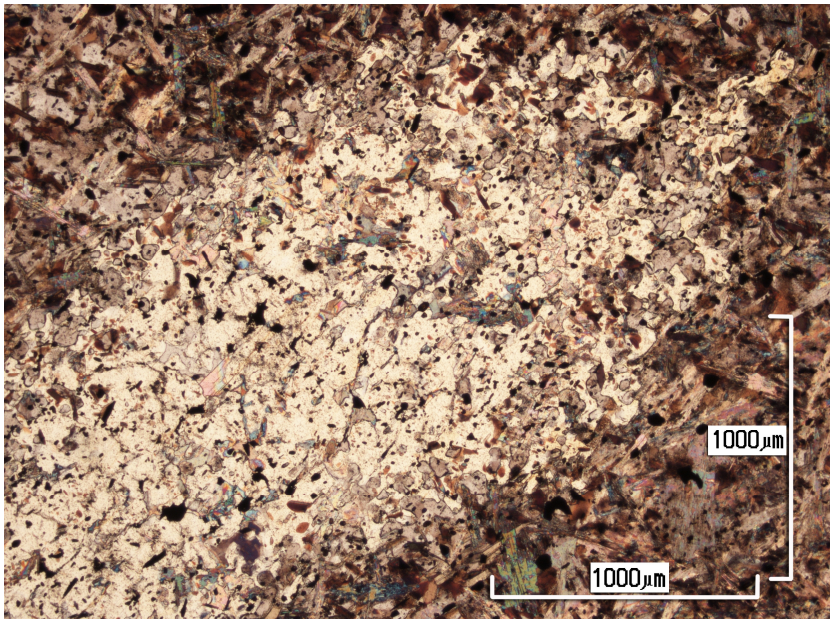


**Fig. 19.** Photomicrograph of sample DM08-54 under crossed polars. A large andalusite poikiloblast dominates most of the image. In the photomicrograph the poikiloblast covers and area of roughly 3.6 $mm^2$. It can be seen to contain inclusions of biotite, muscovite, ilmenite, quartz and/or plagioclase.

DM08-56

Minerals present: bi + pl + q + tml + ilm + mu. Biotite and quartz appear to be the most abundant minerals in the sample. Biotites are mostly subhedral and display a preferred orientation. Ilmenite occurs in low density as either acicular, or more equant grains. A granoblastic texture dominates the sample, though some 120º grain boundaries are present.

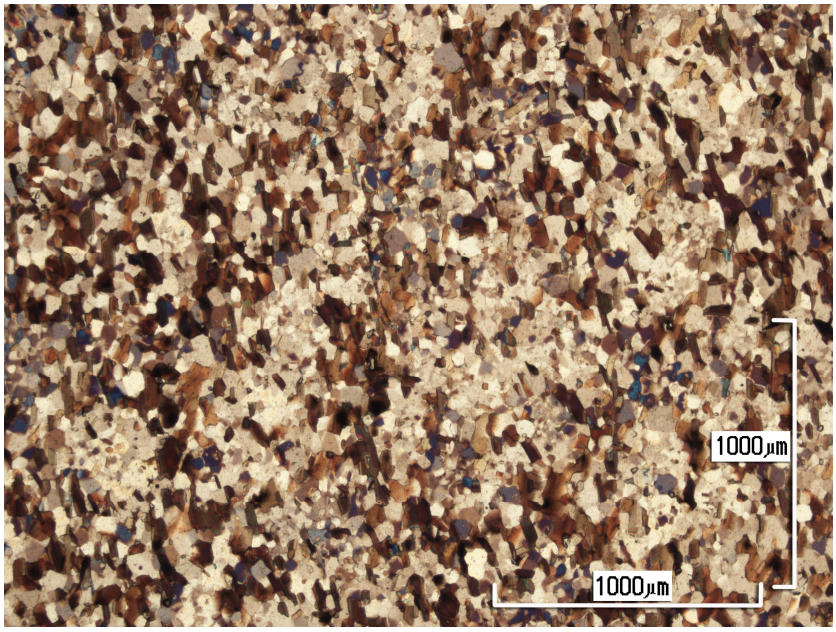


**Fig. 20.** Photomicrograph of sample DM08-56 under crossed polars.

DM08-58

Minerals present: pl + bi + q + mu + tml + ilm + ctd. As in most samples biotite and quartz are the predominant minerals present. Biotite ranges from euhedral to anhedral, but a dominance of subhedral grains was interpreted. Ilmenite is mostly subhedral, though euhedral and anhedral crystals are present. This mineral occurs either as relatively equant grains, or as acicular crystals. A granoblastic texture dominates the sample, though some 120º grain boundaries are present. A very slight compositional banding appears to be visible in the sample with the naked eye.

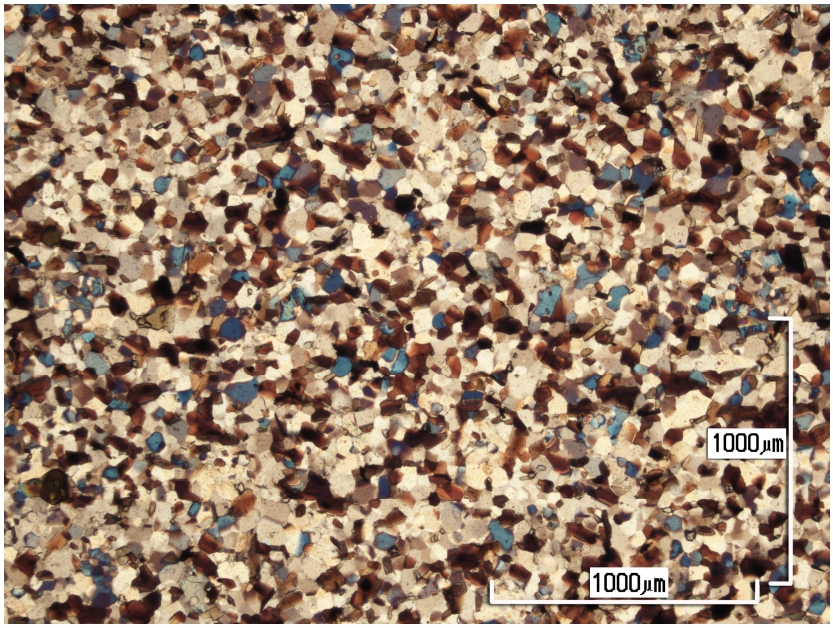


**Fig. 21.** Photomicrograph of sample DM08-58 under crossed polars.

DM08-62

Minerals present: pl + bi + ilm + mu + q. A "patchy" texture is present (Fig. 22). The sample is more finely grained than most other samples and is dominated by quartz and biotite. Many clusters of biotite display a decussate texture and biotite is randomly orientated. The biotite grains are mostly euhedral to subhedral. Ilmenite occurs in relatively low density as acicular to equant grains. A granoblastic texture dominates the sample, though some 120º grain boundaries are present.

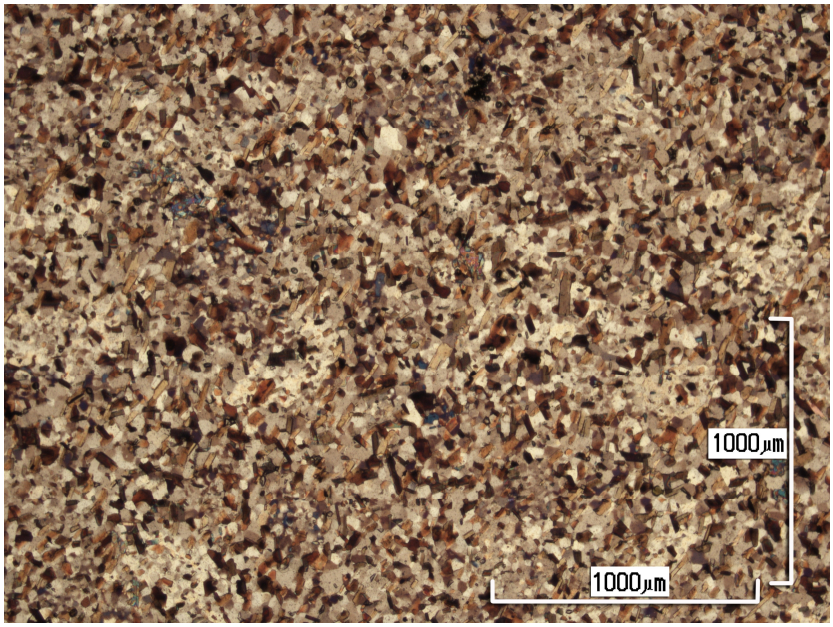


**Fig. 22.** Photomicrograph of sample DM08-62 under crossed polars.

DM08-63

Minerals present: q + bi + pl + mu + ilm + ctd. The sample is very finely grained with the majority more equant grains below 80 μm in diameter and the bulk of elongated grains below 110 μm in length. DY08-63 also displays the same "patchy" appearance as in DM08-62. Biotite appears to be the dominant mineral and is randomly orientated. The sample contains relatively little ilmenite compared to most other samples. Furthermore, the ilmenite is mostly relatively equant. Chloritoid is present as acicular crystals of mainly minute sizes, mostly well below 50 μm in length. Adjacent quartz grains display granoblastic relations forming the dominant texture in the sample.

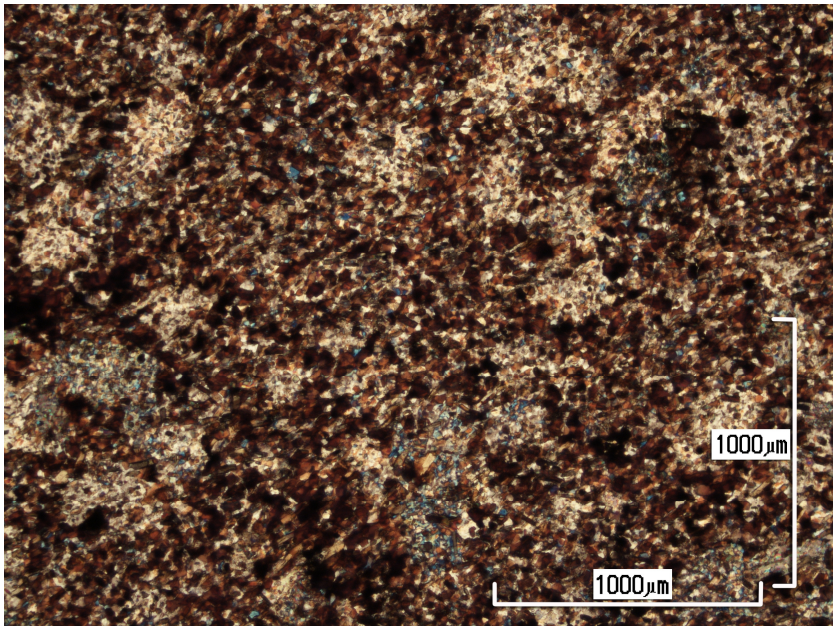


**Fig. 23.** Photomicrograph of sample DM08-63 under crossed polars.

DM08-64

Minerals present: pl + bi + ilm + mu + q + ctd. Quartz and biotite dominate the sample. Quartz displays a granoblastic texture. Biotite is randomly orientated, often exhibiting deccusate texture. As in DM08-63, ilmenite is rather sparse and mostly equant. Finally, similar to DM08-63, the sample is full of porphyroblast-sized “patches” with low relief and low interference colours.

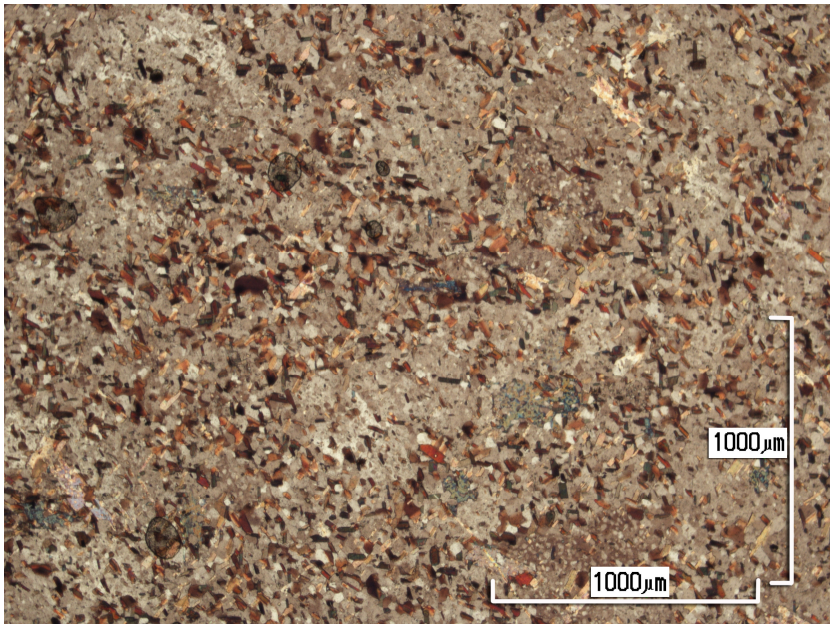


**Fig. 24.** Photomicrograph of sample DM08-64 under crossed polars.

DY09-16

Minerals present: pl + q + bi + mu + ilm + str. Banding and foliation are present. Biotite is possibly the most abundant mineral in the sample, but this is hard to discern due to fine grained nature of much of the sample. Large biotite grains tend to parallel foliation and appear to be porphyroblasts (Fig. 24). Staurolite occurs as euhedral to subhedral porphyroblasts with inclusions of ilmenite and plagioclase. Certain staurolite crystal rims have been replaced by muscovite. Ilmenite is randomly orientated and mostly subhedral and acicular, though equant grains are present. Muscovite and plagioclase are evident in the sample's matrix, which is quite fine-grained with typical grain sizes below 30 µm. Biotite twins (cruciform) are present.


**Fig. 25.** Photomicrograph of sample DY09-16 under crossed polars.

DY09-18A

Minerals present: pl + q + g + bi + mu + ilm. Sample is banded with alternating granoblastic quartz-dominated layers and finer-grained layers that seem to be dominated by biotite. The sample possibly contains tourmaline. Garnets are present as euhedral porphyroblasts. Ilmenite is mostly acicular and subhedral, but range from euhedral-anhedral. This phase is randomly orientated.

DY09-18B

Minerals present: pl + q + g + bi + mu + ilm. Quartz appears to be the most abundant mineral in the sample, followed closely by biotite. A slightly folded banding is present. Garnets are mostly euhedral and contain inclusions of ilmenite, plagioclase, biotite and quartz. These porphyroblasts are typically 200-550 µm in diameter. The foliation consists of bands that have matrixes of varying grain-size. Micas are possibly more abundant in bands of finer-grained matrix. Ilmenite seems to mostly be sub-parallel to parallel to foliation. Acicular and equant ilmenite is present in near-equal proportions. Ilmenite is mostly subhedral-anhedral.

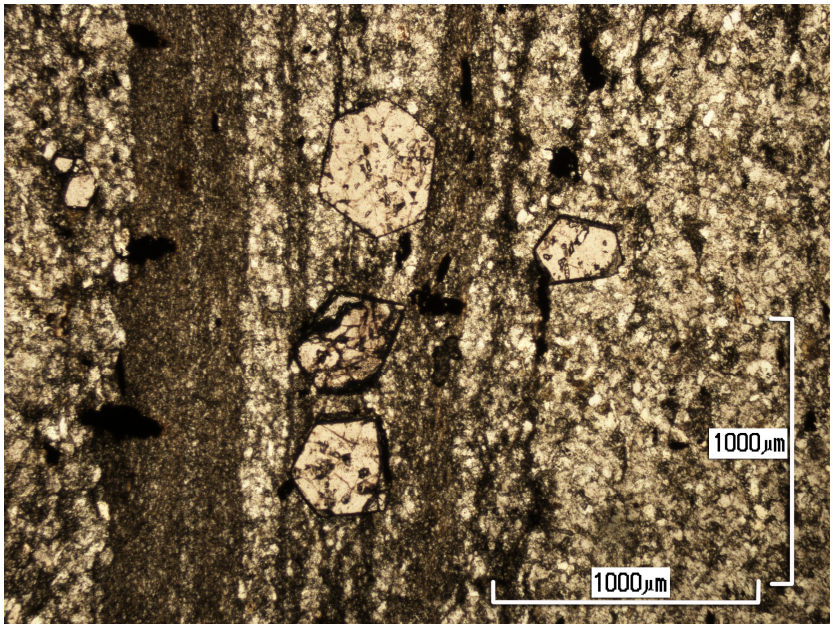


**Fig. 26.** Photomicrograph of sample DY09-18B under crossed polars. Euhedral garnet crystals are clearly visible.

DY09-54

Minerals present: pl + bi + mu + q + g + and + str + ilm. Large crystals of biotite and muscovite are ubiquitous and display a preferred orientation. Biotite appears to be the most abundant mineral in the sample. It often has grain sizes with average diameters above 270 µm. Muscovite grains are not as common as biotite grains, but often have larger sizes. Garnet porphyroblasts occur throughout the sample, are mainly euhedral and have similar grain sizes than in DY09-18B. These porphyroblasts contain inclusions of ilmenite, biotite and possibly quartz. Staurolite occurs as large porphyroblasts with inclusions of plagioclase, ilmenite and what appear to be minute quartz grains. Andalusite also occurs as large porphyroblasts and has inclusions of plagioclase, ilmenite, biotite, muscovite and quartz. The sample's matrix displays a granoblastic texture. In the matrix quartz appears to be the predominant phase. Compared to other samples relatively little ilmenite is present. The mineral occurs as equant to acicular crystals with the two extremes in near equal proportions.

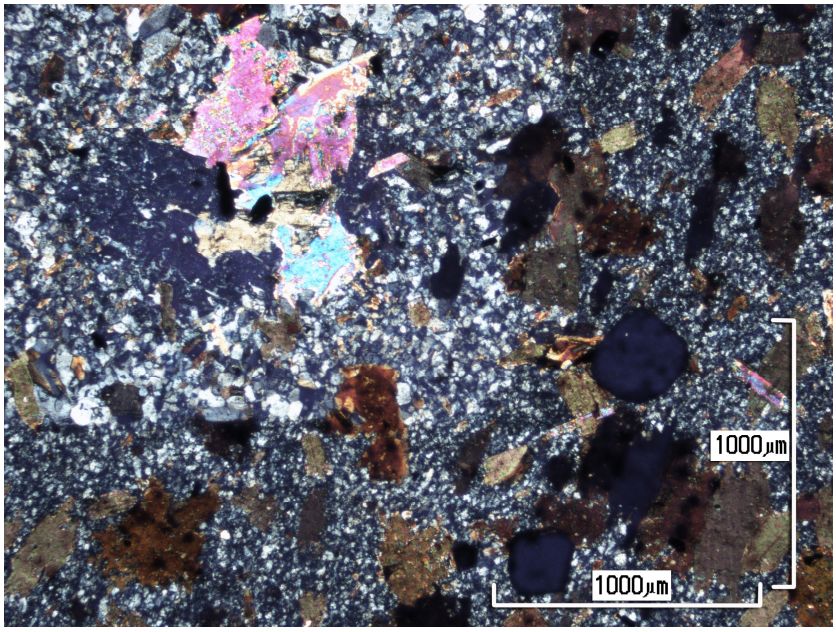


**Fig. 27.** Photomicrograph of sample DY09-54 under crossed polars. A muscovite porphyroblast is visible in top-left portion of the image, while porphyroblasts of garnet are visible in its bottom-right section.

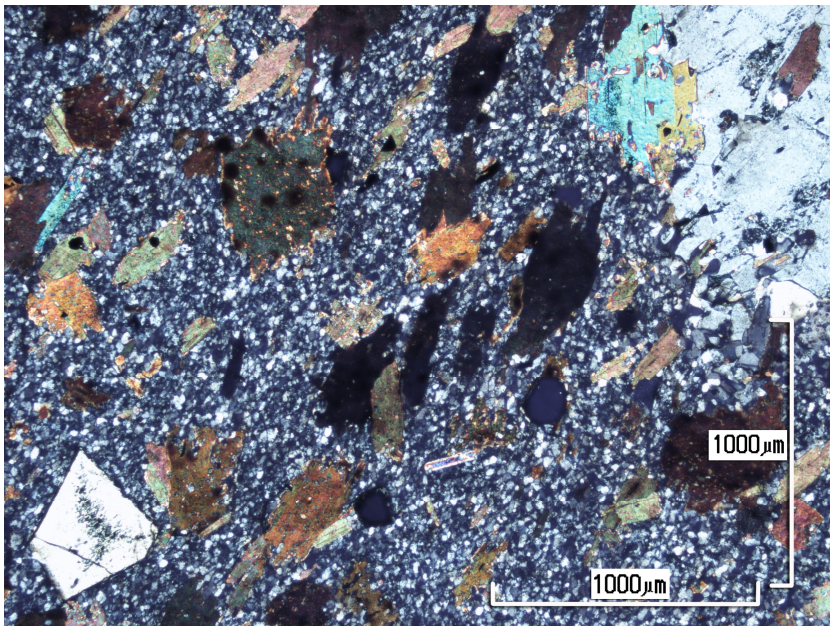


**Fig. 28.** Photomicrograph of sample DY09-54 under crossed polars. The image displays a porphyroblast of staurolite in its bottom-left, a large poikiloblast of andalusite in its top-right and relatively small porphyroblasts of garnet in its lower central portion. A

preferred orientation of biotite and muscovite seems present, with most grains paralleling a direction from the bottom-left to top-right of the photomicrograph.

DY09-56

Minerals present: q + pl + bi + mu + g + and + str + ilm. Biotite and quartz appear to be the dominant minerals in the sample. Large crystals of biotite and muscovite occur throughout the sample. These minerals seem randomly orientated and most often have very thin lath-like shapes. Furthermore, these minerals have similar grain sizes with average diameters that often exceed 270 µm. Andalusite occurs as poikiloblasts and porphyroblasts containing inclusions of plagioclase, minor muscovite, and oxides. Staurolite occurs as porphyroblasts with inclusions of ilmenite, plagioclase, muscovite and possibly quartz. Garnets mostly occur as euhedral porphyroblasts with inclusions of plagioclase, ilmenite and what appears to be quartz. Ilmenite occurs mostly as equant grains, although many acicular crystals of this phase are present. The ilmenite grains are mainly subhedral. The matrix consists mostly of plagioclase and has a granoblastic texture and some 120º grain boundary relationships. Finally, the sample is very similar to DY09-54, in mineralogy, as well as grain shape, -size and -relationships.

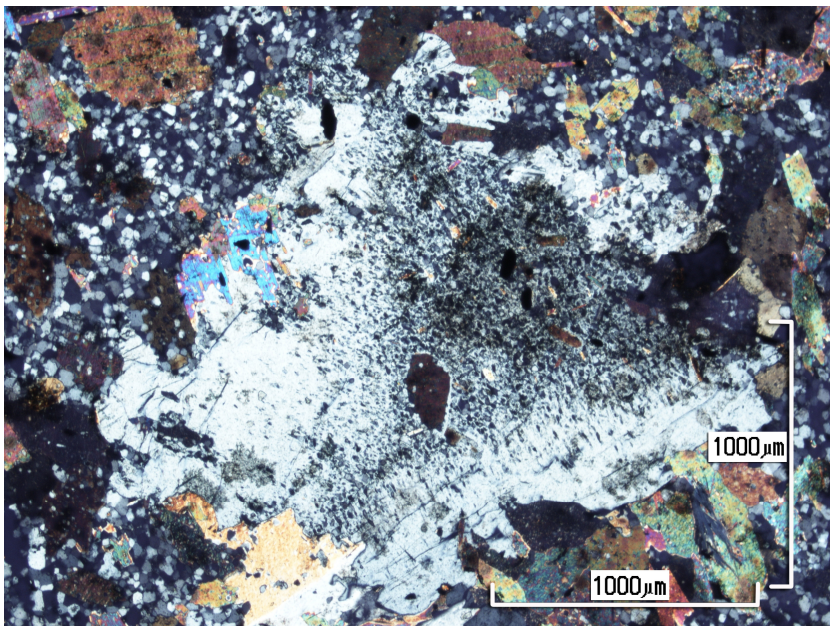


**Fig. 29.** Photomicrograph of sample DY09-56 under crossed polars. A large poikiloblast of andalusite dominates the image. Muscovite, biotite and plagioclase are also clearly visible.

DY09-60A

Minerals present: bi + q + pl + mu + ilm. Biotite and quartz are ubiquitous. Biotites seem to have a preferred orientation. A granoblastic texture dominates the sample, although 120º grain-boundaries are not uncommon. Comparatively little ilmenite is present and these grains are often acicular. Furthermore, ilmenite is of similar grain sizes than in most samples with the majority c-axes measuring less than 190 µm.

DY09-60B

Minerals present: q + pl + bi + mu + ilm. The sample displays slight compositional banding. In spite of this, it is rather homogeneous in terms of grain size, -shape and -relationships. Biotite and quartz are the most abundant minerals in the sample. Biotite displays a slight preference in orientation. This phase occurs as thin lath-like shapes. Quartz is ubiquitous and together with plagioclase displays a granoblastic texture. Ilmenite is very sparse and has grain sizes similar than in DY09-60A.

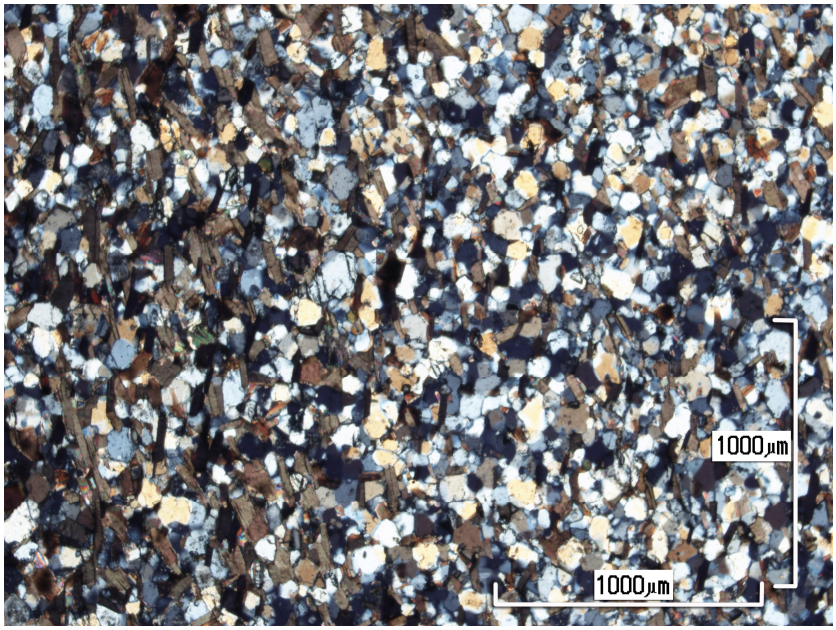


**Fig. 30.** Photomicrograph of sample DY09-60B under crossed polars.

DY09-61

Minerals present: pl + q + bi + mu + tml + ilm. Plagioclase is the most abundant mineral present and quartz is almost as voluminous in large portions of the sample. Biotite possibly displays a preferred orientation. Notably little ilmenite is present.

Ilmenite is mostly of comparatively small grain sizes with most grain diameters smaller than 90 µm. Though acicular crystals of ilmenite are present, this texture is not dominant. A granoblastic texture dominates the sample and is most pronounced in quartz-quartz grain boundaries. However, some decussate grain relationships are present between biotite crystals. Finally, the sample is similar to DY09-60A and DY09-60B in grain size and variation in grain size.

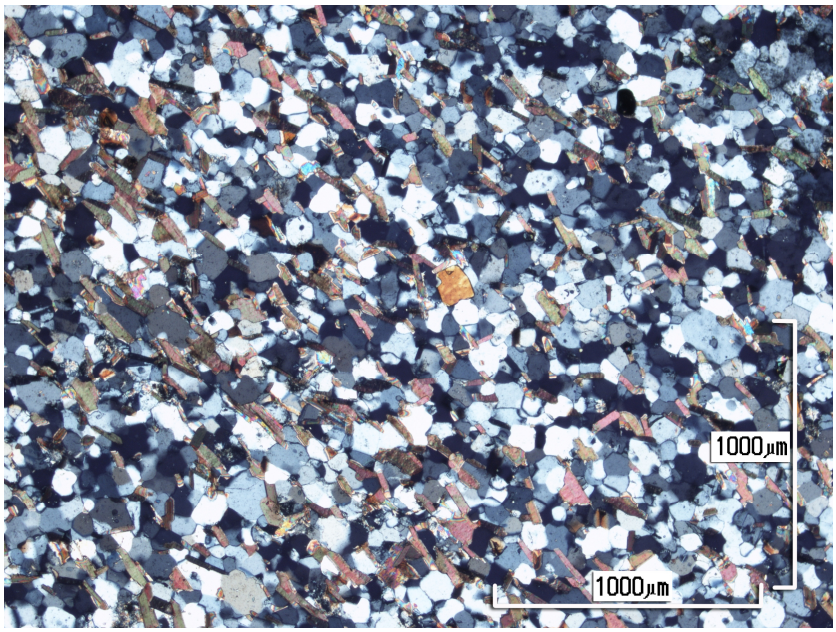


**Fig. 31.** Photomicrograph of sample DY09-61 under crossed polars.

DY09-82

Minerals present: q + pl + bi + mu + str + and + ctd + ilm. The sample displays compositional banding in hand specimen. The banding is however hard to discern in thin-section. Large porphyroblasts of biotite and muscovite are present. Of these, some biotite grains exceed 650 µm in average grain diameter, while a portion of muscovite grains exceed 700 µm in average grain diameter. Biotite porphyroblasts contain inclusions of muscovite, ilmenite and plagioclase. Some of these inferred porphyroblasts have partially regressed to form secondary muscovite. Porphyroblasts and poikiloblasts of andalusite are present. These contain inclusions of muscovite, ilmenite, plagioclase and biotite. Staurolite occurs as porphyroblasts with inclusions of plagioclase, ilmenite, biotite muscovite and quartz. Ilmenite is relatively ubiquitous and mainly acicular. Furthermore,

ilmenite is of comparatively large grain sizes with many grains having c-axes exceeding 280 μm in length.

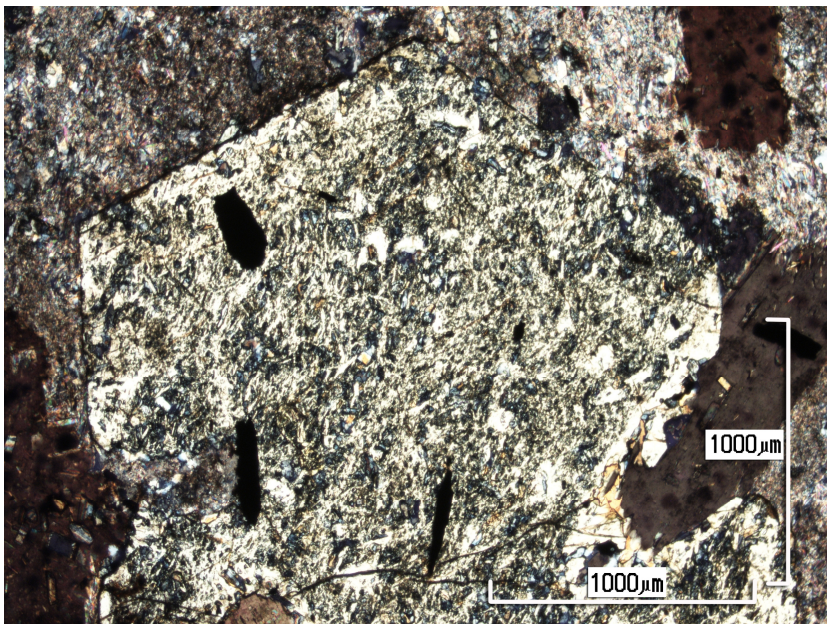


**Fig. 32.** Photomicrograph of sample DY09-82 under crossed polars. A large andalusite porphyroblast, containing acicular ilmenite, dominates the image. In the photomicrograph the porphyroblast covers and area of roughly 3.6 $mm^2$.

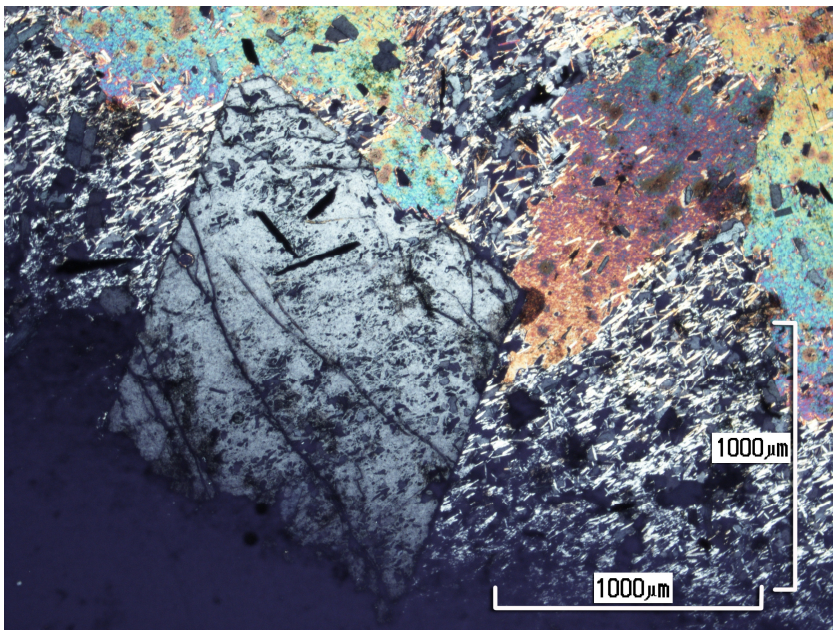


**Fig. 33.** Photomicrograph of sample DY09-82 under crossed polars. A porphyroblast of andalusite and porphyroblasts of muscovite dominate the photomicrograph.

DY09-86A

Minerals present: q + pl + mu + bi + ilm + str + and. Many large porphyroblasts of staurolite are present in sample. These contain inclusions of plagioclase, quartz, ilmenite, muscovite and biotite. Biotite porphyroblasts are also present. These contain inclusions of ilmenite, muscovite and plagioclase. Certain contacts between staurolite and biotite porphyroblasts display a distinct zoning. Furthermore, zoning is also evident in a number of staurolite grains and sometimes at staurolite-staurolite contacts. Muscovite, plagioclase and quartz are abundant in the matrix. Compositional banding is present in the sample and contains micro-folds. As in DY09-82 ilmenite is relatively ubiquitous, of comparatively large grain sizes (similar to those in DY09-82) and mainly acicular. Ilmenite often parallels the sample's banding.

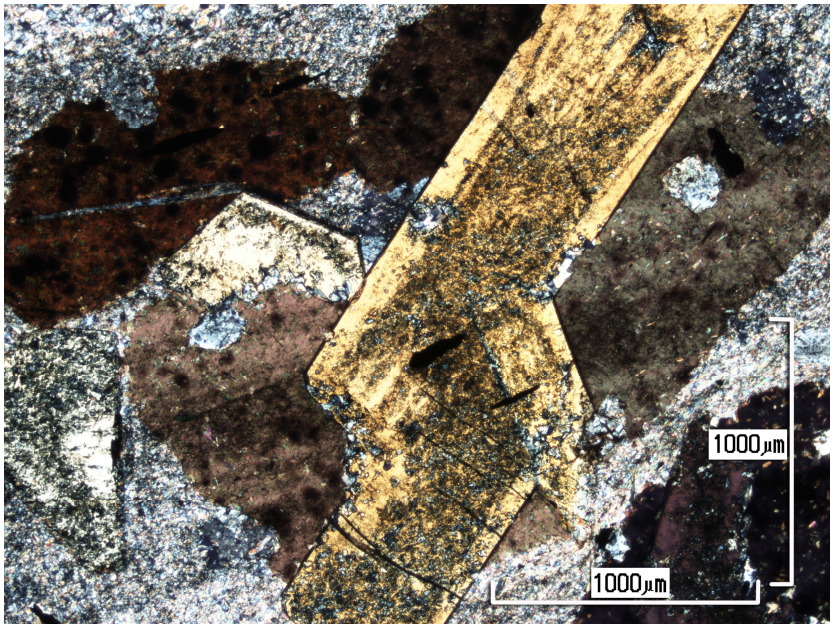


**Fig. 34.** Photomicrograph of sample DY09-86A under crossed polars. Porphyroblasts of biotite and staurolite dominate the image.

DY09-86B

Minerals present: q + pl + bi + mu + ilm + str + and. Staurolite occurs as mostly-euhedral porphyroblasts with inclusions of plagioclase, quartz, minor muscovite and ilmenite. These porphyroblasts have similar sizes than those in DY09-86A. Andalusite occurs as often-euhedral porphyroblasts containing inclusions of plagioclase, ilmenite, muscovite and biotite. The sample's groundmass consists mainly of quartz, muscovite

and plagioclase. Large biotites occur as poikiloblasts with inclusions of quartz, plagioclase, ilmenite and muscovite. A portion of these biotite grains have average diameters exceeding 1200 µm. Ilmenite is similar in size, abundance and texture as in DY09-86A. Compositional banding can be seen with the naked eye and in portions of groundmass. Ilmenite arguably tends to parallel the banding.

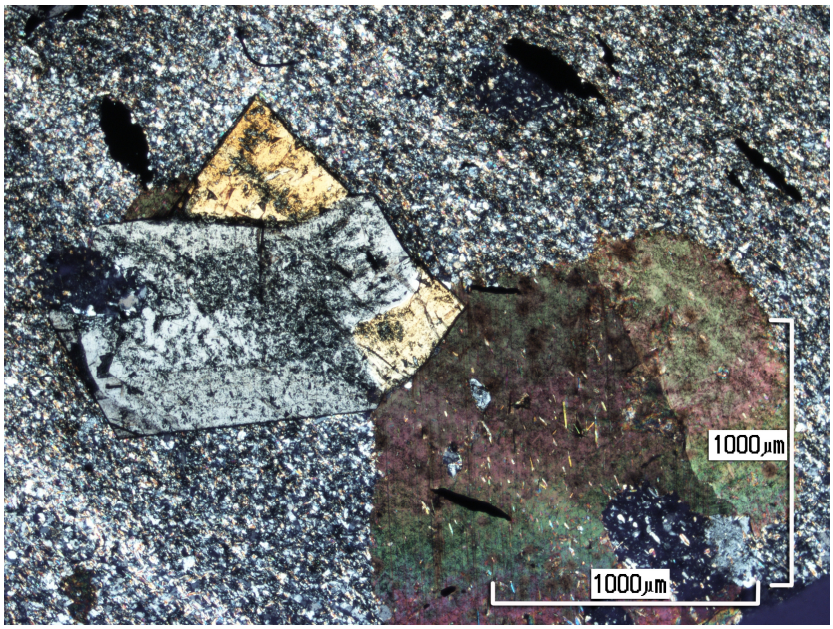


**Fig. 35.** Photomicrograph of sample DY09-86B under crossed polars. A porphyroblasts of biotite together with a porphyroblast of staurolite, which displays twinning, dominate the image.

DY09-87

Minerals present: q + pl + bi + mu + str + ctd + ilm. Compositional banding can be observed in the sample with the naked eye and under microscope. The sample contains large porphyroblasts of staurolite, which in some cases have average diameters exceeding 1500 µm. These contain inclusions of ilmenite, plagioclase, biotite and minor muscovite. Ilmenite is abundant and mainly occurs as comparatively large acicular crystals with c-axes that seldom exceed 300 µm. Large biotite grains are common and are interpreted to be poikiloblasts. These may exceed 1200 µm in average diameter and contain inclusion of ilmenite, muscovite, plagioclase and quartz.

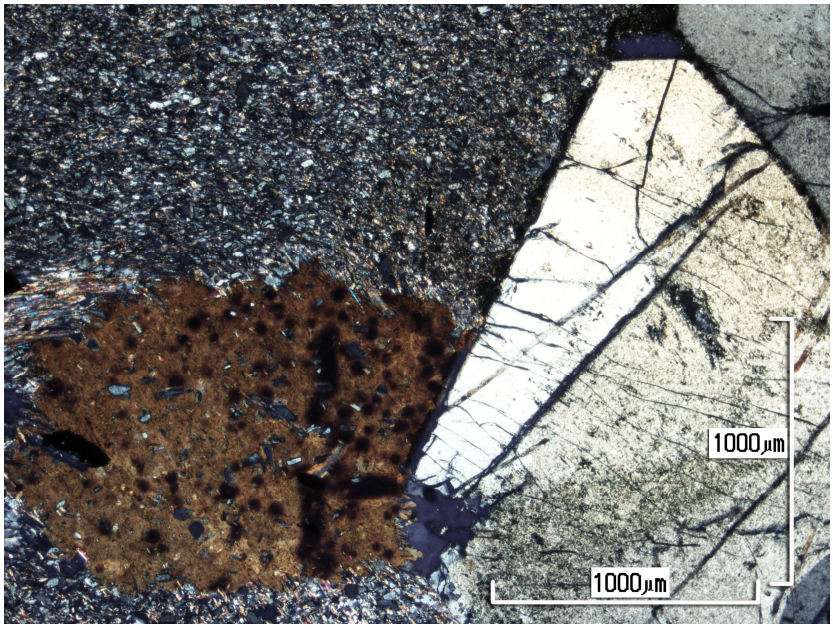


**Fig. 36.** Photomicrograph of sample DY09-87 under crossed polars. A large porphyroblast of staurolite is seen in the right-hand portion of the image and a biotite porphyroblast adjoins it on its left.

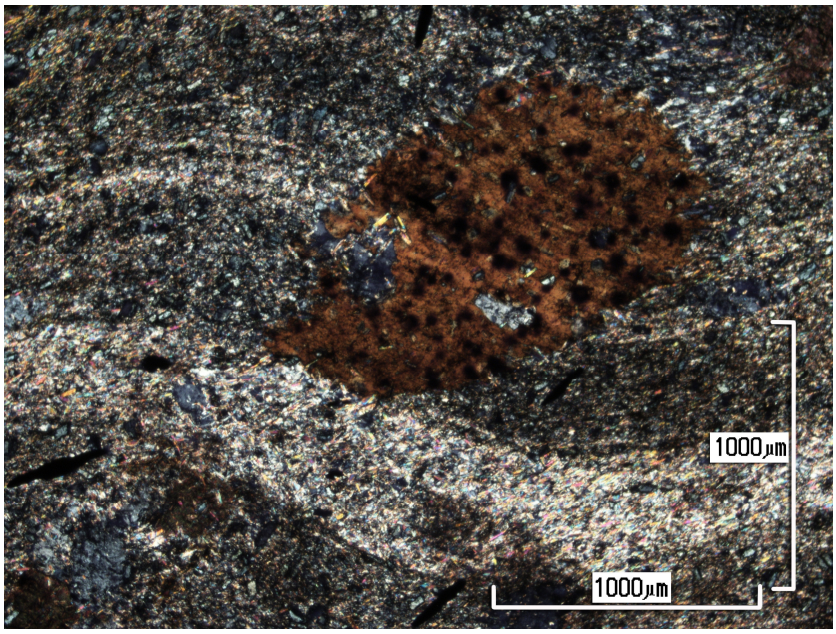


**Fig. 37.** Photomicrograph of sample DY09-87 under crossed polars. In the image a porphyroblast of biotite overlaps with compositional banding, which displays micro-folding.

Below is a summary of the mineral assemblages identified under polarised microscope for each sample (Table 8).

| SAMPLE | MINERAL ASSEMBLAGE |
|---|---|
| DM08-06 | bi + mu + tml + q + pl + ilm |
| DM08-07 | bi + mu + tml + pl + q + ilm |
| DM08-08 | bi + mu + tml + pl + q + ilm |
| DM08-09 | bi + mu + pl + q + tml + ilm |
| DM08-10 | bi + mu + q + ilm + pl + tml |
| DM08-11 | bi + mu + q + ilm + pl + tml |
| DM08-12 | bi + mu + q + ilm + pl + tml |
| DM08-13 | bi + mu + q + ilm + pl |
| DM08-14 | bi + mu + tml + ilm + pl + q |
| DM08-52A | bi + mu + and + sill + q + ilm + pl |
| DM08-52B | bi + mu + and + sill + q + ilm + pl |
| DM08-53 | bi + mu + pl + q + tml + ilm |
| DM08-54 | bi + mu + pl + q + ilm + and + sill |
| DM08-56 | bi + mu + pl + q + tml + ilm |
| DM08-58 | bi + mu + q + tml + ilm + pl + ctd |
| DM08-62 | bi + mu + q + pl + ilm |
| DM08-63 | bi + mu + pl + q + ilm + ctd |
| DM08-64 | bi + mu + q + pl + ctd + ilm |
| DY09-16 | bi + mu + ilm + str + pl + q |
| DY09-18A | bi + mu + pl + q + g + ilm |
| DY09-18B | bi + mu + pl + q + g + ilm |
| DY09-54 | bi + mu + pl + q + g + and + str + ilm |
| DY09-56 | bi + mu + q + pl + g + and + str + ilm |
| DY09-60A | bi + mu + q + pl + ilm |
| DY09-60B | bi + mu + q + pl + ilm |
| DY09-61 | bi + mu + pl + q + tml + ilm |
| DY09-82 | bi + mu + q + pl + str + and + ctd + ilm |
| DY09-86A | bi + mu + q + pl + ilm + str + and |
| DY09-86B | bi + mu + q + pl + str + and + ilm |
| DY09-87 | bi + mu + q + pl + str + ctd + ilm |

**Table 7.** Summary of all identified mineral assemblages from microscope study of sample thin sections.

# CHAPTER 5

## MINERAL AND WHOLE ROCK GEOCHEMISTRY

### 5.1. Whole rock chemistry

The analysed samples, namely DM08-06, DM08-07, DM08-09, DM08-12, DM08-13, DM08-14, DM08-16, DM08-52, DM08-53, DM08-54, DM08-56, DM08-58, DM08-62, DM08-63, DY09-18A, DY09-18B, DY09-40, DY09-54, DY09-56, DY09-60A, DY09-60B, DY09-66, DY09-82, DY09-86B and DY09-87, have widely varying compositions as shown in Table 9. $SiO_2$ contents range from 48.52-69.51 weight % with an average composition of 60.17 %. $TiO_2$ contents vary from 0.69-2.70 weight %, while $Al_2O_3$ and $Fe_2O_3$ contents range from 13.51-26.08 and 6.68-12.60 weight %, respectively. MnO contents range from 0.03-0.12 weight %. MgO and CaO have similar contents, which range from 0.76-4.11 and 0.52-6.22 weight %, respectively. Finally, $Na_2O$ and $K_2O$ have contents varying from 0.29-2.91 and 0.09-7.70 weight %, respectively.

| | **Minimum value (weight %)** | **Maximum value (weight %)** |
|---|---|---|
| **$SiO_2$** | 48.52 | 69.51 |
| **$TiO_2$** | 0.69 | 2.70 |
| **$Al_2O_3$** | 13.51 | 26.08 |
| **$Fe_2O_3$** | 6.68 | 12.60 |
| **MnO** | 0.03 | 0.12 |
| **MgO** | 0.76 | 4.11 |
| **CaO** | 0.52 | 6.22 |
| **$Na_2O$** | 0.29 | 2.91 |
| **$K_2O$** | 0.09 | 7.70 |

**Table 9.** Minimum and maximum values of major oxide bulk-rock weight percentages of all samples analysed by X-ray fluorescence spectroscopy.

Most of the analysed samples were sampled from the Silverton Formation. DY09-18A and DY09-18B were collected from the Timeball Hill Formation and samples DY09-82, DY09-86B and DY09-87 were sampled from the Penge Formation. The samples from the Silverton Formation have compositional ranges similar to those described above. The samples from the Silverton Formation only differ from the ranges described above in their maximum weight % $Al_2O_3$ (25.90 compared to 26.08), minimum weight % MgO (1.34 compared to 0.76), maximum weight percentages of CaO (2.94

compared to 6.22) and $Na_2O$ (1.86 compared to 2.91) and minimum weight % $K_2O$ (2.16 compared to 0.09) (Table 10).

| | Minimum value (weight %) | Maximum value (weight %) | Average composition (weight %) |
|---|---|---|---|
| **$SiO_2$** | 48.52 | 69.51 | 60.82 |
| **$TiO_2$** | 0.69 | 2.70 | 0.96 |
| **$Al_2O_3$** | 13.51 | 25.90 | 17.92 |
| **$Fe_2O_3$** | 6.68 | 12.60 | 8.99 |
| **MnO** | 0.03 | 0.12 | 0.07 |
| **MgO** | 1.34 | 4.11 | 2.83 |
| **CaO** | 0.52 | 2.94 | 1.09 |
| **$Na_2O$** | 0.29 | 1.86 | 1.01 |
| **$K_2O$** | 2.16 | 7.70 | 4.21 |

**Table 10.** Minimum, maximum and average values of major oxide bulk-rock weight percentages of all Silverton Formation samples.

The Timeball Hill samples are inferred to be from the Upper Timeball Hill Shale Member. These samples have $SiO_2$ contents of 59.87 and 60.31 weight %. $TiO_2$ contents are 0.78 and 0.83 weight %, $Al_2O_3$ contents 18.63 and 17.79 weight % and $Fe_2O_3$ contents are 7.37 and 7.14 weight %. MnO contents are 0.07 and 0.09 weight %. MgO contents are 0.79 and 0.76 weight % and CaO contents 6.07 and 6.22 weight %. Finally, $Na_2O$ contents are 2.91 and 2.86 weight % and $K_2O$ contents 0.12 and 0.09 weight %. These, as well as their average weight percentages, are illustrated in Table 11.

| | DY09-18A (weight %) | DY09-18B (weight %) | Average composition (weight %) |
|---|---|---|---|
| **$SiO_2$** | 59.87 | 60.31 | 60.09 |
| **$TiO_2$** | 0.78 | 0.83 | 0.80 |
| **$Al_2O_3$** | 18.63 | 17.79 | 18.21 |
| **$Fe_2O_3$** | 7.37 | 7.14 | 7.25 |
| **MnO** | 0.07 | 0.09 | 0.08 |
| **MgO** | 0.79 | 0.76 | 0.78 |
| **CaO** | 6.07 | 6.22 | 6.15 |
| **$Na_2O$** | 2.91 | 2.86 | 2.88 |
| **$K_2O$** | 0.12 | 0.09 | 0.10 |

**Table 11.** Major oxide bulk-rock weight percentages of samples DY09-18A and DY09-18B with corresponding average compositions.

The Penge Formation samples (DY09-82, DY09-86B and DY09-87) have markedly lower $SiO_2$, MgO, CaO and $Na_2O$ contents than the average for all the other samples. Furthermore, these samples have above average contents of $Al_2O_3$ and $Fe_2O_3$ as compared to the average for all the other samples. The major element compositions of the Penge Formation samples are shown in Table 12.

| | **Minimum value (weight %)** | **Maximum value (weight %)** | **Average composition (weight %)** |
|---|---|---|---|
| $SiO_2$ | 54.81 | 56.96 | 55.91 |
| $TiO_2$ | 0.77 | 0.85 | 0.81 |
| $Al_2O_3$ | 23.39 | 26.08 | 24.38 |
| $Fe_2O_3$ | 10.08 | 10.70 | 10.43 |
| MnO | 0.03 | 0.05 | 0.04 |
| MgO | 0.78 | 0.99 | 0.89 |
| CaO | 0.54 | 0.59 | 0.56 |
| $Na_2O$ | 0.39 | 0.87 | 0.66 |
| $K_2O$ | 3.40 | 3.86 | 3.56 |

**Table 12.** Major oxide bulk-rock weight percentages of samples DY09-82, DY09-86B and DY09-87 with corresponding average compositions.

The average compositions of the Silverton Formation samples can be compared to the Average Silverton Formation shale composition of Reczco (1994) (Table 13). For the comparisons the major oxide compositions of DY09-60A and DY09-60B were replaced by their collective average, because they had been a coherent mass before sampling. Comparing the Silverton Formation samples to the Average Silverton Formation shale of Reczco (1994) shows similarity between these two datasets. Especially good agreement is found in terms of $SiO_2$-, MnO- and $Na_2O$ contents. The average $SiO_2$, MnO and $Na_2O$ contents of the Silverton samples are 60.88, 0.07 and 1.00 weight %, respectively, while those of Reczco (1994) are 60.49, 0.09 and 1.25 weight %, respectively. However, these two datasets show appreciable discrepancy in terms of CaO and $K_2O$ contents. The Silverton pelites have average CaO and $K_2O$ contents of 1.12 and 4.13 weight %, respectively, while those of Reczco (1994) are 1.73 and 2.44 weight %, respectively.

| | **Average composition (weight %)** | **Standard Deviation** | **Reczco (1994) Average Silverton Shale composition (weight %)** | **Reczco (1994)'s Standard deviation** |
|---|---|---|---|---|
| **$SiO_2$** | 60.88 | 6.03 | 60.49 | 7.02 |

| | | | | |
|---|---|---|---|---|
| **$TiO_2$** | 0.96 | 0.52 | 0.69 | 0.24 |
| **$Al_2O_3$** | 17.92 | 2.94 | 15.75 | 3.85 |
| **$Fe_2O_3$** | 8.93 | 1.84 | 6.86 | 3.53 |
| **MnO** | 0.07 | 0.02 | 0.09 | 0.07 |
| **MgO** | 2.84 | 0.60 | 3.24 | 2.95 |
| **CaO** | 1.12 | 0.63 | 1.73 | 3.08 |
| **$Na_2O$** | 1.00 | 0.51 | 1.25 | 1.24 |
| **$K_2O$** | 4.13 | 1.71 | 2.44 | 1.14 |

**Table 13.** Comparison of average major element compositions of all Silverton Formation samples to the Average Silverton Formation shale compositions of Reczco (1994).

When the Timeball Hill Formation samples are compared with the Average Upper Timeball Formation shales of Reczco (1994) (Table 14) good agreement is found in terms of $SiO_2$, $TiO_2$ and MgO contents and considerable differences are found in terms of CaO, $Na_2O$ and $K_2O$ contents. The average $SiO_2$, $TiO_2$ and MgO contents of the Timeball Hill samples are 60.09, 0.80 and 0.78 weight %, respectively, while those of Reczco (1994) are 59.03, 0.70 and 0.87 weight %, respectively. The Timeball Hill samples have average CaO, $Na_2O$ and $K_2O$ contents of 6.15, 2.88 and 0.10, respectively, while those of Reczco (1994) are 0.29, 0.62 and 3.20, respectively.

| | **Average composition (weight %)** | **Reczco (1994) Average Upper Timeball Shale composition (weight %)** |
|---|---|---|
| $SiO_2$ | 60.09 | 59.03 |
| $TiO_2$ | 0.80 | 0.70 |
| $Al_2O_3$ | 18.21 | 20.39 |
| $Fe_2O_3$ | 7.25 | 8.36 |
| MnO | 0.08 | 0.03 |
| MgO | 0.78 | 0.87 |
| CaO | 6.15 | 0.29 |
| $Na_2O$ | 2.88 | 0.62 |
| $K_2O$ | 0.10 | 3.20 |

**Table 14.** Comparison of average major element compositions of all Timeball Hill Formation samples to the Average Upper Timeball Hill Formation shale compositions of Reczco (1994).

The above-mentioned compositional relations for all samples analysed for bulk composition are graphically represented in Figs. 38 to 52. These are binary diagrams of bulk rock composition for all samples (grouped according to formation) compared to the Average Silverton Shale compositions of Reczco (1994).

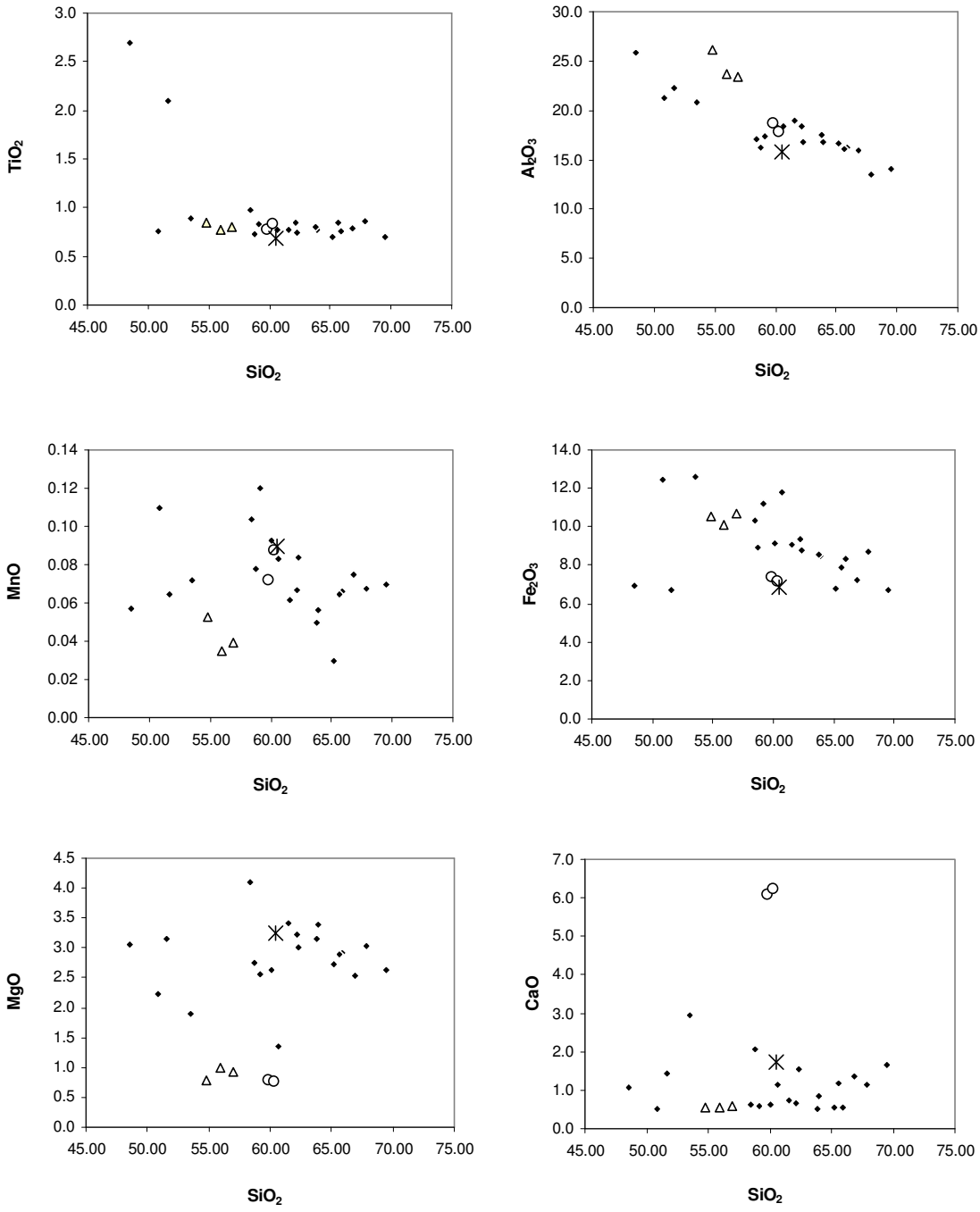


**Figs. 38 to 43.** Binary diagrams of major oxide compositions for all samples compared to the Average Silverton Shale composition of Reczco (1994). The average shale compositions of Reczco (1994) are represented by the asterisks. Samples from the Silverton, Timeball Hill and Penge formations are represented by black diamonds, white octagons and white triangles, respectively.

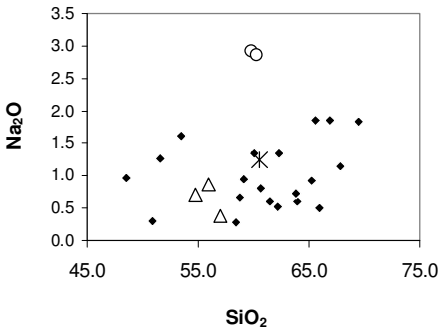


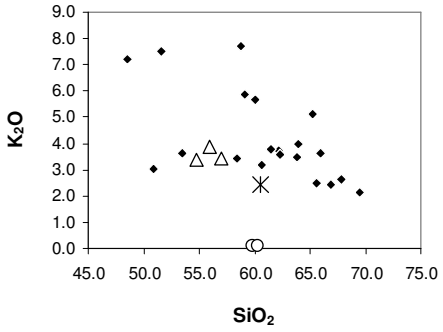


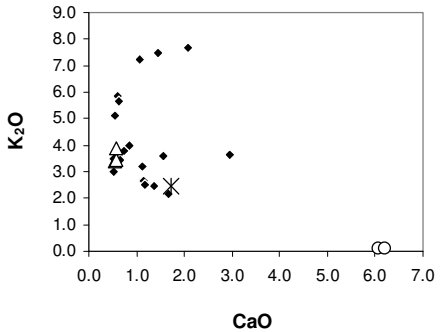


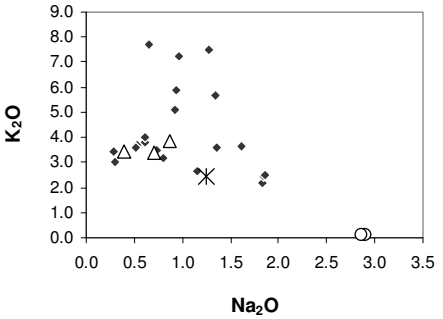


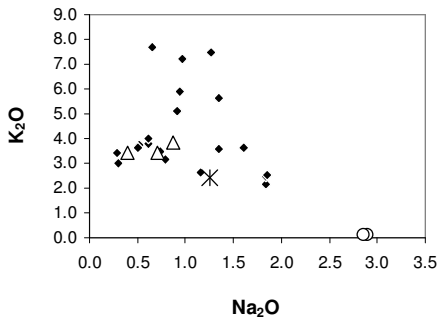


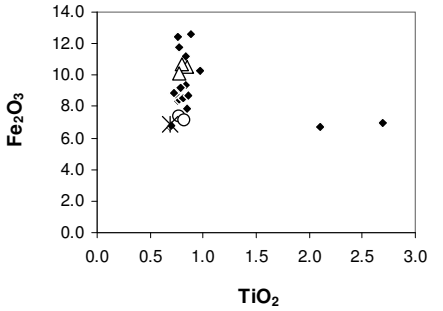


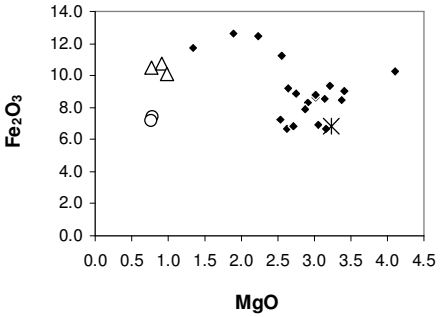


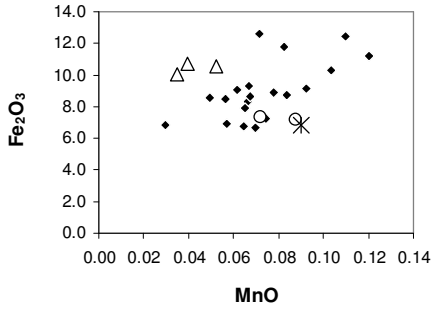


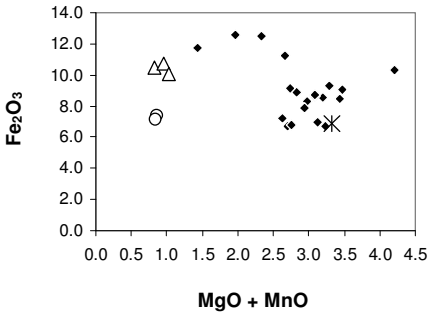


**Figs. 44 to 52.**
Binary diagrams of major oxide compositions for all samples compared to the Average Silverton Shale composition of Reczco (1994). The average shale compositions of Reczco (1994) are represented by the asterisks. Samples from the Silverton, Timeball Hill and Penge formations are represented by black diamonds, white octagons and white triangles, respectively.

In Figs. 38 to 52 the Silverton Formation samples can be seen to have a wide spread of compositions in terms major oxides. While their average compositions may be very similar to the Average Silverton Shale composition of Reczco (1994), some of these samples' major oxide chemistries diverge significantly the Average Silverton Shale composition of Reczco (1994) (Figs. 38 to 52). For most major oxide contents the Silverton Formation samples have relatively evenly spread compositions between maximum and minimum values, however Figs. 38 and 49 show that, except for two samples, all the Silverton Formation samples have very similar $TiO_2$ contents.

In Figs. 38 to 40 it can be seen that the two Timeball Hill Formation samples have $SiO_2$, $TiO_2$, $Al_2O_3$ and MnO contents very similar to the majority of the Silverton Formation samples. These two samples have significantly lower MgO and $K_2O$ contents than the Silverton samples (Figs. 42 and 45). Conversely, the Timeball Hill samples have markedly higher CaO and $Na_2O$ contents than the Silverton samples (Figs. 43 and 44).

The Penge Formation samples plot markedly separate from the majority of the Silverton Formation samples in terms of $Al_2O_3$, MgO and, to a lesser extent, MnO (Figs. 39, 40, 42, 51 and 52). These differences are lower $Al_2O_3$ and MnO contents- and higher MgO contents than the majority of Silverton samples. Finally, the Penge samples plot similarly to the majority of Silverton samples in terms of $TiO_2$, CaO and $K_2O$ (Figs. 38, 45, 46, 47, 48 and 49).

## 5.2. Mineral chemistry

The microprobe data of all analysed samples, namely DM08-52B, DY09-54, DY09-56, DY09-82 and DY09-87, are shown in Tables A3-1 and A3-2 (Appendix A). A description of these samples' mineral chemistries now follows.

DM08-52B

*Biotite*

The number of $Fe^{2+}$ and $Fe^{3+}$ atoms per formula unit (a.p.f.u.) (i.e. per 11 oxygens) range between 1.03-0.90 and 0.10-0.11, respectively. $Al^{3+}$ ranges between 1.73-1.82 a.p.f.u., while $Ti^{4+}$ and $Mg^{2+}$ have values ranging between 0.09-0.17 and 1.06-1.31 a.p.f.u., respectively. Fig. 53 shows how the analysed biotites plot roughly between eastonite/syderophyllite and phlogopite/annite compositions on a SAM diagram. The $X_{Fe}$

[where $X_{Fe}$ = Fe/(Fe+Mg)] and $X_{Na}$ [where $X_{Na}$ = Na/(Na+K)] values of the analysed biotites range between 0.41-0.49 and 0.02-0.05, respectively. Finally, the biotites had $Z_{Ti}$ [where $Z_{Ti}$ = Ti/(Fe+Mg)] values ranging from 0.04-0.08 and Fig. 54 shows a plot of $Z_{Ti}$ versus $X_{Fe}$ for all analysed biotites.

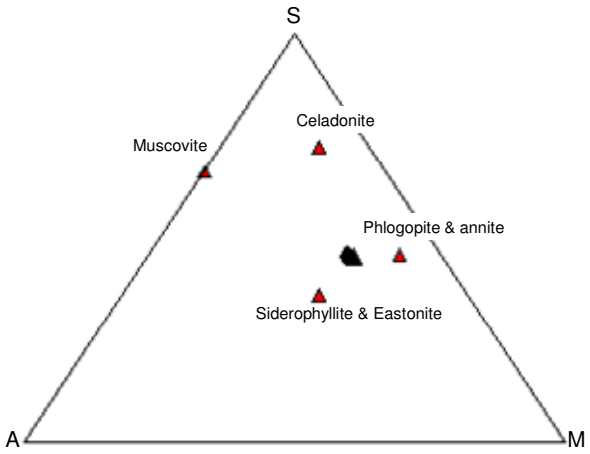


**Fig. 53.** Plot of biotite compositions of sample DM08-52B on the SAM diagram.

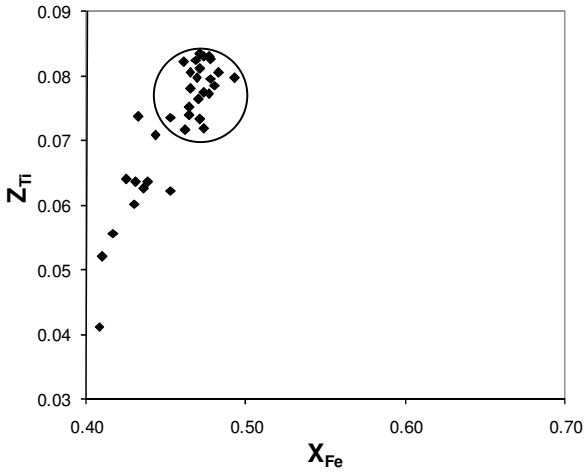


**Fig. 54.** Plot of $Z_{Ti}$ versus $X_{Fe}$ for biotites of DM08-52B. Note the concentration of compositions within the circle and the positive linear trend observed for the plotted compositions below $X_{Fe}$ = 0.45.

*Muscovite*

The analysed muscovites have $Fe^{2+}$ concentrations of 0.039-0.185 a.p.f.u. (i.e. per 11 oxygens). $Al^{3+}$, $Ti^{4+}$ and $Mg^{2+}$ in the analysed muscovites range between 2.48-2.92,

0.009-0.076 and 0.048-1.19 a.p.f.u., respectively. The muscovites are slightly phengetic with $Si^{4+}$ values of 2.93-3.36 a.p.f.u., Fe+Mg values between 0.09-0.38 per 11 oxygens and Na/(Na+K+Ca) values between 0.10-0.12. The $X_{Fe}$ values of the analysed muscovites range between 0.39-0.51 and the $X_{Na}$ values between 0.09-0.13. Fig. 55 illustrates that white micas plot close to the muscovite end-member on the SAM diagram.

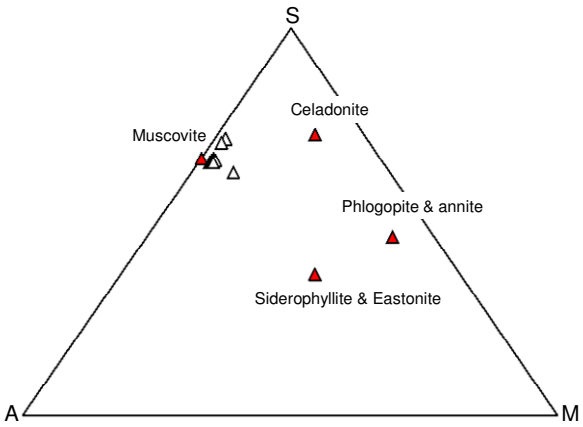


**Fig. 55.** Plot of white mica compositions of DM08-52B on the SAM diagram.

*K-feldspar*

Only two crystals of K-feldspar were analysed owing to the mineral's low concentration in sample DM08-52. Both of these had calcium concentrations below the detection limit of the electron microprobe and they had K/(Na+K+Ca) values of 0.810 and 0.892 respectively, thus plotting close to the orthoclase end-member on an albite-orthoclase-anorthite ternary diagram (Fig. 56).

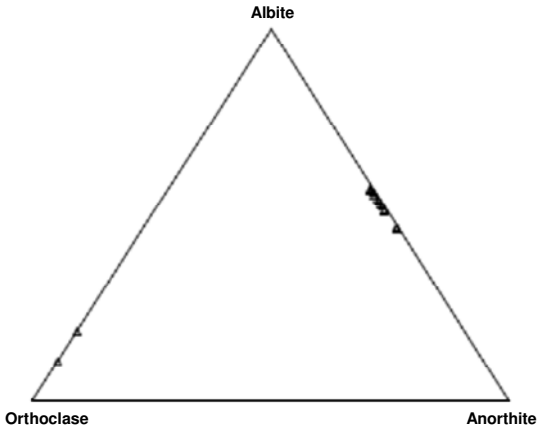


**Fig. 56.** Plot of feldspar compositions of sample DM08-52B on the Al-Or-An ternary diagram. All plagioclases plot roughly between the albite and anorthite end-members and the two probed K-feldspars plot close to the orthoclase end-member.

*Plagioclase*

All analysed plagioclase crystals have low K/(Na+K+Ca) values ranging between 0.003-0.008. Na/(Na+K+Ca) values range between 0.459-0.571 and the probed grains plot centrally between albite and anorthite end-members on an albite-orthoclase-anorthite triangular diagram (Fig. 56).

DY09-54

*Biotite*

Sample DY09-54 has $Fe^{2+}$ and $Fe^{3+}$ concentrations ranging between 1.19-2.02 and 0.13-0.22 a.p.f.u., respectively. $Al^{3+}$ cations ranges between 1.79-1.91 a.p.f.u., while the $Ti^{4+}$ and $Mg^{2+}$ range between values of 0.00-0.11 and 0.18-0.85 a.p.f.u., respectively. Fig. 57 shows that the majority of analyzed biotites plot roughly between eastonite & syderophyllite and phlogopite & annite compositions on the SAM diagram. The $X_{Fe}$ and $X_{Na}$ values of the analysed biotites range between 0.61-0.92 and 0.00-0.34, respectively. Finally, the analyzed biotites have $Z_{Ti}$ values ranging from 0.00 to 0.05 and Fig. 58 shows a plot of $Z_{Ti}$ versus $X_{Fe}$ for all analysed biotites.

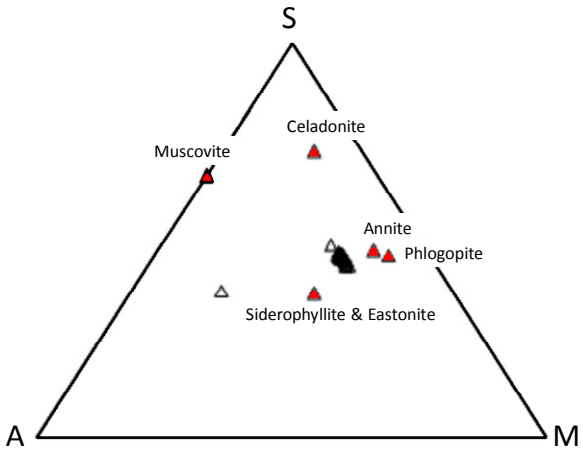


**Fig. 57.** Plot of biotite compositions of sample DY09-54 on the SAM.

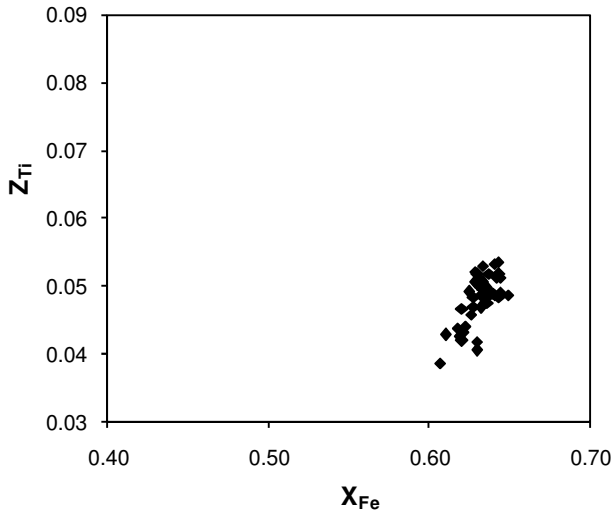


**Fig. 58.** Plot of $Z_{Ti}$ versus $X_{Fe}$ for biotites of sample DY09-54.

*Muscovite*

The analysed muscovites have $Fe^{2+}$ values of 0.01-0.23 a.p.f.u.. $Al^{3+}$, $Ti^{4+}$ and $Mg^{2+}$ in the analysed muscovites have values ranging between 2.02-2.92, 0.00-0.03 and 0.00-0.12 a.p.f.u., respectively. $Si^{4+}$ values range from 3.00-3.79 a.p.f.u., while Fe+Mg- and $X_{Fe}$ values range between 0.01-0.36 a.p.f.u. and 0.51-1.00, respectively. Na/(Na+K+Ca) and $X_{Na}$ values range between 0.15-0.56 and 0.15-0.99, respectively. Fig. 59 shows how close to muscovite the probed white-micas plot on a SAM diagram, although two are markedly phengetic.

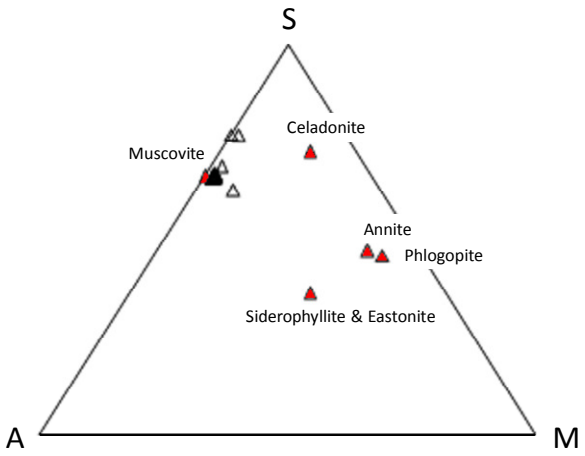


**Fig. 59.** Plot of white mica compositions of sample DY09-54 on the SAM diagram.

*Garnet*

Traverses across garnets from samples DY09-54 and -56 were analysed in order to discern any variations from core to rim. Zoning profiles for DY09-54 reveal the following: $X_{Alm}$ ranges from 0.787-0.827 near the rims to 0.749-0.796 in the cores, $X_{Grs}$ from 0.044-0.061 near the rims to 0.043-0.058 in the cores, $X_{Spss}$ from 0.046-0.089 near the rims to 0.082-0.122 in the cores, $X_{And}$ ranging from 0.000-0.018 near the rims to 0.001-0.010 in the cores, $X_{Pyr}$ ranging from 0.063-0.076 near the rims to 0.067-0.074 in the cores and negligible concentrations of uvarovite (Figs. 60-67). Compositional cross-sections (i.e. zoning profiles) of probed garnets of DY09-54 are shown in Figs. 60-67.

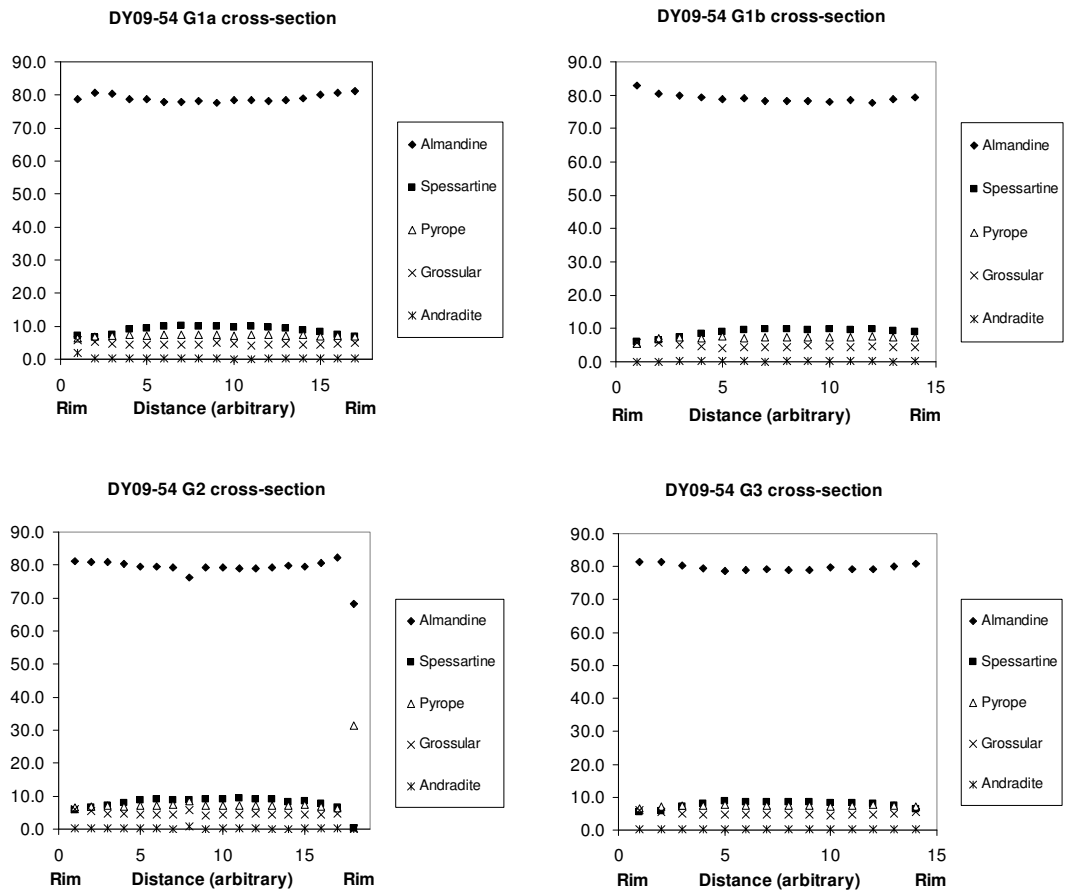


**Figs. 60 to 63.** Diagrams of cross-section microprobe analyses through garnets G1, G2 and G3 of sample DY09-54. Note that the y-axes represent mole percentages.

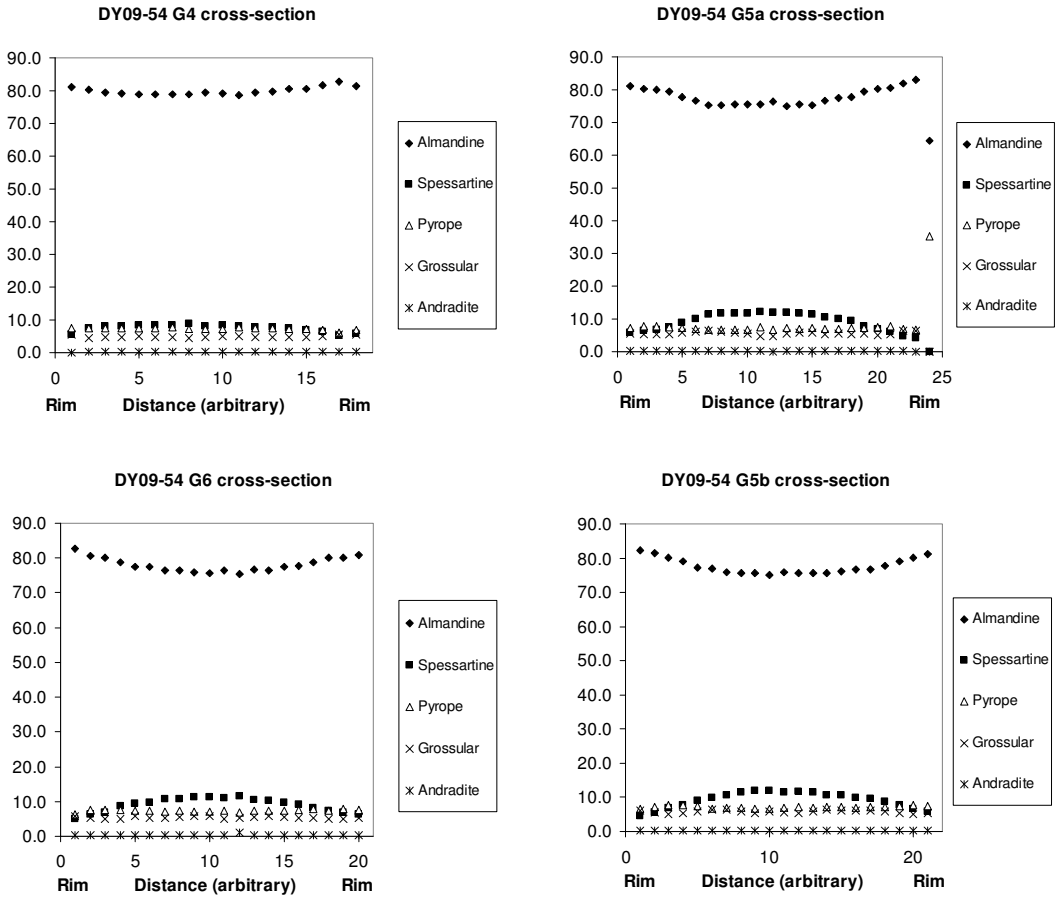


**Figs. 64 to 67.** Diagrams of cross-section microprobe analyses through garnets G4, G5 and G6 of sample DY09-54. Note that the y-axes represent mole percentages.

*Staurolite*

The staurolite grains of DY09-54 have $Fe^{3+}$ and $Zn^{2+}$ concentrations ranging from 1.65-2.00 and 0.07-0.09 a.p.f.u. (i.e. per 23 oxygens), respectively. $X_{Fe}$ values range from 0.83-0.85, while $X_{Mg}$ and $X_{Zn}$ range from 0.10-0.13 and 0.031-0.045, respectively.

*Plagioclase*

All plagioclase crystals have low K/(Na+K+Ca) values that range between 0.002-0.053. These grains plot roughly one third of the way to the Anorthite apex from the Albite apex on an albite-orthoclase-anorthite ternary diagram (Fig. 68). Furthermore, these crystals have Na/(Na+K+Ca) and Ca/(Na+K+Ca) values ranging between 0.571-0.651 and 0.345-0.427, respectively.

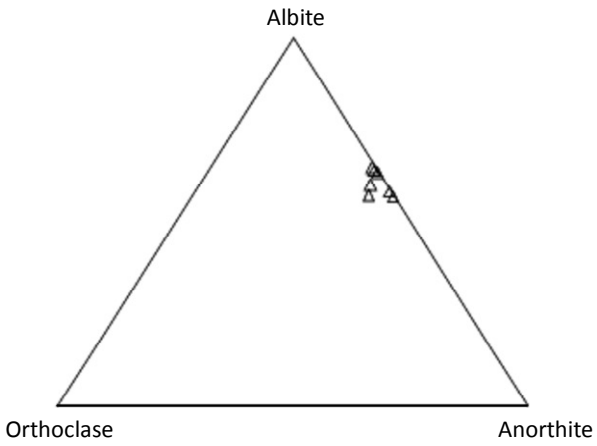


**Fig. 68.** Plot of feldspars of sample DY09-54 on the Al-Or-An triangular diagram.

DY09-56

*Biotite*

The analyzed biotites of DY09-56 have $Fe^{2+}$ and $Fe^{3+}$ concentrations ranging between 1.29-1.42 and 0.14-0.16 a.p.f.u., respectively. $Al^{3+}$ ranges between 1.66-1.94 a.p.f.u., while the $Ti^{4+}$ and $Mg^{2+}$ range between values of 0.08-0.11 and 0.66-0.78 a.p.f.u., respectively. Fig. 69 shows that all but one of the probed biotites plot between eastonite & syderophyllite and phlogopite & annite compositions. The $X_{Fe}$ and $X_{Na}$ values of the analysed biotites range between 0.64-0.70 and 0.04-0.06, respectively. Finally, the analyzed biotites have $Z_{Ti}$ values ranging from 0.04-0.05 and Fig. 70 shows a plot of $Z_{Ti}$ versus $X_{Fe}$ for all analysed biotites.

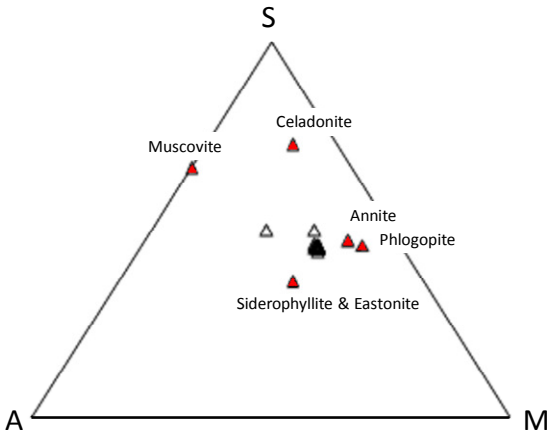


**Fig. 69.** Plot of biotite compositions of sample DY09-56 on the SAM diagram.

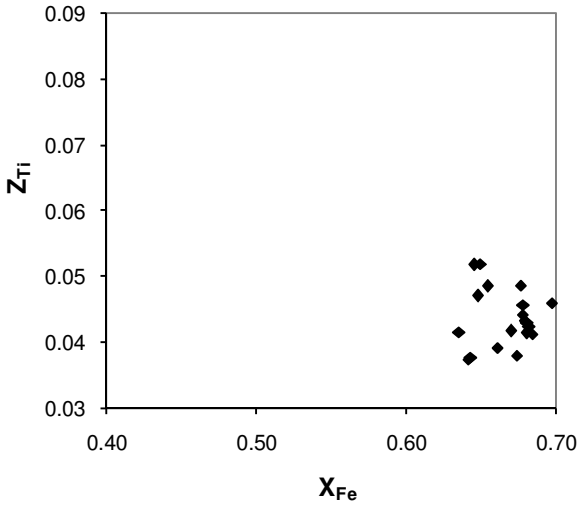


**Fig. 70.** Plot of $Z_{Ti}$ versus $X_{Fe}$ for biotites of DY09-56.

*Garnet*

Zoning profiles for garnets of DY09-56 reveal the following: $X_{Alm}$ range from 0.791-0.803 near the rims to 0.785-0.795 in the cores, $X_{Grs}$ from 0.043-0.052 near the rims to 0.040-0.043 in the cores, $X_{Spss}$ from 0.095-0.102 near the rims to 0.098-0.103 in the cores, $X_{And}$ ranging from 0.000-0.003 near the rims to 0.001-0.002 in the cores, $X_{Pyr}$ ranging from 0.049-0.065 near the rims to 0.063-0.070 in the cores and negligible concentrations of uvarovite (Figs. 71-74). Compositional cross-sections (i.e. zoning profiles) of probed garnets of DY09-56 are shown in Figs. 71-74.

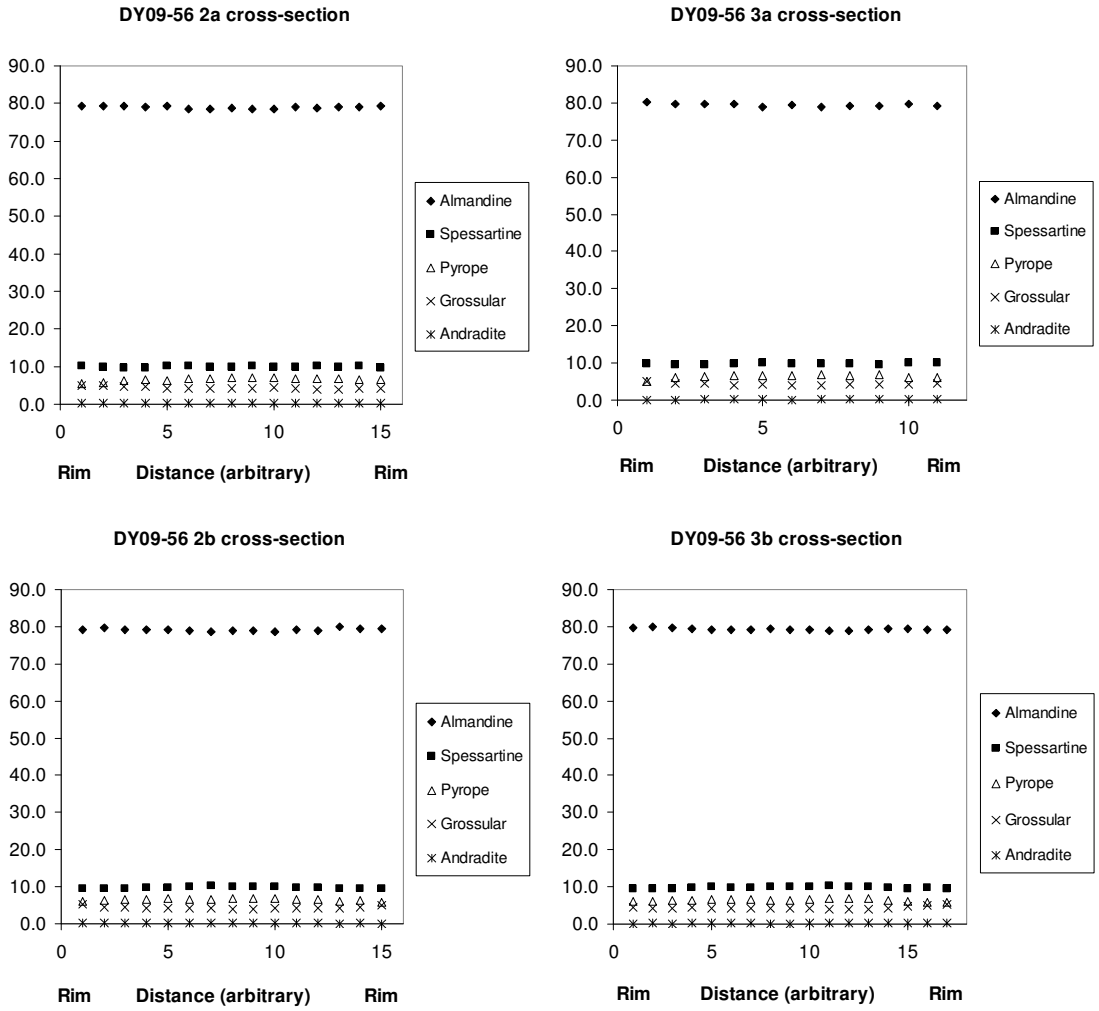


**Figs. 71 to 74.** Diagrams of cross-section microprobe analyses through garnets G1 and G2 of sample DY09-56. Note that the y-axes represent mole percentages.

*Staurolite*

The staurolite grains of DY09-56 have $Fe^{3+}$ and $Zn^{2+}$ concentrations ranging from 1.61-1.79 and 0.02-0.03 a.p.f.u., respectively. $X_{Fe}$ values range from 0.85-0.88, while $X_{Mg}$ and $X_{Zn}$ range from 0.10-0.13 and 0.008-0.014, respectively.

DY09-82

*Biotite*

Biotites of DY09-82 have $Fe^{2+}$ and $Fe^{3+}$ concentrations ranging between 1.33-1.50 and 0.15-0.17 a.p.f.u., respectively. $Al^{3+}$ ranges between 1.78-1.87 a.p.f.u., while the $Ti^{4+}$ and $Mg^{2+}$ concentrations range between 0.09-0.12 and 0.74-0.83 a.p.f.u., respectively. Fig.

75 shows that all but one of the analyzed biotites plot closest to the annite end-member and roughly between eastonite & syderophyllite and phlogopite & annite on the SAM diagram. The $X_{Fe}$ and $X_{Na}$ values of the analysed biotites range between 0.65-0.68 and 0.04-0.06, respectively. Finally, the analyzed biotites have $Z_{Ti}$ values ranging from 0.04 to 0.06 and Fig. 76 shows a plot of $Z_{Ti}$ versus $X_{Fe}$ for all analysed biotites.

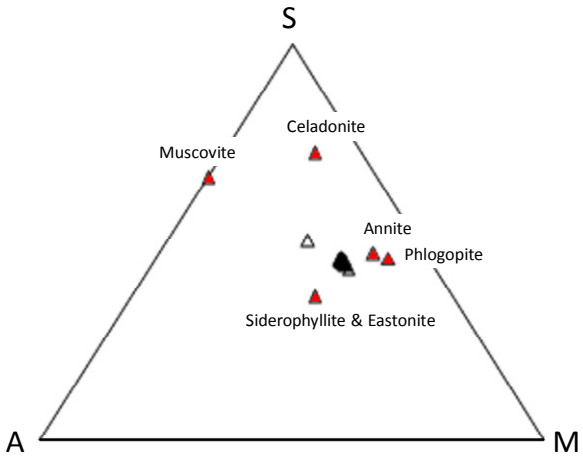


**Fig. 75.** Plot of biotite compositions of sample DY09-82 on the SAM diagram.

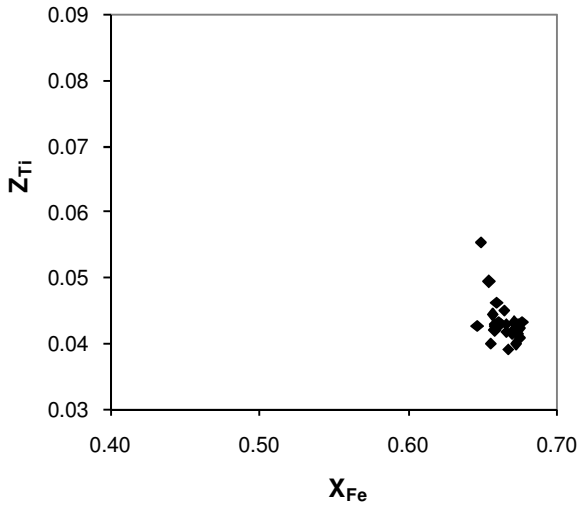


**Fig. 76.** Plot of $Z_{Ti}$ versus $X_{Fe}$ for biotites of DY09-82.

*Muscovite*

The analysed muscovites have $Fe^{2+}$ concentrations of 0.05-0.07 a.p.f.u.. $Al^{3+}$, $Ti^{4+}$ and $Mg^{2+}$ concentrations in the analysed muscovites range between 2.80-2.93, 0.01-0.01 and 0.03-0.04 a.p.f.u., respectively. $Si^{4+}$ concentrations range from 3.00-3.11 a.p.f.u., while Fe+Mg- and $X_{Fe}$ values range between 0.09-0.10 a.p.f.u. and 0.57-0.73, respectively. The Na/(Na+K+Ca) and $X_{Na}$ values both range between 0.24-0.29. Fig. 77 shows that all probed white-micas approach pure-muscovite compositions.

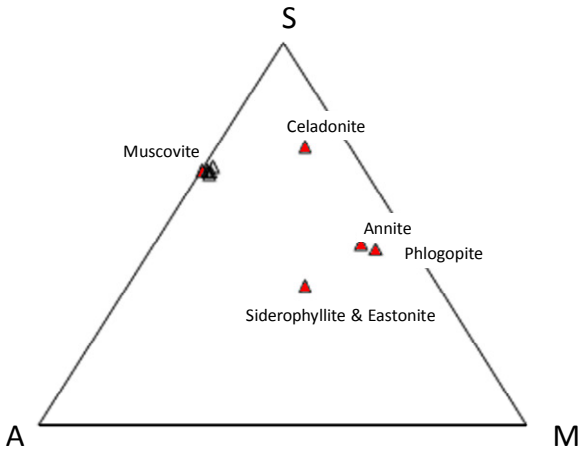


**Fig. 77.** Plot of white mica compositions of sample DY09-82 on the SAM diagram.

*Staurolite*

The staurolite grains of DY09-82 have $Fe^{3+}$ and $Zn^{2+}$ concentrations ranging from 1.68-1.82 and 0.00-0.01 a.p.f.u., respectively. $X_{Fe}$ values range from 0.87-0.90, while $X_{Mg}$ and $X_{Zn}$ range from 0.10-0.12 and 0.000-0.005, respectively.

DY09-87

*Biotite*

Biotites of DY09-82 have $Fe^{2+}$ and $Fe^{3+}$ concentrations ranging between 1.27-1.39 and 0.14-0.15 a.p.f.u., respectively. $Al^{3+}$ concentrations range between 1.80-1.85 a.p.f.u., while the $Ti^{4+}$ and $Mg^{2+}$ range between values of 0.09-0.12 and 0.77-0.86 a.p.f.u., respectively. Fig. 78 shows that all but one of the probed biotites plot closest to an annite-composition and roughly between eastonite & syderophyllite and phlogopite & annite compositions. The $X_{Fe}$ and $X_{Na}$ values of the analysed biotites range between 0.60-0.63

and 0.02-0.06, respectively. Finally, the analyzed biotites have $Z_{Ti}$ values ranging from 0.04 to 0.06 and Fig. 79 shows a plot of $Z_{Ti}$ versus $X_{Fe}$ for all analysed biotites.

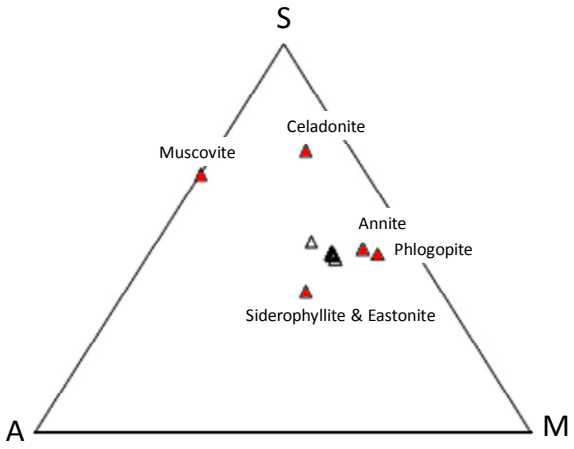


**Fig. 78.** Plot of biotite compositions of sample DY09-87 on the SAM diagram.

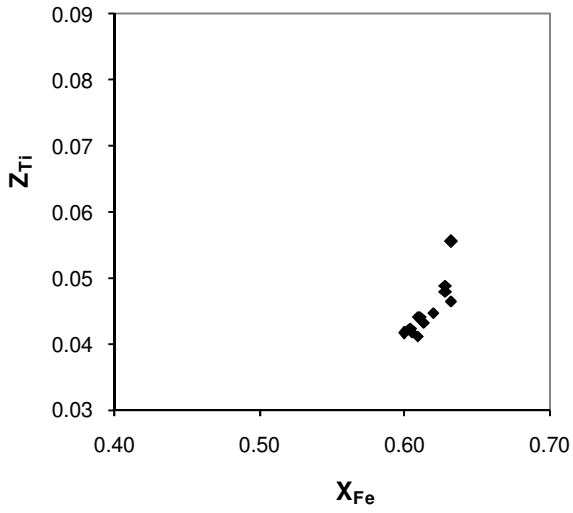


**Fig. 79.** Plot of $Z_{Ti}$ versus $X_{Fe}$ for biotites of sample DY09-87.

*Muscovite*

Only one point of a single muscovite grain was analysed for sample DY09-87. The analysed muscovite has a $Fe^{2+}$ concentration of 0.06 a.p.f.u.. $Al^{3+}$, $Ti^{4+}$, $Mg^{2+}$ and $Si^{4+}$ concentrations are 2.87, 0.01, 0.04 and 3.06 a.p.f.u., respectively. The Fe+Mg and

$X_{Fe}$ values are 0.10 and 0.60, respectively, while the Na/(Na+K+Ca) and $X_{Na}$ values are both 0.23. Fig. 80 shows that the white-mica has a near pure-muscovite composition.

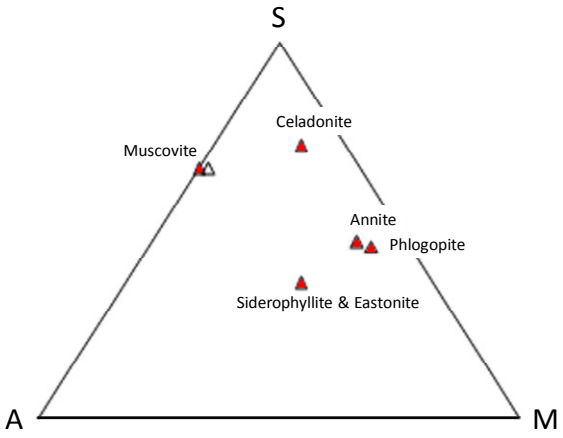


**Fig. 80.** Plot of white mica composition of sample DY09-87 on the SAM diagram.

*Staurolite*

The staurolite grains of DY09-87 have $Fe^{3+}$ and $Zn^{2+}$ concentrations ranging from 1.61-1.94 and 0.00-0.01 a.p.f.u., respectively. $X_{Fe}$ values range from 0.86-0.90, while $X_{Mg}$ and $X_{Zn}$ range from 0.09-0.14 and 0.000-0.006, respectively.

*Plagioclase*

Similar to sample DY09-54, all analysed plagioclase crystals have low K/(Na+K+Ca) values ranging between 0.001-0.016 and plot roughly one third of the way to the anorthite apex from the albite apex on an albite-orthoclase-anorthite ternary diagram (Fig. 81). These crystals have Na/(Na+K+Ca) and Ca/(Na+K+Ca) values ranging between 0.651-0.679 and 0.305-0.348, respectively.

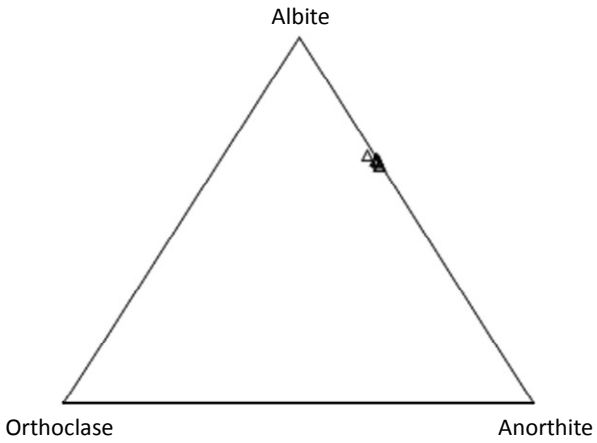


**Fig. 81.** Plot of feldspars of sample DY09-87 on the Al-Or-An ternary diagram.

# CHAPTER 6

## MINERAL EQUILIBRIA MODELING

The solid solution phases used in modelling have been named in the Methodology subchapter. Now follow short explanations for these solid solutions (ignoring the datasets from which they originate): St(HP) = staurolite; Chl(HP) = chlorite; Opx(HP) = orthopyroxene; TiBio(HP) = Ti-Fe-Mg-Mn-bearing biotite; Gt(HP) = garnet; Ep(HP) = epidote; Ctd(HP) = chloroid; IlGHPy = ilmenite-geikielite-pyrophanite solution; hCrd = cordierite; melt(HP) = melt; feldspar = feldspar (both plagioclase- and K-feldspars) and Mica(CH2) = all species of mica. Finally, some these solid solutions are further abbreviated in the following pseudosections as follows: St(HP) = St; Chl(HP) = Chl; TiBio(HP) = TiBio; Gt(HP) = Gt; Ctd(HP) = Ctd; IlGHPy = ilm; melt(HP) = melt; Mica(CH2) = Mica.

Concerning the PT-readings taken from pseudosections note the following: Thermometric readings were taken to the nearest interval of 5 °C for single readings, while readings for temperature ranges were taken so as to exaggerate the ranges to the first outlying factor of 5 °C, e.g. if measurements gave roughly 2543-2968 bar, it was taken as 2540-2970 bar. Pressure readings were rounded off to the nearest interval of 10 bar for single readings, while readings for pressure ranges were noted so as to exaggerate the ranges to the first outlying factor of 10 bar.

### 6.1. Primary thermobarometric results

The pseudosections of two samples, that were constructed in the MnNCKFMASHT system, contained assemblage-fields matching that which was identified under microscope (Figs. 82 and 84). These samples are DY09-54 and DY09-56. For DY09-86B a pseudosection produced in the NCKFMASHT system contains an assemblage-field matching the minerals that were identified in for this sample (Fig. 86).

DY09-54:

In the pseudosection of DY09-54 the identified assemblage pl + bi + mu + q + g + and + str + oxides is represents a thin rectangular P-T field, ranging from 530-565 ºC and 2250-2970 bar (Fig. 82).

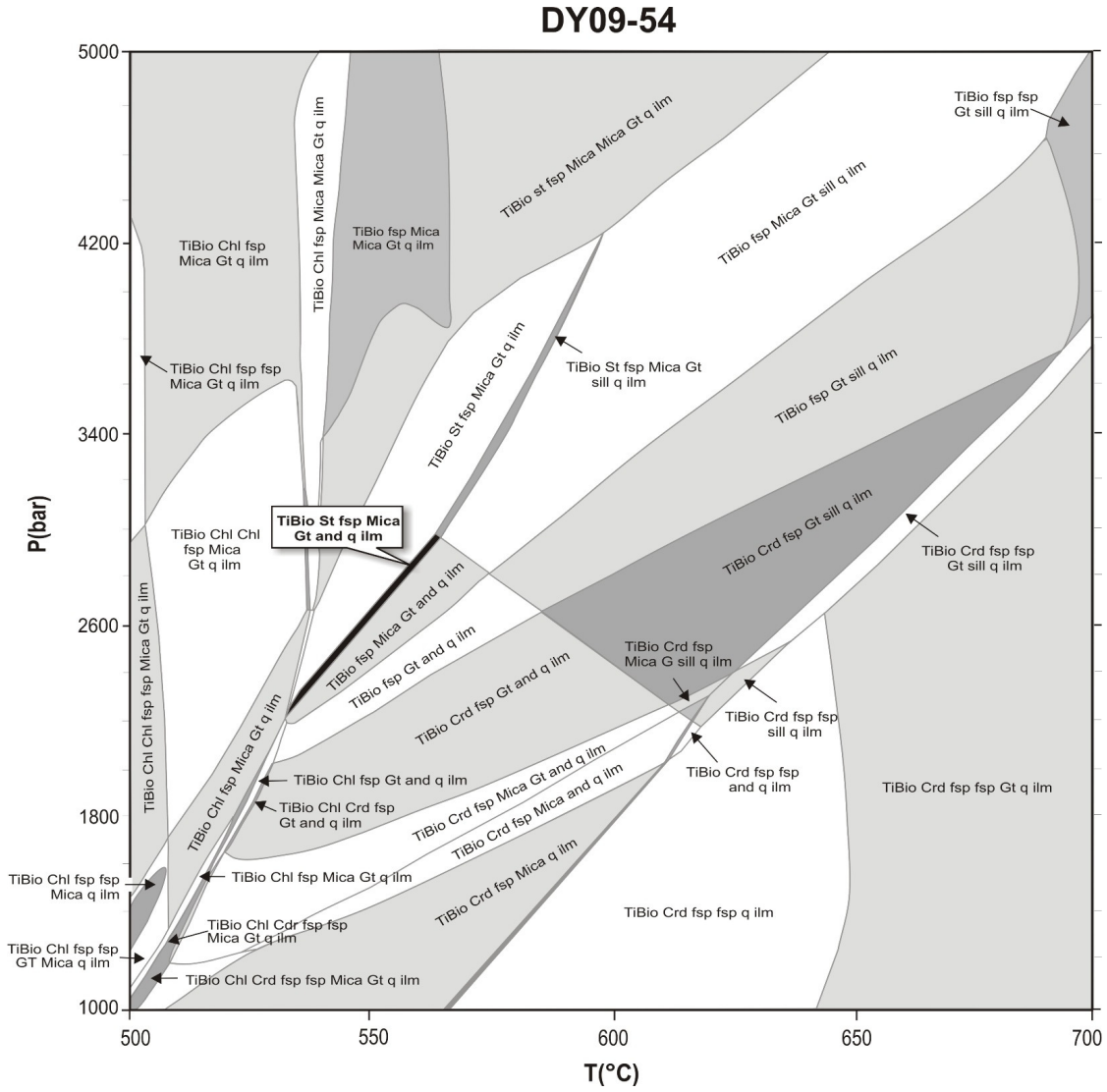


**Fig. 82.** Pseudosection of DY09-54 constructed in the MnNCKFMASKT system using Perplex. The field matching the identified mineral assemblage is filled-in with black.

Isopleths of Fe-Mg-Ca-Mn ratios in garnet, as well as Fe-Mg ratios in biotite, were constructed for the sample. The isopleth-modelling results for DY09-54 now follow:

For the garnets of DY09-54 the following isopleths were produced:

1) $Fe^{2+}/(Fe^{2+}+Mg)$, transecting through the identified mineral assemblage (pl + bi + mu + q + g + and + str + oxides) at a fraction of 0.94 and at 550 ºC and 2720 bar. Electron probe micro-analysis of this sample's garnets gave a range of 0.909-0.920, which does not overlap with the modelled isopleths.

2) $Fe^{2+}/(Fe^{2+}+Mg+Ca)$, which trend semi-parallel to the identified assemblage field. None of these isopleths, modelled at maximum resolution (0.005 intervals), cut through the assemblage field, although the fraction 0.915 nearly transects the field in its low-pressure and -temperature section. It can however be inferred that the fractions 0.913 and 0.914 would cut through the assemblage field. Electron probe micro-analysis of these garnets gave a range of 0.852-0.873, which does not overlap with the isopleths that would transect the assemblage.

3) $Fe^{2+}/(Fe^{2+}+Mg+Ca+Mn)$, transecting through the identified mineral assemblage at fractions ranging from 0.78-0.82 and at temperatures and pressures ranging over the whole assemblage's field (530-565 ºC and 2250-2970 bar). Electron probe micro-analysis of these garnets gave a range of 0.749-0.796. The isopleth range 0.78-0.795 spans 530-540 ºC and 2250-2440 bar.

4) $Ca/(Fe^{2+}+Mg+Ca+Mn)$, which trend semi-parallel to the identified assemblage field. At maximum resolution none of these isopleths cut through the assemblage field, although the fraction 0.045 nearly crosses the field in its high-pressure and -temperature section. It can however be inferred that a fraction of 0.044 would cut through the assemblage field. Electron probe micro-analysis of these garnets gave a range of 0.043-0.061.

5) $Mn/(Fe^{2+}+Mg+Ca+Mn)$, transecting through the identified mineral assemblage at fractions ranging from 0.09-0.14, which cover most of the assemblage's P-T range. Electron probe micro-analysis of these garnets gave a range of 0.081-0.122. The isopleths 0.090-0.120 cut the assemblage across the range 545-565 ºC and 2540-2970 bar (Fig. 83).

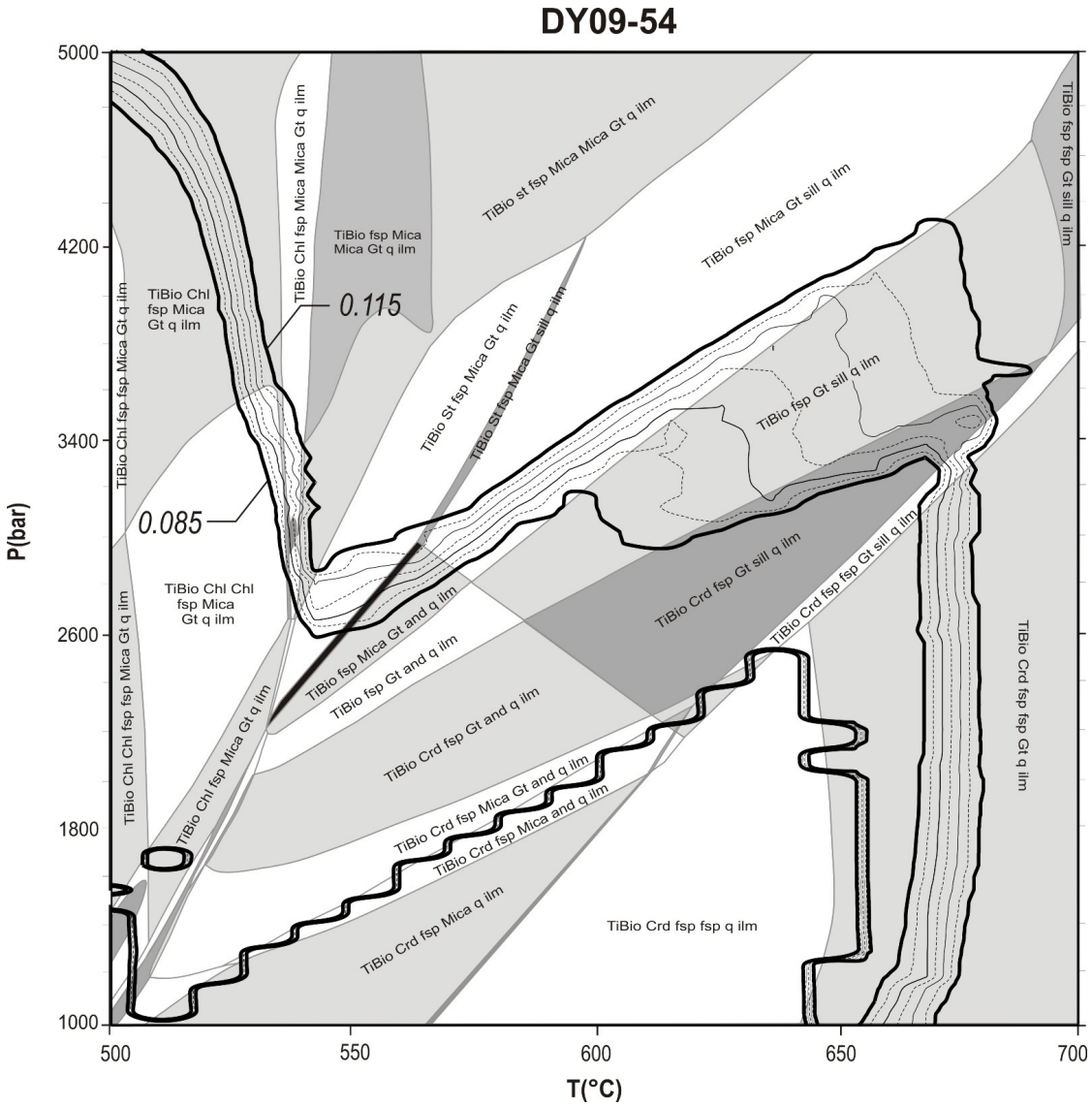


**Fig. 83.** Pseudosection of DY09-54 with isopleths of MnO/(MnO+CaO+FeO+MgO) for ratios 0.085, 0.090, 0.095, 0.100, 0.105, 0.110, 0.115 and 0.120.

For the biotites of DY09-54 isopleths of $Fe^{2+}/(Fe^{2+}+Mg)$ were constructed. These cut the identified mineral assemblage at ratios of 0.83 and 0.835 and a number of times throughout its range (530-565 ºC and 2250-2970 bar). Electron probe micro-analysis of this sample's biotites gave a range of 0.61-0.92.

DY09-56:

In the pseudosection of DY09-56 the identified assemblage q + pl + bi + mu + g + and + str + oxides is again represented by a thin rectangular P-T field, but which ranges from 530-565 ºC and 2120-2950 bar (Fig. 84).

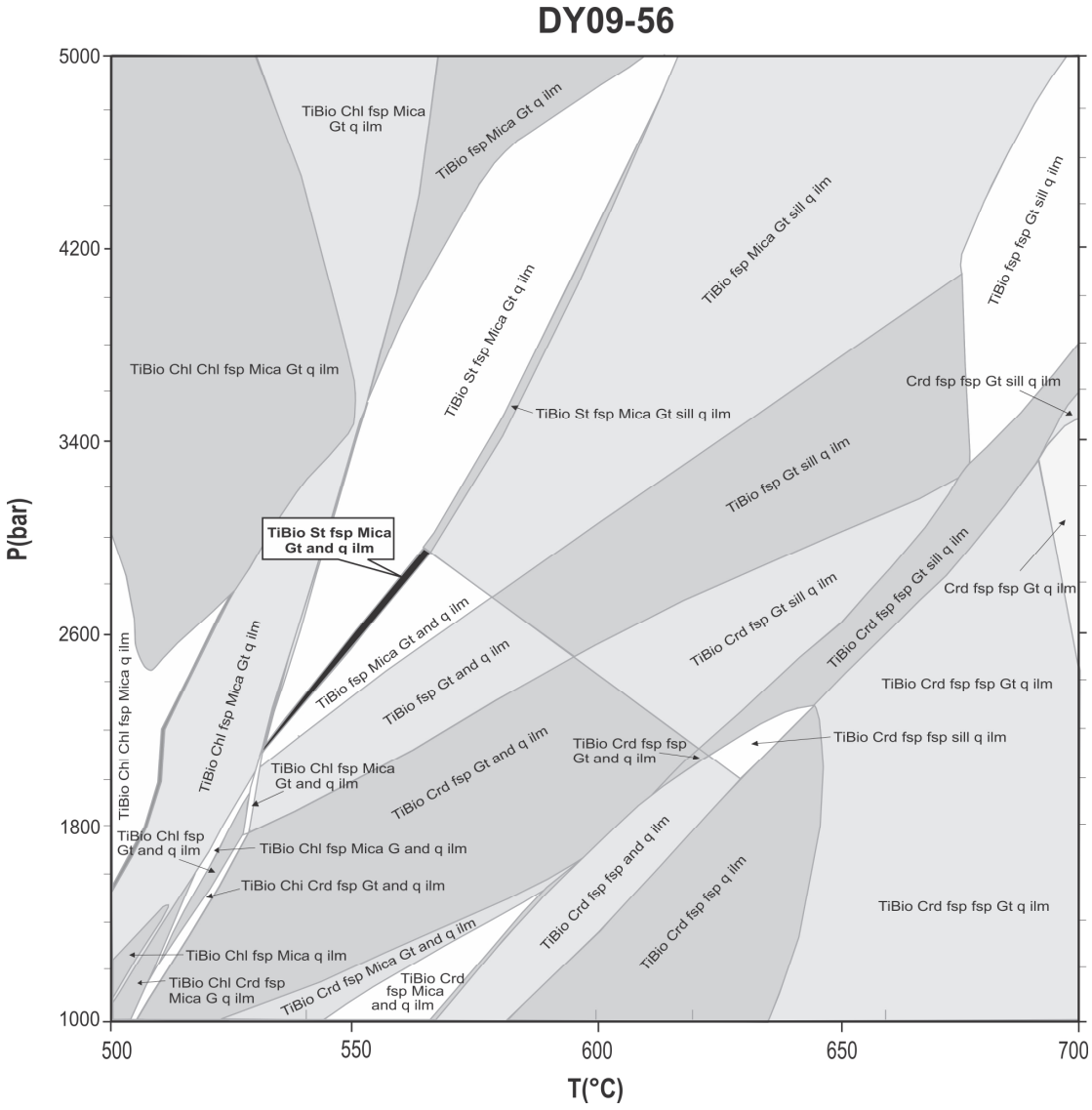


**Fig. 84.** Pseudosection of DY09-56 constructed in the MnNCKFMASKT system using Perplex. The field matching the identified mineral assemblage is filled-in with black.

For the garnets of DY09-56 similar isopleths than those for DY09-54 were produced. They are:

1) $Fe^{2+}/(Fe^{2+}+Mg)$, of which the fraction 0.965 transects through the identified mineral assemblage (q + pl + bi + mu + g + and + str + oxides) twice, at 555 ºC and 2710 bar and 565 ºC and 2910 bar, respectively. Electron probe micro-analysis of this sample's garnets gave a range of 0.918-0.927, which does not overlap with the isopleth XFe = 0.965.

2) $Fe^{2+}/(Fe^{2+}+Mg+Ca)$, where the fractions 0.920 and 0.925 transect the identified mineral assemblage at 535 ºC and 2230 bar and 540 ºC and 2360 bar, respectively. Electron probe micro-analysis of these garnets gave a range of 0.874-0.883, which does not overlap with the above-mentioned isopleths.

3) $Fe^{2+}/(Fe^{2+}+Mg+Ca+Mn)$, transecting through the identified mineral assemblage at fractions ranging from 0.80-0.84 and at temperatures and pressures ranging over the whole assemblage's field (530-565 ºC and 2120-2950 bar). Electron probe micro-analysis of these garnets gave a range of 0.785-0.795, which does not overlap with the above-mentioned isopleths.

4) $Ca/(Fe^{2+}+Mg+Ca+Mn)$, where the isopleth $Ca/(Fe^{2+}+Mg+Ca+Mn) = 0.045$ trends semi-parallel to the identified mineral assemblage and very nearly intersects it. Furthermore, the assemblage lies between the isopleths of fractions 0.045 and 0.040 and it can be inferred that the fraction 0.044 would cut through the assemblage. Electron probe micro-analysis of these garnets gave a range of 0.041-0.044.

5) $Mn/(Fe^{2+}+Mg+Ca+Mn)$, transecting through the identified mineral assemblage at a fraction of 0.10 and at 550 ºC and 2650 bar. Electron probe micro-analysis of these garnets gave a range of 0.098-0.103 (Fig. 85).

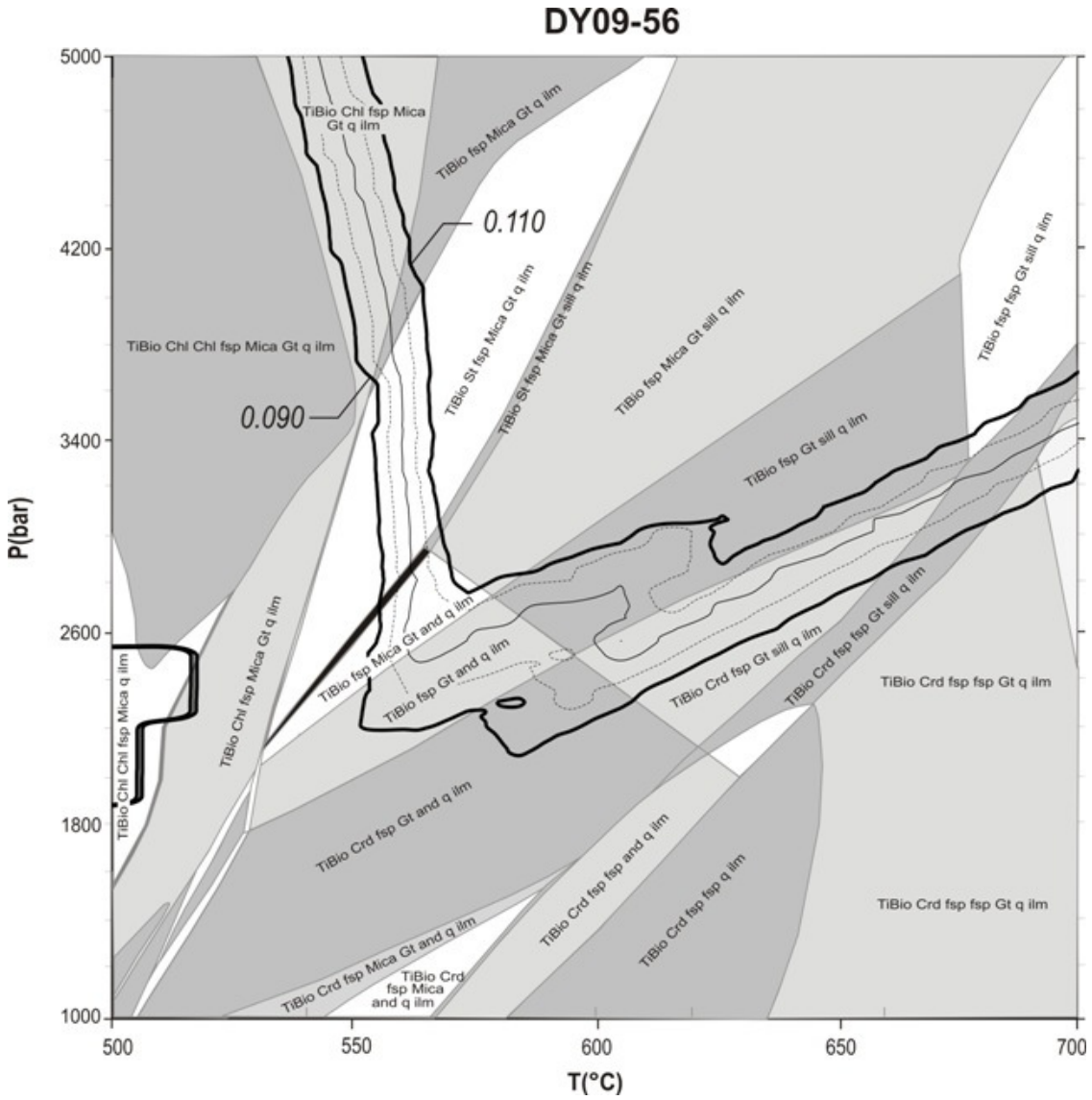


**Fig. 85.** Pseudosection of DY09-54 with isopleths of MnO/(MnO+CaO+FeO+MgO) for ratios 0.090, 0.095, 0.100, 0.105 and 0.110.

As was done for DY09-54, isopleths of $Fe^{2+}/(Fe^{2+}+Mg)$ were constructed for the biotites of DY09-56. These cut the identified mineral assemblage at a ratio of 0.86 and with a slope paralleling that of the assemblage, so that the isopleth spans the full range of the assemblage-field (530-565 ºC and 2120-2950 bar). Electron probe micro-analysis of this sample's biotites gave a range of 0.64-0.70, which does not overlap with the above-mentioned isopleth.

DY09-86B:

Modelling of DY09-86B in the MnNCKFMASHT system arguably produces an unrealistically large field of garnet-stability. However, the resultant pseudosection contains a field that matches the petrographically-identified mineral assemblage, except that it contains garnet. This nearly-matching field is restricted to 530-570 °C and 2080-2970 bar. As mentioned, when this sample is modelled in the NCKFMASHT system a field exactly matching that observed under microscope is obtained (Fig. 86). This field is restricted to 530-570 °C and 2080-2930 bar (Fig. 86).

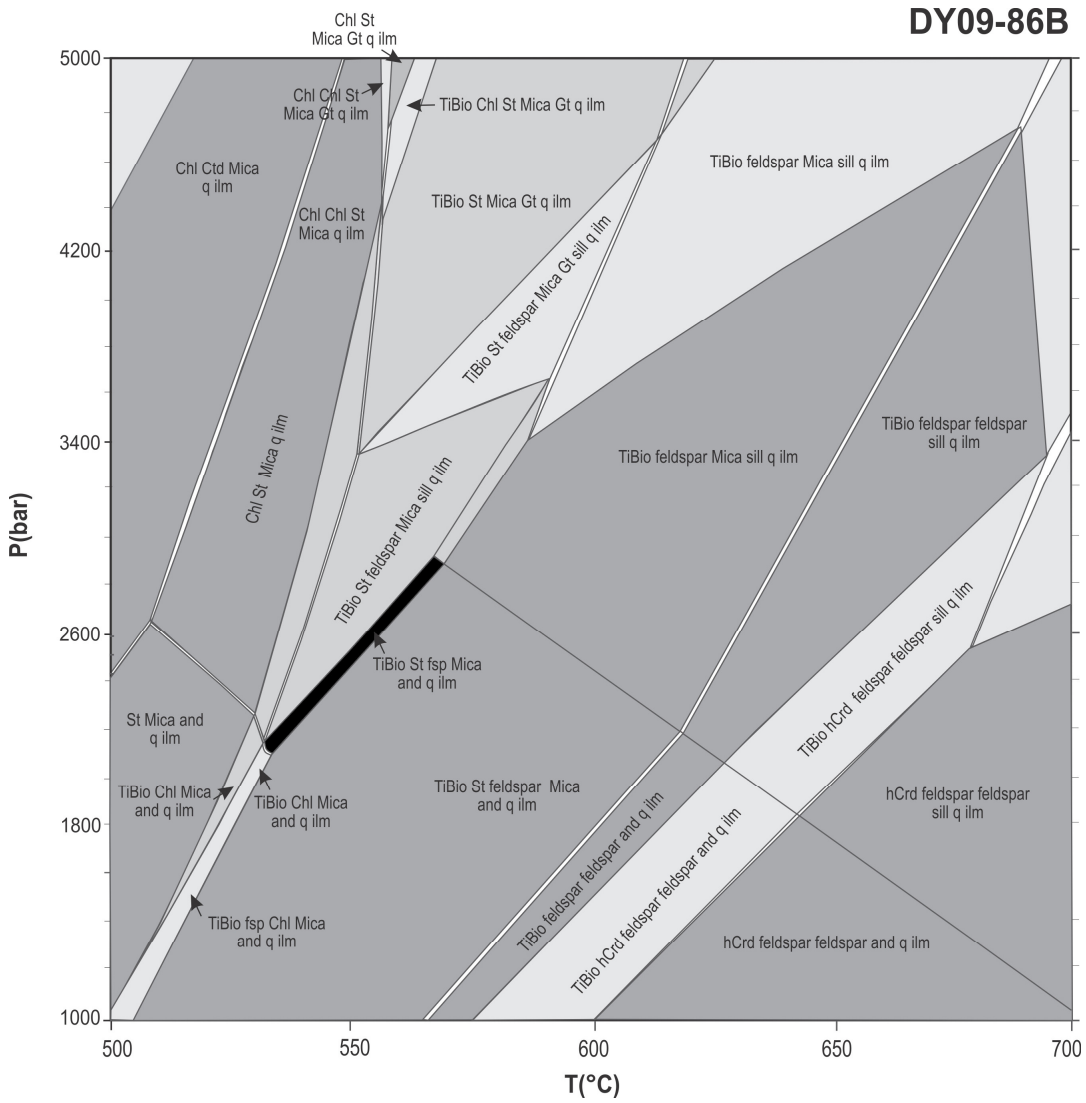


**Fig. 86.** Pseudosection of DY09-86B constructed in the NCKFMASKT system using Perplex. The field matching the identified mineral assemblage is filled-in with black.

## 6.2. Indirect Inferences of Pressure and Temperature

For a number of samples more indirect P-T estimates can be drawn. These are samples that did not contain assemblage-fields corresponding to those observed under microscope, but that contain a number of metamorphic minerals that can serve to give a broad P-T range of peak metamorphism. These samples are DM08-52B, DM08-54, DM08-63 and DY09-82. Furthermore, samples DM08-52B, DM08-54, DM08-63 arguably show unrealistically large fields for garnet-stability. These samples were therefore re-modelled in the NCKFMASHT system (as opposed to modelling in the MnNCKFMASHT system) to give more realistic ranges of garnet-stability.

The pseudosection of DM08-52B contains a field nearly matching the identified mineral assemblage: and + sill + bi + mu + q + ilm + pl, namely one containing sill + bi + mu + q + ilm + pl + ru. This field is restricted to >630 °C and >3700 bar.

DM08-54 produced similar results to that of DM08-52B. It also contains a field that matches the identified assemblage, except that the modelled field includes rutile. This field is restricted to >665 °C and >3850 bar.

The pseudosection of DM08-63 contains an assemblage: TiBio(HP) + hCrd, feldspar + Mica(CH2) + q + ilm. The only difference between this assemblage and that which was observed under microscope is that it contains no chloritoid. However, this modelled field is restricted to <650 °C and <3300 bar.

In the pseudosection of DY09-82 fields containing andalusite, staurolite and biotite span a P-T range of 530-590 ºC and 2090- 2940 bar. Adding plagioclase (represented by “feldspar” in the modelling) as a parameter narrows the temperature range negligibly and does not at all influence the temperature range.

# CHAPTER 7

## DISCUSSION

The results of DY09-54 and DY09-56 should be regarded as having most credence as their pseudosections contain fields exactly matching the petrographically-identified mineral assemblages. In addition the modelled isopleths of these two samples agree fairly well with corresponding analysed mineral-chemistries. These results are 530-565 ºC & 2250-2970 bar and 530-565 ºC & 2120-2950 bar for DY09-54 and DY09-56, respectively. Furthermore, modelled isopleths of MnO/(MnO+CaO+FeO+MgO) suggest refined estimates of 545-565 ºC and 2540-2970 bar for DY09-54 and 550 ± 5 ºC and 2650 bar for DY09-56. The error on the latter reading is due to the uncertainty in single temperature readings from pseudosections, as explained in the start of the results section.

Concerning the isopleths that didn't agree with probed mineral chemistries, namely $Fe^{2+}/(Fe^{2+}+Mg)$ and $Fe^{2+}/(Fe^{2+}+Mg+Ca)$ for garnet in DY09-54 and DY09-56, $Fe^{2+}/(Fe^{2+}+Mg+Ca+Mn)$ for garnet in DY09-56, $Ca/(Fe^{2+}+Mg+Ca+Mn)$ for garnet in DY09-54 and $Fe^{2+}/(Fe^{2+}+Mg)$ for biotite in DY09-54 and DY09-56, it was necessary to investigate whether the discrepancies were not possibly due to errors implicit to the modelling. Two main possible sources of significant error in the modelling was identified, namely standard deviation of the XRF data propagated through modelling for both pseudosections and isopleths, and secondly the propagation of errors on enthalpies of formation of modelled phases from the Holland and Powell (1998) dataset through modelling. Of these, the propagated errors from Holland and Powell (1998) and those from standard deviations on XRF data (propagated-) for isopleths were found to be negligible. The errors obtained from propagating the XRF standard deviations through modelling for pseudosections were found to average a) roughly 1°C and 20 bar for DY09-54 on reaction lines of the identified mineral assemblage and b) less than 1 °C and roughly 10 bar for DY09-56 on reaction lines of its identified mineral assemblage. However, these errors are too small to be the cause of the lack of overlap between probed mineral chemistries and modelled isopleths for $Fe^{2+}/(Fe^{2+}+Mg)$ and $Fe^{2+}/(Fe^{2+}+Mg+Ca)$ for garnet in DY09-54 and DY09-56, $Fe^{2+}/(Fe^{2+}+Mg+Ca+Mn)$ for garnet in DY09-56,

Ca/($Fe^{2+}$+Mg+Ca+Mn) for garnet in DY09-54 and $Fe^{2+}$/($Fe^{2+}$+Mg) for biotite in DY09-54 and DY09-56.

The errors discussed above should then be applied to the P-T estimates for DY09-54 and DY09-56. However, they only modify the P-T estimates in terms of pressure, because temperature estimates were measured to the nearest factor of 5 °C, while the errors obtained for temperature were 1 °C and <1 °C for DY09-54 and DY09-56, respectively. When errors on pressure estimates, namely ± 20 bar for DY09-54 and ± 10 bar for DY09-56, are then added to unrefined estimates we obtain 530-565 ºC and 2230-2990 bar for DY09-54 and 530-565 ºC and 2110-2960 bar for DY09-56, which overlap between 530-565 ºC and 2230-2960 bar. When these errors are added to the estimates refined by MnO/(MnO+CaO+FeO+MgO) isopleth modelling, we obtain 545-565 ºC and 2520-2990 bar for DY09-54 and 550 ± 5 ºC and 2650 ± 10 bar for DY09-56. Furthermore, the overlap of these refined estimates gives 550 ± 5 ºC and 2650 ± 20 bar.

Samples DY09-82 and DY09-86B give results agreeing fairly well with DY09-54 and DY09-56. DY09-82 produced 530-590 ºC and 2090- 2940 bar from the presence of andalusite, staurolite, biotite and plagioclase. DY09-86B yielded 530-570 °C and 2080-2930 bar in the NCKFMASHT system and 530-570 °C and 2080-2970 bar in the MnNCKFMASHT system (as based on the presence of str + and + q + pl + bi + mu + ilm).

The reason why DY09-86B fails to produce a pseudosection with a field that exactly matches it's petrographically-identified mineral assemblage in the MnNCKFMASHT system, but succeeds in doing so in the NCKFMASHT system is related to the predicted influence of Mn on the stability of garnet. If DY09-86B is first modelled in the NCKFMASHT system garnet is roughly restricted to pressures above 3300 bar at temperatures below 680 °C and to pressures above 2500 bar at temperatures above 680 °C. If Mn is then added as a modelling parameter, the predicted stability field of garnet increases to lower temperatures and -pressures. This increase is so pronounced that the predicted stability field of garnet increases from covering roughly 20% of the modelled PT-window to covering more than 80% of its area. Not surprisingly, the garnet-field then overlaps with the field that previously agreed with the petrographically-

identified mineral assemblage for the sample. It therefore seems likely that for DY09-86B the predicted stability field of garnet was exaggerated for the MnNCKFMASHT system and it is justifiable to regard the inferred P-T estimates for this sample in the MnNCKFMASHT system as inferior to the P-T estimates for the sample in the NCKFMASHT system. A reason for the erroneous modelling of the stability of garnet could likely be uncertainty in the activity-composition relations for Mn-bearing phases at low temperatures. Similar arguments can be used to justify the suggestion that DM08-52B, DM08-54 and DM08-63 produced exaggerated stability fields for garnet in the MnNCKFMASHT system. For these pseudosections uncertainty in the activity-composition relations for Mn-bearing phases at low temperatures would also be a likely cause for the largely-increased stability fields.

The agreement in results between DY09-54, DY09-56, DY09-82 and DY09-86B is significant in terms of their spatial relationships. As can be seen in Fig. 2A, DY09-54 and DY09-56 were samples from the same location, while DY09-82 and DY09-86B were samples close to one another and roughly 4 km from DY09-54 and DY09-56. The structural relationship between these two groups can be inferred from their coordinates and dip-and-strike readings taken in their vicinities. An average dip and dip-direction of 35° and 163.5°, respectively, was measured at the locality where DY09-82 was sampled. Furthermore, roughly between the sampling localities of DY09-54 and DY09-56, and those of DY09-82 and DY09-86B, an average dip and dip-direction of 28° and 167°, respectively, was taken on quartzite outcrops. Averaging these two groups of measurements gives a dip and dip-direction of 31.5° and 165°, respectively. Using these values together with the distance between DY09-54 and DY09-82, which is approximately 3.6 km, it can be inferred that the difference in stratigraphic depth between these two samples must have roughly been 2.1 km. Therefore, it can be assumed that the difference in peak-metamorphic pressure between samples DY09-54 and DY09-56 and samples DY09-82 and DY09-86B should be roughly equal to 0.57 kbar, as based on the formula:

$$P = \rho g h \qquad (1)$$

where P = pressure,

$\rho$ = density = 2750 kg/m$^3$ (average Pretoria Group density of Molyneux and Klinkert (1978))

g = gravity = 9.8 m/s$^2$

and h = height (or depth) = 2100 m.

Assuming that their pseudosections are accurate, the overlap of DY09-54 and DY09-56's pressure results gives a minimum metamorphic pressure of 2230 bar. If one then only considers the modelling of DY09-86B in the NCKFMASHT system and its overlap with DY09-82, a maximum metamorphic pressure of 2930 bar is obtained for the area of their sampling. It then follows that the difference in stratigraphic depth suggests: a) that DY09-54 and DY09-56 should have a maximum metamorphic pressure of 2360 bar (if the modelling results of DY09-86B in the NCKFMASHT system are accurate), or b) that the minimum metamorphic pressure of DY09-82 and DY09-86B should be 2800 bar (if the modelling results of DY09-54 are accurate). However, modelled-isopleth data for DY09-82 and DY09-86B do not support the accuracy of their pseudosections. Therefore, it is more valid to use the P-T estimates for DY09-54 and DY09-56 to refine the inferred estimates of DY09-82 and DY09-86B, than vice-versa. In conclusion, if the pseudosections of DY09-54 and DY09-56 are accurate, then it can be inferred (from difference in stratigraphic depth) that DY09-82 and DY09-86B should have undergone minimum peak metamorphic pressures of 2800 bar. This narrows these inferred peak metamorphic pressure ranges to 2800-2940 bar for DY09-82 and to 2800-2930 bar for DY09-86B (in the NCKFMASHT system).

The P-T inferences from DM08-52B, DM08-54 and DM08-63 are rather unspecific, producing either minimum-, or maximum P-T values. There is also a large disparity for the inferred results of DM08-52B and DM08-54 (>630 °C & >3700 bar and >665 °C & >3850 bar, respectively) as compared to the results of DM08-63, DY09-54, DY09-56, DY09-82 and DY09-86B (<650 °C and <3300 bar for DM08-63 and between 530-590 °C and 2080-2970 bar for the other samples). To illustrate the size of this disparity we can use formula (1). If an average density of 2750 kg/m$^3$ was assumed, the difference in depth needed to produce an extra 1000 bar of pressure would be 3.7 km. This is then very roughly a minimum difference in depth required to explain the difference in pressure estimates between the two groups of samples. If we then also

consider that DM08-52B and DM08-54 were not sampled from much different stratigraphic depths (and probably from shallower stratigraphy) than DM08-63, DY09-54, DY09-56, DY09-82 and DY09-86B (as can be seen in Fig. 2A) it seems most likely that the inferred results of DM08-52B and DM08-54 are erroneous. Conversely, the inferred P-T results of DM08-63, though unspecific, are in agreement with the results produced by DY09-54, DY09-56, DY09-82 and DY09-86B.

The P-T results for samples DY09-54, DY09-56, DY09-82, DY09-86B and DM08-63 can now be compared to those from literature. The pressure result for DY09-54 is 2230-2990 bar, although MnO/(MnO+CaO+FeO+MgO) isopleths suggest that this be refined to 2520-2990 bar. DY09-56 produced a pressure estimate of 2110-2960 bar, which MnO/(MnO+CaO+FeO+MgO) isopleths suggest should be refined to approximately 2650 ± 10 bar. These results agree well with those of DY09-82 and DY09-86B, which are 2090- 2940 bar for DY09-82 and 2080-2930 bar for DY09-86B (in the NCKFMASHT system). Furthermore, the pressure estimates for these two samples can arguably be refined to 2800-2940 bar for DY09-82, and 2800-2930 bar for DY09-86B (in the NCKFMASHT system). Finally, the pressure results for DM08-63 are <3300 bar. Comparing these results in bulk, which gives a minimum value of 2080 bar and maximum value of 3300 bar, to the literature shows good agreement to the majority of Bushveld aureole barometry done after the nineteen-eightees, which typically produced estimates in the region of 3 kbar (Uken, 1998, Waters and Lovegrove, 2002, Johnson *et al*., 2003, Johnson *et al*., 2004, Kaneko *et al*., 2005). Furthermore, the barometry of Uken (1998), Waters and Lovegrove (2002), Johnson *et al*. (2003), Johnson *et al*., (2004) and Kaneko *et al*., (2005), which all produced pressures in the region of 3 kbar, were all performed on rocks of the Eastern Bushveld aureole. Finally, when we compare the results of DY09-54 and DY09-56 (which are the most reliable estimates from this study) to pressure estimates produced by Kaneko *et al*., (2005) for metapelites sampled relatively close to the sampling location of DY09-54 and DY09-56 we again find good agreement in results. The estimates by Kaneko *et al*., (2005) are 0.20-0.28 GPa for a location 5km west of Penge and 0.18-0.24 GPa for a location roughly 10 km south-west of Penge (of which the former lies closest to samples DY09-54 and DY09-56) and those of DY09-54 and DY09-56 are 2230-2990 and 2110-2960 bar, respectively, and when

refined by isopleths for MnO/(MnO+CaO+FeO+MgO) 2520-2990 bar and 2650 ± 10 bar, respectively. Table 15 shows all pressure estimates used for the above comparisons.

| **This study:** | | **Previous workers:** | |
|---|---|---|---|
| **Sample** | **Pressure (kbar)** | **Author** | **Pressure (kbar)** |
| DY09-54 | 2.23-2.99, although XMn isopleths suggest 2.52-2.99 | Uken (1998) | 2.8-3.2 |
| DY09-56 | 2.11-2.96, although XMn isopleths suggest approximately 2.65 ± 0.01 | Waters and Lovegrove (2002) | 3.0 ± 0.5 |
| DY09-82 | 2.09-2.94; minimum value should arguably be 2.80 | Johnson *et al.* (2003) | 3.5 ± 1.5 |
| DY09-86B | 2.08-2.93; minimum value should arguably be 2.80 | Johnson *et al.* (2004) | around 3 kbar |
| DM08-63 | <3.30 | Kaneko *et al.* (2005) | 1.5-2.5, 2.2-3.1, 2.0-2.8 and 1.8-2.4 (ignoring pressures calculated at contact) |

**Table 15.** Table of comparison between the barometric results from this study and those produced by previous studies. All the results in the table were performed for the Eastern Bushveld Complex aureole and after the nineteen-eightees.

The pressure estimates obtained from the pseudosections of DY09-54 and DY09-56 can be translated to the depth of these samples at the time of peak metamorphism. Using formula (1) to solve for depth and assuming an average density of 2750 kg/m$^3$, the inferred pressure of 2230-2990 bar for DY09-54 translates to a depth of 8.3-11 km. Likewise, the pressure estimate of 2110-2960 bar for DY09-56 converts to a depth of 7.9-11 km. However, a rock density of 2750 kg/m$^3$ is not representative of a load consisting of a significant proportion of mafic rocks of the Rustenburg Layered Suite, as would have been the case with samples DY09-54 and DY09-56. Let us then consider the likely thickness of load due to Pretoria Group strata. Eriksson *et al.* (1991) gives stratigraphic thickness data of Pretoria Group formations at, amongst other locations, Malipsdrift and Penge. Samples DY09-54 and DY09-56 were collected roughly between these two locations and the thickness data at these two locations has therefore been averaged for the purpose of this study. These averaged data suggests that the Pretoria Group floor rocks

that overlay DY09-54 and DY09-56 were at least 1950 m, or 2460 m, thick, depending on whether they were collected from the Upper-, or Lower Timeball Hill shales (i.e. the Magaliesberg, Silverton, Daspoort, Strubenkop, Dwaalheuwel, Hekpoort and Boshoek formations have an averaged accumulate thickness of roughly 1950 m, while these plus the Upper Shale and Klapperkop members of the Timeball Hill Formation give an approximate accumulate thickness of 2460 m). Assuming the samples were collected from the Lower Timeball Hill shales, the Pretoria Group strata in the floor of the Bushveld Complex probably represents at least 2460 m of overburden, if averaging the data from Eriksson *et al.* (1991) gives thicknesses representative of the sampling locality. This represents a contribution of at least 660 bar to the pressure that the samples were subjected to during peak metamorphism (again derived using formula (1) and an average density of 2750 kg/m$^3$). If we then assume that the remainder of peak metamorphic pressure was due to the load of the RLS, we can deduce the thickness of such a load using formula (1) and a representative density for the RLS. For this purpose we can use 3000 kg/m$^3$, derived from the average density for the RLS of Ashwal *et al.* (2003) (3.02 ± 0.24 g/cm$^3$). This then gives us a thickness for overlying RLS during peak metamorphism of 5.3-7.8 km. If we assume that the samples were collected from the Upper Timeball Hill shales, in which case the Pretoria Group strata in the floor rocks represents at least 1950 m according to averaged data (and at least 520 bar of load pressure), then the same logic suggests a thickness of 5.8-8.3 km for the RLS above samples DY09-54 and DY09-56 during peak metamorphism. Considering that the RLS has a maximum thickness of ~8 km (Cawthorn and Walraven, 1998), these deduced maximum thicknesses for the RLS seem excessive. However, no account was made for the contribution that Pretoria Group rocks in the roof to the Bushveld Complex, or in the form of xenoliths, would have made to load pressure, neither was any account made for possible load due to the mainly rhyolitic Rooiberg Group and/or the Lebowa Granite Suite. Regarding the former, a small proportion of the load should have been due to Pretoria Group strata that formed the roof of the RLS. The Vermont, Lakenvlei, Steenkampsberg and Houtenberg formations are not accounted for in the floor rocks in the vicinity of the sampling locality. Although these strata would have been largely assimilated by the RLS and would only have represented a minimal proportion of load (as roof rocks and xenoliths), accounting their

contribution to the lithostatic pressure would make the inferred load thickness of RLS rocks, more reasonable. The contribution that the Rooiberg Group and/or the Lebowa Granite Suite might have made to the lithostatic pressure is difficult to determine due to field relations and uncertainty between the chronology of peak metamorphism and the intrusion of the Lebowa granites. Considering field relations, it is however reasonable to assume that rocks of the Rooiberg Group and/or the Lebowa Granite Suite made a significant contribution to the pile of rock that overlay samples DY09-54 and DY09-56 during peak metamorphism. If this is the case, then the apparent load thickness of the RLS would be even more reasonable. Finally, another contributor to the peak metamorphic pressure could have been directed stress. Considering that some samples displayed preferred orientations of certain mineral grains, this is feasible. However, evidence of anisotropic stress was not on a whole characteristic of the samples studied under microscope. Furthermore, as discussed above, it is the opinion of the author that the peak metamorphic pressures can be accounted for by lithostatic pressure alone.

Considering the above, we can attempt to make a more accurate estimate for the true depth of samples DY09-54 and DY09-56 during peak metamorphism. Let us assume that 1000 bar of the peak metamorphic pressure was due to load caused by Pretoria Group strata (roof rocks included) and rocks of the Rooiberg Group and/or the Lebowa Granite Suite, and that these had an average density of 2750 kg/m$^3$, and that the remainder of peak metamorphic pressure was caused by the load of the RLS, with an average density of 3000 kg/m$^3$. Furthermore, let us use the overlap of the pressure estimates for DY09-54 and DY09-56, ignoring isopleths (i.e. 2230-2960 bar). Then using formula (1) to solve for the thickness (depth) of these two groups of load, we obtain a total load thickness of 7.9-10.4 km above DY09-54 and DY09-56 during peak metamorphism, of which 4.2-6.7 km of load thickness would have been rocks of the RLS. Note that the assumption that 1000 bar of load pressure was due to rocks of the Pretoria Group, as well as the Rooiberg Group and/or the Lebowa Granite Suite, implies that roughly 410 bar of pressure, or approximately 1.5 km of load thickness, was due to the Rooiberg Group and/or the Lebowa Granite Suite, providing that Pretoria Group rocks in the roof of the Complex and in the form of xenoliths were negligible.

The chief uncertainty in estimating the crustal depth of samples DY09-54 and DY09-56 during peak metamorphism thus seems to stem from uncertainty of the thickness of the pile of rock that overlay the RLS during peak metamorphism.

An attempt can now be made at estimating the crustal depth of the base of the RLS directly above samples DY09-54 and DY09-56 during peak metamorphism. As it is unsure whether the samples were collected from the Upper- or Lower Timeball Hill shales, let us assume an intermediate thickness of overlying Pretoria Group strata in the floor to the Complex (again using averaged thickness data from Eriksson *et al.*, 1991), namely a thickness of 2350 m (remembering that 2460 m and 1950 m were minimum thicknesses for their respective scenarios). Let us also assume that the RLS was overlaid by 1.5 km of felsic rock with an average density of 2750 kg/m$^3$. This would imply that the lithostatic pressure at the base of the RLS would have been 1597-2327 bar (using formula (1) and a density of 2750 kg/m$^3$). According to our second assumption 404 bar of pressure is due to material that overlay the RLS, therefore 1193-1923 bar of pressure would have been due to the RLS alone, which converts to a thickness of 4058-6541 m (derived using formula (1) and a density of 3000 kg/m$^3$). Adding this to the assumed 1.5 km of overlying material gives us the base of the RLS at a crustal depth of 5.6-8.0 km.

The thermometric results for DY09-54 and DY09-56 can be compared to modelled palaeogeotherms to illustrate the amount of thermal energy that was responsible for their metamorphism. For this purpose we can consider the geotherm that Gibson and Jones (2002) modelled for the central Kaapvaal Craton for late-Archaean to Palaeoproterozoic times, namely 15-20 K/km. Using the upper limit of this estimate (20 K/km) and our final maximum estimate for the crustal depth of samples DY09-54 and DY09-56 (10.4 km), implies that in the absence of all non-radiogenic heat sources the samples would have reached temperatures no higher than 210 °C. Thus, the thermometric results of the samples, namely 530-565 °C, suggest that peak metamorphism elevated their temperatures by no less than 320-355 °C, assuming that no thermal metamorphic effect was active on the samples just prior to the intrusion of the Bushveld Complex. This large addition of thermal energy could only have been due to the voluminous magmas of the RLS.

# CHAPTER 8

## CONCLUSIONS

Two samples, namely DY09-54 and DY09-56, produced desirable results via modelling in the MnNCKFMASHT system using Perplex. From these samples it can be concluded that the pressure and temperature of peak metamorphism of the metapelites of the Timeball Hill Formation (as caused by the intrusion of the RLS) roughly 36 km northwest of Penge, was 530-565 ºC and 2230-2990 bar for DY09-54 and 530-565 ºC and 2110-2960 bar for DY09-56, which overlap between 530-565 ºC and 2230-2960 bar. From the overlap of their pressure estimates it follows that at the time of peak metamorphism these samples were arguably at depths of roughly 7.9-10.4 km, in which case the RLS would have had a thickness of 4.2-6.7 km directly above the samples. However, exact determination of the depth of the samples during peak metamorphism is difficult due to uncertainty of the thickness of the rock pile that overlay the RLS during peak metamorphism. Nonetheless, if it is assumed that the load of Pretoria Group strata in the floor to the Complex had a thickness of 2350 m and that a 1.5 km thick pile of felsic rock was present above the RLS during peak metamorphism, then the base of the RLS must have been at a crustal depth of 5.6-8.0 km (directly above samples DY09-54 and DY09-56 and during peak metamorphism).

Considering the modelled palaeogeotherms of Gibson and Jones (2002) for the central Kaapvaal Craton and the above-mentioned peak-metamorphic depth estimate for samples DY09-54 and DY09-56, it appears that peak metamorphism elevated the samples' temperatures by no less than 320-355 °C, assuming that no thermal metamorphic effect was active on the samples just prior to the intrusion of the BIC.

Finally, the barometric results of samples DY09-54 and DY09-56 agree well with post-nineteen-eightees results from the Literature. This is especially true for the barometric results produced for a location roughly 5 km west of Penge by Kaneko *et al.*, (2005), which lies relatively close to the sampling location of DY09-54 and DY09-56.

# REFERENCES

Abraham, K. and Schreyer, W. (1973). Petrology of ferruginous hornfels from Riekensglück, Harz Mountains, Germany. *Contributions to Mineralogy and Petrology*, **40**, 275-292.

Ashwal, L.D., Webb, S.J. and Knoper, M.W. (2003). Cyclicity in layered intrusions as revealed by near-continuous geophysical and petrological measurements in the Bushveld Complex, South Africa. *EGS-AGU-EUG Joint Assembly*, **5**: Nice, France, Geophysical Research Abstracts, 03223.

Berg, J.H. (1977). Regional geobarometry in the contact aureole of the anorthositic Nain Complex, Labrador. *Journal of Petrology*, **18**, 399-430.

Bhattacharya, A. (1986). Some geobarometers involving cordierite in the $FeO$-$Al_2O_3$-$SiO_2(H_2O)$ system: refinements, thermodynamic calibration, and applicability in granulite facies rocks. *Contributions to Mineralogy and Petrology*, **94**, 387-394.

Blain, M.R. (1974). The occurrence of andalusite in the lower Daspoort and Timeball Hill shales of the Pretoria Series in the Western Transvaal. *Unpublished Report of the Geological Survey of South Africa*, 1974-0086.

Blain, M.R. (1975). The occurrence of andalusite in the metamorphic aureole of the Bushveld Complex in the Eastern Transvaal. *Unpublished Report of the Geological Survey of South Africa*, 1975-0103.

Bohlen, S. R. and Boettcher, A. L. (1981). High ‐ pressure stability and thermodynamic properties of $CoSiO_3$. *Geophysical Research Letters*, **8** (6), 575-578.

Bowlen, S.R., Wall, V.J. and Boettcher, A.L. (1983). Experimental investigation and application of garnet granulite equilibria. *Contributions to Mineralogy and Petrology*, **83**, 52-61.

Buick, I.S., Gibson, R.L., Cartwright, I., Maas, R., Wallmach, T. and Uken, R. (2000). Fluid flow in metacarbonates associated with emplacement of the Bushveld Complex, South Africa. *Journal of Geochemical Exploration*, **69-70**, 391-395.

Buick, I.S., Maas, R. and Gibson, R. (2001). Precise U-Pb titanite age constraints on the emplacement of the Bushveld Complex, South Africa. *Journal of the Geological Society, London*, **158**, 3-6.

Buick, I.S., Stevens, G. and Gibson, R.L. (2004). The role of water retention in the anatexis of metapelites in the Bushveld Complex aureole, South Africa: an experimental study. *Journal of Petrology*, **45**, 1777-1797.

Burt, D.M. (1971). The system Fe-Si-C-O-H: A model for metamorphosed iron formations. Yearbk., Carnegie Inst., Washington, **71**, 435-443.

Button, A. (1973). A regional study of the stratigraphy and development of the Traansvaal Basin in the eastern and northeastern Transvaal. *Ph. D. dissertation*, University Witwatersrand, Johannesburg, South Africa, 352 pp.

Button, A. (1975). Stratigraphy and attitude of the floor of the Bushveld Complex in the eastern Transvaal. Economic Geology Research unit, University of the Witwatersrand Information Circular, **96**, 13pp.

Button, A. (1976). Stratigraphy and relations to the Bushveld floor in the Eastern Transvaal. *Transactions of the Geological Society of South Africa*, **79**, 3-12.

Catuneanu, O. and Eriksson, P.G. (1999). The sequence stratigraphic concept and the Precambrian rock record: an example from the 2.7-2.1 Ga Transvaal Supergroup, Kaapvaal craton. *Precambrian Research*, **97**, 215-251.

Cawthorn, R.G., Cooper, G.R.J. and Webb, S.J. (1998). Connectivity between the western and eastern limbs of the Bushveld Complex. *South African Journal of Geology*, **101**, 291-298.

Cawthorn, R.G. and McKenna, N., (2006). The extension of the western limb, Bushveld Complex (South Africa), at Cullinan Diamond Mine. *Mineralogical Magazine*, **71** (3), 241-256.

Cawthorn, R.G. and Walraven, F. (1998). Emplacement and crystallization time for the Bushveld Complex. *Journal of Petrology*, **39**, 1669-1687.

Clarke, B., Uken, R. and Reinhardt, J. (2009). Structural and compositional constraints on the emplacement of the Bushveld Complex, South Africa. *Lithos*, **111**, 21-36.

Coggon, R. and Holland, T. J. B. (2002). Mixing properties of phengitic micas and revised garnet–phengite thermobarometers. *Journal of Metamorphic Geology*, **20**, 683–696.

Department of Mineral and Energy Affairs and the Geological Survey (1986). 2430 Pilgrim's Rest (1:250000 Geological Series). Government Printer, Pretoria, (One sheet).

De Waal, S.A. (1963). Die plooikompleks van die Sisteem Transvaal noord van Marble Hall en die meegaande metamorfe en intrusiegesteentes. *M. Sc. thesis*, University of Pretoria, Pretoria, South Africa, 86 pp.

Droop, G.T.R. (1987). A general equation for estimating $Fe^{3+}$ concentrations in ferromagnesian silicates and oxides using stoichiometric criteria. *Mineralogical Magazine*, **51**, 431-437.

Dymoke, P. and Sandiford, M. (1992). Phase relations in the Buchan facies series pelitic assemblage: calculations with application to the andalusite-staurolite paragenesis in the Mount Lofty Ranges, South Australia. *Contributions to Mineralogy and Petrology*, **110**, 121-132.

Eales, H.V. and Cawthorn, R.G. (1996). The Bushveld Complex. In: Cawthorn, R.G. (Ed.), Layered Intrusions. Elsevier, Amsterdam, pp. 181-230.

Engelbrecht, J.P. (1976). Meta-sediments of the Pretoria Group in the Enzelsberg area, Marico District. *Transactions of the Geological Society of South Africa*, **79** (1), 61-75.

Engelbrecht, J.P. (1988). Die Bosveld kompleks en sy vloergesteentes in die omgewing van Nietverdiend, Wes-Transvaal: *Ph.D. thesis*, University of Pretoria, Pretoria, South Africa, 327 pp.

Engelbrecht, J.P. (1990). Contact metamorphic processes related to the aureole of the Bushveld Complex in the Marico District, western Transvaal, South Africa. *South African Journal of Geology*, **93**, 339-349.

Eriksson, P.G., Hattingh, P.J. and Altermann, W. (1995). An overview of the geology of the Transvaal Sequence and Bushveld Complex, South Africa. *Mineralium Deposita*, **30**, 98-111.

Eriksson, P.G., Schreiber, U.M. and Van der Neut, M. (1991). A review of the sedimentology of the Early Proterozoic Pretoria Group, Transvaal Sequence, South Africa: implications for tectonic setting. *Journal of African Earth Science*, **13**, 107-119.

Evans, B.W. (1965). Application of a reaction-rate method to the breakdown equilibria of muscovite and muscovite plus quartz. *American Journal of Science*, **263**, 647-667.

Ferry and Spear (1978). Experimental calibration of the partitioning of Fe and Mg between biotite and garnet. *Contributions to Mineralogy and Petrology*, **66**, 113-117.

Frost, B.R. (1979). Contact metamorphism of serpentinite, chloritic Blackwall and Rodingite at Paddy-Go-Easy Pass, central Cascades, Washington. *Journal of Petrology*, **16**, 272-313.

Fuhrman. M.L. and Lindsley, D.H. (1988). Ternary-feldspar modeling and thermometry. *American Mineralogist*, **73**, 201-215

Fyfe, W.S., Turner, F.J. and Verhoogen, J. (1958). Metamorphic reactions and metamorphic facies. *Geological Society of America Memoirs*, **73**.

Gau, W.J. (1907). Geological notes on a portion of the Bushveld in the neighbourhood of the junction of the Elands and Olifants rivers. *Transactions of the Geological Society of South Africa*, **XI**, (1906), 67-73.

Ghent, E.D. (1976). Plagioclase – garnet – Al2SiO5 – quartz: a potential geobarometer – geothermometers. *American Mineralogist*, **61**, 710-714.

Gibson, R.L. and Jones, M.Q.W. (2002). Late Archaean to Palaeoproterozoic geotherms in the Kaapvaal craton, South Africa: constraints on the thermal evolution of the Witwatersrand Basin. *Basin Research*, **14**, 169-181.

Hall, A. L., (1932). The Bushveld Igneous Complex of the Central Transvaal: *Memoirs of the Geological Survey of South Africa*, **28**, 560 pp.

Hammerbeck, E.C.I. (1986). Andalusite in the metamorphic aureole of the Bushveld Complex. In: Mineral Deposits of Southern Africa. Anhaeusser, C.R. and Maske, S. *eds*., Vols. I&II, 993-1004. Geological Society of South Africa, Johannesburg.

Harris, N. (1981). The application of spinel-bearing metapelites to P/T determinations: an example from south India. *Contributions to Mineralogy and Petrology*, **76**, 229-233.

Harris, N., McMillan, A., Holness, M., Uken, R., Watkeys, M., Rogers, N. and Fallick, A., (2003). Melt generation and fluid flow in the thermal aureole of the Bushveld Complex. *Journal of Petrology,* **44** (6), 1031-1054.

Hartzer, F. J. (1987). Die geologie van die Krokodilrivierfragment, Transvaal. *M. Sc. thesis*, Rand Afrikaans University, Johannesburg, South Africa, 201 pp.

Hartzer, F. J. (1994). Transvaal inliers: geology and relationship with the Bushveld Complex. *Ph. D. dissertation*, Rand Afrikaans University, Johannesburg, South Africa, 415 pp.

Hartzer, F.J. 1995. Transvaal Supergroup inliers: geology, tectonic development and relationship with the Bushveld complex, South Africa. *Journal of African Earth Sciences*, **21**, 521-547.

Hensen, D.J. and Green, D.H. (1973). Experimental study of the stability of cordierite and garnet in pelitic compositions at high pressures and temperatures. III Synthesis of experimental data and geological applications, *Contributions to Mineralogy and Petrology*, **38**, 151-166.

Hodges, K.V. and Spear, F.S. (1982). Geothermometry, geobarometry and the $Al_2SiO_5$ triple point at Mt. Moosilauke, New Hampshire. *American Mineralogist*, **67**, 175-198.

Holdaway, M.J. and Lee, S.M. (1977). Fe-Mg cordierite stability in high-grade politic rocks based on experimental, theoretical and natural observations. *Contributions to Mineralogy and Petrology*, **63**, 175-198.

Holland, T.J.B. and Powell, R. (1990). An internally-consistent thermodynamic dataset with uncertainties and correlations: the system $Na_2O$-$K_2O$-CaO-MgO-MnO-FeO-$Fe_2O_3$-$Al_2O_3$-$SiO_2$-$TiO_2$-C-$H_2$-$O_2$. *Journal of Metamorphic Geology*, **8**, 89-124.

Holland, T.J.B. and Powell, R. (1998). An internally consistent thermodynamic data set for phases of petrological interest. *Journal of Metamorphic Geology*, **16**, 309-343.

Holland, T.J.B. and Powell, R. (2001). Calculation of phase relations involving haplogranitic melts using an internally-consistent thermodynamic data set. *Journal of Petrology*, **42**, 673-683.

Holtz, F. and Johannes, W. (1991). Genesis of peraluminous granites I. Experimental investigation of melt compositions at 3 and 5 kb and various $H_2O$ activities. *Journal of Petrology,* **32**, 935-958.

Hsu, L.G. and Burnham, C.W. (1969). Phase relations in the system $Fe_3Al_2Si_3O_{12}$-$Mg_3Al_2Si_3O_{12}$-$H_2O$ at 2.0 kilobars. *Geological Society of America Bulletin*, **80**, 2393-2408.

Hulbert, L.J. and Sharpe, M.R. (1981). Institute for geological research on the Bushveld Complex: Annual report. University of Pretoria, South Africa, pp. 30-42.

Human, D.R. (1975). The geology and metamorphic petrology of part of the basal argillaceous zone, Daspoort Stage, Pretoria Series of the Farm Havercroft, North Eastern Transvaal. *Petros*, **6**, 25-43.

Human, D.R. and Collins, L.A. (1986). The Havercroft-Streatham Andalusite Deposit, Eastern Transvaal. In: Anhaeusser, C.R. & Maske, S., (Eds.), *Mineral Deposits of Southern Africa*. Geological Society of South Africa, Johannesburg, 1005-1008.

Impala Platinum Holdings Limited (2004). Annual Report 2004. Impala Platinum Holdings Limited, 157 pp.

Johnson, T.E., Gibson, R.L., Brown, M., Buick, I.S. and Cartwright, I., (2003). Partial melting of metapelitic rocks beneath the Bushveld Complex, South Africa. *Journal of Petrology,* **44** (5), 789-813.

Johnson, T.E., Brown, M., Gibson, R. and Wing, B., (2004). Spinel-cordierite symplectites replacing andalusite: evidence for melt-assisted diapirism in the Bushveld Complex, South Africa. *Journal of Metamorphic Geology,* **22**, 529-545.

Kaneko, Y. and Miyano, T. (1990). Contact metamorphism by the Bushveld Complex in the northeastern Transvaal, South Africa. *Journal of Mineralogy, Petrology and Economic Geology*, **85**, 66-81.

Kaneko, Y. and Miyano, T. (2004). Recalibration of mutually consistent garnet-biotite and garnet-cordierite geothermometers. *Lithos*, **73**, 255-269.

Kaneko, Y., Miyano, T. and van Reenen, D.D. (1990a). Intrusion plane of the Bushveld Complex inferred from the contact metamorphosed Pretoria Group, northeastern Transvaal, South Africa. Scientific Report, Institute of Geoscience, University Tsukuba, Sec. B. vol. 11, pp. 11-22.

Kaneko, Y., Miyano, T. and van Reenen, D.D. (1990b). Occurrences of fibrolite in the eastern Bushveld contact aureole, South Africa. Annual Report, Institute of Geoscience, University Tsukuba, no. 16, 80-85.

Kaneko, Y., Miyano, T. and van Reenen, D.D. (2000). Pseudomorphs and ghost structures of some aluminous silicate minerals in pelitic hornfelses of the Timeball Hill Formation, Transvaal Supergroup, in the northeastern Transvaal, South Africa. Annual Report, Institute of Geoscience, University Tsukuba, no. 26, 41-46.

Kaneko, Y., Tsunogae, T. and Miyano, T. (2005). Crystal size distribution in garnets from the northeastern Bushveld contact aureole. *American Mineralogist*, **90**, 1422-1433.

Koziol, A.M. and Newton, R.C. (1988). Redetermination of the anorthite breakdown reaction and improvement of the plagioclase-garnet-$Al_2SiO_5$-quartz geobarometer. *American Mineralogist*, **73**, 216-223.

Kretz, R. (1982). Transfer and exchange equilibria in a portion of the pyroxene quadrilateral as deduced from natural and experimental data. *Geochiica et Cosmochimica Acta.,* **46**, 411-421.

Lal, R.K. and Seifert, F. (1979). The reaction cordierite + olivine = orthopyroxene + spinel in the system Mg-Fe-Al-Si-O-H. *Neues Jahrbuch für Mineralogie, Monatshefte*, **8**, 225-232.

Le Breton, N. and Thompson, A.B. (1988). Fluid absent (dehydration) melting of biotite in metapelites in the early stages of crustal anatexis. *Contributions to Mineralogy and Petrology*, **99**, 226-237.

Lindsley, D.H. (1983). Pyroxene thermometry. *American Mineralogist,* **68**, 477-493.

Mavimbela, P.K. (2012). Metamorphism in the Contact Aureole of the Eastern Limb of the Bushveld Complex. *M. Sc. thesis*, University of Pretoria, Pretoria, South Africa, 140 pp.

Miyano, T., Beukes, N.J. and van Reenen, D.D. (1987). Metamorphic evidence for early post-Bushveld sills in the Penge Iron Formation, Transvaal Sequence, Eastern Transvaal. *South African Journal of Geology*, **90** (1), 37-43.

Mizuno, K. (2000). Granulite metamorphism of pelitic rocks adjacent to the Bushveld Complex contact in the northeastern Transvaal area, South Africa, 164 p. *Ph. D. thesis*, University of Tsukuba, Ibaraki, Japan.

Mizuno, K. and Miyano, T. (1999). Two-pyroxene geothermometry in the Bushveld Complex contact in the northeastern Transvaal, South Africa. Annual Report, Institute of Geoscience, University Tsukuba, no. 25, 47-50.

Mizuno, K., Miyano, T. and Tojo, S. (1999). Melt textures in orthopyroxene-bearing hornfels in the contact metamorphic aureole of the Bushveld Complex, eastern Transvaal, South Africa. Scientific Report, Institute of Geoscience, University Tsukuba, Sec. B, vol. 21, 1-11.

Molyneux, T. G. & Klinkert, P. S., (1978). A structural interpretation of part of the eastern mafic lobe of the Bushveld Complex and its surrounds. *Transactions of the Geological Society of South Africa*, **81**, 359–368.

Nell, J. (1984). Geochemical and thermodynamic controls on the formation of mineral assemblages from the metamorphic aureole of the Bushveld complex in the Potgietersrus area. *M. Sc. thesis*, University of Pretoria, Pretoria, South Africa.

Newton, R.C. and Haselton, H.T. (1981). Thermodynamics of the garnet-plagioclase-$Al_2SiO_5$-quartz geobarometer. In: R.C. Newton, A. Navrotsky, and B.J. Wood, Eds., Thermodynamics of Minerals and Melts, pp. 131-147, Springer, New York.

Newton, R.C. and Perkins, D. (1982). Thermodynamic calibration of geobarometers based on the assemblages garnet-plagioclase-orthopyroxene(clinopyroxene)-quartz. *American Mineralogist*, **67**, 203-222.

Otto, J. W. and Wylie, P. J. (1993). Relationships between silicate melts and carbonate precipitating melts in CaO-MgO-$Si0_2$-$C0_2$-$H_20$ at 2 kbar. *Mineralogy Petrology*, **48**, 343-365.

Patiňo Douce, A.E. and Harris, N. (1998). Experimental constraints on Himalayan anatexis. *Journal of Petrology*, **39**, 689-710.

Pattison, D.R.M., Spear, F.S., Debuhr, C.L., Cheney, J.T. and Guidotti, C.V. (2002). Thermodynamic modeling of the reaction muscovite + cordierite → $Al_2SiO_5$ + biotite + quartz + $H_2O$: Constraints from natural assemblages and implications for metapelitic petrogenetic grids. *Journal of Metamorphic Geology*, **20**, 99-118.

Perchuk, L.L. (1977). Thermodynamic control of metamorphic processes. In: Saxena, S.K. and Bhattacharji, S. (Eds.), *Energetics of Geological Processes*. Springer and Verlag, New York, 285-352.

Perchuk, L.L., Podlesskii, K.K. and Aranovich, L.Ya. (1981). Thermodynamic properties of end-member minerals from natural paragenesis. In: Newton, R.C., Navrotsky, A. and Woods, B.J. (Eds.). *Thermodynamics of minerals and melts*. 304 pp.

Perkins and Chipera (1985). Garnet-orthopyroxene-plagioclase-quartz barometry: refinement and application to the English River subprovince and the Minnesota River valley. *Contributions to Mineralogy and Petrology*, **89**, 69-80.

Pitra, P. and De Waal, S.A., (2001). High-temperature, low-pressure metamorphism and development of prograde symplectites, Marble Hall Fragment, Bushveld Complex (South Africa). *Journal of Metamorphic Geology,* **19**, 311-325.

Pouchou, J.L. and Pichoir, F. (1991). Quantitative analysis of homogeneous or stratified microvolumes applying the model "PAP". In: Heinrich, K.F.J. and Newbury, D.E. (Eds.), Electron Probe Quantitation. Plenum Press, New York.

Powell, R. (1978). The thermodynamics of pyroxene geotherms. Royal Society [London] Philosophy Transactions, A, **288**, 457-469.

Powell and Holland (1988). An internally consistent dataset with uncertainties and correlations: 3. Applications to geobarometry, worked examples and computer program. *Journal of Metamorphic Geology,* **6**, 173-204.

Raheim, A. and Green, D.H. (1974). Experimental determination of the temperature and pressure dependence of the Fe-Mg partition coefficient for coexisting garnet and clinopyroxene. *Contributions to Mineralogy and Petrology*, **48**, 178-203.

Reczco, B.F.F. (1994). The geochemistry of the sedimentary rocks of the Pretoria Group, Transvaal Sequence. *Ph. D. thesis,* University of Pretoria, Pretoria, South Africa, 385 pp.

Richardson, S.W., Gilbert, M.C. and Bell, P.M. (1969). Experimental determination of kyanite-andalusite and andalusite-sillimanite equilibria; the aluminium silicate triple point. *American Journal of Science*, **267**, 259-272.

Sakai, S. and Kawasaki, T. (1997). An experimental study of Fe-Mg partitioning between orthopyroxene and cordierite in the Mg-rich portion of the $Mg_3Al_2Si_3O_{12}$-$Fe_3Al_2Si_3O_{12}$ system at atmospheric pressure: Calibration of its geothermometry for high-temperature granulites and igneous rocks. *Proceeding of NIPR Symposium of Antarctic Geoscience,* **10**, 165-177.

Sharpe, M.R. (1982). The floor contact of the eastern Bushveld Complex: field relations and petrography. Institute for Geological Research on the Bushveld Complex, University of Pretoria, Research Report, **36**, 43 pp.

Sharpe and Chadwich (1982), Structures in Transvaal Sequence rocks within and adjacent to the Eastern Bushveld Complex. *Transactions of the Geological Society of South Africa*, **85**, 29-41.

Sharpe, M.R. and Fortsch, E. (1981). Grandite garnet in metamorphosed stromatolites from the Houtenberg Formation, eastern Transvaal. Institute for Geological Research on the Bushveld Complex, University of Pretoria, Research Report, **31**, 14 pp.

Schmid, R. and Wood, B.J. (1976). Phase relationships in granulite metapelites from the Ivrea-Verbano zone (northern Italy). *Contributions to Mineralogy and Petrology*, **54**, 255-279.

Schreyer, W. (1976). Experimental metamorphic petrology at low pressures and high temperatures. In: Bailey, D.K. and MacDonald, R,. eds., The evolution of crystalline rocks. Academic Press, London, 261-331.

Schwellnus, J.S.I., Engelbrecht, L.N.J., Coertze, F.J., Russel, H.D., Malherbe, S.J., Van Rooyen, D.P. and Cooke, R. (1962). The Geology of the Olifants River area, Transvaal. Expl. 1:250 000 scale, Sheet 2429B Chuniespoort and 2430A Wolkberg. Geological Survey of South Africa, 87 pp.

Scoates, J.S. and Friedman, R.M. (2007). Determining that age and cooling history of the world's largest layered intrusion: U-Pb zircon-rutile geochronology of the Merensky Reef, Bushveld Complex, South Africa. EOS Trans. AGU 88 (52) Fall Meeting. Supplement., Abstract V43A-1102.

Thompson, A.B. (1976). Mineral reactions in pelitic rocks: II. Calculation of some P-T-X (Fe-Mg) phase relations. *American Journal of Science*, **276**, 425-454.

Turner, F.J. (1968). Metamorphic petrology: Mineralogical and field aspects. McGraw-Hill, New York, 403 pp.

Uken, R., (1998). The geology and structure of the Bushveld Complex metamorphic aureole in the Olifants River area. *Ph. D. thesis*, University of Natal, Durban.

Vielzeuf, D. (1983). The spinel and quartz associations in high grade xenoliths from Tallante (S.E. Spain) and their potential use in geothermometry and barometry. *Contributions to Mineralogy and Petrology*, **82**, 301-311.

Von Gruenewaldt, G. (1991). Precambrian sedimentary basins of southern Africa conference: Excursion guide, Bushveld Complex. Department of Geology, University of Pretoria, South Africa.

Wallmach, T., Hatton, C.J. and Droop, G.T.R. (1989). Extreme facies of contact metamorphism developed in calc-silicate xenoliths in the eastern Bushveld Complex. *Canadian Mineralogist*, **27**, 509-523.

Wallmach, T., Hatton, C.J., De Waal, S.A. and Gibson, R.L. (1995). Retrogressive hydration of calc-silicate xenoliths in the eastern Bushveld complex: evidence for late magmatic fluid movement. *Journal of African Earth Sciences*, **21**, 633-646.

Walraven, F., Armstrong, R.A. and Kruger, F.J. (1990). A chronostratigraphic framework for the north-central Kaapvaal Craton, the Bushveld Complex and Vredefort structure. *Tectonophysics*, **171**, 23-48.

Waters, D.J. and Lovegrove, D.P., (2002). Assessing the extent of disequilibrium and overstepping of prograde metamorphic reactions in metapelites from the Bushveld Complex aureole, South Africa. *Journal of Metamorphic Geology,* **20**, 135-149.

Webb, S.J., Cawthorn, R.G., Nguuri, T. and James, D. (2004). Gravity modeling of Bushveld Complex connectivity supported by Southern African Seismic Experiment results. *South African Journal of Geology*, **107**, 207-218.

Wells, P.R.A. (1977). Pyroxene Thermometry in Simple and Complex Systems. *Contributions to Mineralogy and Petrology,* **62**, 129-139.

Wells, P.R.A. (1976). Late Archaean metamorphism in the Buksefjorden silicic crust, southern west Greenland. *Contributions to Mineralogy and Petrology*, **56**, 229-242.

Wells, P.R.A. (1979). Chemical and thermal evolution of Archean sialic crust, Southern West Greenland. *Journal of Petrology*, **20**, 187-226.

Wells (1983). In: Mizuno, K. and Miyano, T. (1999). Two-pyroxene geothermometry in the Bushveld Complex contact in the northeastern Transvaal, South Africa. Annual Report, Institute of Geoscience, University Tsukuba, no. 25, 47-50.

Wells, P.R.A. and Richardson, S.W. (1979). Thermal evolution of metamorphic rocks in the Central Highlands of Scotland. In: Harris, A.L., Holland, C.H. and Leake, B.E. (eds.). Caledonides of the Bristish Isles – Reviewed. Geological Society of London, Special Publication 8, 339-344.

Willemse, J. (1959). The "floor" of the Bushveld Igneous Complex and its relationships, with special reference to the eastern Transvaal*. Anniversary Address by the President, 14 pp.

Winkler, H.G.F. (1970). Abolition of metamorphic facies, introduction of the four divisions of metamorphic stages, and of a classification based on isograds in common rocks. *Neues Jahrbuch für Mineralogie, Monatshefte*, **5**, 189-248.

Winkler, H.G.F. (1976). Petrogenesis of metamorphic rocks, Springer-Verlag, New York, 334 pp.

Wood, B.J. and Banno, S. (1973). Garnet-Orthopyroxene and Orthopyroxene-Clinopyroxene Relationships in Simple and Complex Systems. *Contributions to Mineralogy and Petrology,* **42**, 109-124.

Wood, B.J. (1974). Solubility of alumina in orthopyroxene coexisting with garnet. *Contributions to Mineralogy and Petrology*, **46**, 1-15.

Wood, B.J. and Fraser, D. G. (1976), Elementary Thermodynamics for Geologists. Oxford University Press, 303 pp.

# APPENDIX

**CONTENTS:**

## APPENDIX A

### Table A1. List of all collected samples with corresponding GPS-coordinates.

| Sample | Decimal Degrees South | Decimal Degrees East | Sample | Decimal Degrees South | Decimal Degrees East |
|---|---|---|---|---|---|
| **DM08-01** | 24.72106 | 30.35008 | **DM08-40** | 24.64728 | 30.38828 |
| **DM08-02** | 24.72106 | 30.35008 | **DM08-41** | 24.64500 | 30.38744 |
| **DM08-03** | 24.72106 | 30.35008 | **DM08-42** | 24.64503 | 30.38719 |
| **DM08-04** | 24.72106 | 30.35008 | **DM08-43** | 24.64550 | 30.38414 |
| **DM08-05** | 24.72106 | 30.35008 | **DM08-44** | 24.64550 | 30.38414 |
| **DM08-06** | 24.74464 | 30.36858 | **DM08-45** | 24.65467 | 30.40097 |
| **DM08-07** | 24.74422 | 30.36936 | **DM08-46** | 24.65428 | 30.40058 |
| **DM08-08** | 24.73072 | 30.36506 | **DM08-47** | 24.65736 | 30.40464 |
| **DM08-09** | 24.73072 | 30.36506 | **DM08-48** | 24.65736 | 30.40464 |
| **DM08-10** | 24.73072 | 30.36506 | **DM08-49** | 24.65756 | 30.40508 |
| **DM08-11** | 24.73072 | 30.36506 | **DM08-50** | 24.77036 | 30.36514 |
| **DM08-12** | 24.73050 | 30.36647 | **DM08-51** | 24.77036 | 30.36514 |
| **DM08-13** | 24.73036 | 30.36717 | **DM08-52** | 24.77036 | 30.36514 |
| **DM08-14** | 24.73081 | 30.37236 | **DM08-53** | 24.77036 | 30.36514 |
| **DM08-15** | 24.73033 | 30.36764 | **DM08-54** | 24.77036 | 30.36514 |
| **DM08-16** | 24.73033 | 30.36764 | **DM08-55** | 24.74622 | 30.37906 |
| **DM08-17** | 24.65464 | 30.40064 | **DM08-56** | 24.74622 | 30.37906 |
| **DM08-18** | 24.67589 | 30.49611 | **DM08-57** | 24.74622 | 30.37906 |
| **DM08-19** | 24.67589 | 30.49611 | **DM08-58** | 24.74622 | 30.37906 |
| **DM08-20** | 24.67589 | 30.49611 | **DM08-59** | 24.74661 | 30.38039 |
| **DM08-21** | 24.67589 | 30.49611 | **DM08-60** | 24.74661 | 30.38039 |
| **DM08-22** | 24.67419 | 30.49675 | **DM08-61** | 24.74683 | 30.38061 |
| **DM08-23** | 24.67419 | 30.49675 | **DM08-62** | 24.74683 | 30.38061 |
| **DM08-24** | 24.67317 | 30.49842 | **DM08-63** | 24.74703 | 30.38117 |
| **DM08-25** | 24.67303 | 30.49856 | **DM08-64** | 24.74703 | 30.38117 |
| **DM08-26** | 24.72111 | 30.52714 | **DY09-01** | 24.75769 | 30.54025 |
| **DM08-27** | 24.72111 | 30.52714 | **DY09-02** | 24.75774 | 30.54015 |
| **DM08-28** | 24.72111 | 30.52714 | **DY09-03** | 24.75769 | 30.54032 |
| **DM08-29** | 24.67622 | 30.49617 | **DY09-04** | 24.75772 | 30.54025 |
| **DM08-30** | 24.67622 | 30.49617 | **DY09-05** | 24.6788 | 30.57738 |
| **DM08-31** | 24.64728 | 30.38900 | **DY09-06** | 24.68583 | 30.58032 |
| **DM08-32** | 24.64728 | 30.38900 | **DY09-07** | 24.68583 | 30.58032 |
| **DM08-33** | 24.64733 | 30.38847 | **DY9-08** | 24.77468 | 30.53147 |
| **DM08-34** | 24.64733 | 30.38847 | **DY09-09** | 24.77468 | 30.53147 |
| **DM08-35** | 24.64733 | 30.38847 | **DY09-10** | 25.00806 | 30.50034 |
| **DM08-36** | 24.64733 | 30.38847 | **DY09-11** | 25.00806 | 30.50034 |
| **DM08-37** | 24.64733 | 30.38847 | **DY09-12** | 24.65738 | 30.40508 |
| **DM08-38** | 24.64728 | 30.38828 | **DY09-13** | 24.51694 | 30.28766 |
| **DM08-39** | 24.64728 | 30.38828 | **DY09-14** | 24.51721 | 30.28796 |

**Table A1 continued..**

| Sample | Decimal Degrees South | Decimal Degrees East | Sample | Decimal Degrees South | Decimal Degrees East |
|---|---|---|---|---|---|
| **DY09-15** | 24.51691 | 30.28757 | **DY09-57** | 24.20998 | 29.97972 |
| **DY09-16** | 24.33107 | 30.20568 | **DY09-58** | 24.78203 | 30.27543 |
| **DY09-17** | 24.33107 | 30.20568 | **DY09-59** | 24.81916 | 30.37236 |
| **DY09-18 A+B** | 24.33179 | 30.20554 | **DY09-60 A+B** | 24.83502 | 30.33565 |
| **DY09-19** | 24.73384 | 30.53707 | **DY09-61** | 24.83502 | 30.33565 |
| **DY09-20** | 24.73384 | 30.53707 | **DY09-62** | 24.91372 | 30.31354 |
| **DY09-21** | 24.73384 | 30.53707 | **DY09-63** | 25.07595 | 30.40930 |
| **DY09-22** | 24.73384 | 30.53707 | **DY09-64** | 25.07595 | 30.40930 |
| **DY09-23** | 24.75769 | 30.54025 | **DY09-65** | 25.07595 | 30.40930 |
| **DY09-24** | 24.75769 | 30.54025 | **DY09-66** | 25.07596 | 30.40910 |
| **DY09-25** | 24.75197 | 30.54900 | **DY09-67** | 25.07596 | 30.40910 |
| **DY09-26** | 24.34603 | 30.14832 | **DY09-68** | 24.95166 | 30.37232 |
| **DY09-27** | 24.34546 | 30.14859 | **DY09-69** | 24.95166 | 30.37232 |
| **DY09-28** | 24.34493 | 30.14818 | **DY09-70** | 24.95166 | 30.37232 |
| **DY09-29** | 24.34466 | 30.14811 | **DY09-71** | 24.95166 | 30.37232 |
| **DY09-30** | 24.34629 | 30.14838 | **DY09-72** | 24.74233 | 30.55352 |
| **DY09-31** | 24.34671 | 30.14864 | **DY09-73** | 24.74233 | 30.55352 |
| **DY09-32** | 24.33488 | 30.14618 | **DY09-74** | 24.74233 | 30.55352 |
| **DY09-33** | 24.33488 | 30.14618 | **DY09-75** | 24.74233 | 30.55352 |
| **DY09-34** | 24.33488 | 30.14618 | **DY09-76** | 24.66517 | 30.60777 |
| **DY09-35** | 24.33488 | 30.14618 | **DY09-77** | 24.66517 | 30.60777 |
| **DY09-36** | 24.33488 | 30.14618 | **DY09-78** | 24.66517 | 30.60777 |
| **DY09-37** | 24.33335 | 30.14916 | **DY09-79** | 24.66517 | 30.60777 |
| **DY09-38** | 24.33335 | 30.14916 | **DY09-80** | 24.66517 | 30.60777 |
| **DY09-39** | 24.33335 | 30.14916 | **DY09-81** | 24.18557 | 29.99162 |
| **DY09-40** | 24.33335 | 30.14916 | **DY09-82** | 24.18557 | 29.99162 |
| **DY09-41** | 24.33347 | 30.14901 | **DY09-83** | 24.18557 | 29.99162 |
| **DY09-42** | 24.33705 | 30.14603 | **DY09-84** | 24.18557 | 29.99162 |
| **DY09-43** | 24.33705 | 30.14603 | **DY09-85** | 24.18557 | 29.99162 |
| **DY09-44** | 24.36852 | 30.17475 | **DY09-86** | 24.18175 | 29.99305 |
| **DY09-45** | 24.36846 | 30.17426 | **DY09-87** | 24.18175 | 29.99305 |
| **DY09-46** | 24.26824 | 30.03738 | | | |
| **DY09-47** | 24.26824 | 30.03738 | | | |
| **DY09-48** | 24.26824 | 30.03738 | | | |
| **DY09-49** | 24.26824 | 30.03738 | | | |
| **DY09-50** | 24.26824 | 30.03738 | | | |
| **DY09-51** | 24.21491 | 29.95563 | | | |
| **DY09-52** | 24.21491 | 29.95563 | | | |
| **DY09-53** | 24.20998 | 29.97972 | | | |
| **DY09-54** | 24.20998 | 29.97972 | | | |
| **DY09-55** | 24.20998 | 29.97972 | | | |
| **DY09-56** | 24.20998 | 29.97972 | | | |

**Table A2. Whole-rock chemistry of all samples analyzed by X-ray fluorescence spectroscopy with relevant standard-data preceding the DM08- and DY09- samples, respectively.**

| % | GSNcert | GSN | DM08-06 | DM08-07 | DM08-13 | DM08-09 | DM08-12 | DM08-14 |
|---|---|---|---|---|---|---|---|---|
| $SiO_2$ | **65.80** | 66.22 | 62.18 | 61.53 | 65.94 | 63.92 | 69.51 | 63.81 |
| $TiO_2$ | **0.68** | 0.67 | 0.84 | 0.77 | 0.76 | 0.78 | 0.69 | 0.81 |
| $Al_2O_3$ | **14.67** | 15.21 | 18.33 | 18.90 | 16.25 | 16.75 | 14.02 | 17.46 |
| $Fe_2O_3$ | **3.75** | 3.77 | 9.35 | 9.07 | 8.33 | 8.44 | 6.68 | 8.54 |
| MnO | **0.06** | 0.05 | 0.07 | 0.06 | 0.07 | 0.06 | 0.07 | 0.05 |
| MgO | **2.30** | 2.25 | 3.22 | 3.40 | 2.90 | 3.38 | 2.63 | 3.15 |
| CaO | **2.50** | 2.69 | 0.68 | 0.74 | 0.56 | 0.84 | 1.67 | 0.52 |
| $Na_2O$ | **3.77** | 3.75 | 0.52 | 0.61 | 0.51 | 0.61 | 1.83 | 0.73 |
| $K_2O$ | **4.63** | 4.61 | 3.72 | 3.78 | 3.61 | 4.00 | 2.16 | 3.48 |
| $P_2O_5$ | **0.28** | 0.28 | 0.08 | 0.09 | 0.00 | 0.15 | 0.09 | 0.05 |
| $Cr_2O_3$ | **0.008** | 0.01 | 0.03 | 0.03 | 0.03 | 0.03 | 0.02 | 0.03 |
| NiO | **0.0043** | 0.02 | 0.02 | 0.02 | 0.02 | 0.02 | 0.01 | 0.02 |
| $V_2O_5$ | **0.01** | 0.01 | 0.01 | 0.04 | 0.00 | 0.03 | 0.00 | 0.01 |
| $ZrO_2$ | **0.03** | 0.02 | 0.01 | 0.00 | 0.02 | 0.02 | 0.01 | 0.02 |
| LOI | **1.32** | 1.29 | 0.77 | 0.73 | 0.82 | 0.89 | 0.49 | 1.14 |
| TOTAL | **99.82** | 100.87 | 99.83 | 99.75 | 99.82 | 99.91 | 99.88 | 99.82 |
| | | | | | | | | |
| % | DM08-16 | DM08-52 | DM08-53 | DM08-54 | DM08-56 | DM08-58 | DM08-62 | DM08-63 |
| $SiO_2$ | 58.42 | 48.52 | 65.21 | 51.61 | 67.87 | 66.88 | 65.63 | 62.32 |
| $TiO_2$ | 0.97 | 2.70 | 0.70 | 2.10 | 0.86 | 0.79 | 0.84 | 0.74 |
| $Al_2O_3$ | 17.13 | 25.90 | 16.69 | 22.28 | 13.51 | 15.92 | 16.14 | 16.84 |
| $Fe_2O_3$ | 10.28 | 6.94 | 6.80 | 6.71 | 8.67 | 7.22 | 7.90 | 8.75 |
| MnO | 0.10 | 0.06 | 0.03 | 0.06 | 0.07 | 0.07 | 0.06 | 0.08 |
| MgO | 4.11 | 3.06 | 2.72 | 3.16 | 3.02 | 2.54 | 2.88 | 3.01 |
| CaO | 0.64 | 1.07 | 0.55 | 1.44 | 1.15 | 1.36 | 1.17 | 1.55 |
| $Na_2O$ | 0.29 | 0.97 | 0.92 | 1.27 | 1.15 | 1.84 | 1.86 | 1.35 |
| $K_2O$ | 3.45 | 7.22 | 5.11 | 7.49 | 2.64 | 2.45 | 2.50 | 3.59 |
| $P_2O_5$ | 0.06 | 0.14 | 0.16 | 0.09 | 0.13 | 0.13 | 0.05 | 0.07 |
| $Cr_2O_3$ | 0.04 | 0.05 | 0.03 | 0.05 | 0.01 | 0.03 | 0.03 | 0.02 |
| NiO | 0.02 | 0.02 | 0.02 | 0.02 | 0.02 | 0.02 | 0.02 | 0.02 |
| $V_2O_5$ | 0.04 | 0.07 | 0.00 | 0.03 | 0.03 | 0.03 | 0.03 | 0.03 |
| $ZrO_2$ | 0.00 | 0.02 | 0.03 | 0.01 | 0.01 | 0.01 | 0.02 | 0.01 |
| LOI | 4.29 | 2.24 | 0.69 | 1.85 | 0.68 | 0.57 | 0.75 | 1.18 |
| TOTAL | 99.85 | 98.98 | 99.65 | 98.19 | 99.82 | 99.88 | 99.88 | 99.57 |

**Table A2 continued..**

| % | GSNcert | GSN | DY09-18A | DY09-18B | DY09-40 | DY09-54 | DY09-56 | DY09-60A |
|---|---|---|---|---|---|---|---|---|
| $SiO_2$ | **65.80** | 65.76 | 59.87 | 60.31 | 58.75 | 53.52 | 60.66 | 59.17 |
| $TiO_2$ | **0.68** | 0.68 | 0.78 | 0.83 | 0.72 | 0.89 | 0.77 | 0.83 |
| $Al_2O_3$ | **14.67** | 15.07 | 18.63 | 17.79 | 16.25 | 20.77 | 18.32 | 17.36 |
| $Fe_2O_3$ | **3.75** | 3.74 | 7.37 | 7.14 | 8.90 | 12.60 | 11.76 | 11.22 |
| MnO | **0.06** | 0.05 | 0.07 | 0.09 | 0.08 | 0.07 | 0.08 | 0.12 |
| MgO | **2.30** | 2.21 | 0.79 | 0.76 | 2.75 | 1.89 | 1.34 | 2.55 |
| CaO | **2.50** | 2.65 | 6.07 | 6.22 | 2.08 | 2.94 | 1.12 | 0.60 |
| $Na_2O$ | **3.77** | 3.83 | 2.91 | 2.86 | 0.66 | 1.61 | 0.80 | 0.94 |
| $K_2O$ | **4.63** | 4.62 | 0.12 | 0.09 | 7.70 | 3.62 | 3.18 | 5.87 |
| $P_2O_5$ | **0.28** | 0.29 | 0.93 | 1.58 | 0.77 | 0.95 | 0.96 | 0.09 |
| $Cr_2O_3$ | **0.008** | 0.01 | 0.03 | 0.05 | 0.02 | 0.04 | 0.04 | 0.03 |
| NiO | **0.0043** | 0.02 | 0.02 | <0.01 | 0.04 | 0.04 | 0.01 | 0.02 |
| $V_2O_5$ | **0.01** | 0.01 | 0.00 | 0.03 | 0.03 | 0.04 | 0.03 | 0.01 |
| $ZrO_2$ | **0.03** | 0.02 | 0.01 | 0.03 | 0.04 | 0.00 | 0.03 | 0.00 |
| LOI | **1.32** | 1.29 | 2.26 | 2.10 | 1.04 | 0.77 | 0.79 | 0.68 |
| TOTAL | **99.82** | 100.26 | 99.86 | 99.87 | 99.82 | 99.78 | 99.89 | 99.49 |
| | | | | | | | | |
| % | DY09-60B | DY09-66 | DY09-82 | DY09-86B | DY09-87 | | | |
| $SiO_2$ | 60.09 | 50.83 | 54.81 | 56.96 | 55.95 | | | |
| $TiO_2$ | 0.79 | 0.76 | 0.85 | 0.79 | 0.77 | | | |
| $Al_2O_3$ | 18.42 | 21.21 | 26.08 | 23.39 | 23.66 | | | |
| $Fe_2O_3$ | 9.17 | 12.46 | 10.51 | 10.70 | 10.08 | | | |
| MnO | 0.09 | 0.11 | 0.05 | 0.04 | 0.03 | | | |
| MgO | 2.64 | 2.23 | 0.78 | 0.91 | 0.99 | | | |
| CaO | 0.62 | 0.53 | 0.54 | 0.59 | 0.56 | | | |
| $Na_2O$ | 1.35 | 0.30 | 0.70 | 0.39 | 0.87 | | | |
| $K_2O$ | 5.64 | 3.02 | 3.40 | 3.42 | 3.86 | | | |
| $P_2O_5$ | 0.10 | 0.00 | 0.29 | 1.03 | 0.07 | | | |
| $Cr_2O_3$ | 0.03 | 0.42 | 0.04 | 0.02 | 0.05 | | | |
| NiO | 0.02 | 0.12 | 0.04 | 0.03 | 0.01 | | | |
| $V_2O_5$ | 0.00 | 0.06 | 0.02 | 0.02 | 0.04 | | | |
| $ZrO_2$ | 0.00 | 0.00 | 0.02 | <0.01 | <0.01 | | | |
| LOI | 0.86 | 4.98 | 1.81 | 1.54 | 2.92 | | | |
| TOTAL | 99.83 | 97.03 | 99.94 | 99.84 | 99.89 | | | |

**Table A3-1. EMPA data of sample DM08-52.**

| Point | $Na_2O$ | MgO | $Al_2O_3$ | $SiO_2$ | $K_2O$ | CaO | $TiO_2$ | FeO | BaO | $Cr_2O_3$ | MnO | ZnO | Total |
|---|---|---|---|---|---|---|---|---|---|---|---|---|---|
| **3/1 .** | 0.63 | 0.54 | 32.81 | 52.37 | 8.88 | 0.00 | 0.59 | 0.84 | 1.19 | 0.00 | 0.01 | 0.01 | 97.87 |
| **4/1 .** | 0.24 | 9.86 | 19.85 | 34.65 | 9.38 | 0.00 | 2.88 | 17.76 | 0.40 | 0.18 | 0.09 | 0.04 | 95.32 |
| **5/1 .** | 0.29 | 9.96 | 19.77 | 34.17 | 9.24 | 0.00 | 2.69 | 17.72 | 0.41 | 0.14 | 0.03 | 0.00 | 94.40 |
| **6/1 .** | 0.18 | 9.43 | 20.11 | 34.66 | 9.23 | 0.01 | 2.93 | 18.13 | 0.52 | 0.17 | 0.07 | 0.02 | 95.45 |
| **7/1 .** | 0.14 | 10.57 | 20.05 | 34.57 | 8.80 | 0.01 | 2.38 | 17.29 | 0.38 | 0.12 | 0.05 | 0.00 | 94.36 |
| **8/1 .** | 0.24 | 10.84 | 20.21 | 35.19 | 9.29 | 0.04 | 2.43 | 16.74 | 0.30 | 0.14 | 0.10 | 0.00 | 95.52 |
| **9/1 .** | 0.01 | 0.03 | 63.73 | 36.28 | 0.00 | 0.00 | 0.08 | 0.33 | 0.00 | 0.03 | 0.01 | 0.00 | 100.51 |
| **10/1 .** | 0.02 | 0.07 | 63.48 | 36.17 | 0.00 | 0.00 | 0.09 | 0.40 | 0.00 | 0.02 | 0.00 | 0.00 | 100.23 |
| **11/1 .** | 0.01 | 0.04 | 64.09 | 36.14 | 0.00 | 0.01 | 0.09 | 0.34 | 0.00 | 0.00 | 0.00 | 0.00 | 100.72 |
| **12/1 .** | 0.01 | 0.22 | 63.22 | 36.11 | 0.01 | 0.00 | 0.25 | 0.77 | 0.00 | 0.03 | 0.00 | 0.00 | 100.62 |
| **13/1 .** | 0.01 | 0.04 | 64.18 | 35.92 | 0.00 | 0.01 | 0.12 | 0.36 | 0.06 | 0.00 | 0.00 | 0.00 | 100.70 |
| **14/1 .** | 0.01 | 0.04 | 64.13 | 36.09 | 0.00 | 0.02 | 0.08 | 0.32 | 0.01 | 0.00 | 0.00 | 0.00 | 100.70 |
| **15/1 .** | 0.00 | 0.04 | 63.93 | 36.00 | 0.02 | 0.01 | 0.04 | 0.31 | 0.00 | 0.00 | 0.02 | 0.00 | 100.39 |
| **16/1 .** | 2.01 | 0.00 | 19.76 | 62.30 | 13.01 | 0.00 | 0.06 | 0.09 | 3.17 | 0.00 | 0.00 | 0.01 | 100.42 |
| **17/1 .** | 0.76 | 0.68 | 36.31 | 44.71 | 8.62 | 0.00 | 1.09 | 0.92 | 1.16 | 0.08 | 0.00 | 0.00 | 94.33 |
| **18/1 .** | 0.81 | 0.69 | 36.44 | 45.94 | 10.22 | 0.00 | 0.73 | 0.89 | 0.89 | 0.01 | 0.00 | 0.00 | 96.62 |
| **20/1 .** | 0.76 | 0.61 | 36.45 | 45.96 | 9.97 | 0.10 | 0.71 | 1.09 | 0.92 | 0.00 | 0.00 | 0.00 | 96.57 |
| **21/1 .** | 0.32 | 10.04 | 20.46 | 35.34 | 9.12 | 0.00 | 3.03 | 18.20 | 0.36 | 0.10 | 0.11 | 0.05 | 97.13 |
| **22/1 .** | 0.27 | 10.16 | 20.64 | 35.78 | 9.38 | 0.02 | 2.96 | 18.11 | 0.36 | 0.11 | 0.13 | 0.01 | 97.93 |
| **23/1 .** | 0.01 | 0.07 | 0.00 | 0.02 | 0.00 | 0.05 | 53.35 | 44.69 | 0.08 | 0.04 | 2.26 | 0.08 | 100.65 |
| **24/1 .** | 0.00 | 0.14 | 0.03 | 0.04 | 0.00 | 0.02 | 53.60 | 44.78 | 0.21 | 0.00 | 1.79 | 0.00 | 100.60 |
| **25/1 .** | 0.01 | 0.12 | 0.03 | 0.01 | 0.00 | 0.01 | 53.33 | 44.65 | 0.12 | 0.01 | 1.93 | 0.00 | 100.22 |
| **26/1 .** | 0.02 | 0.10 | 0.02 | 0.00 | 0.01 | 0.01 | 53.34 | 44.36 | 0.09 | 0.01 | 1.84 | 0.00 | 99.81 |
| **27/1 .** | 0.70 | 0.65 | 35.96 | 45.11 | 8.70 | 0.00 | 1.30 | 0.92 | 0.72 | 0.06 | 0.02 | 0.00 | 94.14 |
| **29/1 .** | 0.73 | 0.76 | 35.73 | 44.79 | 9.24 | 0.02 | 0.89 | 1.30 | 0.65 | 0.00 | 0.00 | 0.00 | 94.09 |
| **30/1 .** | 6.67 | 0.00 | 29.45 | 53.92 | 0.11 | 10.37 | 0.01 | 0.06 | 0.03 | 0.02 | 0.03 | 0.00 | 100.67 |
| **31/1 .** | 6.97 | 0.00 | 28.97 | 55.22 | 0.13 | 9.55 | 0.02 | 0.04 | 0.00 | 0.02 | 0.00 | 0.00 | 100.92 |
| **32/1 .** | 7.06 | 0.00 | 28.70 | 55.49 | 0.16 | 9.56 | 0.02 | 0.06 | 0.00 | 0.00 | 0.04 | 0.00 | 101.08 |
| **33/1 .** | 0.77 | 0.68 | 36.57 | 45.01 | 9.04 | 0.00 | 0.82 | 0.79 | 0.64 | 0.01 | 0.02 | 0.00 | 94.35 |
| **34/1 .** | 0.79 | 0.75 | 36.82 | 45.83 | 10.33 | 0.00 | 0.49 | 0.95 | 0.66 | 0.01 | 0.00 | 0.00 | 96.62 |
| **35/1 .** | 0.73 | 0.81 | 36.82 | 45.41 | 9.15 | 0.00 | 0.23 | 0.93 | 0.96 | 0.00 | 0.01 | 0.00 | 95.05 |
| **36/1 .** | 0.03 | 0.03 | 0.03 | 0.09 | 0.00 | 0.02 | 53.41 | 44.14 | 0.03 | 0.00 | 2.70 | 0.06 | 100.54 |
| **37/1 .** | 0.02 | 0.03 | 0.03 | 0.01 | 0.02 | 0.06 | 53.61 | 43.97 | 0.19 | 0.06 | 2.41 | 0.03 | 100.45 |
| **38/1 .** | 0.00 | 0.03 | 0.04 | 0.04 | 0.00 | 0.05 | 53.23 | 43.87 | 0.11 | 0.05 | 2.36 | 0.01 | 99.79 |
| **39/1 .** | 0.02 | 0.08 | 61.93 | 35.44 | 0.07 | 0.00 | 0.07 | 0.29 | 0.02 | 0.02 | 0.00 | 0.04 | 97.97 |
| **40/1 .** | 0.73 | 0.59 | 36.37 | 45.85 | 10.37 | 0.00 | 1.33 | 1.01 | 0.64 | 0.17 | 0.00 | 0.01 | 97.07 |
| **41/1 .** | 0.78 | 0.74 | 36.70 | 44.90 | 9.20 | 0.00 | 0.38 | 0.90 | 0.93 | 0.00 | 0.01 | 0.00 | 94.55 |
| **42/1 .** | 0.77 | 0.77 | 36.29 | 45.62 | 10.19 | 0.00 | 0.40 | 0.99 | 0.71 | 0.00 | 0.00 | 0.00 | 95.74 |
| **43/1 .** | 0.79 | 0.61 | 35.08 | 42.75 | 8.30 | 3.99 | 0.61 | 0.76 | 0.56 | 0.00 | 0.04 | 0.00 | 93.49 |
| **44/1 .** | 0.73 | 0.74 | 36.43 | 44.85 | 9.79 | 0.00 | 0.90 | 0.92 | 2.27 | 0.00 | 0.00 | 0.01 | 96.64 |
| **45/1 .** | 0.75 | 0.71 | 36.91 | 45.36 | 9.15 | 0.00 | 0.37 | 0.95 | 0.86 | 0.00 | 0.00 | 0.00 | 95.05 |

**Table A3-1 continued..**

| Point | $Na_2O$ | MgO | $Al_2O_3$ | $SiO_2$ | $K_2O$ | CaO | $TiO_2$ | FeO | BaO | $Cr_2O_3$ | MnO | ZnO | Total |
|---|---|---|---|---|---|---|---|---|---|---|---|---|---|
| **46/1 .** | 0.80 | 0.71 | 37.12 | 45.06 | 10.09 | 0.00 | 0.38 | 0.92 | 1.47 | 0.00 | 0.00 | 0.00 | 96.55 |
| **47/1 .** | 0.77 | 0.69 | 36.51 | 45.43 | 8.52 | 0.00 | 0.75 | 1.01 | 0.63 | 0.03 | 0.00 | 0.00 | 94.33 |
| **48/1 .** | 0.75 | 0.70 | 36.23 | 45.50 | 10.22 | 0.02 | 1.22 | 0.95 | 0.53 | 0.01 | 0.01 | 0.00 | 96.14 |
| **49/1 .** | 0.82 | 0.55 | 37.03 | 44.93 | 8.93 | 0.00 | 0.48 | 1.01 | 0.57 | 0.00 | 0.03 | 0.00 | 94.35 |
| **50/1 .** | 0.76 | 0.71 | 37.01 | 45.71 | 10.35 | 0.02 | 0.46 | 1.05 | 1.19 | 0.00 | 0.00 | 0.00 | 97.26 |
| **51/1 .** | 0.24 | 10.98 | 20.10 | 34.56 | 9.03 | 0.01 | 2.82 | 16.55 | 0.55 | 0.16 | 0.04 | 0.02 | 95.05 |
| **52/1 .** | 0.75 | 0.62 | 36.37 | 45.56 | 10.36 | 0.00 | 1.35 | 0.92 | 0.59 | 0.18 | 0.01 | 0.00 | 96.71 |
| **53/1 .** | 0.76 | 0.69 | 37.08 | 45.42 | 8.62 | 0.00 | 0.77 | 0.95 | 0.42 | 0.00 | 0.00 | 0.00 | 94.70 |
| **54/1 .** | 0.75 | 0.71 | 36.93 | 46.12 | 10.25 | 0.00 | 0.56 | 0.84 | 0.60 | 0.00 | 0.00 | 0.02 | 96.79 |
| **55/1 .** | 0.80 | 0.69 | 36.62 | 45.25 | 8.72 | 0.00 | 0.51 | 0.94 | 0.53 | 0.00 | 0.00 | 0.00 | 94.06 |
| **56/1 .** | 0.60 | 0.53 | 26.66 | 64.33 | 7.53 | 0.00 | 0.26 | 0.60 | 0.63 | 0.00 | 0.00 | 0.03 | 101.16 |
| **57/1 .** | 0.13 | 11.44 | 20.67 | 35.38 | 9.41 | 0.00 | 2.16 | 16.16 | 0.70 | 0.02 | 0.07 | 0.00 | 96.13 |
| **58/1 .** | 0.65 | 1.89 | 34.47 | 43.65 | 9.82 | 0.12 | 1.13 | 3.26 | 1.25 | 0.01 | 0.00 | 0.00 | 96.27 |
| **59/1 .** | 0.00 | 0.10 | 64.02 | 36.12 | 0.00 | 0.00 | 0.14 | 0.44 | 0.00 | 0.01 | 0.00 | 0.02 | 100.85 |
| **60/1 .** | 0.02 | 0.02 | 63.93 | 36.14 | 0.00 | 0.00 | 0.14 | 0.26 | 0.00 | 0.08 | 0.01 | 0.00 | 100.59 |
| **61/1 .** | 0.76 | 0.47 | 36.54 | 43.96 | 8.20 | 0.00 | 1.48 | 0.82 | 2.61 | 0.04 | 0.00 | 0.00 | 94.88 |
| **62/1 .** | 0.05 | 0.03 | 61.46 | 36.07 | 0.01 | 0.01 | 0.01 | 0.20 | 0.00 | 0.04 | 0.00 | 0.00 | 97.87 |
| **63/1 .** | 0.01 | 0.04 | 64.02 | 36.30 | 0.01 | 0.00 | 0.03 | 0.31 | 0.04 | 0.07 | 0.00 | 0.00 | 100.81 |
| **64/1 .** | 0.01 | 0.02 | 64.17 | 36.34 | 0.01 | 0.00 | 0.04 | 0.25 | 0.00 | 0.00 | 0.01 | 0.04 | 100.89 |
| **65/1 .** | 0.01 | 0.01 | 63.94 | 36.20 | 0.00 | 0.00 | 0.03 | 0.21 | 0.01 | 0.01 | 0.02 | 0.00 | 100.45 |
| **66/1 .** | 0.02 | 0.03 | 64.11 | 36.28 | 0.00 | 0.00 | 0.04 | 0.28 | 0.07 | 0.04 | 0.01 | 0.00 | 100.89 |
| **67/1 .** | 0.01 | 0.03 | 64.02 | 36.49 | 0.00 | 0.00 | 0.01 | 0.31 | 0.00 | 0.08 | 0.01 | 0.00 | 100.97 |
| **68/1 .** | 0.00 | 0.04 | 64.28 | 36.15 | 0.00 | 0.00 | 0.03 | 0.27 | 0.00 | 0.00 | 0.00 | 0.01 | 100.79 |
| **69/1 .** | 0.01 | 0.03 | 0.06 | 0.00 | 0.00 | 0.00 | 53.29 | 44.87 | 0.15 | 0.04 | 1.39 | 0.09 | 99.93 |
| **70/1 .** | 0.00 | 0.02 | 0.09 | 0.06 | 0.00 | 0.00 | 53.28 | 45.07 | 0.06 | 0.00 | 1.48 | 0.03 | 100.08 |
| **72/1 .** | 0.00 | 0.02 | 63.93 | 36.09 | 0.01 | 0.00 | 0.07 | 0.27 | 0.04 | 0.07 | 0.01 | 0.00 | 100.51 |
| **73/1 .** | 0.00 | 0.03 | 63.70 | 36.28 | 0.00 | 0.00 | 0.06 | 0.30 | 0.00 | 0.07 | 0.01 | 0.01 | 100.47 |
| **74/1 .** | 0.01 | 0.03 | 64.00 | 36.26 | 0.00 | 0.00 | 0.06 | 0.24 | 0.02 | 0.09 | 0.01 | 0.02 | 100.73 |
| **75/1 .** | 0.81 | 0.62 | 36.76 | 44.73 | 8.96 | 0.00 | 0.89 | 1.03 | 0.77 | 0.03 | 0.03 | 0.02 | 94.63 |
| **76/1 .** | 0.75 | 0.59 | 36.60 | 45.52 | 10.32 | 0.00 | 0.90 | 0.99 | 0.56 | 0.04 | 0.00 | 0.04 | 96.31 |
| **77/1 .** | 0.81 | 0.61 | 36.17 | 44.99 | 8.77 | 0.00 | 1.14 | 0.97 | 0.52 | 0.07 | 0.01 | 0.04 | 94.09 |
| **78/1 .** | 0.78 | 0.60 | 36.78 | 45.29 | 10.20 | 0.01 | 0.86 | 1.02 | 0.98 | 0.07 | 0.02 | 0.01 | 96.61 |
| **79/1 .** | 6.83 | 0.00 | 29.16 | 54.60 | 0.10 | 9.93 | 0.02 | 0.03 | 0.03 | 0.02 | 0.01 | 0.02 | 100.74 |
| **80/1 .** | 6.22 | 0.00 | 29.78 | 53.29 | 0.10 | 10.74 | 0.02 | 0.02 | 0.02 | 0.00 | 0.01 | 0.00 | 100.21 |
| **81/1 .** | 6.50 | 0.00 | 29.50 | 54.27 | 0.12 | 10.49 | 0.05 | 0.03 | 0.03 | 0.03 | 0.01 | 0.01 | 101.04 |
| **82/1 .** | 5.62 | 0.00 | 30.66 | 52.82 | 0.08 | 11.87 | 0.02 | 0.07 | 0.03 | 0.03 | 0.01 | 0.00 | 101.21 |
| **83/1 .** | 5.65 | 0.01 | 30.56 | 52.74 | 0.07 | 11.72 | 0.03 | 0.06 | 0.03 | 0.02 | 0.02 | 0.00 | 100.92 |
| **84/1 .** | 6.54 | 0.00 | 29.23 | 54.47 | 0.06 | 10.16 | 0.03 | 0.07 | 0.00 | 0.02 | 0.00 | 0.00 | 100.57 |
| **85/1 .** | 0.18 | 10.13 | 20.47 | 35.38 | 9.38 | 0.06 | 2.67 | 17.22 | 0.38 | 0.14 | 0.12 | 0.06 | 96.19 |
| **86/1 .** | 0.01 | 0.07 | 0.07 | 0.11 | 0.00 | 0.13 | 53.21 | 42.36 | 0.14 | 0.06 | 2.40 | 0.05 | 98.60 |
| **87/1 .** | 0.02 | 0.06 | 0.03 | 0.04 | 0.02 | 0.09 | 53.56 | 42.74 | 0.07 | 0.00 | 2.22 | 0.00 | 98.85 |

**Table A3-1 continued..**

| Point | $Na_2O$ | MgO | $Al_2O_3$ | $SiO_2$ | K2O | CaO | $TiO_2$ | FeO | BaO | $Cr_2O_3$ | MnO | ZnO | Total |
|---|---|---|---|---|---|---|---|---|---|---|---|---|---|
| **88/1 .** | 0.23 | 9.89 | 19.61 | 34.81 | 9.20 | 0.00 | 3.00 | 17.42 | 0.39 | 0.15 | 0.10 | 0.04 | 94.84 |
| **89/1 .** | 0.23 | 10.07 | 20.31 | 35.07 | 9.17 | 0.01 | 2.99 | 17.60 | 0.39 | 0.15 | 0.16 | 0.01 | 96.15 |
| **90/1 .** | 0.21 | 9.73 | 20.10 | 34.99 | 9.25 | 0.03 | 2.99 | 16.98 | 0.42 | 0.14 | 0.09 | 0.00 | 94.94 |
| **91/1 .** | 0.20 | 9.90 | 20.17 | 35.12 | 8.90 | 0.01 | 2.95 | 17.02 | 0.49 | 0.15 | 0.09 | 0.04 | 95.04 |
| **92/1 .** | 0.21 | 10.07 | 20.16 | 35.25 | 9.36 | 0.01 | 3.04 | 17.05 | 0.43 | 0.19 | 0.13 | 0.05 | 95.93 |
| **93/1 .** | 0.16 | 10.82 | 20.25 | 34.64 | 8.26 | 0.01 | 2.88 | 17.71 | 0.38 | 0.14 | 0.08 | 0.00 | 95.32 |
| **94/1 .** | 0.23 | 9.71 | 20.02 | 35.06 | 9.25 | 0.03 | 3.03 | 17.11 | 0.39 | 0.15 | 0.11 | 0.00 | 95.08 |
| **95/1 .** | 0.18 | 9.90 | 20.01 | 35.05 | 9.24 | 0.05 | 2.86 | 17.04 | 0.42 | 0.17 | 0.09 | 0.05 | 95.08 |
| **96/1 .** | 0.00 | 0.06 | 0.02 | 0.04 | 0.03 | 0.01 | 53.29 | 43.66 | 0.06 | 0.02 | 2.40 | 0.00 | 99.59 |
| **97/1 .** | 0.01 | 0.08 | 0.05 | 0.00 | 0.08 | 0.02 | 53.33 | 43.90 | 0.04 | 0.03 | 2.27 | 0.00 | 99.81 |
| **98/1 .** | 0.24 | 9.80 | 19.92 | 34.70 | 9.47 | 0.00 | 3.07 | 17.75 | 0.43 | 0.19 | 0.10 | 0.00 | 95.67 |
| **99/1 .** | 0.25 | 9.80 | 19.83 | 34.65 | 9.36 | 0.00 | 3.02 | 18.11 | 0.61 | 0.16 | 0.10 | 0.00 | 95.89 |
| **100/1 .** | 6.99 | 0.00 | 29.11 | 55.12 | 0.09 | 9.84 | 0.01 | 0.08 | 0.02 | 0.03 | 0.00 | 0.00 | 101.30 |
| **101/1 .** | 6.34 | 0.01 | 30.16 | 53.70 | 0.07 | 10.77 | 0.02 | 0.12 | 0.02 | 0.00 | 0.00 | 0.00 | 101.22 |
| **102/1 .** | 6.42 | 0.00 | 29.75 | 54.42 | 0.05 | 10.54 | 0.02 | 0.08 | 0.01 | 0.00 | 0.01 | 0.00 | 101.31 |
| **103/1 .** | 5.60 | 0.00 | 30.64 | 52.34 | 0.07 | 11.77 | 0.00 | 0.07 | 0.03 | 0.00 | 0.02 | 0.03 | 100.56 |
| **104/1 .** | 6.38 | 0.00 | 29.74 | 54.11 | 0.09 | 10.51 | 0.04 | 0.11 | 0.06 | 0.02 | 0.00 | 0.00 | 101.06 |
| **105/1 .** | 0.23 | 9.83 | 20.11 | 35.15 | 9.34 | 0.00 | 3.09 | 17.76 | 0.39 | 0.12 | 0.10 | 0.03 | 96.16 |
| **106/1 .** | 0.23 | 9.96 | 19.93 | 35.27 | 9.41 | 0.04 | 3.11 | 17.75 | 0.41 | 0.08 | 0.08 | 0.02 | 96.29 |
| **107/1 .** | 0.76 | 0.66 | 36.36 | 44.80 | 8.57 | 0.00 | 1.08 | 0.97 | 0.86 | 0.22 | 0.01 | 0.00 | 94.29 |
| **108/1 .** | 0.19 | 11.30 | 20.19 | 35.01 | 9.46 | 0.00 | 2.49 | 16.54 | 0.47 | 0.17 | 0.14 | 0.05 | 96.00 |
| **109/1 .** | 0.24 | 11.01 | 20.47 | 34.92 | 9.23 | 0.00 | 2.42 | 16.86 | 0.54 | 0.11 | 0.11 | 0.00 | 95.92 |
| **110/1 .** | 0.18 | 11.10 | 20.10 | 35.22 | 9.48 | 0.00 | 2.32 | 16.58 | 0.49 | 0.14 | 0.09 | 0.01 | 95.72 |
| **111/1 .** | 0.25 | 10.06 | 20.09 | 34.93 | 9.32 | 0.00 | 2.76 | 17.73 | 0.47 | 0.17 | 0.09 | 0.00 | 95.88 |
| **112/1 .** | 0.70 | 0.60 | 35.95 | 44.73 | 10.02 | 0.00 | 1.01 | 0.96 | 1.11 | 0.13 | 0.00 | 0.02 | 95.22 |
| **113/1 .** | 0.19 | 9.49 | 20.19 | 34.78 | 9.34 | 0.00 | 2.84 | 17.36 | 0.71 | 0.29 | 0.06 | 0.00 | 95.25 |
| **114/1 .** | 0.17 | 10.37 | 19.72 | 34.38 | 9.30 | 0.00 | 2.83 | 17.79 | 0.45 | 0.17 | 0.04 | 0.00 | 95.23 |
| **115/1 .** | 0.18 | 10.02 | 19.42 | 34.82 | 9.40 | 0.05 | 2.86 | 17.59 | 0.47 | 0.20 | 0.07 | 0.03 | 95.09 |
| **116/1 .** | 0.24 | 10.31 | 20.17 | 34.67 | 9.24 | 0.00 | 2.86 | 17.68 | 0.55 | 0.18 | 0.07 | 0.02 | 95.99 |
| **117/1 .** | 0.04 | 3.79 | 6.44 | 74.78 | 3.47 | 0.02 | 0.84 | 5.89 | 0.23 | 0.03 | 0.00 | 0.00 | 95.51 |
| **118/1 .** | 0.81 | 0.70 | 35.80 | 44.95 | 10.07 | 0.01 | 0.87 | 1.08 | 0.60 | 0.00 | 0.01 | 0.01 | 94.91 |
| **120/1 .** | 0.73 | 0.57 | 32.91 | 49.82 | 9.01 | 0.00 | 0.33 | 0.71 | 1.02 | 0.00 | 0.00 | 0.02 | 95.14 |
| **121/1 .** | 0.19 | 10.93 | 20.19 | 35.39 | 9.42 | 0.00 | 2.75 | 17.20 | 0.37 | 0.09 | 0.09 | 0.02 | 96.63 |
| **122/1 .** | 0.77 | 0.82 | 36.15 | 44.68 | 9.88 | 0.00 | 0.17 | 0.99 | 1.31 | 0.00 | 0.02 | 0.00 | 94.81 |
| **123/1 .** | 0.81 | 0.71 | 36.56 | 44.30 | 9.46 | 0.00 | 0.34 | 0.93 | 1.66 | 0.00 | 0.01 | 0.00 | 94.78 |
| **124/1 .** | 0.81 | 0.75 | 37.04 | 44.84 | 9.86 | 0.00 | 0.22 | 0.94 | 1.77 | 0.00 | 0.00 | 0.00 | 96.23 |
| **125/1 .** | 0.29 | 11.77 | 20.67 | 35.29 | 9.30 | 0.00 | 1.62 | 16.04 | 0.37 | 0.06 | 0.12 | 0.00 | 95.54 |
| **126/1 .** | 0.00 | 0.04 | 63.94 | 36.14 | 0.02 | 0.00 | 0.05 | 0.28 | 0.00 | 0.04 | 0.00 | 0.00 | 100.51 |
| **127/1 .** | 0.25 | 11.64 | 20.62 | 35.32 | 9.09 | 0.00 | 2.03 | 16.01 | 0.29 | 0.08 | 0.11 | 0.00 | 95.44 |
| **128/1 .** | 0.70 | 0.64 | 35.73 | 45.37 | 10.48 | 0.00 | 0.91 | 0.99 | 0.63 | 0.16 | 0.01 | 0.00 | 95.61 |
| **129/1 .** | 0.00 | 0.00 | 0.06 | 0.12 | 0.16 | 0.00 | 99.07 | 0.11 | 0.15 | 0.22 | 0.00 | 0.00 | 99.91 |

**Table A3-1 continued..**

| Point | $Na_2O$ | MgO | $Al_2O_3$ | $SiO_2$ | $K_2O$ | CaO | $TiO_2$ | FeO | BaO | $Cr_2O_3$ | MnO | ZnO | Total |
|---|---|---|---|---|---|---|---|---|---|---|---|---|---|
| **130 / 1 .** | 0.77 | 0.64 | 36.07 | 44.76 | 9.94 | 0.01 | 1.14 | 0.93 | 1.31 | 0.14 | 0.00 | 0.00 | 95.71 |
| **131 / 1 .** | 0.26 | 11.08 | 20.29 | 35.15 | 9.24 | 0.01 | 2.45 | 16.59 | 0.44 | 0.17 | 0.12 | 0.00 | 95.82 |
| **132 / 1 .** | 6.99 | 0.00 | 28.95 | 54.92 | 0.07 | 9.72 | 0.06 | 0.12 | 0.00 | 0.00 | 0.00 | 0.04 | 100.90 |
| **134 / 1 .** | 6.91 | 0.01 | 29.04 | 54.73 | 0.11 | 9.99 | 0.02 | 0.15 | 0.03 | 0.02 | 0.02 | 0.04 | 101.07 |
| **135 / 1 .** | 6.64 | 0.00 | 29.23 | 54.40 | 0.08 | 10.10 | 0.03 | 0.11 | 0.09 | 0.03 | 0.02 | 0.04 | 100.76 |
| **136 / 1 .** | 7.13 | 0.00 | 28.89 | 55.21 | 0.08 | 9.59 | 0.02 | 0.13 | 0.00 | 0.01 | 0.04 | 0.00 | 101.09 |
| **137 / 1 .** | 0.03 | 0.01 | 61.09 | 37.60 | 0.22 | 0.02 | 0.02 | 0.12 | 0.27 | 0.28 | 0.01 | 0.00 | 99.69 |
| **138 / 1 .** | 0.29 | 8.02 | 25.58 | 37.76 | 9.49 | 0.01 | 2.47 | 13.73 | 0.75 | 0.07 | 0.06 | 0.00 | 98.23 |
| **139 / 1 .** | 0.76 | 0.66 | 35.69 | 44.76 | 8.56 | 0.00 | 1.35 | 0.92 | 0.66 | 0.20 | 0.00 | 0.00 | 93.55 |
| **140 / 1 .** | 0.77 | 0.69 | 36.03 | 45.40 | 10.40 | 0.02 | 0.87 | 0.97 | 0.62 | 0.08 | 0.01 | 0.01 | 95.87 |

**Table A3-2. EMPA data of samples DY09-54, -56, -82 and -87.**

| Point | $Na_2O$ | MgO | $Al_2O_3$ | $SiO_2$ | $K_2O$ | CaO | $TiO_2$ | $Cr_2O_3$ | MnO | FeO | ZnO | Total |
|---|---|---|---|---|---|---|---|---|---|---|---|---|
| **1 / 1 .** | 0.09 | 1.28 | 18.06 | 29.52 | 0.03 | 2.10 | 0.00 | 0.00 | 2.50 | 35.78 | 0.06 | 89.43 |
| **2 / 1 .** | 0.03 | 1.69 | 21.67 | 36.02 | 0.00 | 1.88 | 0.00 | 0.03 | 2.86 | 36.62 | 0.00 | 100.79 |
| **3 / 1 .** | 0.02 | 1.70 | 21.48 | 35.48 | 0.00 | 1.67 | 0.01 | 0.00 | 3.15 | 35.82 | 0.00 | 99.33 |
| **4 / 1 .** | 0.03 | 1.77 | 21.59 | 35.15 | 0.00 | 1.60 | 0.02 | 0.01 | 3.72 | 35.60 | 0.02 | 99.52 |
| **5 / 1 .** | 0.03 | 1.72 | 21.68 | 35.72 | 0.00 | 1.59 | 0.01 | 0.00 | 3.96 | 35.50 | 0.00 | 100.22 |
| **6 / 1 .** | 0.03 | 1.80 | 21.57 | 35.70 | 0.01 | 1.57 | 0.03 | 0.00 | 4.16 | 35.29 | 0.00 | 100.16 |
| **7 / 1 .** | 0.03 | 1.76 | 21.41 | 35.78 | 0.00 | 1.54 | 0.00 | 0.02 | 4.35 | 35.07 | 0.00 | 99.97 |
| **8 / 1 .** | 0.03 | 1.79 | 21.57 | 36.16 | 0.00 | 1.58 | 0.00 | 0.01 | 4.23 | 34.87 | 0.00 | 100.25 |
| **9 / 1 .** | 0.03 | 1.79 | 21.48 | 36.06 | 0.00 | 1.71 | 0.06 | 0.05 | 4.21 | 34.51 | 0.00 | 99.93 |
| **10 / 1 .** | 0.03 | 1.74 | 21.29 | 36.06 | 0.00 | 1.62 | 0.03 | 0.04 | 4.13 | 34.64 | 0.03 | 99.62 |
| **11 / 1 .** | 0.03 | 1.80 | 21.45 | 36.30 | 0.01 | 1.46 | 0.05 | 0.06 | 4.20 | 34.79 | 0.02 | 100.17 |
| **12 / 1 .** | 0.04 | 1.82 | 21.57 | 36.12 | 0.00 | 1.54 | 0.00 | 0.01 | 4.12 | 34.95 | 0.01 | 100.18 |
| **13 / 1 .** | 0.03 | 1.77 | 21.46 | 36.24 | 0.00 | 1.68 | 0.04 | 0.02 | 3.97 | 35.14 | 0.00 | 100.34 |
| **14 / 1 .** | 0.03 | 1.78 | 21.38 | 36.20 | 0.01 | 1.58 | 0.00 | 0.02 | 3.80 | 35.55 | 0.00 | 100.36 |
| **15 / 1 .** | 0.02 | 1.71 | 21.53 | 36.35 | 0.00 | 1.57 | 0.00 | 0.01 | 3.50 | 36.01 | 0.02 | 100.72 |
| **16 / 1 .** | 0.03 | 1.76 | 21.41 | 36.23 | 0.02 | 1.65 | 0.02 | 0.02 | 3.14 | 36.06 | 0.00 | 100.34 |
| **17 / 1 .** | 0.03 | 1.64 | 21.60 | 35.94 | 0.01 | 1.76 | 0.01 | 0.00 | 2.90 | 35.81 | 0.00 | 99.70 |
| **18 / 1 .** | 0.06 | 1.22 | 18.02 | 42.61 | 0.00 | 1.72 | 0.00 | 0.03 | 2.31 | 32.61 | 0.00 | 98.58 |
| **19 / 1 .** | 0.00 | 1.79 | 21.79 | 36.98 | 0.00 | 2.02 | 0.03 | 0.00 | 2.87 | 35.90 | 0.00 | 101.38 |
| **20 / 1 .** | 0.01 | 1.76 | 21.38 | 36.09 | 0.00 | 1.83 | 0.00 | 0.04 | 3.15 | 35.93 | 0.02 | 100.20 |
| **21 / 1 .** | 0.01 | 1.73 | 21.31 | 36.29 | 0.01 | 1.66 | 0.00 | 0.03 | 3.66 | 35.68 | 0.00 | 100.37 |
| **22 / 1 .** | 0.02 | 1.86 | 21.37 | 35.87 | 0.00 | 1.49 | 0.02 | 0.04 | 3.86 | 35.44 | 0.02 | 99.99 |
| **23 / 1 .** | 0.05 | 1.69 | 21.55 | 36.11 | 0.00 | 1.55 | 0.03 | 0.02 | 4.02 | 35.14 | 0.01 | 100.17 |
| **24 / 1 .** | 0.03 | 1.80 | 21.55 | 36.25 | 0.00 | 1.51 | 0.07 | 0.02 | 4.20 | 34.71 | 0.01 | 100.15 |
| **25 / 1 .** | 0.02 | 1.76 | 21.59 | 36.05 | 0.00 | 1.54 | 0.06 | 0.03 | 4.18 | 34.96 | 0.00 | 100.19 |
| **26 / 1 .** | 0.04 | 1.79 | 21.67 | 36.37 | 0.00 | 1.70 | 0.00 | 0.04 | 4.05 | 34.93 | 0.00 | 100.59 |
| **27 / 1 .** | 0.02 | 1.77 | 21.42 | 35.89 | 0.00 | 1.60 | 0.05 | 0.05 | 4.16 | 35.03 | 0.00 | 99.99 |
| **28 / 1 .** | 0.02 | 1.80 | 21.60 | 36.35 | 0.00 | 1.56 | 0.02 | 0.00 | 4.09 | 35.35 | 0.00 | 100.79 |
| **29 / 1 .** | 0.02 | 1.85 | 21.56 | 35.98 | 0.00 | 1.62 | 0.03 | 0.01 | 4.13 | 35.12 | 0.04 | 100.35 |
| **30 / 1 .** | 0.05 | 1.82 | 21.56 | 36.38 | 0.02 | 1.51 | 0.01 | 0.00 | 3.93 | 35.20 | 0.03 | 100.53 |
| **31 / 1 .** | 0.04 | 1.77 | 21.35 | 36.24 | 0.00 | 1.54 | 0.00 | 0.01 | 3.81 | 35.63 | 0.03 | 100.42 |
| **32 / 1 .** | 0.00 | 1.82 | 21.44 | 36.16 | 0.00 | 1.65 | 0.00 | 0.02 | 3.75 | 35.82 | 0.00 | 100.66 |
| **33 / 1 .** | 0.26 | 7.14 | 20.97 | 34.38 | 7.89 | 0.04 | 1.62 | 0.06 | 0.09 | 22.84 | 0.00 | 95.29 |
| **34 / 1 .** | 0.28 | 6.65 | 20.54 | 34.72 | 8.71 | 0.05 | 1.80 | 0.08 | 0.05 | 23.02 | 0.00 | 95.91 |
| **35 / 1 .** | 0.29 | 6.85 | 20.16 | 34.25 | 8.86 | 0.02 | 1.85 | 0.08 | 0.06 | 22.98 | 0.03 | 95.44 |
| **36 / 1 .** | 0.27 | 6.76 | 20.14 | 34.50 | 8.58 | 0.00 | 1.84 | 0.06 | 0.03 | 22.88 | 0.02 | 95.10 |
| **37 / 1 .** | 0.29 | 6.76 | 19.95 | 33.95 | 8.57 | 0.01 | 1.88 | 0.06 | 0.05 | 22.66 | 0.04 | 94.21 |
| **38 / 1 .** | 0.23 | 6.73 | 20.69 | 34.46 | 8.84 | 0.00 | 1.93 | 0.07 | 0.06 | 23.05 | 0.00 | 96.06 |
| **39 / 1 .** | 0.28 | 7.23 | 20.12 | 32.40 | 7.08 | 0.00 | 1.81 | 0.07 | 0.05 | 24.16 | 0.01 | 93.21 |
| **40 / 1 .** | 0.27 | 6.51 | 19.96 | 33.76 | 8.70 | 0.27 | 1.91 | 0.08 | 0.06 | 22.95 | 0.05 | 94.52 |
| **41 / 1 .** | 0.25 | 6.71 | 20.44 | 34.50 | 8.67 | 0.00 | 1.73 | 0.10 | 0.02 | 22.44 | 0.04 | 94.91 |
| **42 / 1 .** | 0.01 | 1.62 | 21.40 | 36.11 | 0.03 | 2.13 | 0.01 | 0.00 | 2.47 | 36.21 | 0.02 | 100.00 |
| **43 / 1 .** | 0.04 | 1.64 | 21.52 | 36.05 | 0.00 | 1.93 | 0.00 | 0.02 | 2.81 | 36.23 | 0.00 | 100.24 |

**Table A3-2 continued..**

| Point | $Na_2O$ | MgO | $Al_2O_3$ | $SiO_2$ | $K_2O$ | CaO | $TiO_2$ | $Cr_2O_3$ | MnO | FeO | ZnO | Total |
|---|---|---|---|---|---|---|---|---|---|---|---|---|
| **44 / 1 .** | 0.01 | 1.72 | 21.44 | 36.28 | 0.00 | 1.68 | 0.03 | 0.03 | 3.01 | 36.37 | 0.00 | 100.55 |
| **45 / 1 .** | 0.02 | 1.68 | 21.66 | 36.40 | 0.00 | 1.61 | 0.00 | 0.00 | 3.48 | 36.19 | 0.03 | 101.08 |
| **46 / 1 .** | 0.03 | 1.72 | 21.41 | 36.20 | 0.00 | 1.51 | 0.00 | 0.00 | 3.76 | 35.59 | 0.01 | 100.23 |
| **47 / 1 .** | 0.04 | 1.73 | 21.26 | 36.39 | 0.00 | 1.52 | 0.02 | 0.03 | 3.87 | 35.56 | 0.01 | 100.44 |
| **48 / 1 .** | 0.02 | 1.81 | 21.52 | 36.27 | 0.00 | 1.49 | 0.03 | 0.01 | 3.79 | 35.06 | 0.02 | 100.01 |
| **49 / 1 .** | 0.38 | 1.79 | 20.11 | 31.12 | 0.09 | 1.89 | 0.02 | 0.02 | 3.21 | 32.34 | 0.00 | 90.97 |
| **50 / 1 .** | 0.02 | 1.76 | 21.44 | 36.36 | 0.01 | 1.49 | 0.08 | 0.00 | 3.88 | 35.42 | 0.00 | 100.46 |
| **51 / 1 .** | 0.04 | 1.76 | 21.48 | 36.35 | 0.03 | 1.58 | 0.04 | 0.03 | 3.86 | 35.78 | 0.00 | 100.95 |
| **52 / 1 .** | 0.04 | 1.74 | 21.45 | 35.84 | 0.03 | 1.52 | 0.04 | 0.01 | 3.91 | 35.32 | 0.01 | 99.90 |
| **53 / 1 .** | 0.05 | 1.71 | 21.45 | 36.00 | 0.00 | 1.66 | 0.03 | 0.04 | 3.84 | 35.20 | 0.00 | 99.98 |
| **54 / 1 .** | 0.04 | 1.75 | 21.35 | 36.13 | 0.00 | 1.52 | 0.04 | 0.00 | 3.85 | 35.19 | 0.03 | 99.90 |
| **55 / 1 .** | 0.04 | 1.73 | 21.40 | 35.94 | 0.01 | 1.54 | 0.05 | 0.03 | 3.54 | 35.30 | 0.04 | 99.62 |
| **56 / 1 .** | 0.02 | 1.78 | 21.37 | 35.99 | 0.00 | 1.55 | 0.01 | 0.05 | 3.58 | 35.40 | 0.00 | 99.75 |
| **57 / 1 .** | 0.02 | 1.64 | 21.50 | 35.88 | 0.04 | 1.56 | 0.05 | 0.04 | 3.32 | 35.76 | 0.02 | 99.84 |
| **58 / 1 .** | 0.00 | 1.51 | 21.42 | 36.09 | 0.01 | 1.66 | 0.06 | 0.04 | 2.84 | 36.44 | 0.00 | 100.08 |
| **59 / 1 .** | 0.34 | 5.75 | 19.89 | 33.46 | 8.67 | 0.04 | 1.84 | 0.11 | 0.11 | 22.32 | 0.07 | 92.61 |
| **60 / 1 .** | 6.66 | 0.03 | 25.07 | 57.09 | 0.59 | 7.31 | 0.05 | 0.01 | 0.00 | 0.35 | 0.00 | 97.17 |
| **61 / 1 .** | 0.32 | 6.38 | 20.31 | 33.88 | 8.61 | 0.06 | 1.90 | 0.09 | 0.06 | 22.74 | 0.05 | 94.40 |
| **62 / 1 .** | 0.27 | 7.20 | 19.80 | 32.92 | 7.75 | 0.00 | 1.87 | 0.08 | 0.04 | 23.74 | 0.00 | 93.67 |
| **63 / 1 .** | 0.27 | 6.73 | 19.80 | 34.03 | 8.73 | 0.00 | 1.84 | 0.06 | 0.05 | 23.01 | 0.03 | 94.55 |
| **64 / 1 .** | 0.31 | 6.72 | 20.01 | 34.15 | 8.67 | 0.00 | 1.81 | 0.07 | 0.04 | 23.22 | 0.03 | 95.02 |
| **65 / 1 .** | 0.30 | 6.50 | 19.92 | 33.50 | 8.35 | 0.03 | 1.87 | 0.08 | 0.04 | 23.24 | 0.02 | 93.87 |
| **66 / 1 .** | 0.26 | 6.92 | 19.93 | 32.87 | 7.87 | 0.04 | 1.83 | 0.05 | 0.02 | 24.00 | 0.06 | 93.85 |
| **67 / 1 .** | 0.30 | 6.37 | 20.09 | 33.92 | 8.53 | 0.04 | 1.75 | 0.09 | 0.02 | 23.30 | 0.03 | 94.45 |
| **68 / 1 .** | 0.31 | 6.54 | 20.04 | 33.83 | 8.54 | 0.01 | 1.76 | 0.04 | 0.05 | 23.12 | 0.02 | 94.27 |
| **69 / 1 .** | 0.28 | 6.60 | 19.73 | 33.67 | 8.17 | 0.14 | 1.80 | 0.10 | 0.03 | 23.72 | 0.01 | 94.26 |
| **70 / 1 .** | 0.30 | 6.62 | 19.69 | 33.85 | 8.66 | 0.02 | 1.88 | 0.09 | 0.01 | 23.08 | 0.00 | 94.20 |
| **71 / 1 .** | 0.27 | 6.83 | 19.15 | 32.67 | 8.03 | 0.03 | 1.83 | 0.07 | 0.06 | 23.26 | 0.03 | 92.23 |
| **72 / 1 .** | 0.23 | 6.79 | 19.91 | 34.06 | 8.66 | 0.00 | 1.85 | 0.05 | 0.04 | 23.07 | 0.01 | 94.67 |
| **73 / 1 .** | 0.26 | 6.49 | 19.83 | 33.57 | 8.63 | 0.00 | 1.74 | 0.12 | 0.01 | 22.27 | 0.05 | 92.98 |
| **74 / 1 .** | 0.23 | 6.65 | 19.89 | 33.33 | 8.44 | 0.00 | 1.76 | 0.10 | 0.01 | 23.02 | 0.03 | 93.47 |
| **75 / 1 .** | 0.22 | 6.88 | 20.02 | 34.21 | 8.24 | 0.01 | 1.54 | 0.09 | 0.04 | 23.15 | 0.04 | 94.45 |
| **76 / 1 .** | 0.24 | 6.89 | 20.08 | 34.42 | 8.43 | 0.00 | 1.56 | 0.09 | 0.04 | 22.41 | 0.02 | 94.18 |
| **77 / 1 .** | 0.22 | 7.17 | 20.15 | 33.57 | 8.13 | 0.00 | 1.59 | 0.10 | 0.05 | 23.09 | 0.05 | 94.14 |
| **78 / 1 .** | 0.16 | 7.18 | 20.59 | 32.46 | 6.42 | 0.09 | 1.56 | 0.08 | 0.06 | 24.21 | 0.04 | 92.85 |
| **79 / 1 .** | 0.54 | 6.36 | 20.12 | 34.99 | 8.52 | 0.17 | 1.81 | 0.08 | 0.07 | 22.60 | 0.03 | 95.27 |
| **80 / 1 .** | 0.21 | 6.76 | 20.16 | 34.14 | 8.68 | 0.02 | 1.82 | 0.09 | 0.08 | 22.80 | 0.02 | 94.79 |
| **81 / 1 .** | 6.78 | 0.00 | 26.56 | 55.91 | 0.03 | 8.66 | 0.05 | 0.00 | 0.00 | 0.08 | 0.00 | 98.06 |
| **82 / 1 .** | 6.56 | 0.00 | 27.16 | 56.03 | 0.04 | 8.87 | 0.00 | 0.03 | 0.01 | 0.07 | 0.00 | 98.78 |
| **83 / 1 .** | 0.57 | 0.00 | 3.15 | 90.43 | 0.00 | 1.06 | 0.00 | 0.00 | 0.00 | 0.09 | 0.04 | 95.35 |
| **84 / 1 .** | 6.15 | 0.02 | 26.92 | 58.92 | 0.87 | 7.26 | 0.02 | 0.00 | 0.00 | 0.14 | 0.00 | 100.29 |
| **85 / 1 .** | 0.00 | 1.63 | 21.86 | 36.28 | 0.00 | 2.13 | 0.03 | 0.03 | 2.35 | 36.79 | 0.00 | 101.10 |
| **86 / 1 .** | 0.01 | 1.72 | 21.63 | 36.03 | 0.00 | 1.94 | 0.05 | 0.02 | 2.44 | 36.40 | 0.01 | 100.25 |

**Table A3-2 continued..**

| Point | $Na_2O$ | MgO | $Al_2O_3$ | $SiO_2$ | $K_2O$ | CaO | $TiO_2$ | $Cr_2O_3$ | MnO | FeO | ZnO | Total |
|---|---|---|---|---|---|---|---|---|---|---|---|---|
| **87 / 1 .** | 0.01 | 1.76 | 21.58 | 35.84 | 0.00 | 1.78 | 0.00 | 0.01 | 3.01 | 36.37 | 0.01 | 100.37 |
| **88 / 1 .** | 0.03 | 1.84 | 21.58 | 36.26 | 0.00 | 1.69 | 0.00 | 0.02 | 3.39 | 35.97 | 0.00 | 100.77 |
| **89 / 1 .** | 0.03 | 1.86 | 21.52 | 36.03 | 0.00 | 1.68 | 0.03 | 0.04 | 3.71 | 35.32 | 0.00 | 100.22 |
| **90 / 1 .** | 0.03 | 1.78 | 21.54 | 36.10 | 0.00 | 1.71 | 0.02 | 0.02 | 3.62 | 35.74 | 0.00 | 100.56 |
| **91 / 1 .** | 0.02 | 1.79 | 21.36 | 36.09 | 0.01 | 1.67 | 0.04 | 0.01 | 3.64 | 35.41 | 0.00 | 100.05 |
| **92 / 1 .** | 0.03 | 1.78 | 21.46 | 36.08 | 0.00 | 1.67 | 0.04 | 0.07 | 3.69 | 35.31 | 0.02 | 100.14 |
| **93 / 1 .** | 0.04 | 1.82 | 21.34 | 36.17 | 0.00 | 1.61 | 0.00 | 0.03 | 3.69 | 35.28 | 0.01 | 99.99 |
| **94 / 1 .** | 0.03 | 1.76 | 21.20 | 36.09 | 0.03 | 1.58 | 0.02 | 0.02 | 3.55 | 35.46 | 0.02 | 99.76 |
| **95 / 1 .** | 0.01 | 1.83 | 21.69 | 36.08 | 0.00 | 1.64 | 0.00 | 0.06 | 3.53 | 35.62 | 0.01 | 100.47 |
| **96 / 1 .** | 0.02 | 1.84 | 21.46 | 35.92 | 0.00 | 1.65 | 0.04 | 0.04 | 3.43 | 35.86 | 0.00 | 100.26 |
| **97 / 1 .** | 0.03 | 1.79 | 21.43 | 36.35 | 0.00 | 1.78 | 0.01 | 0.02 | 3.21 | 36.00 | 0.00 | 100.61 |
| **98 / 1 .** | 0.01 | 1.73 | 21.49 | 36.19 | 0.00 | 1.95 | 0.00 | 0.02 | 2.66 | 36.41 | 0.00 | 100.47 |
| **99 / 1 .** | 0.16 | 1.88 | 22.87 | 39.15 | 0.02 | 1.95 | 0.05 | 0.02 | 2.37 | 35.69 | 0.00 | 104.17 |
| **100 / 1 .** | 0.02 | 1.82 | 21.57 | 35.97 | 0.00 | 1.60 | 0.00 | 0.06 | 3.19 | 36.05 | 0.00 | 100.28 |
| **101 / 1 .** | 0.04 | 1.81 | 21.39 | 36.14 | 0.01 | 1.69 | 0.04 | 0.03 | 3.40 | 35.55 | 0.00 | 100.10 |
| **102 / 1 .** | 0.02 | 1.81 | 21.52 | 36.06 | 0.00 | 1.70 | 0.03 | 0.06 | 3.49 | 35.36 | 0.00 | 100.06 |
| **103 / 1 .** | 0.01 | 1.82 | 21.52 | 36.13 | 0.00 | 1.75 | 0.04 | 0.02 | 3.54 | 35.47 | 0.00 | 100.30 |
| **104 / 1 .** | 0.03 | 1.84 | 21.63 | 35.97 | 0.00 | 1.70 | 0.01 | 0.00 | 3.53 | 35.63 | 0.00 | 100.34 |
| **105 / 1 .** | 0.03 | 1.87 | 21.46 | 35.92 | 0.00 | 1.65 | 0.00 | 0.10 | 3.57 | 35.24 | 0.00 | 99.84 |
| **106 / 1 .** | 0.04 | 1.76 | 21.49 | 35.74 | 0.00 | 1.57 | 0.02 | 0.03 | 3.80 | 35.42 | 0.01 | 99.88 |
| **107 / 1 .** | 0.03 | 1.77 | 21.56 | 36.32 | 0.00 | 1.70 | 0.05 | 0.02 | 3.51 | 35.67 | 0.03 | 100.66 |
| **108 / 1 .** | 0.03 | 1.74 | 21.58 | 36.10 | 0.01 | 1.77 | 0.02 | 0.02 | 3.55 | 35.48 | 0.01 | 100.32 |
| **109 / 1 .** | 0.03 | 1.90 | 21.52 | 35.79 | 0.00 | 1.78 | 0.05 | 0.00 | 3.42 | 35.39 | 0.00 | 99.87 |
| **110 / 1 .** | 0.03 | 1.82 | 21.53 | 35.83 | 0.00 | 1.68 | 0.00 | 0.04 | 3.31 | 35.84 | 0.00 | 100.08 |
| **111 / 1 .** | 0.03 | 1.81 | 21.61 | 36.05 | 0.00 | 1.67 | 0.00 | 0.02 | 3.34 | 36.04 | 0.00 | 100.57 |
| **112 / 1 .** | 0.02 | 1.77 | 21.40 | 36.16 | 0.01 | 1.62 | 0.03 | 0.03 | 3.17 | 35.85 | 0.02 | 100.07 |
| **113 / 1 .** | 0.00 | 1.77 | 21.37 | 35.98 | 0.00 | 1.65 | 0.00 | 0.01 | 3.00 | 36.19 | 0.00 | 99.98 |
| **114 / 1 .** | 0.02 | 1.66 | 21.49 | 36.07 | 0.00 | 1.76 | 0.02 | 0.04 | 2.72 | 36.53 | 0.00 | 100.32 |
| **115 / 1 .** | 0.03 | 1.47 | 21.46 | 36.13 | 0.00 | 2.01 | 0.02 | 0.00 | 2.23 | 37.19 | 0.00 | 100.54 |
| **116 / 1 .** | 2.71 | 0.00 | 8.00 | 86.09 | 0.00 | 2.19 | 0.04 | 0.02 | 0.02 | 0.62 | 0.00 | 99.71 |
| **117 / 1 .** | 0.01 | 1.72 | 21.56 | 36.21 | 0.00 | 1.96 | 0.03 | 0.00 | 2.45 | 36.54 | 0.02 | 100.49 |
| **118 / 1 .** | 0.02 | 1.79 | 21.81 | 36.32 | 0.01 | 1.96 | 0.02 | 0.00 | 2.45 | 36.64 | 0.00 | 101.01 |
| **119 / 1 .** | 0.04 | 1.90 | 21.50 | 36.21 | 0.00 | 1.84 | 0.02 | 0.01 | 2.77 | 36.21 | 0.01 | 100.52 |
| **120 / 1 .** | 0.03 | 1.85 | 21.52 | 35.94 | 0.00 | 1.83 | 0.00 | 0.06 | 2.88 | 35.70 | 0.00 | 99.80 |
| **121 / 1 .** | 0.04 | 1.80 | 21.57 | 35.64 | 0.00 | 1.87 | 0.01 | 0.03 | 3.17 | 35.77 | 0.01 | 99.90 |
| **122 / 1 .** | 0.00 | 1.73 | 21.65 | 36.09 | 0.00 | 2.07 | 0.05 | 0.00 | 3.82 | 34.85 | 0.00 | 100.26 |
| **123 / 1 .** | 0.02 | 1.70 | 21.72 | 36.04 | 0.00 | 2.14 | 0.06 | 0.02 | 4.21 | 34.37 | 0.05 | 100.34 |
| **124 / 1 .** | 0.02 | 1.61 | 21.41 | 36.52 | 0.00 | 2.29 | 0.02 | 0.00 | 4.91 | 34.11 | 0.03 | 100.91 |
| **125 / 1 .** | 0.04 | 1.62 | 21.55 | 35.90 | 0.00 | 2.15 | 0.05 | 0.00 | 4.95 | 34.07 | 0.00 | 100.31 |
| **126 / 1 .** | 0.02 | 1.64 | 21.58 | 36.43 | 0.00 | 2.07 | 0.05 | 0.05 | 5.05 | 33.81 | 0.00 | 100.70 |
| **127 / 1 .** | 0.05 | 1.64 | 21.39 | 35.92 | 0.00 | 1.97 | 0.03 | 0.00 | 4.99 | 33.77 | 0.00 | 99.75 |
| **128 / 1 .** | 0.02 | 1.80 | 21.52 | 36.29 | 0.02 | 1.66 | 0.06 | 0.00 | 5.22 | 34.22 | 0.00 | 100.81 |
| **129 / 1 .** | 0.03 | 1.64 | 21.28 | 36.01 | 0.00 | 1.65 | 0.00 | 0.00 | 5.06 | 33.73 | 0.01 | 99.42 |

**Table A3-2 continued..**

| Point | $Na_2O$ | MgO | $Al_2O_3$ | $SiO_2$ | $K_2O$ | CaO | $TiO_2$ | $Cr_2O_3$ | MnO | FeO | ZnO | Total |
|---|---|---|---|---|---|---|---|---|---|---|---|---|
| **130 / 1 .** | 0.04 | 1.72 | 21.47 | 35.99 | 0.00 | 1.99 | 0.04 | 0.01 | 5.11 | 33.99 | 0.00 | 100.35 |
| **131 / 1 .** | 0.04 | 1.67 | 21.62 | 36.30 | 0.01 | 2.04 | 0.02 | 0.00 | 5.02 | 33.79 | 0.00 | 100.51 |
| **132 / 1 .** | 0.03 | 1.75 | 21.53 | 36.30 | 0.00 | 2.08 | 0.04 | 0.00 | 4.85 | 34.56 | 0.00 | 101.14 |
| **133 / 1 .** | 0.01 | 1.69 | 21.24 | 35.98 | 0.00 | 1.88 | 0.06 | 0.01 | 4.54 | 34.32 | 0.00 | 99.74 |
| **134 / 1 .** | 0.03 | 1.67 | 21.44 | 36.12 | 0.01 | 1.97 | 0.05 | 0.01 | 4.21 | 35.08 | 0.00 | 100.59 |
| **135 / 1 .** | 0.02 | 1.77 | 21.58 | 36.23 | 0.00 | 1.89 | 0.02 | 0.04 | 4.04 | 35.09 | 0.01 | 100.67 |
| **136 / 1 .** | 0.03 | 1.76 | 21.67 | 36.51 | 0.00 | 1.96 | 0.03 | 0.01 | 3.31 | 35.79 | 0.00 | 101.06 |
| **137 / 1 .** | 0.01 | 1.81 | 21.59 | 36.01 | 0.00 | 1.79 | 0.00 | 0.00 | 2.99 | 36.18 | 0.00 | 100.37 |
| **138 / 1 .** | 0.01 | 1.84 | 21.47 | 35.80 | 0.00 | 1.88 | 0.06 | 0.04 | 2.57 | 36.55 | 0.02 | 100.24 |
| **139 / 1 .** | 0.02 | 1.68 | 21.40 | 36.08 | 0.01 | 2.24 | 0.03 | 0.02 | 1.96 | 36.93 | 0.00 | 100.38 |
| **140 / 1 .** | 0.03 | 1.57 | 21.16 | 35.69 | 0.28 | 2.10 | 0.17 | 0.00 | 1.78 | 35.55 | 0.01 | 98.35 |
| **141 / 1 .** | 0.29 | 6.97 | 19.97 | 34.20 | 8.83 | 0.00 | 1.95 | 0.04 | 0.04 | 22.69 | 0.04 | 95.01 |
| **142 / 1 .** | 0.75 | 0.00 | 3.64 | 92.65 | 0.00 | 1.02 | 0.02 | 0.00 | 0.05 | 0.42 | 0.00 | 98.55 |
| **143 / 1 .** | 0.00 | 1.64 | 21.69 | 36.25 | 0.02 | 2.14 | 0.01 | 0.00 | 1.98 | 36.76 | 0.01 | 100.50 |
| **144 / 1 .** | 0.01 | 1.73 | 21.59 | 36.10 | 0.01 | 1.94 | 0.04 | 0.00 | 2.39 | 36.17 | 0.00 | 99.98 |
| **145 / 1 .** | 0.01 | 1.88 | 21.46 | 35.81 | 0.00 | 1.77 | 0.00 | 0.02 | 2.89 | 36.11 | 0.00 | 99.94 |
| **146 / 1 .** | 0.00 | 1.84 | 21.41 | 35.90 | 0.01 | 1.83 | 0.03 | 0.04 | 3.33 | 35.23 | 0.00 | 99.60 |
| **147 / 1 .** | 0.03 | 1.78 | 21.66 | 36.10 | 0.00 | 2.13 | 0.00 | 0.07 | 3.86 | 35.00 | 0.00 | 100.63 |
| **148 / 1 .** | 0.02 | 1.62 | 21.30 | 36.09 | 0.00 | 2.20 | 0.06 | 0.01 | 4.24 | 34.20 | 0.00 | 99.75 |
| **149 / 1 .** | 0.00 | 1.69 | 21.46 | 36.16 | 0.00 | 2.24 | 0.03 | 0.00 | 4.53 | 34.28 | 0.03 | 100.43 |
| **150 / 1 .** | 0.00 | 1.64 | 21.53 | 35.92 | 0.01 | 2.11 | 0.07 | 0.02 | 4.83 | 34.20 | 0.00 | 100.34 |
| **151 / 1 .** | 0.07 | 1.56 | 21.20 | 35.19 | 0.00 | 1.87 | 0.08 | 0.02 | 5.02 | 34.09 | 0.05 | 99.15 |
| **152 / 1 .** | 0.03 | 1.62 | 21.54 | 35.89 | 0.00 | 2.03 | 0.03 | 0.04 | 5.09 | 33.91 | 0.00 | 100.19 |
| **153 / 1 .** | 0.03 | 1.68 | 21.24 | 36.26 | 0.00 | 1.96 | 0.00 | 0.04 | 4.89 | 33.63 | 0.02 | 99.75 |
| **154 / 1 .** | 0.04 | 1.72 | 21.44 | 36.11 | 0.00 | 1.87 | 0.06 | 0.00 | 5.03 | 33.72 | 0.00 | 99.99 |
| **155 / 1 .** | 0.05 | 1.66 | 21.35 | 36.08 | 0.00 | 2.07 | 0.07 | 0.04 | 4.89 | 34.07 | 0.00 | 100.27 |
| **156 / 1 .** | 0.04 | 1.75 | 21.36 | 36.42 | 0.01 | 2.25 | 0.07 | 0.03 | 4.60 | 34.41 | 0.00 | 100.94 |
| **157 / 1 .** | 0.02 | 1.72 | 21.42 | 36.21 | 0.02 | 2.12 | 0.03 | 0.01 | 4.52 | 34.27 | 0.03 | 100.36 |
| **158 / 1 .** | 0.03 | 1.71 | 21.44 | 36.50 | 0.00 | 2.16 | 0.01 | 0.03 | 4.30 | 34.81 | 0.00 | 101.00 |
| **159 / 1 .** | 0.01 | 1.77 | 21.58 | 36.28 | 0.00 | 2.17 | 0.01 | 0.01 | 4.08 | 35.12 | 0.02 | 101.05 |
| **160 / 1 .** | 0.02 | 1.76 | 21.35 | 35.96 | 0.01 | 2.06 | 0.04 | 0.00 | 3.78 | 35.07 | 0.00 | 100.05 |
| **161 / 1 .** | 0.03 | 1.81 | 21.48 | 36.13 | 0.00 | 1.93 | 0.04 | 0.00 | 3.30 | 35.68 | 0.00 | 100.39 |
| **162 / 1 .** | 0.01 | 1.89 | 21.36 | 36.22 | 0.00 | 1.81 | 0.00 | 0.04 | 2.84 | 36.53 | 0.06 | 100.74 |
| **163 / 1 .** | 0.02 | 1.79 | 21.38 | 36.02 | 0.00 | 1.85 | 0.02 | 0.06 | 2.46 | 36.38 | 0.00 | 99.99 |
| **164 / 1 .** | 1.22 | 0.36 | 36.12 | 45.06 | 8.50 | 0.04 | 0.31 | 0.07 | 0.01 | 0.99 | 0.00 | 92.69 |
| **165 / 1 .** | 1.25 | 0.38 | 35.93 | 43.99 | 9.33 | 0.00 | 0.37 | 0.06 | 0.03 | 0.98 | 0.00 | 92.33 |
| **166 / 1 .** | 1.21 | 0.44 | 36.12 | 44.64 | 8.34 | 0.02 | 0.36 | 0.07 | 0.02 | 1.10 | 0.02 | 92.34 |
| **167 / 1 .** | 1.25 | 0.39 | 36.73 | 44.95 | 9.40 | 0.00 | 0.40 | 0.04 | 0.00 | 0.93 | 0.01 | 94.12 |
| **168 / 1 .** | 1.24 | 0.37 | 37.10 | 45.96 | 8.47 | 0.01 | 0.30 | 0.07 | 0.00 | 0.93 | 0.01 | 94.46 |
| **169 / 1 .** | 1.18 | 0.42 | 36.60 | 44.59 | 9.27 | 0.02 | 0.42 | 0.06 | 0.00 | 0.95 | 0.01 | 93.52 |
| **170 / 1 .** | 0.02 | 0.00 | 0.16 | 97.77 | 0.04 | 0.00 | 0.01 | 0.00 | 0.00 | 0.22 | 0.01 | 98.23 |
| **171 / 1 .** | 1.24 | 0.33 | 36.63 | 44.39 | 9.30 | 0.00 | 0.32 | 0.05 | 0.01 | 0.94 | 0.00 | 93.22 |
| **172 / 1 .** | 1.16 | 0.40 | 36.42 | 46.53 | 8.30 | 0.03 | 0.47 | 0.05 | 0.00 | 0.86 | 0.03 | 94.23 |

**Table A3-2 continued..**

| Point | $Na_2O$ | MgO | $Al_2O_3$ | $SiO_2$ | $K_2O$ | CaO | $TiO_2$ | $Cr_2O_3$ | MnO | FeO | ZnO | Total |
|---|---|---|---|---|---|---|---|---|---|---|---|---|
| **173 / 1 .** | 7.12 | 0.00 | 26.98 | 57.21 | 0.02 | 8.58 | 0.02 | 0.01 | 0.05 | 0.43 | 0.00 | 100.44 |
| **174 / 1 .** | 0.06 | 1.49 | 20.21 | 35.44 | 0.00 | 2.00 | 0.03 | 0.02 | 2.10 | 36.66 | 0.00 | 98.01 |
| **175 / 1 .** | 0.00 | 1.82 | 21.58 | 35.75 | 0.02 | 1.85 | 0.05 | 0.03 | 2.64 | 36.46 | 0.00 | 100.20 |
| **176 / 1 .** | 0.03 | 1.87 | 21.52 | 36.23 | 0.00 | 1.79 | 0.01 | 0.04 | 2.94 | 35.93 | 0.04 | 100.40 |
| **177 / 1 .** | 0.00 | 0.03 | 0.18 | 2.59 | 0.00 | 6.43 | 0.04 | 0.00 | 0.00 | 2.18 | 0.00 | 11.44 |
| **178 / 1 .** | 0.01 | 1.80 | 21.31 | 35.79 | 0.00 | 1.74 | 0.05 | 0.00 | 3.60 | 34.95 | 0.02 | 99.26 |
| **179 / 1 .** | 0.02 | 1.77 | 21.49 | 36.13 | 0.00 | 1.99 | 0.05 | 0.00 | 3.99 | 34.73 | 0.00 | 100.17 |
| **180 / 1 .** | 0.02 | 1.80 | 21.48 | 36.20 | 0.01 | 1.80 | 0.06 | 0.00 | 4.19 | 34.71 | 0.00 | 100.27 |
| **181 / 1 .** | 0.03 | 1.72 | 21.62 | 36.00 | 0.00 | 1.88 | 0.09 | 0.02 | 4.61 | 34.41 | 0.00 | 100.38 |
| **182 / 1 .** | 0.04 | 1.75 | 21.35 | 36.13 | 0.02 | 1.90 | 0.09 | 0.01 | 4.59 | 34.29 | 0.03 | 100.22 |
| **183 / 1 .** | 0.03 | 1.71 | 21.56 | 36.21 | 0.00 | 2.06 | 0.07 | 0.00 | 4.77 | 34.18 | 0.00 | 100.58 |
| **184 / 1 .** | 0.04 | 1.73 | 21.63 | 36.35 | 0.01 | 2.02 | 0.02 | 0.00 | 4.86 | 34.13 | 0.00 | 100.79 |
| **185 / 1 .** | 0.06 | 1.77 | 21.53 | 36.36 | 0.02 | 1.77 | 0.03 | 0.07 | 4.75 | 34.10 | 0.02 | 100.46 |
| **186 / 1 .** | 0.84 | 0.32 | 2.31 | 3.20 | 0.01 | 0.34 | 0.02 | 0.04 | 3.42 | 27.55 | 0.03 | 38.07 |
| **187 / 1 .** | 0.05 | 1.47 | 19.02 | 31.94 | 0.01 | 1.89 | 0.07 | 0.04 | 4.38 | 33.81 | 0.00 | 92.68 |
| **188 / 1 .** | 0.04 | 1.78 | 21.51 | 36.45 | 0.00 | 1.92 | 0.05 | 0.01 | 4.51 | 34.68 | 0.03 | 100.99 |
| **189 / 1 .** | 0.02 | 1.76 | 21.53 | 36.21 | 0.01 | 2.06 | 0.09 | 0.01 | 4.40 | 34.60 | 0.00 | 100.69 |
| **190 / 1 .** | 0.01 | 1.74 | 21.71 | 36.04 | 0.00 | 1.95 | 0.00 | 0.06 | 4.08 | 34.76 | 0.00 | 100.35 |
| **191 / 1 .** | 0.03 | 1.82 | 21.61 | 36.08 | 0.00 | 1.90 | 0.04 | 0.04 | 3.86 | 35.26 | 0.00 | 100.65 |
| **192 / 1 .** | 0.03 | 1.88 | 21.63 | 36.10 | 0.00 | 1.84 | 0.01 | 0.01 | 3.45 | 35.48 | 0.00 | 100.43 |
| **193 / 1 .** | 0.02 | 1.77 | 21.53 | 35.96 | 0.00 | 1.75 | 0.01 | 0.00 | 3.10 | 35.87 | 0.00 | 100.00 |
| **194 / 1 .** | 0.03 | 1.91 | 21.69 | 36.35 | 0.00 | 1.79 | 0.01 | 0.03 | 2.97 | 36.13 | 0.00 | 100.92 |
| **195 / 1 .** | 0.04 | 1.85 | 21.33 | 36.22 | 0.00 | 1.86 | 0.01 | 0.01 | 2.63 | 36.24 | 0.00 | 100.19 |
| **196 / 1 .** | 1.14 | 0.40 | 36.44 | 45.98 | 8.51 | 0.00 | 0.53 | 0.09 | 0.00 | 0.87 | 0.01 | 93.97 |
| **197 / 1 .** | 1.24 | 0.35 | 36.65 | 44.69 | 9.54 | 0.00 | 0.45 | 0.08 | 0.00 | 0.93 | 0.00 | 93.94 |
| **198 / 1 .** | 1.17 | 0.37 | 36.78 | 46.72 | 8.27 | 0.00 | 0.47 | 0.07 | 0.00 | 0.91 | 0.00 | 94.77 |
| **199 / 1 .** | 1.19 | 0.41 | 36.87 | 45.32 | 9.58 | 0.00 | 0.47 | 0.07 | 0.02 | 0.87 | 0.00 | 94.81 |
| **200 / 1 .** | 1.18 | 0.43 | 36.45 | 46.30 | 8.12 | 0.00 | 0.43 | 0.08 | 0.00 | 0.97 | 0.00 | 93.96 |
| **201 / 1 .** | 1.16 | 0.44 | 36.44 | 45.02 | 9.41 | 0.00 | 0.49 | 0.05 | 0.01 | 0.92 | 0.00 | 93.94 |
| **202 / 1 .** | 0.94 | 1.22 | 34.56 | 43.62 | 7.86 | 0.00 | 0.40 | 0.07 | 0.02 | 4.06 | 0.01 | 92.76 |
| **203 / 1 .** | 1.16 | 0.41 | 36.06 | 44.94 | 9.29 | 0.00 | 0.50 | 0.07 | 0.03 | 0.88 | 0.00 | 93.34 |
| **204 / 1 .** | 1.20 | 0.43 | 36.81 | 46.58 | 8.16 | 0.00 | 0.49 | 0.05 | 0.00 | 0.99 | 0.00 | 94.71 |
| **205 / 1 .** | 1.26 | 0.34 | 36.73 | 44.61 | 9.42 | 0.03 | 0.26 | 0.08 | 0.01 | 1.04 | 0.00 | 93.77 |
| **206 / 1 .** | 0.63 | 0.50 | 23.24 | 31.71 | 3.69 | 3.45 | 19.23 | 0.05 | 0.12 | 14.50 | 0.01 | 97.13 |
| **207 / 1 .** | 0.38 | 2.99 | 22.33 | 27.61 | 1.31 | 2.86 | 22.74 | 0.05 | 0.21 | 22.51 | 0.09 | 103.08 |
| **208 / 1 .** | 0.38 | 2.36 | 24.03 | 28.60 | 1.46 | 1.65 | 17.96 | 0.00 | 0.21 | 21.42 | 0.04 | 98.10 |
| **209 / 1 .** | 0.56 | 1.52 | 29.13 | 35.78 | 2.64 | 2.42 | 9.11 | 0.03 | 0.06 | 10.42 | 0.00 | 91.68 |
| **210 / 1 .** | 0.52 | 0.23 | 25.73 | 55.26 | 3.62 | 0.02 | 0.10 | 0.00 | 0.01 | 1.06 | 0.00 | 86.55 |
| **211 / 1 .** | 0.23 | 7.25 | 21.05 | 33.65 | 6.82 | 0.68 | 1.48 | 0.06 | 0.04 | 23.12 | 0.05 | 94.44 |
| **212 / 1 .** | 2.40 | 4.53 | 20.83 | 48.93 | 5.93 | 1.31 | 1.12 | 0.10 | 0.01 | 15.54 | 0.02 | 100.72 |
| **213 / 1 .** | 1.18 | 0.40 | 36.80 | 44.87 | 9.57 | 0.02 | 0.32 | 0.08 | 0.00 | 1.09 | 0.04 | 94.37 |
| **214 / 1 .** | 6.51 | 0.00 | 27.36 | 55.46 | 0.06 | 9.27 | 0.05 | 0.00 | 0.01 | 0.19 | 0.00 | 98.93 |
| **215 / 1 .** | 0.92 | 0.26 | 32.59 | 46.08 | 4.29 | 0.61 | 0.19 | 0.03 | 0.02 | 1.30 | 0.00 | 86.30 |

**Table A3-2 continued..**

| Point | $Na_2O$ | MgO | $Al_2O_3$ | $SiO_2$ | $K_2O$ | CaO | $TiO_2$ | $Cr_2O_3$ | MnO | FeO | ZnO | Total |
|---|---|---|---|---|---|---|---|---|---|---|---|---|
| **216 / 1 .** | 1.19 | 0.50 | 36.49 | 46.34 | 8.40 | 0.01 | 0.38 | 0.02 | 0.00 | 0.94 | 0.05 | 94.32 |
| **217 / 1 .** | 1.09 | 0.44 | 36.47 | 45.25 | 9.27 | 0.00 | 0.36 | 0.08 | 0.02 | 1.00 | 0.02 | 93.99 |
| **218 / 1 .** | 1.17 | 0.41 | 36.64 | 46.13 | 8.18 | 0.00 | 0.44 | 0.07 | 0.00 | 0.98 | 0.00 | 94.03 |
| **219 / 1 .** | 1.20 | 0.39 | 36.57 | 44.49 | 9.42 | 0.02 | 0.35 | 0.09 | 0.01 | 1.01 | 0.02 | 93.57 |
| **220 / 1 .** | 1.19 | 0.42 | 36.40 | 46.31 | 8.45 | 0.00 | 0.35 | 0.08 | 0.02 | 1.02 | 0.00 | 94.23 |
| **221 / 1 .** | 1.21 | 0.38 | 36.70 | 44.97 | 9.43 | 0.00 | 0.27 | 0.06 | 0.02 | 1.03 | 0.00 | 94.08 |
| **222 / 1 .** | 1.18 | 0.44 | 36.44 | 45.52 | 8.31 | 0.00 | 0.26 | 0.09 | 0.01 | 1.06 | 0.00 | 93.32 |
| **223 / 1 .** | 0.32 | 6.91 | 20.32 | 34.25 | 8.57 | 0.00 | 1.69 | 0.10 | 0.04 | 22.39 | 0.04 | 94.63 |
| **224 / 1 .** | 0.31 | 6.98 | 20.18 | 33.90 | 8.54 | 0.00 | 1.62 | 0.08 | 0.01 | 22.79 | 0.02 | 94.43 |
| **225 / 1 .** | 0.27 | 6.98 | 20.49 | 33.67 | 8.12 | 0.02 | 1.53 | 0.05 | 0.05 | 22.61 | 0.07 | 93.86 |
| **226 / 1 .** | 0.32 | 7.39 | 20.34 | 34.24 | 8.29 | 0.03 | 1.44 | 0.08 | 0.02 | 22.61 | 0.03 | 94.79 |
| **227 / 1 .** | 0.27 | 7.30 | 20.62 | 34.27 | 8.28 | 0.02 | 1.59 | 0.08 | 0.04 | 22.63 | 0.00 | 95.11 |
| **228 / 1 .** | 1.13 | 0.03 | 2.62 | 4.56 | 0.06 | 0.41 | 50.75 | 0.00 | 0.35 | 43.73 | 0.06 | 103.72 |
| **229 / 1 .** | 0.00 | 0.03 | 0.00 | 2.37 | 0.05 | 0.01 | 52.68 | 0.02 | 0.36 | 44.94 | 0.10 | 100.54 |
| **230 / 1 .** | 2.39 | 0.07 | 12.50 | 23.43 | 0.05 | 2.87 | 34.46 | 0.00 | 0.28 | 30.52 | 0.04 | 106.60 |
| **231 / 1 .** | 0.40 | 0.00 | 0.59 | 1.20 | 0.07 | 0.08 | 52.83 | 0.00 | 0.33 | 45.36 | 0.04 | 100.92 |
| **232 / 1 .** | 3.75 | 0.08 | 17.78 | 70.86 | 0.07 | 6.11 | 0.03 | 0.03 | 0.00 | 0.28 | 0.00 | 98.98 |
| **233 / 1 .** | 0.01 | 1.20 | 54.39 | 27.28 | 0.00 | 0.00 | 0.50 | 0.01 | 0.12 | 14.19 | 0.68 | 98.40 |
| **234 / 1 .** | 0.03 | 1.19 | 54.52 | 26.84 | 0.00 | 0.02 | 0.54 | 0.06 | 0.11 | 14.16 | 0.78 | 98.26 |
| **235 / 1 .** | 0.02 | 1.20 | 54.90 | 27.03 | 0.00 | 0.01 | 0.54 | 0.04 | 0.11 | 14.39 | 0.76 | 98.99 |
| **236 / 1 .** | 0.03 | 1.16 | 55.01 | 26.48 | 0.00 | 0.01 | 0.44 | 0.04 | 0.12 | 14.33 | 0.70 | 98.33 |
| **237 / 1 .** | 0.02 | 1.11 | 55.07 | 26.86 | 0.00 | 0.02 | 0.48 | 0.10 | 0.10 | 14.31 | 0.79 | 98.86 |
| **238 / 1 .** | 0.02 | 1.14 | 54.74 | 26.82 | 0.00 | 0.01 | 0.40 | 0.02 | 0.11 | 14.40 | 0.74 | 98.40 |
| **239 / 1 .** | 0.30 | 0.95 | 54.23 | 27.38 | 0.01 | 0.12 | 0.42 | 0.07 | 0.12 | 14.35 | 0.86 | 98.82 |
| **240 / 1 .** | 0.04 | 0.99 | 56.53 | 25.67 | 0.00 | 0.00 | 0.33 | 0.08 | 0.13 | 14.49 | 0.88 | 99.14 |
| **241 / 1 .** | 0.02 | 1.04 | 55.25 | 28.04 | 0.00 | 0.00 | 0.36 | 0.04 | 0.13 | 14.51 | 0.79 | 100.20 |
| **242 / 1 .** | 0.02 | 1.13 | 54.84 | 26.72 | 0.01 | 0.00 | 0.37 | 0.05 | 0.13 | 14.32 | 0.82 | 98.40 |
| **243 / 1 .** | 0.00 | 0.36 | 19.69 | 64.53 | 0.00 | 0.02 | 0.18 | 0.03 | 0.06 | 5.91 | 0.27 | 91.06 |
| **244 / 1 .** | 0.03 | 1.17 | 54.77 | 26.55 | 0.00 | 0.00 | 0.39 | 0.06 | 0.11 | 14.37 | 0.84 | 98.29 |
| **245 / 1 .** | 0.02 | 1.20 | 54.73 | 26.54 | 0.00 | 0.00 | 0.37 | 0.05 | 0.15 | 14.80 | 0.76 | 98.62 |
| **246 / 1 .** | 0.04 | 1.22 | 54.92 | 26.77 | 0.00 | 0.01 | 0.43 | 0.03 | 0.16 | 14.68 | 0.69 | 98.94 |
| **247 / 1 .** | 0.02 | 1.14 | 54.71 | 26.85 | 0.01 | 0.00 | 0.36 | 0.06 | 0.13 | 14.50 | 0.78 | 98.56 |
| **248 / 1 .** | 0.05 | 1.13 | 53.00 | 25.79 | 0.00 | 0.01 | 0.38 | 0.04 | 0.11 | 14.60 | 0.74 | 95.86 |
| **249 / 1 .** | 0.02 | 1.15 | 54.65 | 26.82 | 0.00 | 0.02 | 0.41 | 0.05 | 0.14 | 14.52 | 0.73 | 98.50 |
| **250 / 1 .** | 0.02 | 1.22 | 54.49 | 26.84 | 0.00 | 0.00 | 0.41 | 0.03 | 0.09 | 14.74 | 0.74 | 98.57 |
| **251 / 1 .** | 0.12 | 1.36 | 50.55 | 27.60 | 0.16 | 0.22 | 0.50 | 0.04 | 0.09 | 16.90 | 0.71 | 98.25 |
| **252 / 1 .** | 0.01 | 1.24 | 54.86 | 26.95 | 0.01 | 0.00 | 0.44 | 0.05 | 0.13 | 14.74 | 0.71 | 99.15 |
| **253 / 1 .** | 0.02 | 1.17 | 53.72 | 28.04 | 0.00 | 0.00 | 0.38 | 0.03 | 0.14 | 14.46 | 0.77 | 98.74 |
| **254 / 1 .** | 0.03 | 1.23 | 55.02 | 26.46 | 0.00 | 0.00 | 0.45 | 0.04 | 0.12 | 14.56 | 0.76 | 98.66 |
| **255 / 1 .** | 0.02 | 1.21 | 54.70 | 26.45 | 0.00 | 0.02 | 0.45 | 0.01 | 0.14 | 14.49 | 0.76 | 98.26 |
| **256 / 1 .** | 0.02 | 1.25 | 54.59 | 26.60 | 0.00 | 0.00 | 0.49 | 0.06 | 0.16 | 14.48 | 0.72 | 98.37 |
| **257 / 1 .** | 0.03 | 1.21 | 55.09 | 26.65 | 0.01 | 0.00 | 0.49 | 0.01 | 0.14 | 14.68 | 0.80 | 99.11 |
| **258 / 1 .** | 0.02 | 1.11 | 54.81 | 26.17 | 0.01 | 0.00 | 0.48 | 0.03 | 0.15 | 14.59 | 0.76 | 98.13 |

**Table A3-2 continued..**

| Point | $Na_2O$ | MgO | $Al_2O_3$ | $SiO_2$ | $K_2O$ | CaO | $TiO_2$ | $Cr_2O_3$ | MnO | FeO | ZnO | Total |
|---|---|---|---|---|---|---|---|---|---|---|---|---|
| **259 / 1 .** | 0.02 | 1.08 | 55.37 | 26.33 | 0.00 | 0.00 | 0.50 | 0.05 | 0.15 | 14.43 | 0.76 | 98.69 |
| **260 / 1 .** | 0.04 | 1.05 | 53.75 | 26.16 | 0.00 | 0.00 | 0.59 | 0.10 | 0.10 | 14.16 | 0.73 | 96.69 |
| **261 / 1 .** | 0.02 | 1.00 | 54.95 | 26.46 | 0.01 | 0.01 | 0.56 | 0.05 | 0.12 | 14.35 | 0.85 | 98.38 |
| **262 / 1 .** | 1.17 | 0.40 | 35.97 | 44.48 | 7.80 | 0.04 | 0.35 | 0.07 | 0.02 | 0.94 | 0.00 | 91.24 |
| **263 / 1 .** | 1.19 | 0.42 | 36.93 | 45.73 | 9.38 | 0.00 | 0.36 | 0.07 | 0.01 | 0.98 | 0.00 | 95.07 |
| **264 / 1 .** | 1.22 | 0.38 | 36.48 | 45.31 | 8.39 | 0.07 | 0.37 | 0.06 | 0.00 | 0.92 | 0.01 | 93.23 |
| **265 / 1 .** | 1.19 | 0.40 | 36.40 | 44.18 | 9.19 | 0.04 | 0.37 | 0.08 | 0.00 | 0.95 | 0.00 | 92.79 |
| **266 / 1 .** | 1.07 | 0.42 | 36.53 | 45.60 | 7.79 | 0.01 | 0.36 | 0.03 | 0.00 | 0.90 | 0.01 | 92.73 |
| **267 / 1 .** | 1.04 | 0.44 | 35.05 | 43.34 | 7.74 | 0.14 | 0.39 | 0.07 | 0.00 | 1.11 | 0.01 | 89.32 |
| **268 / 1 .** | 0.01 | 0.11 | 0.42 | 96.84 | 0.20 | 0.03 | 0.07 | 0.00 | 0.00 | 0.66 | 0.00 | 98.34 |
| **269 / 1 .** | 7.64 | 0.00 | 25.79 | 57.74 | 0.09 | 7.57 | 0.00 | 0.01 | 0.00 | 0.15 | 0.00 | 99.01 |
| **270 / 1 .** | 0.91 | 5.85 | 20.71 | 35.45 | 7.20 | 0.67 | 1.58 | 0.05 | 0.05 | 20.61 | 0.03 | 93.11 |
| **271 / 1 .** | 7.21 | 0.00 | 27.22 | 61.67 | 0.04 | 7.40 | 0.00 | 0.00 | 0.00 | 0.10 | 0.00 | 103.65 |
| **272 / 1 .** | 0.37 | 6.61 | 20.29 | 33.89 | 8.59 | 0.07 | 1.67 | 0.08 | 0.04 | 22.48 | 0.00 | 94.09 |
| **273 / 1 .** | 0.36 | 6.55 | 20.37 | 34.16 | 8.60 | 0.12 | 1.73 | 0.08 | 0.06 | 22.39 | 0.01 | 94.42 |
| **274 / 1 .** | 1.19 | 0.01 | 5.45 | 88.41 | 0.02 | 1.59 | 0.02 | 0.02 | 0.01 | 0.29 | 0.01 | 97.03 |
| **275 / 1 .** | 0.27 | 6.45 | 19.83 | 33.41 | 8.53 | 0.04 | 1.84 | 0.07 | 0.03 | 23.11 | 0.01 | 93.59 |
| **276 / 1 .** | 7.94 | 0.03 | 25.77 | 56.91 | 0.08 | 7.61 | 0.03 | 0.01 | 0.00 | 0.35 | 0.00 | 98.75 |
| **277 / 1 .** | 0.27 | 6.42 | 19.63 | 33.47 | 8.77 | 0.00 | 1.73 | 0.06 | 0.03 | 22.98 | 0.00 | 93.36 |
| **278 / 1 .** | 0.32 | 6.80 | 19.90 | 33.33 | 8.59 | 0.04 | 1.83 | 0.04 | 0.04 | 23.00 | 0.03 | 93.91 |
| **279 / 1 .** | 0.28 | 6.71 | 20.01 | 33.65 | 8.91 | 0.00 | 1.74 | 0.06 | 0.07 | 23.24 | 0.01 | 94.68 |
| **280 / 1 .** | 0.24 | 6.75 | 19.95 | 34.25 | 8.79 | 0.00 | 1.74 | 0.06 | 0.03 | 23.24 | 0.00 | 95.07 |
| **281 / 1 .** | 0.23 | 6.76 | 20.02 | 34.17 | 8.67 | 0.00 | 1.78 | 0.05 | 0.03 | 23.06 | 0.00 | 94.77 |
| **282 / 1 .** | 0.27 | 6.88 | 19.48 | 33.57 | 8.58 | 0.00 | 1.91 | 0.06 | 0.04 | 23.25 | 0.02 | 94.06 |
| **283 / 1 .** | 0.21 | 7.04 | 20.11 | 33.52 | 8.16 | 0.02 | 1.71 | 0.10 | 0.03 | 23.36 | 0.07 | 94.33 |
| **284 / 1 .** | 0.03 | 1.08 | 53.94 | 26.77 | 0.00 | 0.02 | 0.53 | 0.09 | 0.23 | 14.64 | 0.28 | 97.62 |
| **285 / 1 .** | 0.04 | 1.09 | 54.21 | 26.56 | 0.00 | 0.01 | 0.52 | 0.09 | 0.21 | 14.67 | 0.20 | 97.61 |
| **286 / 1 .** | 0.18 | 1.03 | 52.96 | 26.48 | 0.01 | 0.09 | 0.47 | 0.06 | 0.18 | 14.67 | 0.21 | 96.35 |
| **287 / 1 .** | 0.02 | 1.08 | 55.06 | 26.68 | 0.00 | 0.04 | 0.50 | 0.07 | 0.20 | 15.02 | 0.23 | 98.89 |
| **288 / 1 .** | 0.01 | 1.02 | 54.94 | 26.69 | 0.00 | 0.02 | 0.61 | 0.03 | 0.23 | 14.88 | 0.17 | 98.59 |
| **289 / 1 .** | 0.01 | 1.14 | 54.54 | 26.59 | 0.00 | 0.00 | 0.52 | 0.05 | 0.19 | 15.11 | 0.21 | 98.35 |
| **290 / 1 .** | 0.02 | 1.00 | 55.87 | 25.78 | 0.02 | 0.00 | 0.39 | 0.07 | 0.22 | 14.91 | 0.26 | 98.53 |
| **291 / 1 .** | 0.00 | 0.98 | 56.07 | 25.69 | 0.01 | 0.00 | 0.37 | 0.05 | 0.22 | 15.10 | 0.24 | 98.74 |
| **292 / 1 .** | 0.00 | 1.00 | 56.10 | 25.54 | 0.00 | 0.00 | 0.37 | 0.04 | 0.21 | 15.05 | 0.21 | 98.54 |
| **293 / 1 .** | 0.01 | 0.98 | 56.21 | 25.18 | 0.00 | 0.00 | 0.36 | 0.04 | 0.20 | 14.96 | 0.28 | 98.23 |
| **294 / 1 .** | 0.01 | 1.02 | 56.36 | 25.44 | 0.00 | 0.00 | 0.30 | 0.06 | 0.19 | 14.96 | 0.28 | 98.61 |
| **295 / 1 .** | 0.01 | 0.31 | 14.93 | 56.38 | 0.00 | 0.00 | 0.11 | 0.02 | 0.16 | 3.80 | 0.07 | 75.79 |
| **296 / 1 .** | 0.02 | 1.00 | 56.39 | 25.50 | 0.00 | 0.01 | 0.30 | 0.05 | 0.19 | 15.17 | 0.24 | 98.86 |
| **297 / 1 .** | 0.00 | 0.90 | 51.33 | 33.95 | 0.01 | 0.00 | 0.31 | 0.02 | 0.24 | 14.50 | 0.20 | 101.46 |
| **298 / 1 .** | 0.01 | 0.02 | 1.19 | 95.42 | 0.01 | 0.02 | 0.00 | 0.01 | 0.01 | 0.50 | 0.02 | 97.22 |
| **299 / 1 .** | 0.01 | 1.01 | 56.11 | 25.56 | 0.00 | 0.01 | 0.33 | 0.05 | 0.23 | 15.09 | 0.25 | 98.65 |
| **300 / 1 .** | 0.01 | 0.99 | 55.42 | 27.23 | 0.00 | 0.02 | 0.28 | 0.03 | 0.25 | 14.87 | 0.27 | 99.38 |
| **301 / 1 .** | 0.00 | 0.01 | 0.16 | 95.25 | 0.00 | 0.00 | 0.02 | 0.02 | 0.00 | 0.26 | 0.00 | 95.72 |

**Table A3-2 continued..**

| Point | $Na_2O$ | MgO | $Al_2O_3$ | $SiO_2$ | $K_2O$ | CaO | $TiO_2$ | $Cr_2O_3$ | MnO | FeO | ZnO | Total |
|---|---|---|---|---|---|---|---|---|---|---|---|---|
| **302 / 1 .** | 0.01 | 0.00 | 0.06 | 98.19 | 0.02 | 0.00 | 0.03 | 0.00 | 0.00 | 0.22 | 0.01 | 98.55 |
| **303 / 1 .** | 0.00 | 0.13 | 2.61 | 93.04 | 0.00 | 0.00 | 0.06 | 0.02 | 0.00 | 0.69 | 0.03 | 96.58 |
| **304 / 1 .** | 0.01 | 0.01 | 0.05 | 98.36 | 0.00 | 0.00 | 0.00 | 0.00 | 0.01 | 0.20 | 0.00 | 98.64 |
| **305 / 1 .** | 0.00 | 0.00 | 0.08 | 97.51 | 0.00 | 0.00 | 0.04 | 0.00 | 0.00 | 0.25 | 0.00 | 97.87 |
| **306 / 1 .** | 0.00 | 1.12 | 55.02 | 26.85 | 0.00 | 0.00 | 0.46 | 0.06 | 0.20 | 14.82 | 0.22 | 98.76 |
| **307 / 1 .** | 0.00 | 0.00 | 0.03 | 97.38 | 0.01 | 0.02 | 0.04 | 0.02 | 0.00 | 0.17 | 0.02 | 97.68 |
| **308 / 1 .** | 0.00 | 0.01 | 0.00 | 97.75 | 0.01 | 0.00 | 0.00 | 0.01 | 0.02 | 0.17 | 0.01 | 97.98 |
| **309 / 1 .** | 0.01 | 1.21 | 54.70 | 27.09 | 0.00 | 0.00 | 0.52 | 0.03 | 0.19 | 15.24 | 0.23 | 99.23 |
| **310 / 1 .** | 0.00 | 1.15 | 55.06 | 26.75 | 0.03 | 0.00 | 0.57 | 0.05 | 0.22 | 15.12 | 0.28 | 99.23 |
| **311 / 1 .** | 0.01 | 1.13 | 55.04 | 26.71 | 0.00 | 0.00 | 0.55 | 0.04 | 0.21 | 15.15 | 0.19 | 99.04 |
| **312 / 1 .** | 0.01 | 1.19 | 54.90 | 26.68 | 0.00 | 0.03 | 0.55 | 0.06 | 0.26 | 15.04 | 0.23 | 98.96 |
| **313 / 1 .** | 0.01 | 1.12 | 54.86 | 26.59 | 0.00 | 0.00 | 0.63 | 0.07 | 0.21 | 15.15 | 0.23 | 98.87 |
| **314 / 1 .** | 0.01 | 1.18 | 54.46 | 26.77 | 0.00 | 0.01 | 0.45 | 0.04 | 0.20 | 15.03 | 0.20 | 98.34 |
| **315 / 1 .** | 0.00 | 1.06 | 54.27 | 26.45 | 0.02 | 0.02 | 0.45 | 0.05 | 0.21 | 15.09 | 0.15 | 97.77 |
| **316 / 1 .** | 0.01 | 1.08 | 54.32 | 26.72 | 0.00 | 0.01 | 0.51 | 0.04 | 0.18 | 15.08 | 0.19 | 98.14 |
| **317 / 1 .** | 0.00 | 1.07 | 54.77 | 26.59 | 0.01 | 0.01 | 0.45 | 0.03 | 0.19 | 15.18 | 0.15 | 98.46 |
| **318 / 1 .** | 0.01 | 0.15 | 7.98 | 81.99 | 0.00 | 0.01 | 0.09 | 0.00 | 0.03 | 2.90 | 0.04 | 93.20 |
| **319 / 1 .** | 0.00 | 1.08 | 54.71 | 26.71 | 0.00 | 0.00 | 0.44 | 0.00 | 0.21 | 15.21 | 0.22 | 98.59 |
| **320 / 1 .** | 0.01 | 1.13 | 51.55 | 33.04 | 0.01 | 0.00 | 0.39 | 0.08 | 0.22 | 14.67 | 0.16 | 101.27 |
| **321 / 1 .** | 0.00 | 1.19 | 54.39 | 26.47 | 0.00 | 0.00 | 0.40 | 0.05 | 0.19 | 15.07 | 0.24 | 98.00 |
| **322 / 1 .** | 0.02 | 1.21 | 54.89 | 26.47 | 0.00 | 0.00 | 0.42 | 0.06 | 0.22 | 15.30 | 0.21 | 98.79 |
| **323 / 1 .** | 0.01 | 1.21 | 54.50 | 26.73 | 0.00 | 0.00 | 0.33 | 0.06 | 0.24 | 14.95 | 0.16 | 98.19 |
| **324 / 1 .** | 0.01 | 1.16 | 54.86 | 26.66 | 0.00 | 0.00 | 0.34 | 0.03 | 0.18 | 15.09 | 0.19 | 98.52 |
| **325 / 1 .** | 0.00 | 1.13 | 54.93 | 26.39 | 0.00 | 0.00 | 0.39 | 0.05 | 0.20 | 15.21 | 0.21 | 98.51 |
| **326 / 1 .** | 0.01 | 1.23 | 53.01 | 30.02 | 0.01 | 0.00 | 0.38 | 0.05 | 0.22 | 15.00 | 0.17 | 100.11 |
| **327 / 1 .** | 0.00 | 1.14 | 55.25 | 26.30 | 0.00 | 0.00 | 0.39 | 0.09 | 0.24 | 15.09 | 0.24 | 98.75 |
| **328 / 1 .** | 0.01 | 1.12 | 54.87 | 26.37 | 0.00 | 0.00 | 0.41 | 0.06 | 0.23 | 14.86 | 0.25 | 98.18 |
| **329 / 1 .** | 0.00 | 1.09 | 55.27 | 27.07 | 0.00 | 0.00 | 0.36 | 0.07 | 0.23 | 15.03 | 0.23 | 99.36 |
| **330 / 1 .** | 0.02 | 1.00 | 56.03 | 27.69 | 0.00 | 0.00 | 0.43 | 0.07 | 0.21 | 14.45 | 0.21 | 100.11 |
| **331 / 1 .** | 0.01 | 0.89 | 45.47 | 51.20 | 0.02 | 0.00 | 0.40 | 0.12 | 0.14 | 12.48 | 0.18 | 110.91 |
| **332 / 1 .** | 0.01 | 1.09 | 54.85 | 26.05 | 0.00 | 0.00 | 0.43 | 0.03 | 0.20 | 15.03 | 0.20 | 97.89 |
| **333 / 1 .** | 0.02 | 1.05 | 55.16 | 26.30 | 0.00 | 0.00 | 0.55 | 0.03 | 0.21 | 15.16 | 0.21 | 98.70 |
| **334 / 1 .** | 0.01 | 1.02 | 55.04 | 26.10 | 0.00 | 0.00 | 0.53 | 0.05 | 0.23 | 15.26 | 0.21 | 98.44 |
| **335 / 1 .** | 0.01 | 1.13 | 54.21 | 26.45 | 0.00 | 0.00 | 0.56 | 0.03 | 0.23 | 15.26 | 0.19 | 98.07 |
| **336 / 1 .** | 0.01 | 1.11 | 55.19 | 25.90 | 0.00 | 0.00 | 0.54 | 0.05 | 0.21 | 14.96 | 0.22 | 98.19 |
| **337 / 1 .** | 0.01 | 1.17 | 54.53 | 29.47 | 0.00 | 0.00 | 0.57 | 0.00 | 0.22 | 14.93 | 0.25 | 101.15 |
| **338 / 1 .** | 0.06 | 0.01 | 0.52 | 97.93 | 0.02 | 0.12 | 0.03 | 0.00 | 0.00 | 0.05 | 0.00 | 98.75 |
| **339 / 1 .** | 0.03 | 0.00 | 0.34 | 97.65 | 0.07 | 0.00 | 0.00 | 0.00 | 0.00 | 0.04 | 0.00 | 98.13 |
| **340 / 1 .** | 0.00 | 0.00 | 0.04 | 97.77 | 0.02 | 0.00 | 0.00 | 0.00 | 0.02 | 0.09 | 0.02 | 97.96 |
| **341 / 1 .** | 0.01 | 0.00 | 0.25 | 96.98 | 0.04 | 0.00 | 0.01 | 0.00 | 0.00 | 0.06 | 0.02 | 97.37 |
| **342 / 1 .** | 0.02 | 0.00 | 0.08 | 100.3 | 0.05 | 0.04 | 0.03 | 0.00 | 0.00 | 0.07 | 0.00 | 100.60 |
| **343 / 1 .** | 0.00 | 0.00 | 0.04 | 97.43 | 0.00 | 0.00 | 0.00 | 0.00 | 0.00 | 0.08 | 0.00 | 97.56 |
| **344 / 1 .** | 0.02 | 0.02 | 63.79 | 35.42 | 0.00 | 0.00 | 0.13 | 0.01 | 0.00 | 0.34 | 0.00 | 99.74 |

**Table A3-2 continued..**

| Point | $Na_2O$ | MgO | $Al_2O_3$ | $SiO_2$ | $K_2O$ | CaO | $TiO_2$ | $Cr_2O_3$ | MnO | FeO | ZnO | Total |
|---|---|---|---|---|---|---|---|---|---|---|---|---|
| **345 / 1 .** | 0.01 | 0.03 | 63.73 | 35.73 | 0.01 | 0.00 | 0.17 | 0.00 | 0.02 | 0.39 | 0.00 | 100.09 |
| **346 / 1 .** | 0.08 | 0.07 | 4.95 | 2.54 | 0.01 | 0.04 | 51.02 | 0.05 | 1.23 | 40.66 | 0.00 | 100.65 |
| **347 / 1 .** | 0.22 | 5.78 | 19.46 | 32.96 | 9.13 | 0.00 | 1.74 | 0.07 | 0.09 | 23.74 | 0.00 | 93.18 |
| **348 / 1 .** | 0.30 | 6.15 | 20.28 | 34.01 | 8.65 | 0.00 | 1.63 | 0.04 | 0.04 | 23.55 | 0.01 | 94.66 |
| **349 / 1 .** | 0.32 | 5.76 | 18.78 | 31.69 | 8.29 | 0.00 | 1.59 | 0.09 | 0.10 | 22.93 | 0.00 | 89.54 |
| **350 / 1 .** | 0.26 | 6.28 | 19.71 | 33.45 | 8.62 | 0.00 | 1.68 | 0.05 | 0.08 | 23.75 | 0.00 | 93.88 |
| **351 / 1 .** | 0.21 | 3.85 | 11.86 | 18.65 | 4.34 | 0.07 | 28.07 | 0.01 | 0.59 | 32.56 | 0.00 | 100.23 |
| **352 / 1 .** | 0.03 | 0.91 | 2.96 | 89.58 | 1.16 | 0.00 | 0.33 | 0.02 | 0.02 | 3.59 | 0.00 | 98.60 |
| **353 / 1 .** | 0.00 | 0.06 | 0.14 | 97.09 | 0.06 | 0.00 | 0.04 | 0.00 | 0.00 | 0.50 | 0.00 | 97.89 |
| **354 / 1 .** | 0.25 | 5.91 | 18.76 | 38.08 | 8.28 | 0.00 | 1.53 | 0.07 | 0.04 | 22.83 | 0.00 | 95.76 |
| **355 / 1 .** | 0.28 | 6.30 | 19.94 | 33.68 | 8.74 | 0.00 | 1.62 | 0.11 | 0.05 | 23.96 | 0.06 | 94.73 |
| **356 / 1 .** | 0.27 | 6.10 | 20.49 | 34.13 | 8.63 | 0.00 | 1.63 | 0.01 | 0.07 | 23.24 | 0.00 | 94.58 |
| **357 / 1 .** | 0.27 | 6.55 | 20.01 | 33.65 | 8.39 | 0.02 | 1.64 | 0.04 | 0.08 | 23.75 | 0.00 | 94.39 |
| **358 / 1 .** | 0.09 | 0.56 | 45.21 | 31.72 | 3.05 | 0.06 | 0.15 | 0.07 | 0.03 | 3.45 | 0.01 | 84.39 |
| **359 / 1 .** | 0.01 | 0.02 | 0.07 | 16.25 | 0.00 | 0.00 | 47.59 | 0.01 | 0.98 | 39.21 | 0.00 | 104.15 |
| **360 / 1 .** | 0.00 | 0.01 | 0.03 | 7.02 | 0.00 | 0.01 | 50.19 | 0.00 | 0.95 | 42.39 | 0.00 | 100.60 |
| **361 / 1 .** | 0.02 | 0.00 | 0.24 | 2.32 | 0.02 | 1.05 | 52.74 | 0.00 | 1.10 | 43.02 | 0.00 | 100.52 |
| **362 / 1 .** | 0.04 | 0.18 | 0.41 | 0.88 | 0.09 | 0.32 | 89.81 | 0.02 | 0.13 | 6.08 | 0.00 | 97.96 |
| **363 / 1 .** | 0.01 | 0.03 | 63.52 | 35.81 | 0.01 | 0.01 | 0.03 | 0.03 | 0.00 | 0.26 | 0.00 | 99.70 |
| **364 / 1 .** | 0.02 | 0.04 | 63.57 | 35.65 | 0.03 | 0.00 | 0.02 | 0.02 | 0.02 | 0.24 | 0.02 | 99.63 |
| **365 / 1 .** | 0.00 | 0.01 | 63.89 | 35.79 | 0.00 | 0.03 | 0.04 | 0.04 | 0.00 | 0.22 | 0.01 | 100.04 |
| **366 / 1 .** | 0.00 | 0.03 | 63.86 | 35.62 | 0.00 | 0.01 | 0.04 | 0.07 | 0.00 | 0.24 | 0.00 | 99.87 |
| **367 / 1 .** | 0.00 | 0.03 | 63.61 | 35.87 | 0.00 | 0.00 | 0.02 | 0.04 | 0.00 | 0.23 | 0.00 | 99.81 |
| **368 / 1 .** | 0.01 | 0.04 | 63.41 | 35.58 | 0.00 | 0.00 | 0.00 | 0.04 | 0.00 | 0.26 | 0.00 | 99.36 |
| **369 / 1 .** | 0.01 | 0.02 | 63.43 | 35.60 | 0.00 | 0.00 | 0.06 | 0.04 | 0.00 | 0.27 | 0.00 | 99.42 |
| **370 / 1 .** | 0.00 | 0.03 | 63.80 | 35.68 | 0.01 | 0.00 | 0.02 | 0.03 | 0.00 | 0.26 | 0.00 | 99.84 |
| **371 / 1 .** | 0.01 | 0.00 | 63.69 | 35.65 | 0.01 | 0.01 | 0.04 | 0.03 | 0.01 | 0.25 | 0.00 | 99.71 |
| **372 / 1 .** | 0.01 | 0.02 | 63.87 | 36.11 | 0.00 | 0.00 | 0.01 | 0.00 | 0.03 | 0.24 | 0.00 | 100.30 |
| **373 / 1 .** | 0.01 | 0.01 | 44.53 | 50.87 | 0.02 | 0.00 | 0.01 | 0.02 | 0.00 | 0.20 | 0.00 | 95.66 |
| **374 / 1 .** | 0.00 | 0.02 | 63.79 | 35.99 | 0.00 | 0.00 | 0.01 | 0.03 | 0.02 | 0.25 | 0.03 | 100.13 |
| **375 / 1 .** | 0.03 | 0.04 | 62.37 | 35.75 | 0.07 | 0.03 | 0.04 | 0.06 | 0.00 | 0.29 | 0.02 | 98.71 |
| **376 / 1 .** | 0.00 | 0.03 | 63.67 | 35.79 | 0.01 | 0.00 | 0.00 | 0.04 | 0.02 | 0.27 | 0.00 | 99.84 |
| **377 / 1 .** | 0.00 | 0.02 | 63.49 | 36.01 | 0.00 | 0.01 | 0.05 | 0.00 | 0.00 | 0.24 | 0.00 | 99.82 |
| **378 / 1 .** | 0.01 | 0.02 | 63.75 | 36.05 | 0.01 | 0.00 | 0.00 | 0.05 | 0.00 | 0.26 | 0.01 | 100.16 |
| **379 / 1 .** | 0.01 | 0.03 | 63.75 | 35.86 | 0.00 | 0.01 | 0.02 | 0.04 | 0.01 | 0.24 | 0.00 | 99.98 |
| **380 / 1 .** | 0.01 | 0.02 | 63.28 | 35.30 | 0.00 | 0.00 | 0.03 | 0.00 | 0.00 | 0.23 | 0.00 | 98.88 |
| **381 / 1 .** | 0.00 | 0.02 | 63.46 | 36.36 | 0.00 | 0.00 | 0.04 | 0.01 | 0.02 | 0.29 | 0.02 | 100.23 |
| **382 / 1 .** | 0.02 | 0.03 | 63.94 | 35.73 | 0.00 | 0.00 | 0.03 | 0.00 | 0.01 | 0.23 | 0.00 | 99.99 |
| **383 / 1 .** | 0.01 | 0.03 | 63.78 | 35.69 | 0.00 | 0.01 | 0.01 | 0.02 | 0.00 | 0.24 | 0.00 | 99.80 |
| **384 / 1 .** | 0.28 | 6.73 | 20.83 | 34.67 | 8.61 | 0.02 | 1.52 | 0.00 | 0.11 | 23.27 | 0.00 | 96.05 |
| **385 / 1 .** | 0.26 | 6.59 | 20.66 | 34.25 | 8.69 | 0.01 | 1.38 | 0.04 | 0.08 | 23.56 | 0.05 | 95.58 |
| **386 / 1 .** | 0.27 | 6.82 | 21.12 | 33.81 | 7.84 | 0.01 | 1.41 | 0.04 | 0.11 | 24.20 | 0.00 | 95.63 |
| **387 / 1 .** | 0.29 | 6.41 | 20.07 | 34.41 | 8.73 | 0.00 | 1.78 | 0.07 | 0.07 | 24.01 | 0.00 | 95.85 |

**Table A3-2 continued..**

| Point | $Na_2O$ | MgO | $Al_2O_3$ | $SiO_2$ | $K_2O$ | CaO | $TiO_2$ | $Cr_2O_3$ | MnO | FeO | ZnO | Total |
|---|---|---|---|---|---|---|---|---|---|---|---|---|
| **388 / 1 .** | 0.33 | 6.44 | 20.16 | 34.39 | 8.73 | 0.00 | 1.89 | 0.09 | 0.06 | 23.69 | 0.01 | 95.79 |
| **389 / 1 .** | 0.33 | 6.37 | 20.29 | 34.00 | 8.61 | 0.01 | 1.84 | 0.07 | 0.08 | 22.93 | 0.00 | 94.54 |
| **390 / 1 .** | 0.30 | 6.45 | 20.07 | 34.04 | 8.74 | 0.00 | 1.71 | 0.08 | 0.10 | 23.56 | 0.00 | 95.05 |
| **391 / 1 .** | 0.24 | 5.98 | 20.84 | 32.94 | 7.66 | 0.00 | 1.37 | 0.09 | 0.09 | 23.06 | 0.01 | 92.28 |
| **392 / 1 .** | 0.31 | 4.27 | 31.17 | 36.87 | 7.02 | 0.04 | 0.99 | 0.05 | 0.05 | 14.86 | 0.01 | 95.64 |
| **393 / 1 .** | 0.30 | 6.31 | 19.83 | 32.93 | 8.69 | 0.01 | 1.46 | 0.11 | 0.07 | 23.29 | 0.04 | 93.05 |
| **394 / 1 .** | 0.30 | 6.37 | 20.27 | 34.21 | 8.93 | 0.00 | 1.90 | 0.05 | 0.09 | 23.73 | 0.03 | 95.87 |
| **395 / 1 .** | 0.31 | 6.38 | 20.13 | 33.42 | 8.74 | 0.00 | 1.73 | 0.03 | 0.05 | 23.91 | 0.00 | 94.71 |
| **396 / 1 .** | 0.33 | 6.36 | 20.20 | 34.06 | 8.59 | 0.00 | 1.79 | 0.04 | 0.07 | 23.92 | 0.00 | 95.37 |
| **397 / 1 .** | 0.01 | 1.29 | 21.39 | 35.85 | 0.03 | 1.72 | 0.10 | 0.00 | 4.34 | 35.67 | 0.00 | 100.39 |
| **398 / 1 .** | 0.03 | 1.40 | 21.62 | 35.87 | 0.00 | 1.71 | 0.07 | 0.01 | 4.17 | 35.51 | 0.00 | 100.39 |
| **399 / 1 .** | 0.04 | 1.52 | 21.59 | 36.44 | 0.02 | 1.65 | 0.02 | 0.02 | 4.16 | 35.79 | 0.02 | 101.27 |
| **400 / 1 .** | 0.02 | 1.56 | 21.46 | 36.21 | 0.00 | 1.68 | 0.01 | 0.06 | 4.11 | 35.38 | 0.01 | 100.50 |
| **401 / 1 .** | 0.02 | 1.56 | 21.82 | 36.40 | 0.00 | 1.45 | 0.00 | 0.05 | 4.32 | 35.58 | 0.01 | 101.22 |
| **402 / 1 .** | 0.02 | 1.67 | 21.68 | 36.13 | 0.01 | 1.49 | 0.05 | 0.05 | 4.34 | 35.44 | 0.06 | 100.93 |
| **403 / 1 .** | 0.01 | 1.67 | 21.56 | 36.04 | 0.00 | 1.49 | 0.00 | 0.04 | 4.27 | 35.52 | 0.00 | 100.59 |
| **404 / 1 .** | 0.02 | 1.68 | 21.55 | 36.18 | 0.00 | 1.44 | 0.00 | 0.00 | 4.29 | 35.38 | 0.00 | 100.56 |
| **405 / 1 .** | 0.06 | 1.69 | 21.55 | 36.09 | 0.00 | 1.46 | 0.00 | 0.04 | 4.32 | 35.18 | 0.00 | 100.39 |
| **406 / 1 .** | 0.03 | 1.73 | 21.69 | 36.32 | 0.00 | 1.53 | 0.05 | 0.02 | 4.20 | 35.13 | 0.02 | 100.73 |
| **407 / 1 .** | 0.02 | 1.65 | 21.57 | 36.13 | 0.00 | 1.43 | 0.00 | 0.05 | 4.28 | 35.34 | 0.02 | 100.49 |
| **408 / 1 .** | 0.03 | 1.64 | 21.49 | 36.17 | 0.01 | 1.43 | 0.03 | 0.00 | 4.33 | 35.65 | 0.06 | 100.85 |
| **409 / 1 .** | 0.01 | 1.63 | 21.45 | 36.16 | 0.00 | 1.41 | 0.04 | 0.02 | 4.28 | 35.35 | 0.03 | 100.39 |
| **410 / 1 .** | 0.04 | 1.59 | 21.60 | 36.02 | 0.02 | 1.46 | 0.00 | 0.01 | 4.29 | 35.45 | 0.00 | 100.48 |
| **411 / 1 .** | 0.01 | 1.58 | 21.49 | 36.13 | 0.00 | 1.51 | 0.00 | 0.00 | 4.09 | 35.62 | 0.00 | 100.43 |
| **412 / 1 .** | 0.01 | 1.46 | 21.65 | 36.08 | 0.00 | 1.80 | 0.03 | 0.00 | 4.07 | 35.11 | 0.00 | 100.22 |
| **413 / 1 .** | 0.04 | 1.53 | 21.54 | 36.23 | 0.00 | 1.57 | 0.03 | 0.02 | 4.06 | 35.48 | 0.00 | 100.51 |
| **414 / 1 .** | 0.01 | 1.63 | 21.63 | 36.24 | 0.01 | 1.58 | 0.01 | 0.01 | 4.09 | 35.65 | 0.00 | 100.85 |
| **415 / 1 .** | 0.02 | 1.57 | 21.56 | 36.05 | 0.00 | 1.46 | 0.00 | 0.00 | 4.20 | 35.69 | 0.00 | 100.55 |
| **416 / 1 .** | 0.02 | 1.64 | 21.58 | 36.27 | 0.00 | 1.48 | 0.02 | 0.00 | 4.14 | 35.63 | 0.00 | 100.78 |
| **417 / 1 .** | 0.02 | 1.62 | 21.52 | 36.08 | 0.00 | 1.49 | 0.00 | 0.02 | 4.24 | 35.14 | 0.05 | 100.17 |
| **418 / 1 .** | 0.01 | 1.59 | 21.49 | 36.08 | 0.00 | 1.49 | 0.00 | 0.01 | 4.39 | 35.11 | 0.00 | 100.15 |
| **419 / 1 .** | 0.01 | 1.64 | 21.56 | 36.11 | 0.00 | 1.44 | 0.02 | 0.01 | 4.23 | 35.60 | 0.00 | 100.62 |
| **420 / 1 .** | 0.04 | 1.66 | 21.60 | 36.16 | 0.00 | 1.44 | 0.02 | 0.03 | 4.26 | 35.56 | 0.00 | 100.77 |
| **421 / 1 .** | 0.02 | 1.70 | 21.71 | 36.29 | 0.01 | 1.45 | 0.00 | 0.00 | 4.35 | 35.09 | 0.06 | 100.67 |
| **422 / 1 .** | 0.02 | 1.61 | 21.59 | 35.93 | 0.00 | 1.47 | 0.04 | 0.04 | 4.15 | 35.33 | 0.03 | 100.21 |
| **423 / 1 .** | 0.02 | 1.61 | 21.54 | 35.95 | 0.00 | 1.54 | 0.00 | 0.06 | 4.15 | 35.61 | 0.00 | 100.48 |
| **424 / 1 .** | 0.01 | 1.49 | 21.51 | 36.42 | 0.00 | 1.49 | 0.02 | 0.00 | 4.12 | 35.66 | 0.01 | 100.73 |
| **425 / 1 .** | 0.04 | 1.55 | 21.62 | 36.58 | 0.00 | 1.56 | 0.05 | 0.02 | 4.16 | 35.78 | 0.04 | 101.38 |
| **426 / 1 .** | 0.03 | 1.44 | 21.60 | 36.25 | 0.01 | 1.71 | 0.02 | 0.00 | 4.05 | 35.12 | 0.03 | 100.26 |
| **427 / 1 .** | 0.02 | 1.18 | 20.30 | 39.07 | 0.00 | 1.65 | 0.01 | 0.00 | 4.17 | 34.48 | 0.03 | 100.91 |
| **428 / 1 .** | 0.01 | 1.49 | 21.74 | 36.28 | 0.00 | 1.58 | 0.01 | 0.03 | 4.07 | 35.47 | 0.00 | 100.67 |
| **429 / 1 .** | 0.01 | 1.55 | 21.59 | 36.40 | 0.01 | 1.55 | 0.04 | 0.00 | 4.05 | 35.81 | 0.00 | 101.02 |
| **430 / 1 .** | 0.05 | 1.57 | 21.39 | 36.11 | 0.00 | 1.39 | 0.00 | 0.00 | 4.17 | 35.49 | 0.00 | 100.17 |

**Table A3-2 continued..**

| Point | $Na_2O$ | MgO | $Al_2O_3$ | $SiO_2$ | $K_2O$ | CaO | $TiO_2$ | $Cr_2O_3$ | MnO | FeO | ZnO | Total |
|---|---|---|---|---|---|---|---|---|---|---|---|---|
| **431 / 1 .** | 0.02 | 1.61 | 21.80 | 35.85 | 0.00 | 1.45 | 0.06 | 0.01 | 4.24 | 35.57 | 0.00 | 100.62 |
| **432 / 1 .** | 0.04 | 1.61 | 21.52 | 36.19 | 0.00 | 1.39 | 0.02 | 0.02 | 4.21 | 35.36 | 0.02 | 100.39 |
| **433 / 1 .** | 0.03 | 1.69 | 21.67 | 36.02 | 0.02 | 1.41 | 0.02 | 0.00 | 4.19 | 35.72 | 0.00 | 100.77 |
| **434 / 1 .** | 0.03 | 1.57 | 21.45 | 35.93 | 0.00 | 1.46 | 0.02 | 0.01 | 4.19 | 35.33 | 0.00 | 100.01 |
| **435 / 1 .** | 0.03 | 1.64 | 21.57 | 36.06 | 0.01 | 1.50 | 0.04 | 0.04 | 4.10 | 35.73 | 0.00 | 100.73 |
| **436 / 1 .** | 0.04 | 1.45 | 21.48 | 36.21 | 0.00 | 1.48 | 0.02 | 0.02 | 4.25 | 35.53 | 0.00 | 100.48 |
| **437 / 1 .** | 0.03 | 1.50 | 21.54 | 36.06 | 0.00 | 1.57 | 0.01 | 0.00 | 4.24 | 35.81 | 0.02 | 100.77 |
| **438 / 1 .** | 0.02 | 1.48 | 21.63 | 35.98 | 0.00 | 1.56 | 0.03 | 0.00 | 4.09 | 34.96 | 0.00 | 99.75 |
| **439 / 1 .** | 0.04 | 1.47 | 21.32 | 35.90 | 0.00 | 1.50 | 0.05 | 0.00 | 4.02 | 35.53 | 0.00 | 99.82 |
| **440 / 1 .** | 0.02 | 1.55 | 21.55 | 36.10 | 0.02 | 1.46 | 0.03 | 0.00 | 4.05 | 35.38 | 0.02 | 100.18 |
| **441 / 1 .** | 0.00 | 1.52 | 21.58 | 36.20 | 0.02 | 1.54 | 0.02 | 0.03 | 4.21 | 35.65 | 0.00 | 100.76 |
| **442 / 1 .** | 0.01 | 1.59 | 21.70 | 36.45 | 0.00 | 1.50 | 0.00 | 0.00 | 4.26 | 35.62 | 0.00 | 101.13 |
| **443 / 1 .** | 0.02 | 1.61 | 21.47 | 36.31 | 0.00 | 1.51 | 0.00 | 0.00 | 4.19 | 35.59 | 0.05 | 100.75 |
| **444 / 1 .** | 0.03 | 1.61 | 21.67 | 36.39 | 0.03 | 1.45 | 0.00 | 0.00 | 4.23 | 35.52 | 0.00 | 100.91 |
| **445 / 1 .** | 0.03 | 1.54 | 21.53 | 36.40 | 0.00 | 1.44 | 0.01 | 0.00 | 4.28 | 35.50 | 0.00 | 100.71 |
| **446 / 1 .** | 0.02 | 1.56 | 21.53 | 36.17 | 0.02 | 1.47 | 0.02 | 0.01 | 4.25 | 35.21 | 0.01 | 100.26 |
| **447 / 1 .** | 0.02 | 1.58 | 21.84 | 36.29 | 0.00 | 1.46 | 0.00 | 0.05 | 4.26 | 35.45 | 0.00 | 100.95 |
| **448 / 1 .** | 0.03 | 1.63 | 21.50 | 35.92 | 0.00 | 1.42 | 0.02 | 0.00 | 4.33 | 35.31 | 0.00 | 100.16 |
| **449 / 1 .** | 0.02 | 1.65 | 21.57 | 35.85 | 0.00 | 1.45 | 0.00 | 0.01 | 4.22 | 35.63 | 0.03 | 100.42 |
| **450 / 1 .** | 0.01 | 1.64 | 21.71 | 36.08 | 0.00 | 1.40 | 0.00 | 0.00 | 4.26 | 35.60 | 0.00 | 100.71 |
| **451 / 1 .** | 0.04 | 1.54 | 21.57 | 36.19 | 0.01 | 1.49 | 0.02 | 0.00 | 4.22 | 35.48 | 0.00 | 100.56 |
| **452 / 1 .** | 0.04 | 1.49 | 21.55 | 36.00 | 0.01 | 1.62 | 0.00 | 0.01 | 4.07 | 35.39 | 0.00 | 100.19 |
| **453 / 1 .** | 0.01 | 1.40 | 21.53 | 36.31 | 0.00 | 1.76 | 0.03 | 0.00 | 4.23 | 35.64 | 0.00 | 100.91 |
| **454 / 1 .** | 0.02 | 1.41 | 21.58 | 36.00 | 0.02 | 1.82 | 0.02 | 0.01 | 4.08 | 35.36 | 0.00 | 100.32 |
| **455 / 1 .** | 0.00 | 0.09 | 2.08 | 90.49 | 0.00 | 0.00 | 0.00 | 0.03 | 0.01 | 1.61 | 0.01 | 94.33 |
| **456 / 1 .** | 0.01 | 1.79 | 41.52 | 24.47 | 0.03 | 0.00 | 0.00 | 0.05 | 0.19 | 25.21 | 0.01 | 93.29 |
| **457 / 1 .** | 0.00 | 1.85 | 41.59 | 24.13 | 0.01 | 0.02 | 0.03 | 0.05 | 0.16 | 25.44 | 0.02 | 93.31 |
| **458 / 1 .** | 0.00 | 1.84 | 41.26 | 24.08 | 0.00 | 0.00 | 0.01 | 0.03 | 0.17 | 25.17 | 0.00 | 92.56 |
| **459 / 1 .** | 0.01 | 1.74 | 41.44 | 23.80 | 0.00 | 0.00 | 0.00 | 0.09 | 0.15 | 25.38 | 0.02 | 92.63 |
| **460 / 1 .** | 0.00 | 0.00 | 0.00 | 0.16 | 0.02 | 0.00 | 52.73 | 0.00 | 0.49 | 46.03 | 0.00 | 99.44 |
| **461 / 1 .** | 0.03 | 0.00 | 0.60 | 0.80 | 0.13 | 0.00 | 50.95 | 0.00 | 0.43 | 44.88 | 0.00 | 97.83 |
| **462 / 1 .** | 0.02 | 0.00 | 0.17 | 14.46 | 0.08 | 0.01 | 48.45 | 0.01 | 0.37 | 41.92 | 0.00 | 105.51 |
| **463 / 1 .** | 0.00 | 0.00 | 0.21 | 0.50 | 0.07 | 0.00 | 52.06 | 0.00 | 0.46 | 45.67 | 0.03 | 99.00 |
| **464 / 1 .** | 0.02 | 1.01 | 55.45 | 27.37 | 0.01 | 0.08 | 0.51 | 0.04 | 0.10 | 14.63 | 0.06 | 99.28 |
| **465 / 1 .** | 0.00 | 0.96 | 55.43 | 26.93 | 0.00 | 0.00 | 0.52 | 0.04 | 0.07 | 15.21 | 0.04 | 99.20 |
| **466 / 1 .** | 0.01 | 1.01 | 55.02 | 26.88 | 0.01 | 0.00 | 0.47 | 0.07 | 0.11 | 15.25 | 0.04 | 98.89 |
| **467 / 1 .** | 0.02 | 1.01 | 54.94 | 26.89 | 0.00 | 0.03 | 0.47 | 0.08 | 0.11 | 15.36 | 0.04 | 98.95 |
| **468 / 1 .** | 0.01 | 1.02 | 54.93 | 27.03 | 0.00 | 0.01 | 0.46 | 0.03 | 0.10 | 15.45 | 0.06 | 99.10 |
| **469 / 1 .** | 0.00 | 1.01 | 55.34 | 26.24 | 0.00 | 0.10 | 0.49 | 0.04 | 0.10 | 15.59 | 0.02 | 98.92 |
| **470 / 1 .** | 0.00 | 1.08 | 55.07 | 26.85 | 0.00 | 0.00 | 0.43 | 0.02 | 0.09 | 15.47 | 0.05 | 99.07 |
| **471 / 1 .** | 0.00 | 1.06 | 54.66 | 26.66 | 0.00 | 0.00 | 0.50 | 0.01 | 0.08 | 15.46 | 0.09 | 98.53 |
| **472 / 1 .** | 0.02 | 1.09 | 54.77 | 27.08 | 0.00 | 0.00 | 0.44 | 0.03 | 0.12 | 15.30 | 0.05 | 98.90 |
| **473 / 1 .** | 0.00 | 1.12 | 54.61 | 26.93 | 0.00 | 0.00 | 0.44 | 0.04 | 0.10 | 15.56 | 0.00 | 98.80 |

**Table A3-2 continued..**

| Point | $Na_2O$ | MgO | $Al_2O_3$ | $SiO_2$ | $K_2O$ | CaO | $TiO_2$ | $Cr_2O_3$ | MnO | FeO | ZnO | Total |
|---|---|---|---|---|---|---|---|---|---|---|---|---|
| **474 / 1 .** | 0.01 | 1.11 | 54.52 | 26.93 | 0.01 | 0.00 | 0.43 | 0.05 | 0.09 | 15.39 | 0.05 | 98.59 |
| **475 / 1 .** | 0.01 | 1.08 | 54.85 | 26.82 | 0.01 | 0.00 | 0.47 | 0.03 | 0.10 | 15.38 | 0.03 | 98.78 |
| **476 / 1 .** | 0.01 | 1.08 | 54.99 | 26.89 | 0.01 | 0.00 | 0.47 | 0.03 | 0.09 | 15.34 | 0.02 | 98.92 |
| **477 / 1 .** | 0.01 | 1.09 | 54.78 | 26.82 | 0.00 | 0.01 | 0.50 | 0.09 | 0.11 | 15.41 | 0.00 | 98.81 |
| **478 / 1 .** | 0.02 | 1.08 | 54.87 | 26.62 | 0.01 | 0.00 | 0.49 | 0.04 | 0.06 | 15.31 | 0.01 | 98.49 |
| **479 / 1 .** | 0.01 | 1.14 | 54.98 | 26.77 | 0.00 | 0.00 | 0.49 | 0.04 | 0.07 | 15.40 | 0.02 | 98.93 |
| **480 / 1 .** | 0.01 | 1.06 | 51.92 | 30.75 | 0.00 | 0.02 | 0.38 | 0.06 | 0.09 | 14.87 | 0.00 | 99.15 |
| **481 / 1 .** | 0.01 | 1.05 | 54.69 | 26.76 | 0.00 | 0.02 | 0.43 | 0.02 | 0.11 | 15.23 | 0.04 | 98.38 |
| **482 / 1 .** | 0.01 | 1.12 | 54.73 | 26.70 | 0.00 | 0.01 | 0.44 | 0.04 | 0.12 | 15.47 | 0.05 | 98.69 |
| **483 / 1 .** | 0.01 | 1.09 | 55.05 | 26.72 | 0.00 | 0.00 | 0.40 | 0.03 | 0.05 | 15.48 | 0.03 | 98.85 |
| **484 / 1 .** | 0.01 | 1.16 | 54.98 | 26.71 | 0.00 | 0.03 | 0.42 | 0.01 | 0.06 | 15.41 | 0.00 | 98.80 |
| **485 / 1 .** | 0.00 | 1.09 | 54.58 | 26.71 | 0.00 | 0.00 | 0.55 | 0.06 | 0.10 | 15.60 | 0.03 | 98.71 |
| **486 / 1 .** | 0.01 | 0.28 | 15.57 | 82.88 | 0.02 | 0.01 | 0.14 | 0.02 | 0.02 | 5.05 | 0.02 | 104.03 |
| **487 / 1 .** | 0.01 | 1.13 | 51.90 | 29.31 | 0.01 | 0.00 | 0.39 | 0.02 | 0.09 | 14.49 | 0.06 | 97.41 |
| **488 / 1 .** | 0.00 | 0.52 | 24.54 | 62.01 | 0.00 | 0.01 | 0.15 | 0.03 | 0.05 | 7.19 | 0.00 | 94.50 |
| **489 / 1 .** | 0.01 | 1.10 | 54.75 | 26.94 | 0.01 | 0.00 | 0.37 | 0.03 | 0.07 | 15.33 | 0.00 | 98.60 |
| **490 / 1 .** | 0.02 | 1.15 | 54.78 | 26.59 | 0.00 | 0.00 | 0.42 | 0.02 | 0.10 | 15.63 | 0.04 | 98.75 |
| **491 / 1 .** | 0.03 | 1.11 | 54.46 | 27.04 | 0.03 | 0.00 | 0.46 | 0.00 | 0.08 | 15.34 | 0.03 | 98.57 |
| **492 / 1 .** | 0.00 | 1.08 | 54.50 | 26.73 | 0.00 | 0.00 | 0.52 | 0.05 | 0.11 | 15.19 | 0.04 | 98.22 |
| **493 / 1 .** | 0.00 | 0.92 | 55.06 | 26.48 | 0.00 | 0.00 | 0.48 | 0.07 | 0.12 | 15.27 | 0.00 | 98.41 |
| **494 / 1 .** | 0.02 | 1.00 | 54.45 | 27.02 | 0.00 | 0.00 | 0.60 | 0.04 | 0.07 | 15.25 | 0.02 | 98.48 |
| **495 / 1 .** | 0.00 | 0.96 | 54.51 | 27.10 | 0.02 | 0.00 | 0.47 | 0.07 | 0.14 | 14.63 | 0.00 | 97.91 |
| **496 / 1 .** | 0.01 | 0.99 | 54.97 | 27.29 | 0.01 | 0.00 | 0.48 | 0.03 | 0.13 | 14.52 | 0.03 | 98.46 |
| **497 / 1 .** | 0.25 | 7.31 | 20.35 | 34.41 | 8.30 | 0.02 | 1.75 | 0.06 | 0.03 | 23.89 | 0.05 | 96.40 |
| **498 / 1 .** | 0.25 | 6.52 | 19.71 | 33.36 | 8.43 | 0.00 | 1.68 | 0.05 | 0.05 | 24.13 | 0.00 | 94.19 |
| **499 / 1 .** | 0.31 | 6.65 | 20.04 | 33.82 | 8.32 | 0.00 | 1.73 | 0.03 | 0.02 | 24.17 | 0.02 | 95.09 |
| **500 / 1 .** | 0.33 | 6.55 | 19.82 | 33.56 | 8.35 | 0.00 | 1.64 | 0.07 | 0.03 | 23.71 | 0.02 | 94.07 |
| **501 / 1 .** | 0.38 | 6.88 | 20.14 | 33.71 | 8.35 | 0.00 | 1.76 | 0.06 | 0.03 | 23.43 | 0.00 | 94.74 |
| **502 / 1 .** | 0.37 | 6.50 | 19.33 | 33.40 | 8.34 | 0.02 | 2.03 | 0.08 | 0.04 | 23.79 | 0.00 | 93.89 |
| **503 / 1 .** | 0.26 | 6.44 | 19.66 | 32.98 | 8.09 | 0.00 | 1.74 | 0.05 | 0.00 | 24.77 | 0.00 | 93.99 |
| **504 / 1 .** | 0.31 | 6.43 | 19.92 | 33.77 | 8.38 | 0.01 | 1.82 | 0.06 | 0.03 | 24.14 | 0.02 | 94.89 |
| **505 / 1 .** | 0.64 | 4.83 | 26.06 | 37.89 | 7.93 | 0.02 | 1.24 | 0.03 | 0.03 | 18.15 | 0.02 | 96.84 |
| **506 / 1 .** | 0.32 | 6.60 | 19.95 | 33.83 | 8.57 | 0.00 | 1.72 | 0.04 | 0.04 | 24.18 | 0.04 | 95.28 |
| **507 / 1 .** | 0.30 | 6.58 | 19.88 | 33.86 | 8.54 | 0.00 | 1.72 | 0.06 | 0.03 | 24.19 | 0.00 | 95.18 |
| **508 / 1 .** | 0.33 | 6.58 | 19.92 | 34.02 | 8.32 | 0.03 | 1.63 | 0.05 | 0.04 | 23.39 | 0.00 | 94.30 |
| **509 / 1 .** | 0.35 | 6.69 | 20.60 | 34.21 | 8.27 | 0.00 | 1.63 | 0.04 | 0.04 | 23.01 | 0.00 | 94.84 |
| **510 / 1 .** | 0.35 | 6.60 | 20.03 | 33.90 | 8.40 | 0.00 | 1.54 | 0.04 | 0.00 | 23.61 | 0.00 | 94.48 |
| **511 / 1 .** | 0.32 | 6.64 | 20.42 | 34.12 | 8.60 | 0.04 | 1.65 | 0.05 | 0.01 | 23.98 | 0.00 | 95.82 |
| **512 / 1 .** | 0.29 | 6.55 | 20.12 | 33.82 | 8.51 | 0.02 | 1.58 | 0.03 | 0.01 | 23.94 | 0.03 | 94.92 |
| **513 / 1 .** | 0.32 | 6.54 | 20.46 | 34.08 | 8.56 | 0.01 | 1.65 | 0.06 | 0.00 | 24.07 | 0.00 | 95.75 |
| **514 / 1 .** | 0.27 | 6.58 | 20.17 | 33.70 | 8.28 | 0.00 | 1.64 | 0.05 | 0.06 | 24.35 | 0.00 | 95.11 |
| **515 / 1 .** | 0.22 | 6.69 | 19.29 | 31.98 | 7.45 | 0.09 | 1.78 | 0.08 | 0.04 | 25.02 | 0.00 | 92.65 |
| **516 / 1 .** | 1.87 | 0.29 | 38.17 | 47.17 | 7.33 | 0.00 | 0.22 | 0.03 | 0.01 | 0.69 | 0.02 | 95.81 |

**Table A3-2 continued..**

| Point | $Na_2O$ | MgO | $Al_2O_3$ | $SiO_2$ | $K_2O$ | CaO | $TiO_2$ | $Cr_2O_3$ | MnO | FeO | ZnO | Total |
|---|---|---|---|---|---|---|---|---|---|---|---|---|
| **517 / 1 .** | 1.90 | 0.24 | 38.06 | 46.27 | 8.26 | 0.00 | 0.25 | 0.05 | 0.01 | 0.63 | 0.00 | 95.66 |
| **518 / 1 .** | 1.77 | 0.24 | 28.97 | 53.34 | 6.38 | 0.05 | 0.19 | 0.02 | 0.00 | 0.57 | 0.00 | 91.54 |
| **519 / 1 .** | 0.47 | 0.03 | 5.77 | 89.16 | 1.18 | 0.00 | 0.04 | 0.00 | 0.03 | 0.13 | 0.00 | 96.81 |
| **520 / 1 .** | 0.29 | 6.80 | 19.93 | 33.06 | 7.56 | 0.00 | 1.74 | 0.10 | 0.00 | 24.19 | 0.00 | 93.67 |
| **521 / 1 .** | 0.35 | 6.67 | 20.40 | 34.27 | 8.37 | 0.02 | 1.78 | 0.06 | 0.08 | 23.58 | 0.00 | 95.59 |
| **522 / 1 .** | 0.30 | 6.66 | 20.30 | 34.28 | 8.43 | 0.00 | 1.68 | 0.04 | 0.03 | 23.31 | 0.06 | 95.09 |
| **523 / 1 .** | 0.35 | 6.76 | 20.48 | 34.52 | 8.41 | 0.00 | 1.71 | 0.05 | 0.05 | 23.53 | 0.00 | 95.85 |
| **524 / 1 .** | 0.33 | 6.82 | 20.23 | 34.00 | 8.09 | 0.08 | 1.57 | 0.04 | 0.07 | 23.12 | 0.00 | 94.36 |
| **525 / 1 .** | 0.31 | 6.73 | 20.46 | 34.29 | 8.44 | 0.00 | 1.66 | 0.04 | 0.06 | 23.11 | 0.00 | 95.11 |
| **526 / 1 .** | 0.36 | 6.87 | 20.14 | 33.93 | 8.36 | 0.00 | 1.71 | 0.04 | 0.05 | 23.56 | 0.00 | 95.01 |
| **527 / 1 .** | 1.92 | 0.27 | 37.72 | 45.44 | 8.44 | 0.00 | 0.23 | 0.03 | 0.00 | 1.27 | 0.03 | 95.34 |
| **528 / 1 .** | 1.92 | 0.34 | 36.85 | 45.64 | 7.18 | 0.00 | 0.28 | 0.04 | 0.01 | 1.07 | 0.03 | 93.35 |
| **529 / 1 .** | 1.78 | 0.41 | 36.34 | 47.52 | 8.47 | 0.02 | 0.27 | 0.06 | 0.00 | 0.98 | 0.02 | 95.87 |
| **530 / 1 .** | 1.84 | 0.23 | 37.43 | 46.29 | 6.96 | 0.04 | 0.12 | 0.06 | 0.03 | 0.69 | 0.00 | 93.70 |
| **531 / 1 .** | 1.85 | 0.26 | 36.60 | 43.88 | 8.11 | 1.38 | 0.19 | 0.03 | 0.00 | 0.64 | 0.00 | 92.95 |
| **532 / 1 .** | 1.82 | 0.29 | 37.59 | 46.41 | 6.83 | 0.01 | 0.24 | 0.06 | 0.00 | 0.71 | 0.00 | 93.95 |
| **533 / 1 .** | 2.04 | 0.22 | 36.49 | 43.15 | 8.21 | 0.04 | 0.22 | 0.03 | 0.00 | 0.65 | 0.02 | 91.08 |
| **534 / 1 .** | 1.99 | 0.27 | 37.07 | 45.65 | 6.97 | 0.03 | 0.10 | 0.03 | 0.00 | 0.61 | 0.00 | 92.72 |
| **535 / 1 .** | 0.01 | 1.93 | 41.63 | 24.04 | 0.01 | 0.04 | 0.03 | 0.06 | 0.17 | 25.06 | 0.00 | 92.98 |
| **536 / 1 .** | 0.00 | 1.89 | 41.62 | 23.80 | 0.00 | 0.05 | 0.03 | 0.04 | 0.16 | 24.93 | 0.02 | 92.54 |
| **537 / 1 .** | 0.00 | 1.88 | 41.51 | 24.26 | 0.03 | 0.00 | 0.01 | 0.08 | 0.17 | 25.55 | 0.01 | 93.49 |
| **538 / 1 .** | 0.01 | 1.81 | 41.43 | 23.99 | 0.01 | 0.00 | 0.00 | 0.06 | 0.17 | 25.43 | 0.00 | 92.91 |
| **539 / 1 .** | 0.00 | 1.84 | 41.49 | 24.15 | 0.00 | 0.00 | 0.00 | 0.03 | 0.18 | 25.46 | 0.00 | 93.15 |
| **540 / 1 .** | 0.00 | 1.09 | 54.68 | 26.79 | 0.00 | 0.00 | 0.56 | 0.08 | 0.08 | 15.35 | 0.04 | 98.67 |
| **541 / 1 .** | 0.01 | 1.15 | 54.79 | 26.98 | 0.00 | 0.03 | 0.55 | 0.07 | 0.08 | 15.18 | 0.03 | 98.87 |
| **542 / 1 .** | 0.00 | 1.14 | 54.99 | 26.79 | 0.00 | 0.00 | 0.62 | 0.04 | 0.09 | 15.06 | 0.08 | 98.82 |
| **543 / 1 .** | 0.01 | 1.12 | 55.00 | 26.97 | 0.00 | 0.00 | 0.49 | 0.05 | 0.11 | 15.19 | 0.03 | 98.97 |
| **544 / 1 .** | 0.00 | 1.11 | 55.00 | 26.76 | 0.00 | 0.01 | 0.57 | 0.06 | 0.08 | 14.92 | 0.07 | 98.59 |
| **545 / 1 .** | 0.00 | 0.01 | 0.08 | 97.62 | 0.02 | 0.00 | 0.15 | 0.00 | 0.00 | 0.40 | 0.03 | 98.31 |
| **546 / 1 .** | 0.01 | 1.22 | 55.08 | 26.92 | 0.00 | 0.00 | 0.41 | 0.04 | 0.07 | 15.13 | 0.04 | 98.93 |
| **547 / 1 .** | 0.01 | 0.00 | 0.07 | 98.28 | 0.00 | 0.00 | 0.05 | 0.00 | 0.00 | 0.28 | 0.02 | 98.70 |
| **548 / 1 .** | 0.01 | 1.22 | 54.83 | 27.28 | 0.00 | 0.01 | 0.47 | 0.00 | 0.03 | 15.03 | 0.10 | 98.99 |
| **549 / 1 .** | 0.00 | 1.23 | 54.71 | 27.13 | 0.00 | 0.00 | 0.43 | 0.01 | 0.08 | 15.22 | 0.06 | 98.86 |
| **550 / 1 .** | 0.00 | 1.17 | 55.10 | 26.86 | 0.01 | 0.00 | 0.48 | 0.01 | 0.09 | 15.15 | 0.05 | 98.93 |
| **551 / 1 .** | 0.01 | 1.21 | 55.08 | 27.01 | 0.00 | 0.00 | 0.44 | 0.03 | 0.10 | 15.17 | 0.08 | 99.13 |
| **552 / 1 .** | 0.02 | 0.14 | 0.00 | 0.04 | 0.00 | 0.00 | 51.95 | 0.06 | 0.35 | 46.76 | 0.00 | 99.32 |
| **553 / 1 .** | 0.01 | 0.14 | 0.01 | 0.21 | 0.00 | 0.02 | 52.19 | 0.01 | 0.35 | 46.73 | 0.00 | 99.66 |
| **554 / 1 .** | 0.01 | 1.14 | 55.25 | 26.61 | 0.01 | 0.01 | 0.43 | 0.05 | 0.11 | 15.08 | 0.09 | 98.79 |
| **555 / 1 .** | 0.01 | 1.16 | 54.86 | 27.04 | 0.01 | 0.01 | 0.47 | 0.00 | 0.08 | 15.18 | 0.04 | 98.87 |
| **556 / 1 .** | 0.02 | 1.26 | 55.38 | 27.21 | 0.00 | 0.00 | 0.44 | 0.05 | 0.08 | 15.25 | 0.04 | 99.72 |
| **557 / 1 .** | 0.00 | 1.20 | 54.76 | 26.93 | 0.00 | 0.00 | 0.42 | 0.00 | 0.09 | 15.19 | 0.05 | 98.66 |
| **558 / 1 .** | 0.00 | 1.24 | 54.78 | 27.02 | 0.00 | 0.00 | 0.39 | 0.05 | 0.07 | 15.08 | 0.08 | 98.72 |
| **559 / 1 .** | 0.02 | 1.18 | 54.94 | 27.09 | 0.00 | 0.01 | 0.40 | 0.04 | 0.06 | 15.18 | 0.09 | 99.02 |

**Table A3-2 continued..**

| Point | $Na_2O$ | MgO | $Al_2O_3$ | $SiO_2$ | $K_2O$ | CaO | $TiO_2$ | $Cr_2O_3$ | MnO | FeO | ZnO | Total |
|---|---|---|---|---|---|---|---|---|---|---|---|---|
| **560 / 1 .** | 0.02 | 1.20 | 55.05 | 26.94 | 0.00 | 0.00 | 0.67 | 0.02 | 0.09 | 15.28 | 0.12 | 99.38 |
| **561 / 1 .** | 0.08 | 1.65 | 49.68 | 24.52 | 0.02 | 0.01 | 0.41 | 0.03 | 0.11 | 15.25 | 0.03 | 91.80 |
| **562 / 1 .** | 0.00 | 1.24 | 55.18 | 27.25 | 0.00 | 0.00 | 0.49 | 0.04 | 0.10 | 15.27 | 0.06 | 99.63 |
| **563 / 1 .** | 0.01 | 1.16 | 54.84 | 27.06 | 0.00 | 0.00 | 0.42 | 0.01 | 0.08 | 15.33 | 0.10 | 99.01 |
| **564 / 1 .** | 0.01 | 1.21 | 54.45 | 27.22 | 0.00 | 0.02 | 0.47 | 0.02 | 0.10 | 14.95 | 0.08 | 98.52 |
| **565 / 1 .** | 0.01 | 0.01 | 1.15 | 91.67 | 0.00 | 0.01 | 0.04 | 0.00 | 0.01 | 0.67 | 0.01 | 93.58 |
| **566 / 1 .** | 0.02 | 1.07 | 55.08 | 26.95 | 0.01 | 0.02 | 0.44 | 0.04 | 0.08 | 14.22 | 0.08 | 98.01 |
| **567 / 1 .** | 0.04 | 0.02 | 0.05 | 62.18 | 0.03 | 0.02 | 21.31 | 0.00 | 0.17 | 13.75 | 0.03 | 97.60 |
| **568 / 1 .** | 0.05 | 0.01 | 0.31 | 15.34 | 0.00 | 0.02 | 46.37 | 0.00 | 0.43 | 39.34 | 0.00 | 101.86 |
| **569 / 1 .** | 0.04 | 0.01 | 0.15 | 0.24 | 0.03 | 0.01 | 52.08 | 0.02 | 0.49 | 44.40 | 0.06 | 97.53 |
| **570 / 1 .** | 0.02 | 0.03 | 0.00 | 11.88 | 0.01 | 0.02 | 48.08 | 0.02 | 0.44 | 41.30 | 0.00 | 101.80 |
| **571 / 1 .** | 0.01 | 0.01 | 0.01 | 0.11 | 0.00 | 0.01 | 0.00 | 0.00 | 0.01 | 0.04 | 0.01 | 0.21 |
| **572 / 1 .** | 0.01 | 0.00 | 0.00 | 0.10 | 0.01 | 0.02 | 0.02 | 0.00 | 0.00 | 0.04 | 0.00 | 0.20 |
| **573 / 1 .** | 0.02 | 0.00 | 0.00 | 0.12 | 0.00 | 0.04 | 0.00 | 0.01 | 0.00 | 0.05 | 0.00 | 0.24 |
| **574 / 1 .** | 0.02 | 1.12 | 54.76 | 26.80 | 0.01 | 0.01 | 0.52 | 0.02 | 0.10 | 15.00 | 0.04 | 98.40 |
| **575 / 1 .** | 0.01 | 1.12 | 54.40 | 27.25 | 0.00 | 0.00 | 0.44 | 0.03 | 0.06 | 15.19 | 0.03 | 98.52 |
| **576 / 1 .** | 0.01 | 1.11 | 54.74 | 26.84 | 0.00 | 0.00 | 0.42 | 0.02 | 0.10 | 14.85 | 0.09 | 98.19 |
| **577 / 1 .** | 0.01 | 1.17 | 54.51 | 27.17 | 0.00 | 0.00 | 0.47 | 0.03 | 0.08 | 15.20 | 0.05 | 98.67 |
| **578 / 1 .** | 0.01 | 1.15 | 54.95 | 27.08 | 0.00 | 0.00 | 0.41 | 0.04 | 0.09 | 14.72 | 0.06 | 98.51 |
| **579 / 1 .** | 0.02 | 0.96 | 52.64 | 26.18 | 0.01 | 0.02 | 0.67 | 0.05 | 0.11 | 16.28 | 0.10 | 97.05 |
| **580 / 1 .** | 0.00 | 1.10 | 54.65 | 26.88 | 0.01 | 0.01 | 0.59 | 0.01 | 0.08 | 15.36 | 0.07 | 98.77 |
| **581 / 1 .** | 0.00 | 1.16 | 55.09 | 26.59 | 0.00 | 0.00 | 0.44 | 0.02 | 0.10 | 15.19 | 0.06 | 98.64 |
| **582 / 1 .** | 0.01 | 1.16 | 54.57 | 26.88 | 0.00 | 0.00 | 0.47 | 0.05 | 0.07 | 15.22 | 0.05 | 98.48 |
| **583 / 1 .** | 0.02 | 1.25 | 55.08 | 27.36 | 0.01 | 0.00 | 0.45 | 0.03 | 0.07 | 13.97 | 0.04 | 98.28 |
| **584 / 1 .** | 0.00 | 0.32 | 16.87 | 6.70 | 0.00 | 0.00 | 0.11 | 0.01 | 0.06 | 11.23 | 0.03 | 35.34 |
| **585 / 1 .** | 0.00 | 1.22 | 54.55 | 27.04 | 0.00 | 0.00 | 0.44 | 0.02 | 0.14 | 14.87 | 0.00 | 98.27 |
| **586 / 1 .** | 0.01 | 1.06 | 54.75 | 26.90 | 0.00 | 0.00 | 0.48 | 0.07 | 0.10 | 14.98 | 0.00 | 98.36 |
| **587 / 1 .** | 0.01 | 1.11 | 54.44 | 27.19 | 0.00 | 0.00 | 0.46 | 0.05 | 0.08 | 14.93 | 0.05 | 98.32 |
| **588 / 1 .** | 0.18 | 6.72 | 20.04 | 34.37 | 8.17 | 0.00 | 2.01 | 0.05 | 0.00 | 22.89 | 0.00 | 94.44 |
| **589 / 1 .** | 0.28 | 7.18 | 20.36 | 34.30 | 8.18 | 0.01 | 1.59 | 0.03 | 0.03 | 22.51 | 0.00 | 94.47 |
| **590 / 1 .** | 0.30 | 7.32 | 20.37 | 35.08 | 8.31 | 0.02 | 1.55 | 0.05 | 0.02 | 22.15 | 0.03 | 95.20 |
| **591 / 1 .** | 0.24 | 7.29 | 19.80 | 34.21 | 8.06 | 0.06 | 1.52 | 0.01 | 0.02 | 22.46 | 0.00 | 93.67 |
| **592 / 1 .** | 0.30 | 7.33 | 20.00 | 34.01 | 8.08 | 0.04 | 1.53 | 0.04 | 0.04 | 22.21 | 0.00 | 93.60 |
| **593 / 1 .** | 0.36 | 6.05 | 23.20 | 36.02 | 7.65 | 0.07 | 1.58 | 0.00 | 0.02 | 18.19 | 0.00 | 93.13 |
| **594 / 1 .** | 0.26 | 7.48 | 20.11 | 34.57 | 8.11 | 0.00 | 1.54 | 0.01 | 0.04 | 22.20 | 0.00 | 94.31 |
| **595 / 1 .** | 0.34 | 7.12 | 20.16 | 34.30 | 8.22 | 0.01 | 1.60 | 0.04 | 0.05 | 22.16 | 0.03 | 94.03 |
| **596 / 1 .** | 0.30 | 7.15 | 20.04 | 34.48 | 8.66 | 0.01 | 1.60 | 0.03 | 0.00 | 22.06 | 0.02 | 94.34 |
| **597 / 1 .** | 0.29 | 7.04 | 19.98 | 33.96 | 8.33 | 0.02 | 1.64 | 0.03 | 0.01 | 22.69 | 0.00 | 94.00 |
| **598 / 1 .** | 0.17 | 6.86 | 19.74 | 34.02 | 8.35 | 0.00 | 1.72 | 0.03 | 0.04 | 23.36 | 0.03 | 94.33 |
| **599 / 1 .** | 0.25 | 7.01 | 20.01 | 34.35 | 8.31 | 0.02 | 1.79 | 0.05 | 0.04 | 23.50 | 0.00 | 95.34 |
| **600 / 1 .** | 0.13 | 7.11 | 19.90 | 33.48 | 7.77 | 0.02 | 1.85 | 0.01 | 0.05 | 23.84 | 0.00 | 94.17 |
| **601 / 1 .** | 1.64 | 0.40 | 36.48 | 45.84 | 8.50 | 0.00 | 0.23 | 0.02 | 0.00 | 1.07 | 0.00 | 94.16 |
| **602 / 1 .** | 0.01 | 0.01 | 0.00 | 0.08 | 0.00 | 0.01 | 0.05 | 0.02 | 0.00 | 0.02 | 0.00 | 0.20 |

**Table A3-2 continued..**

| Point | $Na_2O$ | MgO | $Al_2O_3$ | $SiO_2$ | $K_2O$ | CaO | $TiO_2$ | $Cr_2O_3$ | MnO | FeO | ZnO | Total |
|---|---|---|---|---|---|---|---|---|---|---|---|---|
| **603 / 1 .** | 0.03 | 0.01 | 0.04 | 0.29 | 0.02 | 0.00 | 0.00 | 0.01 | 0.00 | 0.08 | 0.00 | 0.49 |
| **604 / 1 .** | 0.03 | 0.00 | 0.01 | 0.07 | 0.00 | 0.01 | 0.02 | 0.00 | 0.00 | 0.01 | 0.00 | 0.15 |
| **605 / 1 .** | 0.02 | 0.01 | 0.01 | 0.07 | 0.00 | 0.02 | 0.00 | 0.03 | 0.00 | 0.02 | 0.00 | 0.17 |
| **606 / 1 .** | 0.00 | 0.00 | 0.00 | 0.09 | 0.00 | 0.02 | 0.00 | 0.00 | 0.00 | 0.01 | 0.01 | 0.14 |
| **607 / 1 .** | 0.03 | 0.01 | 0.02 | 0.09 | 0.02 | 0.01 | 0.00 | 0.00 | 0.00 | 0.01 | 0.00 | 0.19 |
| **608 / 1 .** | 0.00 | 0.00 | 0.01 | 0.15 | 0.00 | 0.01 | 0.00 | 0.00 | 0.00 | 0.03 | 0.00 | 0.21 |
| **609 / 1 .** | 0.00 | 1.83 | 40.83 | 23.79 | 0.01 | 0.02 | 0.00 | 0.04 | 0.15 | 25.06 | 0.03 | 91.76 |
| **610 / 1 .** | 0.00 | 1.85 | 40.92 | 24.28 | 0.04 | 0.02 | 0.01 | 0.04 | 0.15 | 24.85 | 0.00 | 92.16 |
| **611 / 1 .** | 0.03 | 1.86 | 41.15 | 24.19 | 0.04 | 0.01 | 0.00 | 0.02 | 0.17 | 25.10 | 0.00 | 92.58 |
| **612 / 1 .** | 0.00 | 1.92 | 41.47 | 24.28 | 0.01 | 0.01 | 0.01 | 0.09 | 0.19 | 24.90 | 0.00 | 92.88 |
| **613 / 1 .** | 0.00 | 1.89 | 41.44 | 24.24 | 0.00 | 0.00 | 0.00 | 0.03 | 0.18 | 25.32 | 0.00 | 93.11 |
| **614 / 1 .** | 0.00 | 1.93 | 41.26 | 24.24 | 0.03 | 0.02 | 0.02 | 0.04 | 0.12 | 25.01 | 0.00 | 92.68 |
| **615 / 1 .** | 0.01 | 1.87 | 41.15 | 24.15 | 0.01 | 0.00 | 0.03 | 0.04 | 0.16 | 25.24 | 0.03 | 92.70 |
| **616 / 1 .** | 0.01 | 1.90 | 41.22 | 24.06 | 0.01 | 0.01 | 0.00 | 0.05 | 0.18 | 25.21 | 0.00 | 92.67 |
| **617 / 1 .** | 0.04 | 9.78 | 23.44 | 25.71 | 0.04 | 0.03 | 0.06 | 0.04 | 0.07 | 29.12 | 0.00 | 88.33 |
| **618 / 1 .** | 0.37 | 2.80 | 8.54 | 51.94 | 1.40 | 0.11 | 0.06 | 0.29 | 0.05 | 9.55 | 0.00 | 75.13 |
| **619 / 1 .** | 0.64 | 0.69 | 17.23 | 72.56 | 4.28 | 0.00 | 0.16 | 0.05 | 0.00 | 1.40 | 0.03 | 97.04 |
| **620 / 1 .** | 5.53 | 0.17 | 30.50 | 55.01 | 4.33 | 3.40 | 0.07 | 0.02 | 0.00 | 0.40 | 0.00 | 99.43 |
| **621 / 1 .** | 7.87 | 0.00 | 25.61 | 58.98 | 0.28 | 6.39 | 0.00 | 0.02 | 0.00 | 0.09 | 0.02 | 99.26 |
| **622 / 1 .** | 7.77 | 0.00 | 25.87 | 59.06 | 0.01 | 7.09 | 0.01 | 0.00 | 0.00 | 0.11 | 0.01 | 99.93 |
| **623 / 1 .** | 7.76 | 0.01 | 25.42 | 58.10 | 0.02 | 7.03 | 0.03 | 0.02 | 0.01 | 0.06 | 0.00 | 98.45 |
| **624 / 1 .** | 7.69 | 0.00 | 25.71 | 58.76 | 0.02 | 7.05 | 0.00 | 0.00 | 0.00 | 0.05 | 0.03 | 99.30 |
| **625 / 1 .** | 8.04 | 0.00 | 25.63 | 58.06 | 0.04 | 7.15 | 0.00 | 0.00 | 0.00 | 0.08 | 0.00 | 99.00 |
| **626 / 1 .** | 7.38 | 0.00 | 25.68 | 60.38 | 0.01 | 7.14 | 0.04 | 0.00 | 0.01 | 0.10 | 0.00 | 100.75 |
| **627 / 1 .** | 7.48 | 0.02 | 26.25 | 58.30 | 0.04 | 7.10 | 0.02 | 0.01 | 0.00 | 0.19 | 0.00 | 99.41 |

**Table A4. All dip and strike measurements from field work with corresponding GPS coordinates.**

| Decimal Degrees South | Decimal Degrees East | Dip Direction | Dip | | Decimal Degrees South | Decimal Degrees East | Dip Direction | Dip |
|---|---|---|---|---|---|---|---|---|
| 24.6788 | 30.5774 | 218 | 10 | | 24.2100 | 29.9797 | 176 | 22 |
| 24.6788 | 30.5774 | 212 | 8 | | 24.2100 | 29.9797 | 174 | 27 |
| 24.6788 | 30.5774 | 208 | 6 | | | | | |
| 24.6788 | 30.5774 | 222 | 16 | | 24.7820 | 30.2754 | 353 | 22 |
| 24.6788 | 30.5774 | 202 | 20 | | | | | |
| 24.6788 | 30.5774 | 218 | 8 | | 25.0760 | 30.4091 | 247 | 12 |
| | | | | | 25.0760 | 30.4091 | 230 | 10 |
| 24.7338 | 30.5371 | 282 | 6 | | | | | |
| | | | | | 24.9517 | 30.3723 | 286 | 18 |
| 24.7423 | 30.5535 | 236 | 16 | | 24.9517 | 30.3723 | 270 | 14 |
| 24.7423 | 30.5535 | 201 | 10 | | 24.9517 | 30.3723 | 273 | 14 |
| | | | | | 24.9517 | 30.3723 | 279 | 15 |
| 24.6652 | 30.6078 | 291 | 12 | | | | | |
| 24.6652 | 30.6078 | 252 | 14 | | 24.6760 | 30.4964 | 277 | 6 |
| 24.6652 | 30.6078 | 284 | 20 | | 24.6760 | 30.4964 | 260 | 6 |
| 24.6652 | 30.6078 | 284 | 18 | | | | | |
| | | | | | 24.6758 | 30.4963 | 241 | 6 |
| | | | | | 24.6758 | 30.4963 | 270 | 4 |
| 24.1856 | 29.9916 | 171 | 32 | | | | | |
| 24.1856 | 29.9916 | 159 | 38 | | 24.6754 | 30.4961 | 246 | 4 |
| 24.1856 | 29.9916 | 158 | 34 | | | | | |
| 24.1856 | 29.9916 | 166 | 36 | | 24.7211 | 30.5277 | 199 | 9 |
| | | | | | 24.7211 | 30.5277 | 213 | 6 |
| 24.2100 | 29.9797 | 178 | 38 | | | | | |
| 24.1856 | 29.9916 | 166 | 38 | | 24.7210 | 30.5273 | 256 | 8 |
| | | | | | 24.7210 | 30.5273 | 276 | 5 |
| 25.0081 | 30.5003 | 260 | 10 | | | | | |
| 25.0081 | 30.5003 | 272 | 11 | | 24.7210 | 30.5272 | 252 | 6 |
| | | | | | 24.7210 | 30.5272 | 250 | 4 |
| 24.5172 | 30.2880 | 208 | 10 | | | | | |
| 24.5172 | 30.2880 | 214 | 10 | | 24.7480 | 30.5689 | 163 | 11 |
| 24.5172 | 30.2880 | 218 | 10 | | 24.7480 | 30.5689 | 230 | 7 |
| | | | | | 24.7480 | 30.5689 | 197 | 12 |
| 24.2682 | 30.0374 | 46 | 6 | | 24.7480 | 30.5689 | 231 | 10 |
| 24.2682 | 30.0374 | 97 | 21 | | 24.7480 | 30.5689 | 186 | 6 |
| 24.2682 | 30.0374 | 88 | 16 | | | | | |
| | | | | | 24.4471 | 30.2759 | 204 | 16 |
| 24.2100 | 29.9797 | 170 | 30 | | 24.4471 | 30.2759 | 208 | 16 |
| 24.2100 | 29.9797 | 157 | 36 | | 24.4471 | 30.2759 | 204 | 16 |
| 24.2100 | 29.9797 | 166 | 28 | | 24.4471 | 30.2759 | 216 | 16 |
| 24.2100 | 29.9797 | 158 | 26 | | | | | |

**Table A4 continued..**

| Decimal Degrees South | Decimal Degrees East | Dip Direction | Dip |
|---|---|---|---|
| 24.3615 | 30.0965 | 210 | 16 |
| 24.3615 | 30.0965 | 188 | 33 |
| 24.3615 | 30.0965 | 202 | 21 |
| | | | |
| 24.8355 | 30.3349 | 300 | 16 |
| 24.8355 | 30.3349 | 266 | 14 |
| 24.8355 | 30.3349 | 250 | 14 |
| | | | |
| 24.8931 | 30.3124 | 310 | 5 |
| 24.8931 | 30.3124 | 12 | 8 |
| | | | |
| 24.9137 | 30.3135 | 208 | 22 |
| 24.9137 | 30.3135 | 190 | 14 |
| 24.9137 | 30.3135 | 219 | 14 |
| 24.9137 | 30.3135 | 224 | 10 |
| | | | |
| 25.0760 | 30.4093 | 241 | 22 |
| 25.0760 | 30.4093 | 228 | 19 |
| 25.0760 | 30.4093 | 226 | 22 |

## APPENDIX B

**Fig. B1. Original pseudosection for DY09-54 produced with Perplex in the MnNCKFMASHT system.**

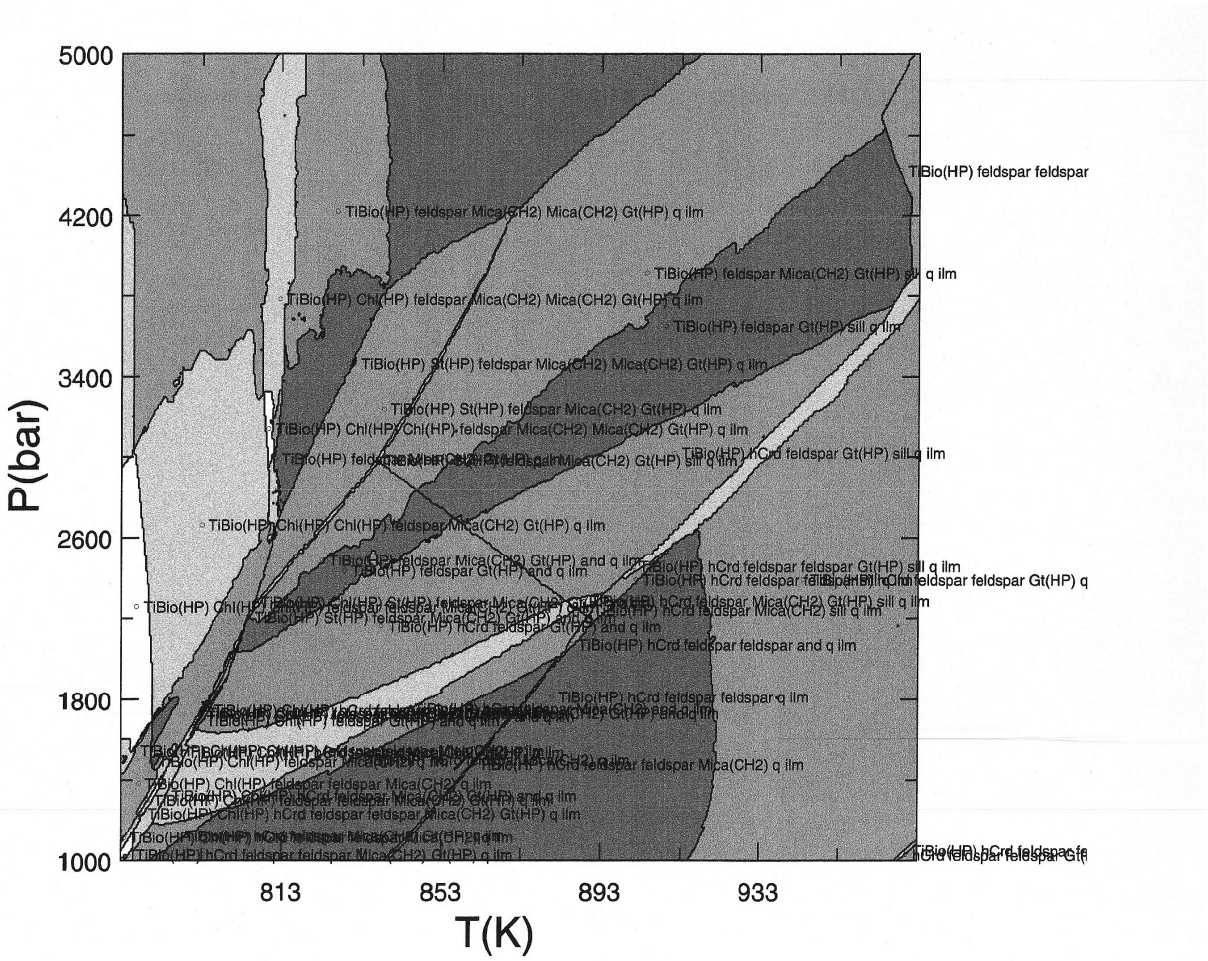

**Fig. B2. Original pseudosection for DY09-56 produced with Perplex in the MnNCKFMASHT system.**

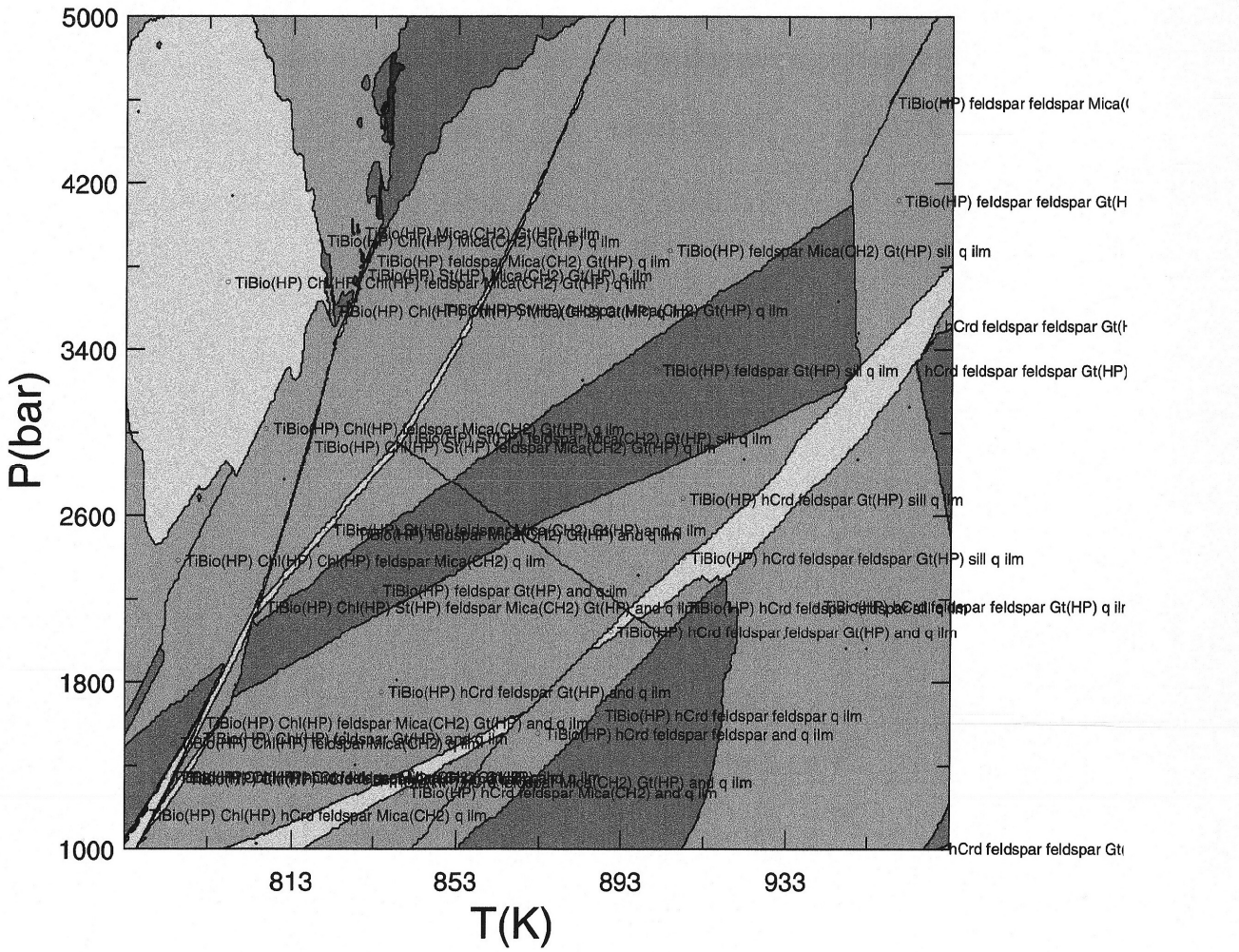

**Fig. B3. Original pseudosection for DY09-86B produced with Perplex in the NCKFMASHT system.**

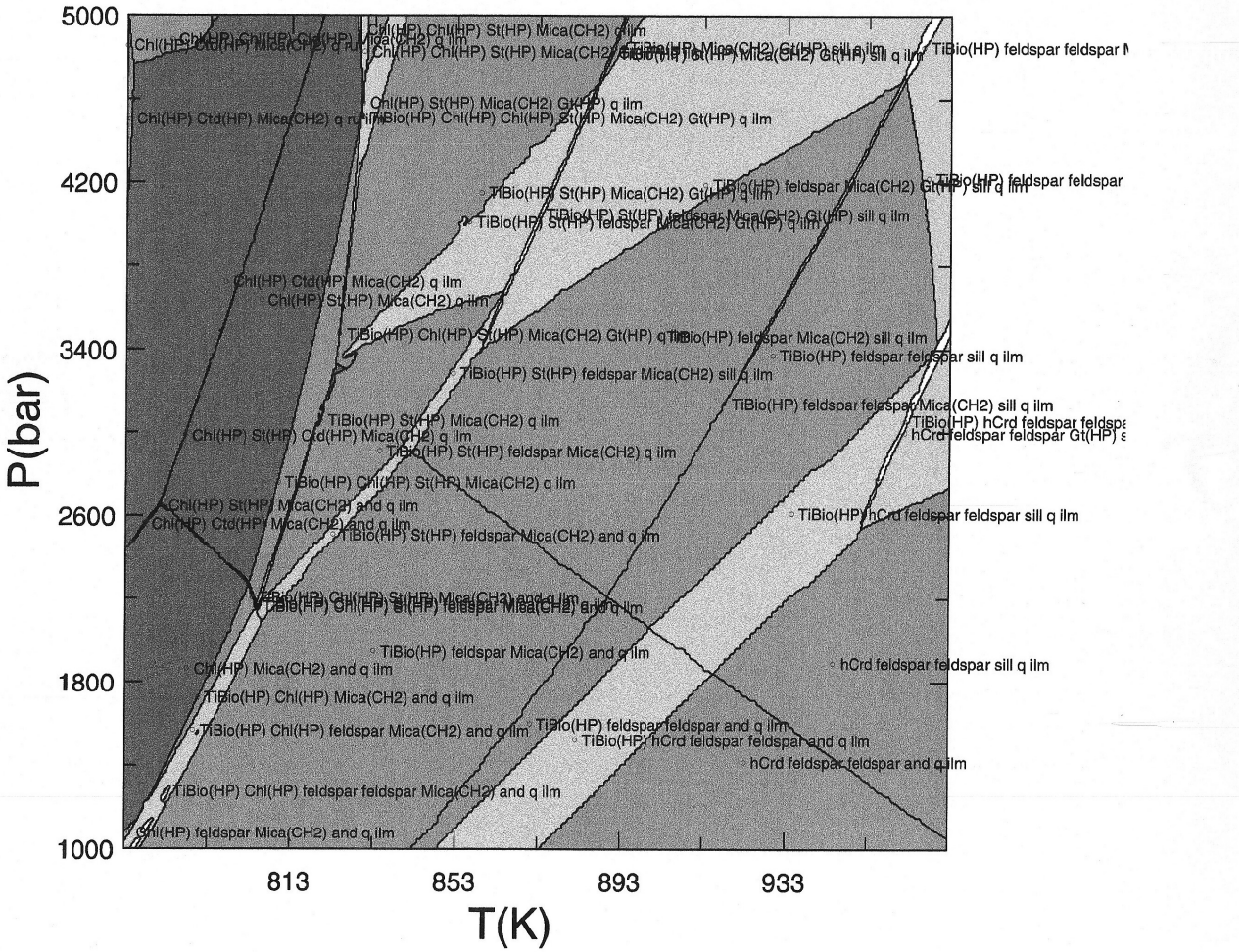

**Fig. B4. Original pseudosection for DM08-52B produced with Perplex in the NCKFMASHT system.**

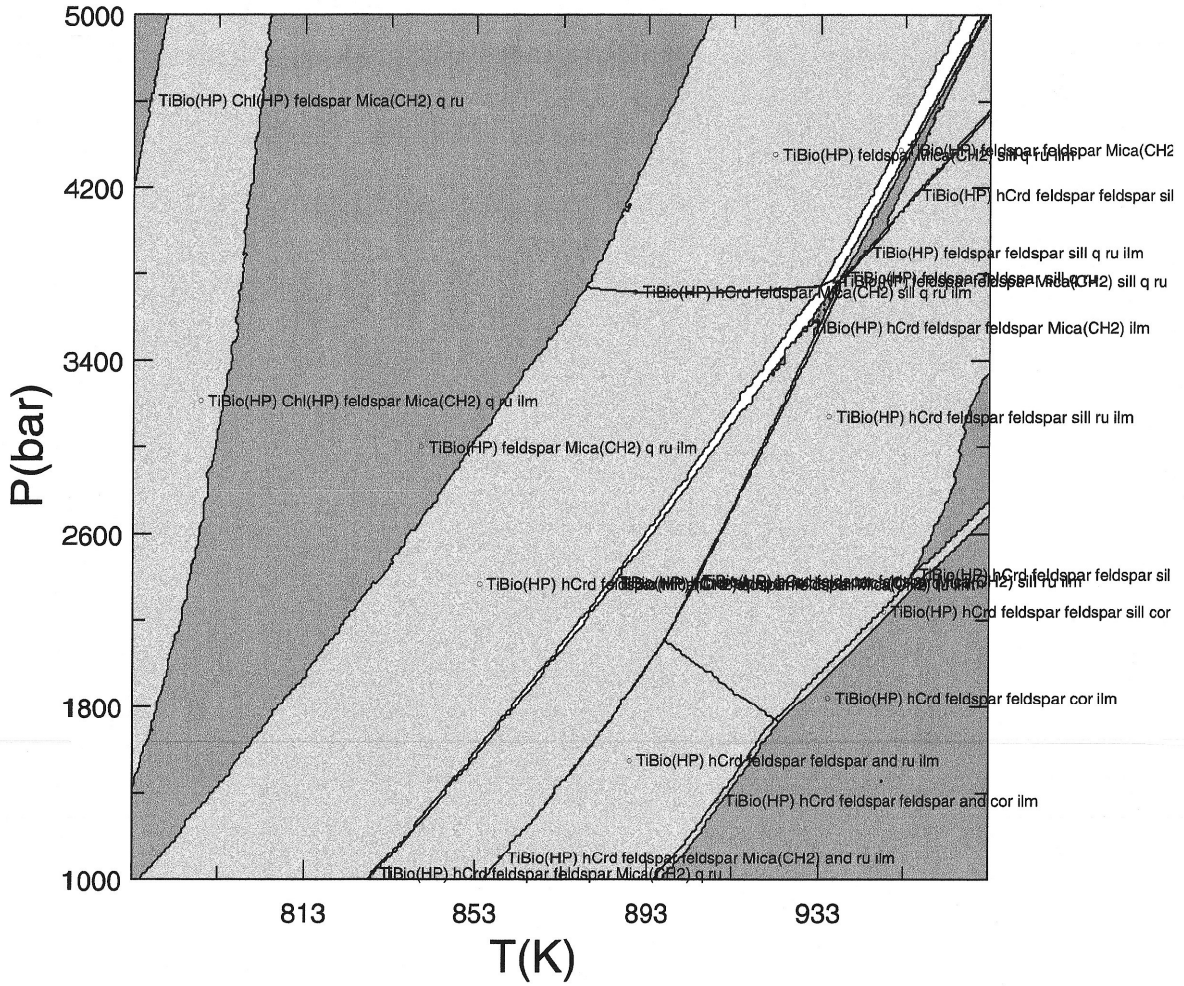

**Fig. B5. Original pseudosection for DM08-54 produced with Perplex in the NCKFMASHT system.**

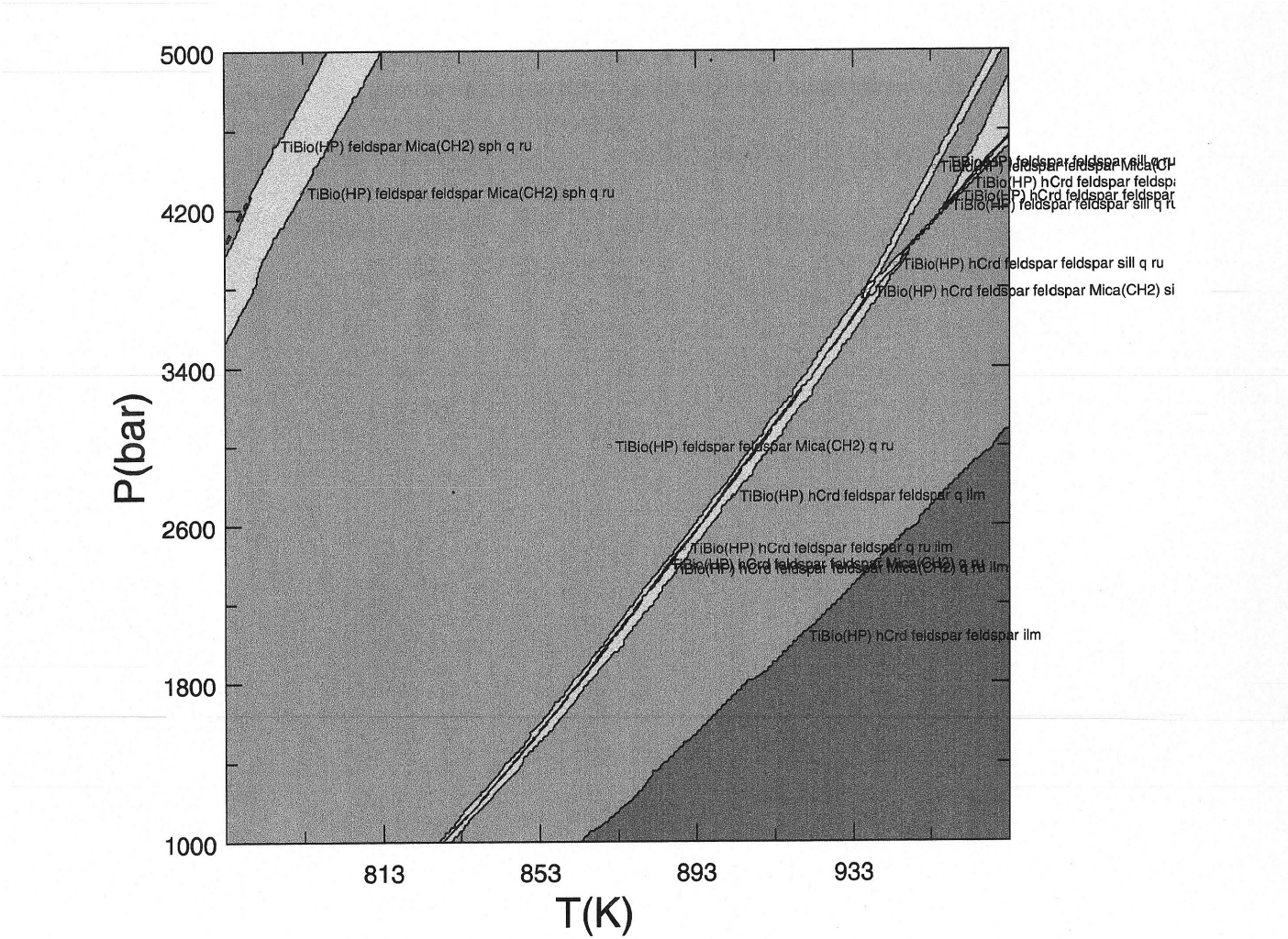

**Fig. B6. Original pseudosection for DM08-63 produced with Perplex in the NCKFMASHT system.**

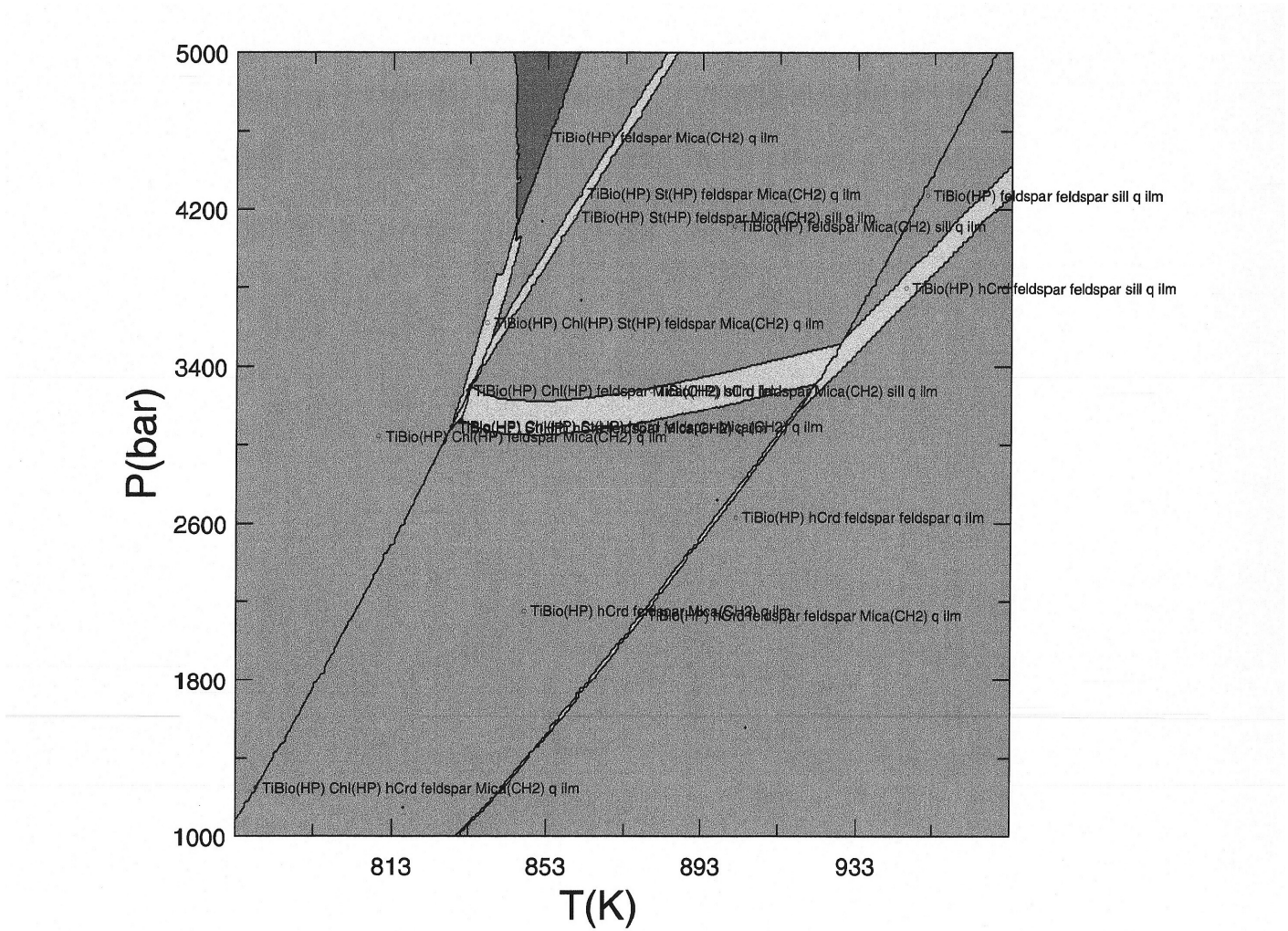

**Fig. B7. Original pseudosection for DM08-82 produced with Perplex in the MnNCKFMASHT system.**

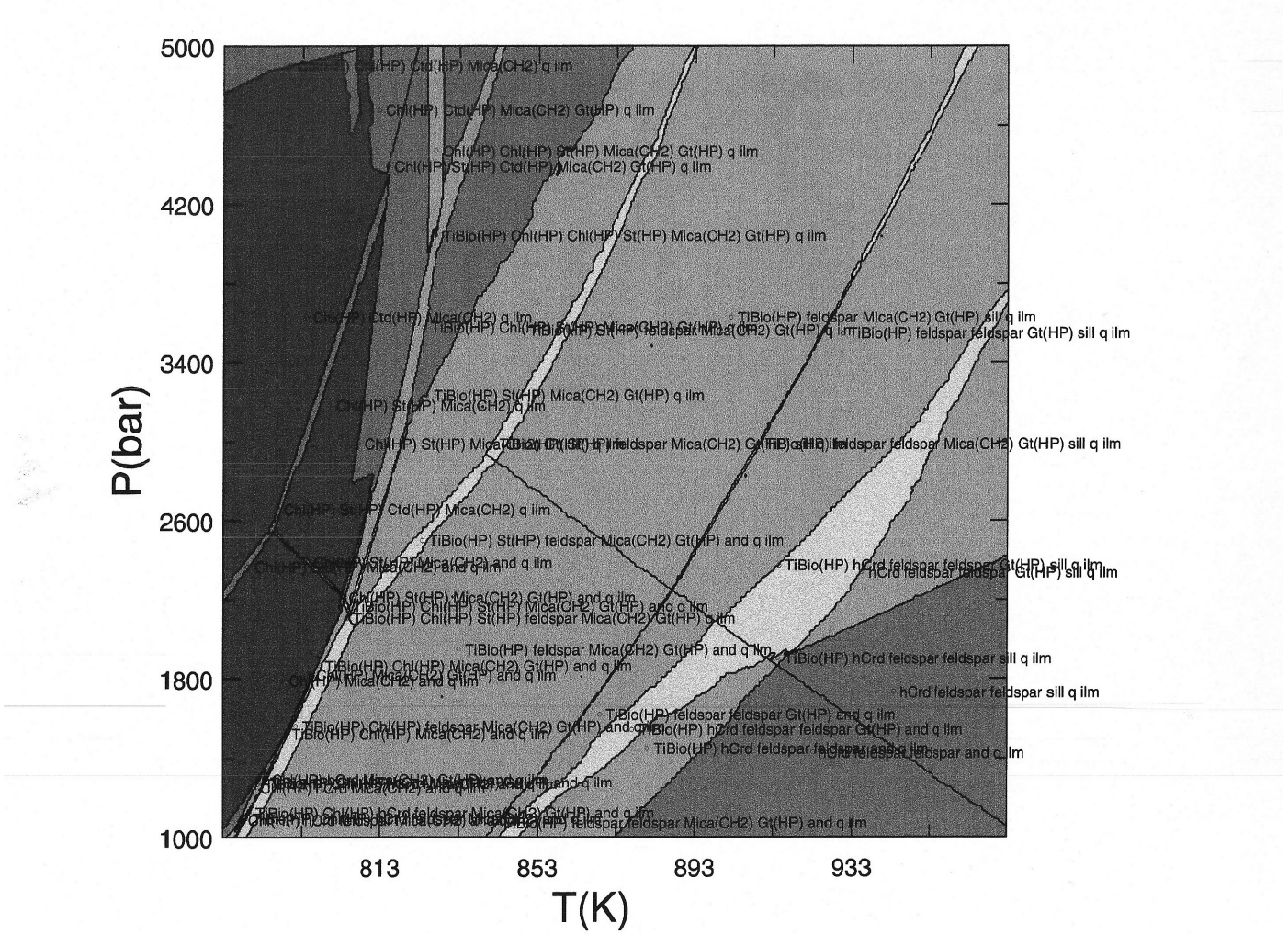

**Fig. B8. Redrafted version of DY09-54 prepared by hand for the purpose of serving as a guide in the final redrafting of DY09-54.**

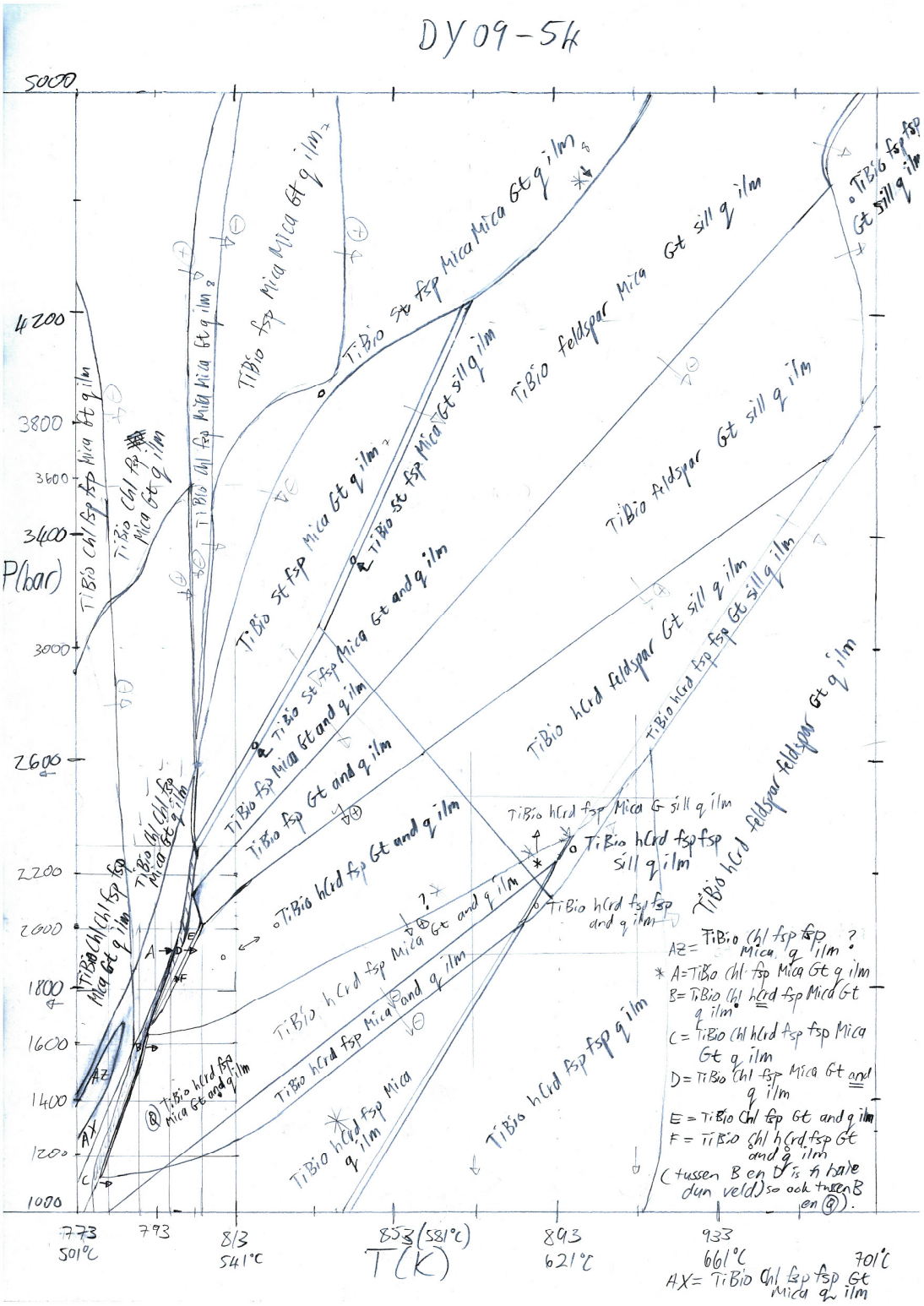

**Fig. B9. Redrafted version of DY09-56 prepared by hand for the purpose of serving as a guide in the final redrafting of DY09-54.**

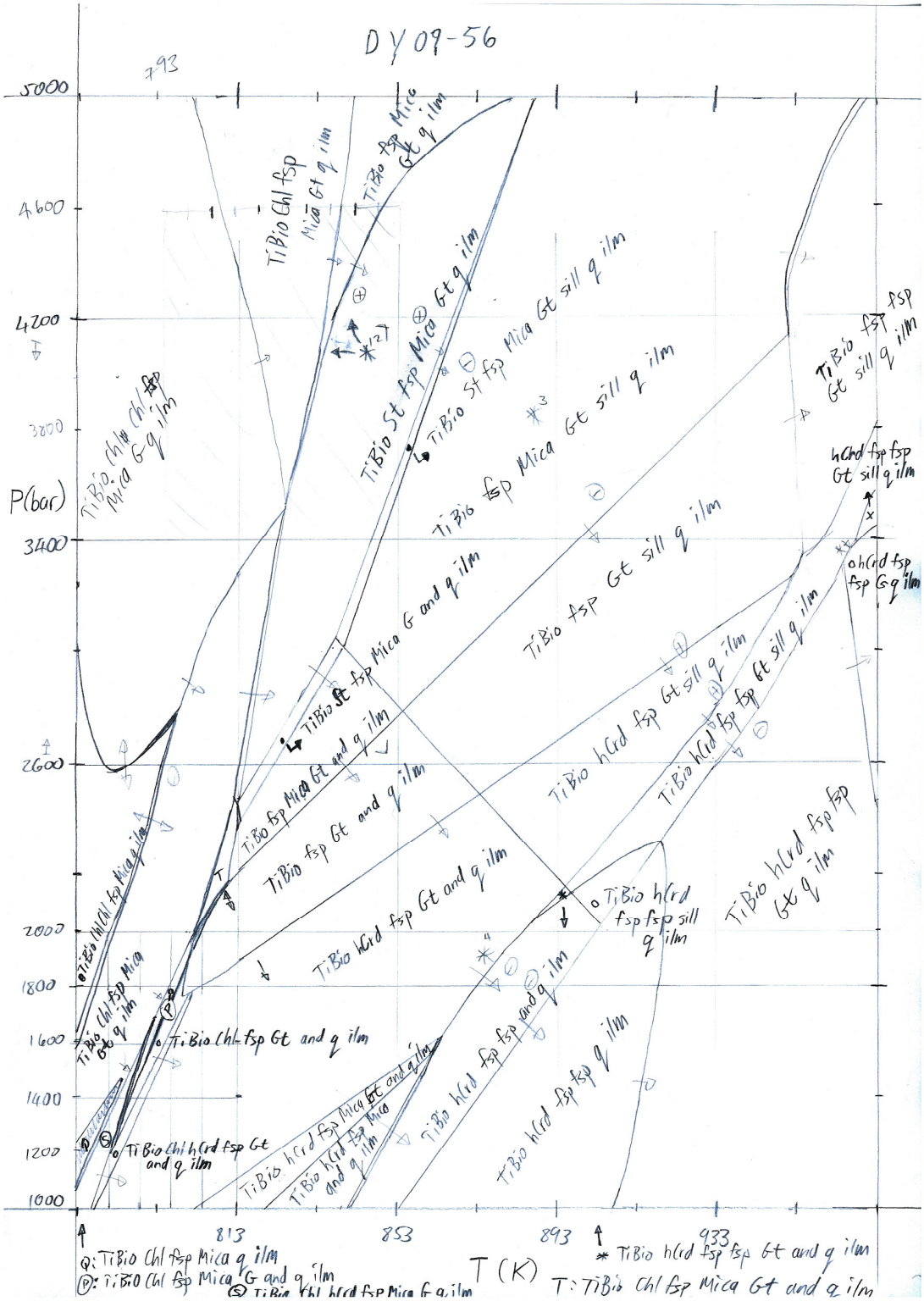

**Fig. B10. Redrafted version of DY09-86B prepared by hand for the purpose of serving as a guide in the final redrafting of DY09-54.**